

© 2009

Yahia M. Tokal-Ahmed

ALL RIGHTS RESERVED

**RESPONSE OF BRIDGE STRUCTURES SUBJECTED TO BLAST LOADS AND
PROTECTION TECHNIQUES TO MITIGATE THE EFFECT OF BLAST
HAZARDS ON BRIDGES**

by

YAHIA M. TOKAL-AHMED

A Dissertation submitted to the
Graduate School – New Brunswick
Rutgers, The State University of New Jersey

In partial fulfillment of the requirements

for the degree of

Doctor of Philosophy

Graduate Program in Civil and Environmental Engineering

Written under the direction of

Dr. Husam S. Najm

and approved by

New Brunswick, New Jersey

January, 2009

ABSTRACT OF THE DISSERTATION

Response of bridge structures subjected to blast loads and protection techniques to mitigate the effect of blast hazards on bridges

by YAHIA M. TOKAL-AHMED

Dissertation Director:

Dr. Husam S. Najm

Bridges are critical to the transportation system especially at the time of crises. They are essential for rescue missions, evacuations, and rapid distribution of aid and medical supplies. Bridges are highly visible and accessible structures which make them valued potential targets for terrorist attacks as their destruction could have significant impact on the nation. An efficient security system can minimize the potential of terrorism, yet it will not completely eliminate the threat. Consequently, critical bridges should be protected and designed to mitigate probable blast hazards.

The primary objective of this investigation is to analyze the effect of blast loads on critical bridge components and bridge global response, and propose protection measures for mitigating blast hazards. This investigation presents an overview of the characteristics of blast loads, pressure distributions, wave propagation and reflection, energy dissipation, and the factors affecting the behavior of structural elements subjected to blast loading.

To simplify the analysis of structural elements subjected to blast loads, blast load response spectra were developed. These spectra are used to transform the dynamic blast loads into equivalent static loads. Blast response spectra can be used to analyze and design individual structural components subjected to blast loads, estimate the required ductility, and estimate the minimum standoff distance for the probable blast hazards.

The global behavior of a typical highway bridge was evaluated using computer simulation. The bridge model was subjected to various blast scenarios applied above or below the bridge deck. The results from these computer simulations were used to identify the vulnerable components in the bridge during a blast hazard as well as estimating the magnitudes and locations of maximum shear forces and bending moments. The results from the computer simulations were compared to those from the response spectral analysis. Thus, protection measures were proposed and evaluated. Protection measures include preventive measures such as standoff distance and added security. They also include improved redundancy through utilizing multiple column bents with double and triple edge columns, using highly ductile materials, longer seat widths, doubly reinforced decks, hold-down devices, and the use of cable auxiliary systems.

DEDICATION

To my parents, for all their love, care, and support.

ACKNOWLEDGEMENTS

First and foremost, I would like to thank God Almighty for guiding me through every step of my life. I wish to express my deepest gratitude to my advisor Dr. Husam Najm, for his guidance, care, support, and encouragement. Working with Dr. Najm was an enriching experience on both the personal and the professional levels. This work was only possible through his guidance and assistance.

I am very grateful to my committee members; Dr. Perumalsamy Balaguru, Dr. Hani Nassif, Dr. Yook-Kong Yong, and Dr. David Coit. I am honored to have them in my committee. I deeply thank them for all their help. I would like to thank Dr. Perumalsamy Balaguru and Dr. Nenad Gucunski for always being so welcoming to my questions and for their guidance and advice. Special thanks to Dr. Edward Nawy for his invaluable advice and assistance. I extend my appreciation to the staff of Civil Engineering Department at Rutgers University for their help and support; Connie Dellamura, Linda Szary, Pat Szary, Azam Kalantari, and Gina Cullari. Also, I am very grateful to my instructors; Dr. Trefor Williams, Dr. Andy Foden, and Suhail Albhaisi.

Thanks to my colleagues at the Civil and Environmental Engineering Department. Special thanks to Dr. Joseph Davis, Kagan Aktas, Amrutha Donaiah, and Ufuk Ates. I would like to express my appreciation and gratitude to Dr. Mohamed Nazir, Dr. Mohamed Arafa, Radwa Omar, Salaheldin Hamed, and Ahmed Shaker.

Finally, I thank my brother and sister for their warm encouragement and love. Most of all, I thank my beloved parents for their kindness, warmth, love, and prayers. Words can not express my appreciation and love to them.

TABLE OF CONTENTS

ABSTRACT OF THE DISSERTATION	ii
DEDICATION	iv
ACKNOWLEDGEMENTS	v
TABLE OF CONTENTS.....	vii
LIST OF TABLES	xi
LIST OF FIGURES	xii
CHAPTER 1: INTRODUCTION	1
1.1 Statement of Problem.....	1
1.2 Research Objectives.....	2
CHAPTER 2: BACKGROUND	5
2.1 Blast Hazards and Attacks against Infrastructure Targets	5
2.2 Designing Bridges for Blast Hazards.....	11
2.3 Characteristics of the Blast Wave.....	16
2.3.1 Types of explosives.....	17
2.3.2 Types of blast scenarios	19
2.3.3 Positive and negative phases.....	20
2.3.4 Incident and reflected pressures.....	21
2.3.5 Cubic root scaling and blast wave parameters	23
2.3.6 Confined versus unconfined blasts	27
2.3.7 Vapor cloud explosions.....	27

2.4	Factors affecting the Behavior of Bridges during Blast loading.....	28
2.5	Comparison of Blast Hazards and Earthquakes Hazards.....	30
2.6	Dynamic Properties of Materials	31
2.7	Strength Increase Factor	32
2.8	Impulsive Load Design.....	33
2.9	Equivalent SDOF Analysis.....	34
2.10	Plastic Design of Structural Members Loaded with Impulsive Loads	35
2.11	Pressure-Impulse (P-I) Diagrams.....	38
2.12	Synopsis	44
CHAPTER 3: RESPONSE SPECTRA FOR BLAST LOADS.....		47
3.1	Variation of Blast Pressure along the Length of Loaded Members.....	48
3.2	Elastic Blast Pressure Response Spectra.....	52
3.2.1	Designing a member for a specific charge weight and standoff distance.	60
3.2.2	Calculating the minimum required standoff distance for a member.....	61
3.3	Inelastic Blast Pressure Response Spectra.....	62
CHAPTER 4: ANALYTICAL INVESTIGATION.....		66
4.1	Analysis Methods.....	66
4.2	ELS Software	68
4.2.1	Applied element method	68
4.2.2	Connectivity between elements	69
4.2.3	Collapse analysis.....	71

4.2.4	Blast wave model	71
4.3	Response of Concrete Columns Subjected to Blast Loads	73
4.3.1	ELS analysis.....	74
4.3.2	Response spectral analysis – Approximate Analysis.....	89
4.3.3	Comparisons and discussions	94
CHAPTER 5: BRIDGE GLOBAL RESPONSE TO BLAST LOADS.....		98
5.1	Below Deck Blast Scenario	103
5.1.1	Blast scenario close to the bridge midspan	103
5.1.2	Blast scenario between the midspan and the bridge pier	112
5.1.3	Blast scenario underneath the bridge bent	114
5.1.4	Hand charge attached to one or more of the columns.....	118
5.2	Above Deck Blast Scenario	119
5.2.1	Blast scenario close to the bridge midspan	120
5.2.2	Blast scenario close to the bridge bent.....	123
5.3	Results and Discussion	125
CHAPTER 6: PROTECTION TECHNIQUES TO MITIGATE BLAST HAZARDS. .		127
6.1	Minimum Standoff Distance and Maximum Charge Weight.....	128
6.2	Highly Ductile Concrete Materials	129
6.2.1	SIFCON	132
6.2.2	SIMCON	134
6.2.3	ECC.....	135

6.3	Redundancy and Continuity.....	139
6.4	Collapse Prevention using Auxiliary Cable Systems.....	147
6.4.1	Equilibrium of the deflected system (Popov, 1990)	150
6.4.2	Castigliano’s first theorem (Oden, 1967).....	154
6.4.3	Prestressed cable system.....	157
6.4.4	Anchorage details of cable system.....	158
CHAPTER 7: CONCLUSIONS AND RECOMMENDATIONS.....		161
7.1	Summary.....	161
7.2	Conclusions and Recommendations	162
7.3	Future Research	165
APPENDIX A.....		166
A.1	Using the Blast Response Spectra to Design a Structural Element Subjected to a Specific Blast Scenario	167
A.2	Calculating the Minimum Required Standoff Distance for a Specific Structural Element	174
APPENDIX B.....		179
	Design of Catenary Cable System to Prevent Progressive Collapse	180
APPENDIX C.....		184
	Cost Analysis of Bridge Protection Measures against Extreme Events	185
REFERENCES		194
CURRICULUM VITA		197

LIST OF TABLES

Table 2.1. Minimum barrier standoffs from bridge piers (FHWA, 2003).....	16
Table 2.2. Desired barrier standoffs from bridge piers (FHWA, 2003)	16
Table 2.3. TNT equivalents for different types of explosive (TM5-1300, 1990).....	18
Table 2.4. Comparing seismic hazards and blast hazards.....	31
Table 2.5. Dynamic Increase Factor for design of reinforced Concrete (TM5-1300, 1990)	32
Table 2.6. Strength Increase Factor (TM5-1300, 1990)	33
Table 2.7. Performance criteria for typical structural components (TM5-1300, 1990)....	43
Table 4.1. Comparison between the maximum shear values of ELS versus SDOF.....	95
Table 4.2. Comparison between the total shear values of ELS versus SDOF	95

LIST OF FIGURES

Fig. 2.1. Murrah Federal Building before explosion (courtesy Associated Press)	6
Fig. 2.2. Murrah Federal Building after explosion (courtesy Associated Press)	6
Fig. 2.3. Severe damage in the Murrah Federal Building (courtesy Associated Press).....	7
Fig. 2.4. Khubar Towers after the terrorist attack (courtesy Associated Press).....	7
Fig. 2.5. WTC towers completely collapsed after the attacks (courtesy Associated Press)	8
Fig. 2.6. Damage done to the Pentagon building (courtesy Associated Press).....	8
Fig. 2.7. Collapse of I-880 ramps near Oakland, CA (courtesy Associated Press)	9
Fig. 2.8. Barge crashing into the river piers of I-40 Bridge in Oklahoma (NTSB, 2002)	10
Fig. 2.9. Collapse of I-40 Bridge in Oklahoma due to vessel impact (NTSB, 2002)	10
Fig. 2.10. Collapse of bridge due to blast (courtesy AFP / Getty Images)	11
Fig. 2.11. Collapse of bridge span due to blast load (GlobalSecurity.org, 1999).....	12
Fig. 2.12. Collapse of truss bridge due to blast (CNN, 2005).....	12
Fig. 2.13. Hemispherical blast waves for ground-level explosion (courtesy Reuters)	19
Fig. 2.14. Pressure-time history for free field blast (TM5-1300, 1990)	21
Fig. 2.15. Angle of incidence (TM5-1300, 1990).....	22
Fig. 2.16. Effect of angle of incidence on the coefficient of reflection (TM5-1300, 1990)	23
.....	23
Fig. 2.17. Blast wave parameters for hemispherical TNT explosion (TM5-1300, 1990).	25
Fig. 2.18. Proposed equation for coefficient of reflected pressure	26
Fig. 2.19. Effect of standoff distance on pressure amplitude (A.T.-BLAST).....	29
Fig. 2.20. Dynamic Load Factor for triangular load (TM5-1300, 1990)	35
Fig. 2.21. Typical resistance curve of elastic-perfectly plastic system.....	36

Fig. 2.22. Typical normalized P-I diagram for a SDOF system (Mays and Smith, 1995)	38
Fig. 2.23. Quasi-static loading	40
Fig. 2.24. Impulsive loading	40
Fig. 2.25. P-I diagram expressed in specific units (ASCE, 1997)	42
Fig. 3.1. Variation of range and angle of incidence along the length of the loaded member	48
Fig. 3.2. Distribution of blast pressure along the length of the loaded member for different values of standoff distances	50
Fig. 3.3. Distribution of blast pressure along the length of the loaded member for different charge weights ($R = 5$ ft).....	51
Fig. 3.4. Response Spectra for $W = 500$ lbs (zero damping)	55
Fig. 3.5. Response Spectra for $W = 1000$ lbs (zero damping)	56
Fig. 3.6. Response Spectra for $R = 3$ ft (zero damping)	57
Fig. 3.7. Response Spectra for $R = 8$ ft (zero damping)	58
Fig. 3.8. Response Spectra for $R = 20$ ft (zero damping)	59
Fig. 3.9. Effect of Damping on the equivalent static pressure ($W = 1000$ lbs).....	63
Fig. 3.10. Plastic pressure values for various ductility limits ($W = 500$ lbs).....	64
Fig. 3.11. Plastic pressure values for various ductility limits ($W = 1000$ lbs).....	65
Fig. 4.1. Comparison between AEM, FEM, and DEM (ELS Technical Manual, 2006)..	69
Fig. 4.2. Connectivity springs between adjacent elements (ELS Technical Manual, 2006)	70
Fig. 4.3. Partial connectivity in AEM (ELS Technical Manual, 2006)	71
Fig. 4.4. Effect of the standoff distance on the time of maximum response	75

Fig. 4.5. Typical time-history response of a concrete column subjected to distant blast load.....	78
Fig. 4.6. Schematics of cracks developed in a concrete column due to variable standoff distances.....	79
Fig. 4.7. Schematics of SFD developed in a concrete column due to variable standoff distances.....	80
Fig. 4.8. Schematics of BMD developed in a concrete column due to variable standoff distances.....	81
Fig. 4.9. Schematics of shear envelope developed in a concrete column due to variable standoff distances.....	82
Fig. 4.10. Schematics of bending moment envelope developed in a concrete column due to variable standoff distances.....	83
Fig. 4.11. Effect of the standoff distance on the magnitude of the reversed response	84
Fig. 4.12. Response of concrete column to various blast scenarios.....	87
Fig. 4.13. Effect of the charge weight on the maximum shear developed in the column.	88
Fig. 4.14. Resistance curve for concrete columns with fixed supports.....	90
Fig. 4.15. Pressure distribution along the length of the column	93
Fig. 4.16. Maximum shear calculated using ELS analysis versus SDOF analysis.....	96
Fig. 4.17. Summation of total shear calculated using ELS analysis versus SDOF analysis	96
Fig. 5.1. Cross section of bridge (Wassef et al, 2003).....	100
Fig. 5.2. Reinforcement details of the bridge model (ELS).....	100
Fig. 5.3. Prestressed girders supported on elastomeric bearing pads.....	101

Fig. 5.4. View of the bridge model prior to being subjected to blast scenarios.....	102
Fig. 5.5. Response of deck slab to a blast scenario from below (scale 1:15)	104
Fig. 5.6. Schematics of the SFD of a bridge girder subjected to below-deck blast scenario	105
Fig. 5.7. Schematics of the BMD of a bridge girder subjected to below-deck blast	106
Fig. 5.8. Separation between the girders and the abutment	108
Fig. 5.9. Fixed bearing connection.....	109
Fig. 5.10. Separation between the bottom flange and the web of the prestressed girders	109
Fig. 5.11. Lateral movement of abutment due to blast waves	110
Fig. 5.12. Schematics of the SFD and BMD of a bridge column subjected to below-deck blast scenario.....	111
Fig. 5.13. Lateral displacement of bridge girders (scale 1:20)	112
Fig. 5.14. Response of the bridge model to a below-deck detonation between the midspan and the pier.....	113
Fig. 5.15. Intermediate bent subjected to lateral bending (scale 1:50)	114
Fig. 5.16. Rising of bridge superstructure if the girders are not restrained against upward movement.....	115
Fig. 5.17. Deformed shape of the intermediate bent (scale 1:25).....	116
Fig. 5.18. Failure in concrete columns for integral piers	117
Fig. 5.19. Cracking at the pier cap and separation between the cap beam and columns	117
Fig. 5.20. Failure in concrete column as a result of a hand emplaced charge	118
Fig. 5.21. Bridge collapse due to the failure in the intermediate pier.....	119

Fig. 5.22. Crushing of concrete at the top of the deck slab.....	121
Fig. 5.23. Initiation of flexural cracks in the cap beam	122
Fig. 5.24. Severe flexural cracking of pier cap and buckling of concrete columns.....	122
Fig. 5.25. Hazards of falling debris.....	123
Fig. 5.26. Response of the bridge model to an above-deck detonation at the bent.....	124
Fig. 6.1. Moment-curvature curve of HPFRC versus RC.....	130
Fig. 6.2. Effect of the fiber volume fraction on the flexural behavior of SIFCON	133
Fig. 6.3. Load-deflection curve for reinforced concrete versus reinforced SIFCON (Fritz et al, 1992)	134
Fig. 6.4. Tensile stress strain behavior of concrete, FRC, and ECC (Li, 2003)	138
Fig. 6.5. Bendable ECC (Li, 2003)	138
Fig. 6.6. Multiple column straddle bent (Route 130 East Brunswick, NJ).....	140
Fig. 6.7. Close view of the multi column bent.....	141
Fig. 6.8. Increased pier redundancy using double and triple edge columns	142
Fig. 6.9. HPFRC wall piers.....	142
Fig. 6.10. Combinations of HPFRC walls and columns.....	143
Fig. 6.11. Encased composite HPFRC columns	145
Fig. 6.12. Effect of pipe thickness on the moment curvature curve	146
Fig. 6.13. Effect of concrete ultimate strain on the moment curvature curve.....	147
Fig. 6.14. Typical detail of cable system in concrete girders	149
Fig. 6.15. Typical detail of cable system in steel girders.....	150
Fig. 6.16. Equilibrium of deflected system of cables for a two-span bridge	151
Fig. 6.17. Equilibrium of deflected system of cables for a multiple-span bridge.....	153

Fig. 6.18. Long single cable system versus multiple short cable systems	155
Fig. 6.19. Effect of the angle of rotation on the requires area of the cables	156
Fig. 6.20. Prestressed cable system a) initial prestressing b) final equilibrium.....	157
Fig. 6.21. Anchored cables at the abutment backwall	160
Fig. 6.22. Anchored cables behind columns	160
Fig. A.1. Response spectra for $W = 1000$ lbs (zero damping).....	169
Fig. A.2. Pressure distribution along the length of the member	171
Fig. B.1. Schematic of the catenary forces in the cable system.....	181
Fig. C.1. Pier section prior to any protection measures	192
Fig. C.2. Pier section designed for minor blast hazards.....	193
Fig. C.3. Pier section designed for major blast hazards	193

CHAPTER 1

INTRODUCTION

1.1 Statement of Problem

One of the challenges associated with blast design is that most of the information related to this phenomenon are scattered in different sources. In addition to the scatter, some of the information is classified and not accessible. It is essential to review the available literature regarding bridge security, types of explosives, characteristics of the blast wave, and the different factors that affect the behavior of bridges during blast scenarios. According to the Federal Highway Administration (NBI, 2006) there are more than 600,000 bridges in the United States. Bridges are essential and critical components of the transportation system especially at the time of crises. They are essential for rescue missions, evacuation, and transporting supplies. Damage in one or more critical bridges can result in hundreds of casualties. In addition, the cost of reconstructing the bridge is significantly high. This reconstruction cost can range from several million dollars for ordinary bridges up to billions of dollars for major bridges. Blast hazards on bridges can be classified as either accidental hazards or intentional blast attacks. The accessibility of

bridges as well as their national importance makes them attractive targets to terrorism. Bridges and other transportation assets are considered to be potential targets to terrorist attacks (Blue Ribbon Panel Report, 2003). Information obtained from terrorists training manuals and the testimonies of captured terrorists revealed that there were planned terrorist attacks against U.S. bridges. In 2001, California received several threats to some of its major bridges (CNN, 2001). Pictures of the Golden Gate Bridge and the Brooklyn Bridge were found with one of the captured terrorists. In 2002, a terrorist plot to destroy the Brooklyn Bridge by using blowtorches to cut through its cables was exposed. Between 1980 and 2006, more than 50 attacks against highway bridges were recorded worldwide (TRB, 2008).

An effective security system will minimize the potential threat of an attack, but it will not entirely eliminate the occurrence of attacks. Critical bridges should be designed to mitigate potential blast scenarios. The current engineering standards used for the design of bridges do not account for designing bridges against blast loading. Hence, it is essential to investigate the effect of blast scenarios on critical bridges and establish guidelines regarding the security of bridges.

1.2 Research Objectives

The primary objective of this investigation is to analyze the effect of blast loads on critical bridge components and bridge global response, and propose protection measures for mitigating blast hazards. The proposed research program will take into account both local and global behavior of bridges. Based on the observations obtained from the

analysis and the response of bridge components, protection measures will be proposed and evaluated. These protection measures aim to minimize the damage and prevent the collapse of bridges subjected to blast hazards. The objectives of this study are the following:

- Understand the fundamentals of blast hazards both qualitatively and quantitatively. The effect of wave propagation, reflected pressure, momentum, and impulse will be studied to evaluate their effect on structural elements. The interaction between the blast waves and the structural material will be examined.
- Develop blast load response spectra to transform the dynamic blast loads into equivalent static loads. Blast response spectra can be used to analyze and design individual structural components subjected to blast loads, estimate the required ductility, and estimate the minimum standoff distance for the different probable blast scenarios.
- Perform computer simulation to evaluate the behavior of individual superstructure and substructure bridge components subjected to blast loads, and the global behavior of bridges subjected to various blast loads applied above or below the bridge deck. The results from these computer simulations will be used to identify the vulnerable components in the bridge during a blast hazard. These results will be compared with a simplified SDOF analysis using the blast load response spectra.

- Evaluate various protection measures and investigate in depth those measures that are efficient, easy to apply, and cost effective. These protection measures include: cable systems to prevent collapse, redundant substructure components, substructure components made using High Performance Fiber Reinforced Concrete (HPFRC), superstructure continuity, and maintaining minimum standoff distance.

CHAPTER 2

BACKGROUND

2.1 Blast Hazards and Attacks against Infrastructure Targets

Recently, the threat of terrorist attacks has become an increasing concern for governments. America was subjected to several terrorist attacks during the past 25 years. In April 1983, the United States embassy in Beirut, Lebanon was subjected to a car bombing attack which killed 63 people. The interest in protecting infrastructure against terrorist attacks and blast hazards was strongly generated after the bombing of the Murrah Federal Building in Oklahoma City in April 1995 (Figs 2.1 through 2.3). This terrorist attack killed 168 people and injured over 600 more. A second wave of interest was generated after the bombing of the Khubar Towers in Saudi Arabia in June 1996 (Fig. 2.4). The buildings were used as housing facilities for foreign military personnel. The explosion killed 19 U.S. servicemen and injured more than 500 people from several countries. However, the collapse of World Trade Center (WTC) Towers in New York City, resulting from the terrorist attack in September 2001, was the key event that raised a high interest level of protecting critical infrastructural targets against blast scenarios (Fig

2.5). Almost 3,000 people were killed in the WTC Towers collapse (CNN, 2002). The Pentagon was also attacked by a hijacked plane (Fig. 2.6).



Fig. 2.1. Murrah Federal Building before explosion (courtesy Associated Press)



Fig. 2.2. Murrah Federal Building after explosion (courtesy Associated Press)



Fig. 2.3. Severe damage in the Murrah Federal Building (courtesy Associated Press)



Fig. 2.4. Khubar Towers after the terrorist attack (courtesy Associated Press)



Fig. 2.5. WTC towers completely collapsed after the attacks (courtesy Associated Press)

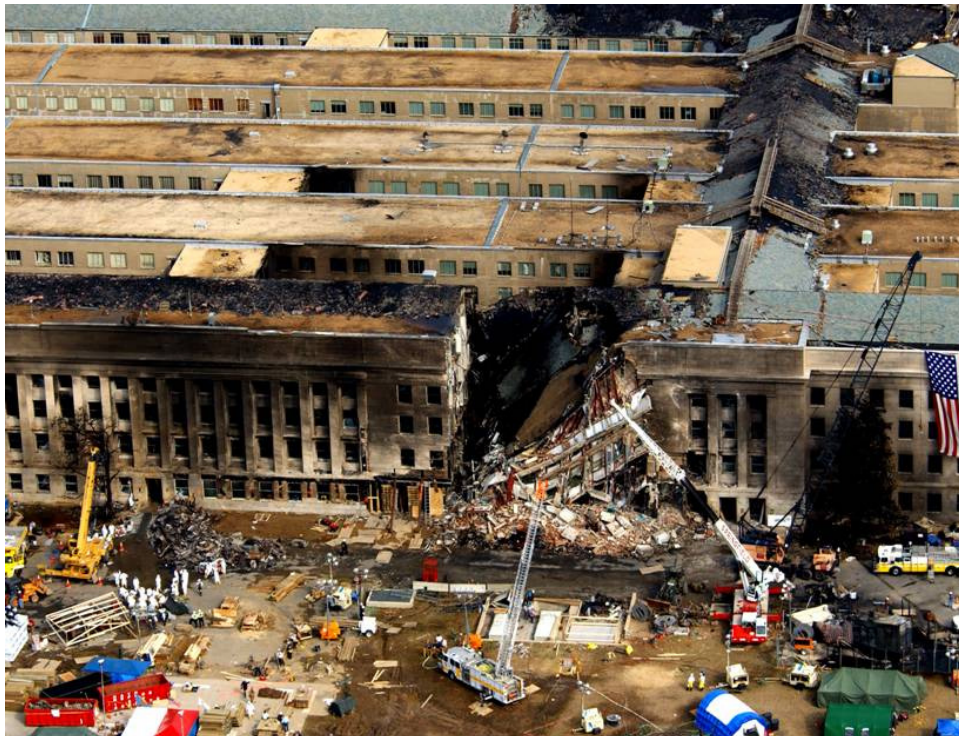


Fig. 2.6. Damage done to the Pentagon building (courtesy Associated Press)

Other hazards on bridges could result from incidents such as fiery crashes of gasoline tankers such as those on I-95 in Connecticut in 2003, and I-880 near San Francisco in 2007 (Fig. 2.7). Both these incidents resulted in the partial collapse of bridges and caused significant damage and disruption to traffic. Vessel impact and truck impacts are also hazardous events to bridges and can result in partial or total collapse of the bridge. An example of such, was the vessel impacts to the river piers of the I-40 Bridge in Oklahoma in 2002 (Figs. 2.8 and 2.9) that resulted in the total collapse of two spans of the bridge. Similarly, a truck impact resulted in the partial collapse of two girders in Pennsylvania in 2007.

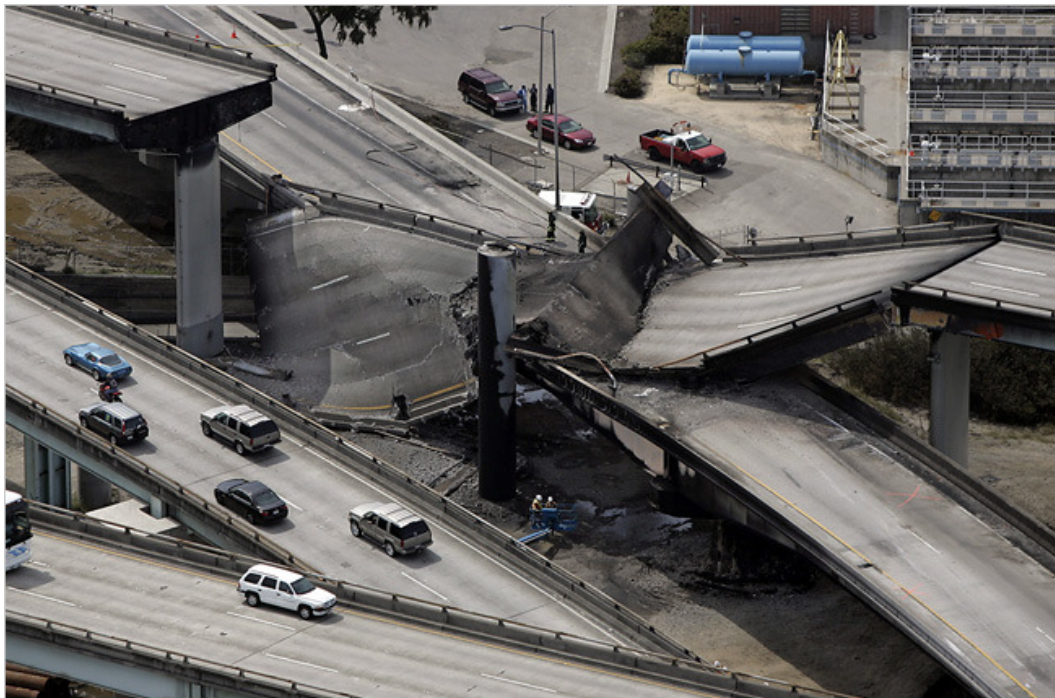


Fig. 2.7. Collapse of I-880 ramps near Oakland, CA (courtesy Associated Press)

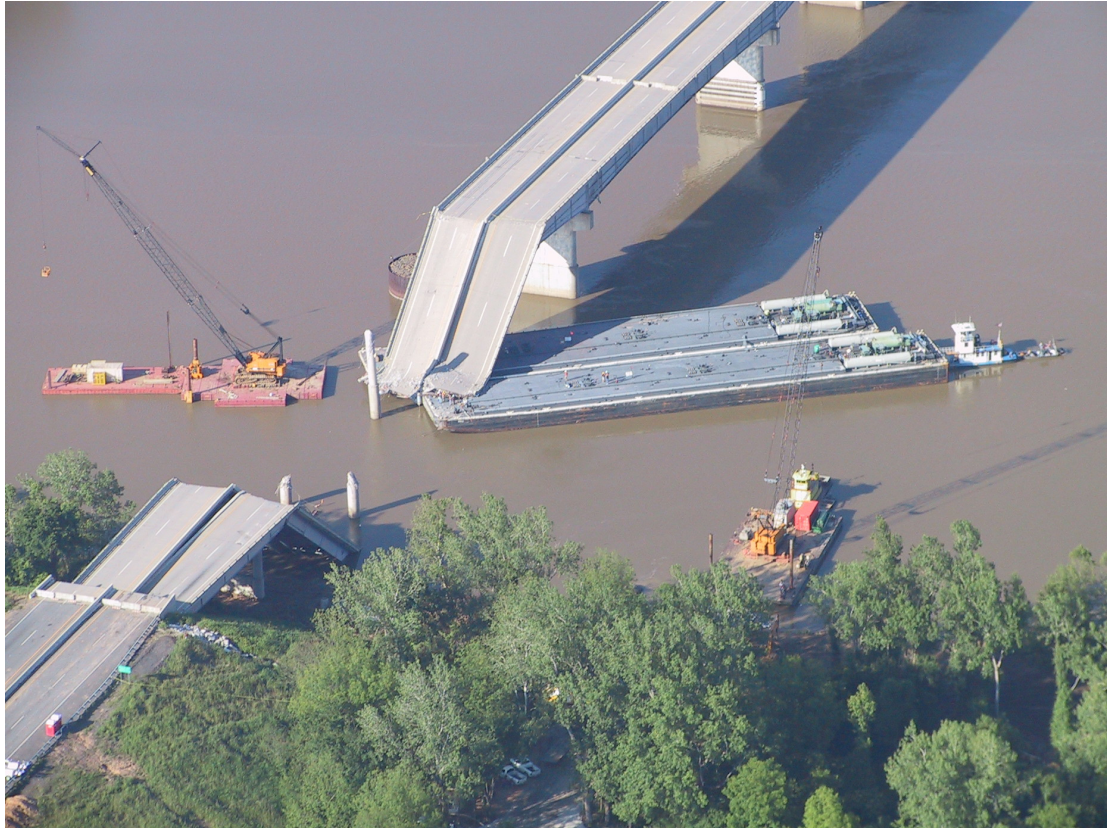


Fig. 2.8. Barge crashing into the river piers of I-40 Bridge in Oklahoma (NTSB, 2002)

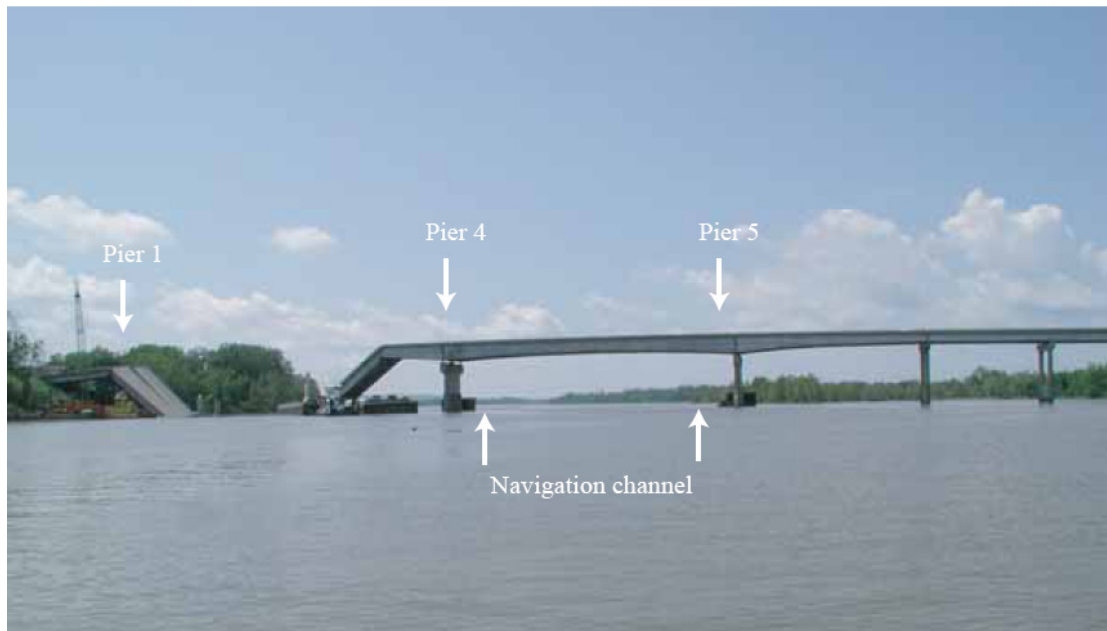


Fig. 2.9. Collapse of I-40 Bridge in Oklahoma due to vessel impact (NTSB, 2002)

2.2 Designing Bridges for Blast Hazards

Adopting an efficient security system is the most effective way to minimize the potential of terrorist attacks. The security system should be visible so that it can scare terrorists away. Many of these security measures are cost-effective such as security surveillance, cameras, preventing parking under the bridge, and proper lighting of the site (Williamson and Winget, 2005). Yet, it is almost impossible to totally eliminate terrorism and other blast hazards. Critical bridges and essential infrastructure elements need to be protected against extreme loads resulting from low probability / high consequence events such as terrorist attacks, blast hazards, and other high impact loads. These bridges have to be designed to mitigate the effect of blast loading due to probable attacks and hazards. Structural engineers should begin considering blast as a type of loading on critical structures. In addition, designing bridges to mitigate blast scenarios will enhance their performance against other extreme events. The devastating effect of blast loads on bridges is shown in Figs. 2.10 through 2.12.



Fig. 2.10. Collapse of bridge due to blast (courtesy AFP / Getty Images)

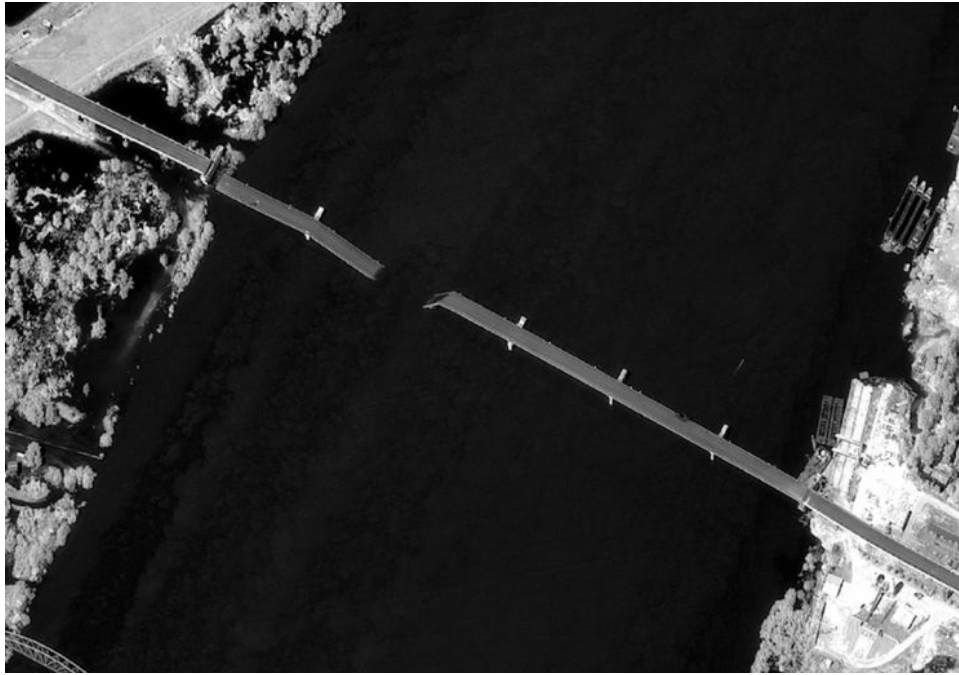


Fig. 2.11. Collapse of bridge span due to blast load (GlobalSecurity.org, 1999)

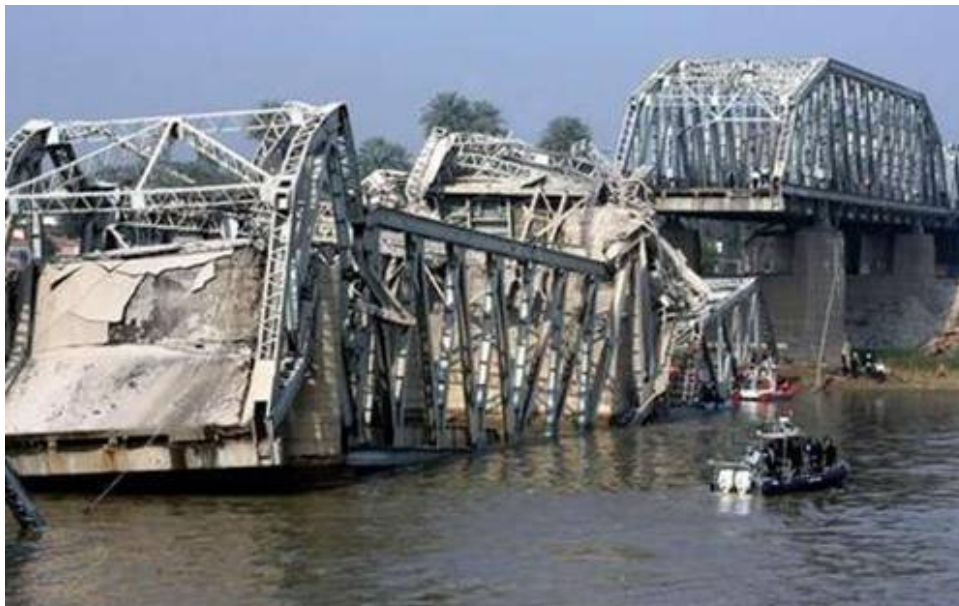


Fig. 2.12. Collapse of truss bridge due to blast (CNN, 2005)

Terrorist attacks are highly unpredictable events, and therefore it is impossible to predict the exact scenario that might take place. More than 50% of the terrorist attacks worldwide are in the form of explosives (FHWA, 2006). Designing bridges to resist all possible combinations of blast scenarios is unpractical and uneconomical. Military structures are usually designed to resist probable blast scenarios and to remain functional after the event. However, it is uneconomical to design bridges and other essential infrastructure components to remain intact after blast attacks.

The philosophy of designing structures against blast loading aims to minimize the damage as much as possible. First, it is important to categorize bridges in terms of their importance (Blue Ribbon Panel Report, 2003). Due to the limited financial resources, prioritization of bridges will ensure that more concern will be directed towards critical bridges. There are several factors that affect the prioritization process. These factors include the national significance of the bridge, availability of alternative routes, average daily traffic, bridge dimensions, criticality to emergency evacuation, and border crossing.

Secondly, a risk assessment should be made to identify the credible threats that can occur and to predict the accepted risk levels and design for the unacceptable levels of damage. A security risk assessment, however, is difficult to quantify. Security risk is a function of the nature of the threat or the attack, the probability of an attack, the probability the attack is successful, the effectiveness of the bridge security system against the attack, and the consequences associated with the bridge damage or collapse due to the attack.

Blast hazards and performance criteria for bridges can be based on a two-level design approach; Level I blast design is an operating level blast in which the bridge remains operational after light blast with minimal to moderate damage, and Level II blast design in which the bridge suffers significant damage but does not collapse under heavy blast loads. The choice of design levels for blast loads depends on many complex factors including detailed analytical investigation, experimental studies, bridge type, and the risk assessment and the consequences of an attack. Categorizing the blast scenario into light blast or heavy blast is a multifaceted challenging task. This categorization depends on the charge weight, the standoff distance, and the properties of the structural element subjected to the blast load. Consequently, the same blast scenario can be categorized differently depending on the geometry, strength, and material of the loaded element. If an 8 ft diameter column is subjected to a charge weight of 1000 lbs at a standoff distance of 15 ft, this scenario can be categorized as a light blast event. On the contrary, if a 3 ft diameter column is subjected to the same scenario, it might be treated as a heavy blast event.

Despite the small weight of hand emplaced explosive devices, they are considered as heavy blast events due to their devastating effect as a result of their almost zero standoff distances. Furthermore, blast scenarios involving heavy trucks are categorized as heavy blast events as trucks can carry up to 30,000 lbs of explosives. Further studies are required to quantify the blast design level for different structural elements.

However, in order to maintain a uniform level of bridge performance against blast hazards, a design level blast load needs to be established for each performance level. For a standardized design procedure, this design level blast load should be independent of the structural properties. The design level blast load should be a function of the charge weight and the standoff distance.

The Blue Ribbon Panel for Bridge Security Assessments (FHWA, 2003) provided estimated values for the minimum standoff distances and the desired standoff distances for typical highway bridges in the United States. These values are presented in tables 2.1 and 2.2, respectively. Yet, these values can only be considered for preliminary analysis as they do not seem to be based on scientific or experimental investigations. Further studies are required to verify these values and establish uniform performance levels and structure specific assessment. In addition, these values are dependant on the thickness of the bridge pier, and therefore need to be standardized to be independent of the geometry of the bridge.

Table 2.1. Minimum barrier standoffs from bridge piers (FHWA, 2003)

Minimum Barrier Standoffs from Bridge Piers (Measured in feet, from face of pier to front of barrier)					
Threat Type	Explosive Weight (lbs TNT)	Pier Thickness (ft)			
		~ 3'	~ 4'	~ 7'	> 8'
Sedan	1,000	8	8	8	8
Passenger Van	4,000	35	25	16	16
Box Truck	10,000	75	75	25	22
Moving Van/Water Truck	30,000	150	100	75	75

Table 2.2. Desired barrier standoffs from bridge piers (FHWA, 2003)

Desired Barrier Standoffs from Bridge Piers (Measured in feet, from face of pier to front of barrier)					
Threat Type	Explosive Weight (lbs TNT)	Pier Thickness (ft)			
		~ 3'	~ 4'	~ 7'	> 8'
Sedan	1,000	15	12	10	10
Passenger Van	4,000	50	35	25	25
Box Truck	10,000	100	100	45	35
Moving Van/Water Truck	30,000	200	150	100	100

2.3 Characteristics of the Blast Wave

To understand the behavior of bridges during a blast event, it is important to study the characteristics of the blast waves and pressures, and to account for the different factors that affect the behavior of bridge components subjected to blast loads.

2.3.1 Types of explosives

An explosion is a phenomenon in which energy is released in a very fast and violent manner and is accompanied by the release of gases and generation of high temperatures. There are different types of explosions; nuclear, physical, and chemical. Explosive volcanic eruptions are classified as natural explosions. Chemical explosives are the most common type of artificial explosives that can occur accidentally or can be caused by terrorist attacks. Chemical explosives are generally in the form of condensed solids or liquids. In a chemical explosion, a rapid oxidation reaction takes place producing pressure waves, also called blast waves (Mays and Smith, 1995).

Explosions are categorized as low explosives or high explosives. Low explosives tend to deflagrate, while high explosives tend to detonate. Deflagration is a subsonic (having a speed less than the speed of sound) combustion process in which the material burns rapidly, while detonation is a supersonic (having a speed more than the speed of sound) decomposition process in which the condensed material burns at a higher rate than that of the low explosives producing what is known as shock waves. Shock waves are transient waves that expand outward from the detonation source into the surrounding air. The duration of blast waves lasts only for few milliseconds.

The process of deflagration is easier to control than detonation. Gun powder is the most common type of low explosives. Fireworks are controlled low explosives. High explosives usually have less energy than many common materials, however, it is their rapid release of the energy that creates the blast pressure which causes the damaging

effect (Kiger and Woodson, 2006). Detonation velocities for high explosives range from 18,000 fps to 25,000 fps. Dynamite was the first high explosive used by engineers. Trinitrotoluene (TNT) is the most common type of high explosives. TNT is commonly used as the reference explosive, other explosives types are usually transformed to an equivalent weight of TNT. These transformation factors are presented in Table 2.3. When a high explosive is detonated, instantly created pressure waves travel away from the detonation source in the form of spherical waves. For a ground-level explosion, those pressure waves are hemispherical as shown in Fig. 2.13.

Table 2.3. TNT equivalents for different types of explosive (TM5-1300, 1990)

Explosive Types	Equivalent mass for pressure	Equivalent mass for impulse	Valid for pressure range (psi)
ANFO	0.82	0.82	1-100
C-4	1.37	1.19	10-100
HBX-1	1.17	1.16	5-20
HBX-3	1.14	0.97	5-25
H-6	1.38	1.15	5-100
Pentolite	1.42	1.00	5-100
TNT	1.00	1.00	All



Fig. 2.13. Hemispherical blast waves for ground-level explosion (courtesy Reuters)

2.3.2 Types of blast scenarios

The behavior of structures subjected to blast loads depends to a great extent on the size of the blast and its proximity to the structure. For large scale blast waves like those produced due to nuclear explosions, the blast wave is significantly huge compared to the size of the structure, and hence the whole structure tends to deform, and the global stiffness of the structure governs the behavior of the structure. A different scenario can take place in cases of explosions resulting from accidents or terrorist attacks. In these explosions, the blast wave is relatively small, and the local behavior of structure components dominates the behavior of the structure. Consequently, it is important to study the individual behavior of the structural components subjected to the blast wave. These components are loaded sequentially as the blast wave travels from the detonation source towards the structure.

2.3.3 *Positive and negative phases*

When a high explosive is detonated in open free air (free field), the induced pressure is divided into two main phases; the positive phase and the negative phase. The positive phase starting point is the time taken by the blast wave to travel from the detonation source to the element, which is known as the time of arrival (TOA). At this point, the pressure rises up instantaneously to the peak incident pressure (P_{so}), and then it starts to decay as the compressed air at the shock front cools down and the pressure falls slightly below the atmospheric pressure. This creates the negative phase (Mays and Smith, 1995). Finally, the pressure stabilizes to match the ambient pressure at the end of the negative phase.

During the positive phase, the elements exposed to the blast wave are subjected to compressive pressure, while during the negative phase they are subjected to suction. The amplitude of the negative phase is much lower than that of the positive phase, and usually the negative phase is neglected in design. Only for light structures, does the negative phase have a significant effect. A typical pressure-time history curve in free field is shown in Fig. 2.14. The positive phase is usually idealized to an equivalent triangular blast load having the same peak pressure and an idealized duration (t_d).

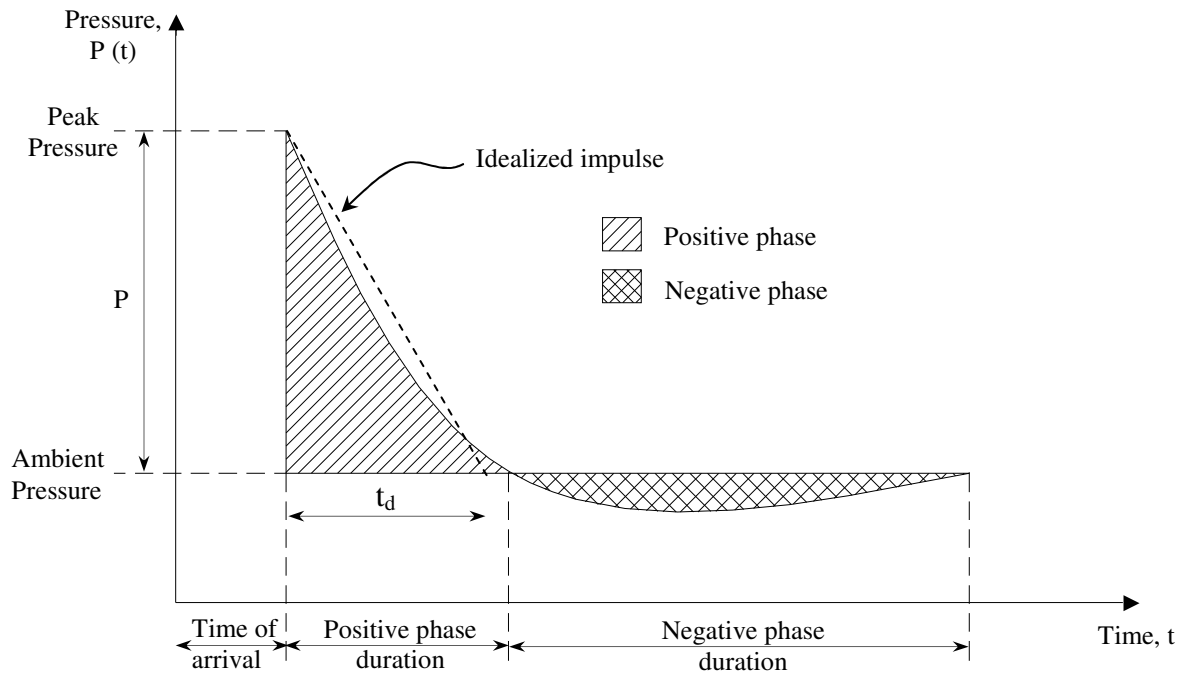


Fig. 2.14. Pressure-time history for free field blast (TM5-1300, 1990)

2.3.4 Incident and reflected pressures

When the incident pressure (P_{so}) waves created by the detonation encounter a solid surface, the pressure undergoes reflection. This reflection is mainly attributed to the compression of air molecules of the pressure wave when they decelerate suddenly and are brought to rest. At this incident, the structure is loaded by the reflected pressure (Mays and Smith, 1995). This reflected pressure (P_r) is of significant higher amplitude than the incident pressure. The value of the reflected pressure depends on the angle of incidence (α) between the detonation source and the point under consideration. It also depends on the value of the incident pressure. The incidence angle can be calculated using the diagram presented in Fig. 2.15. The value of the reflected pressure decreases with the increase in the value of the incidence angle, i.e. the reflected pressure reaches its

maximum value at a zero incidence angle. The effect of the angle of incidence on the magnitude of the reflected pressure is presented in Fig. 2.16. The coefficient of reflection (C_r) is defined as the ratio of the reflected pressure to the incident pressure. For distant explosions, the value of C_r is in the order of 2, while for close blast scenarios, C_r can be as high as 13.

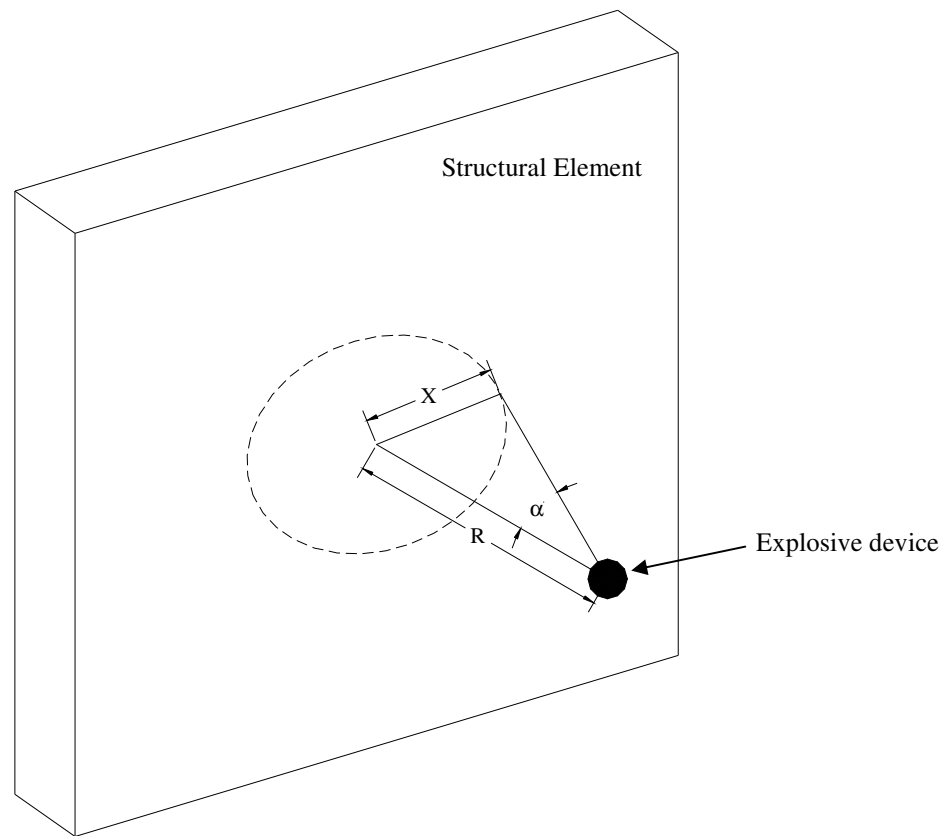


Fig. 2.15. Angle of incidence (TM5-1300, 1990)

Where:

R = perpendicular distance from the center of the explosive device to the loaded element

X = distance between the projection of the charge and the point of concern

α = angle of incidence at the point of concern

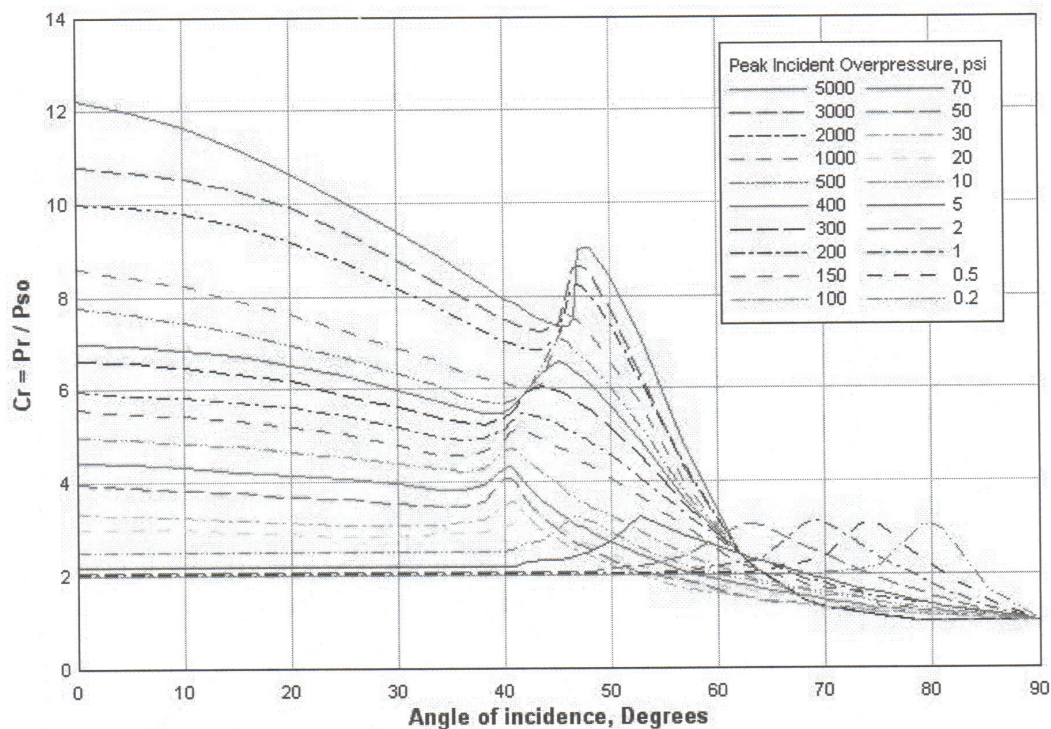


Fig. 2.16. Effect of angle of incidence on the coefficient of reflection (TM5-1300, 1990)

2.3.5 Cubic root scaling and blast wave parameters

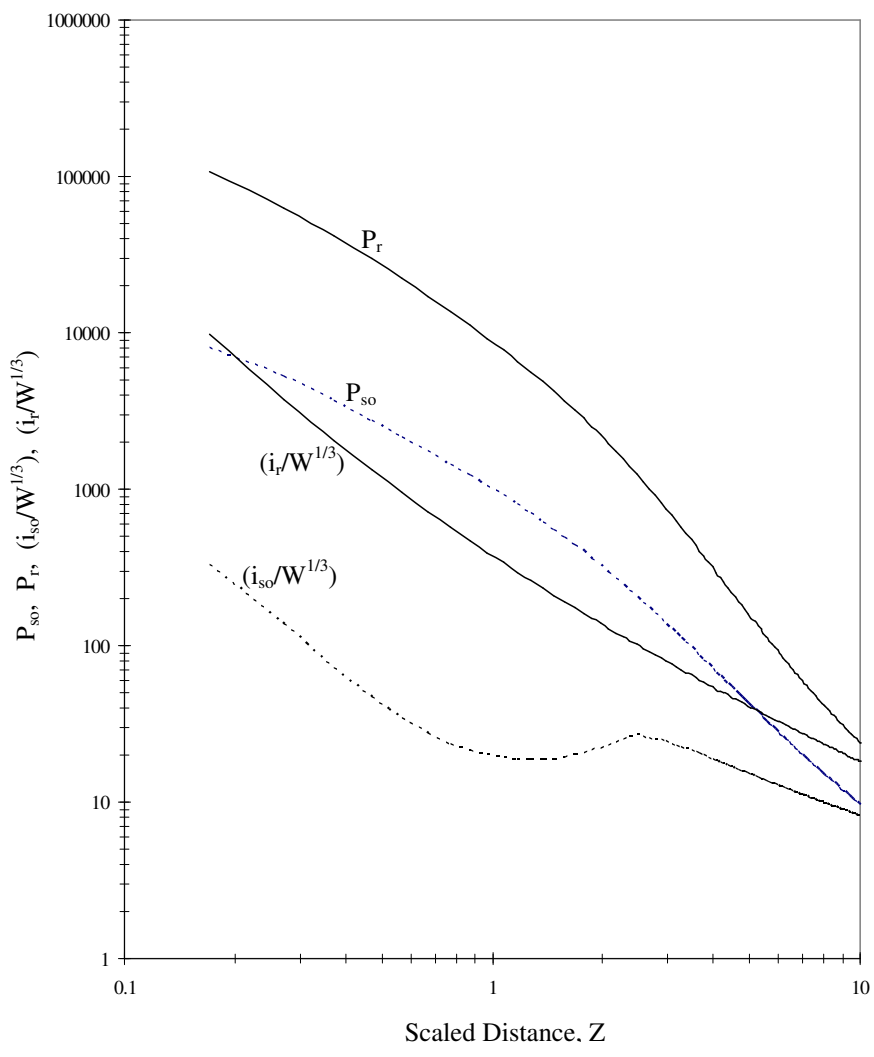
Blast wave parameters include: the incident pressure (P_{so}), reflected pressure (P_r), incident impulse (i_o), reflected impulse (i_r), time of arrival (TOA), positive phase duration, negative phase duration, idealized duration (t_d), and blast wave speed. The impulse is defined as the area under the pressure-time curve. The main two factors in determining the blast wave parameters are the distance from the blast source (range, R) and the charge weight (W). It was verified that the cubic root scaling model proposed by Hopkinson (1915) is representative of the blast wave parameters for different combinations of range and charge weight. Hopkinson stated that the same pressure, either incident or reflected, can be produced from different charge weights as long as the ratios of their ranges are proportional to the cubic root of their charge weights (Eq. 2.1).

$$\frac{R_1}{R_2} = \left(\frac{W_1}{W_2} \right)^{1/3} \quad (2.1)$$

The scaled distance (Z) is defined as the dimensionless ratio of the distance from the center of explosive (R) in feet divided by the cubic root of the charge weight (W) in lbs. This relation is presented in Eq. 2.2. Hopkinson's cubic-root scaling model was confirmed by Kennedy (1946). The intensity of the blast increases with the increase in the cubic root of the charge weight and the decrease in the standoff distance. However, the standoff distance is the dominant parameter in determining the intensity of the pressure. A slight increase in the standoff distance can significantly reduce the induced pressure.

$$Z = \frac{R}{W^{1/3}} \quad (2.2)$$

To illustrate Hopkinson's scaling numerically, assume a charge weight of 1000 lbs at distance 100 ft from a specific target. The pressure produced by this scenario is the same as that produced by a charge weight of 125 lbs at distance 50 ft, and is the same as that produced by a charge weight of 1 lb at distance 10 ft. However, for each of the above scenarios, the duration of the positive phase is different, and hence the impulse is different. The magnitude of the impulse increases with the increase in the charge weight. The United States Department of Defense provided charts relating the blast wave parameters to the scaled distance (TM5-1300, 1990). The blast wave parameters for a ground-level hemispherical wave is presented in Fig. 2.17. These parameters are numerically represented in A.T.-BLAST software developed by the Applied Research Associates (ARA), Inc.



P_{so} = peak positive incident pressure, psi.

P_r = peak positive reflected pressure, psi

$i_s / W^{1/3}$ = scaled unit positive incident impulse, psi-ms/lb^{1/3}

$i_r / W^{1/3}$ = scaled unit positive reflected impulse, psi-ms/lb^{1/3}

Fig. 2.17. Blast wave parameters for hemispherical TNT explosion (TM5-1300, 1990)

For incident pressure values up to 20 psi, Newmark (1956) proposed a simplified equation for computing the coefficient of reflection. This relation is presented in Eq. 2.3. However, for pressure values that exceed 20 psi, there is no available equation relating the coefficient of reflection (C_r) to the scaled distance (Z), such equation is essential to provide better understanding of the sensitivity of C_r to Z especially for small values of Z . Based on TM5-1300, the relation between C_r and Z is drawn in Fig. 2.18. It was observed that for $Z > 20$, C_r is in the range of 2, while for $Z < 20$, C_r varies inversely with Z . Hence, Eqs. 2.4 and 2.5 are proposed to relate C_r and Z .

$$C_r = (2 + 0.05P_{so}) \quad (\text{psi}) \quad (2.3)$$

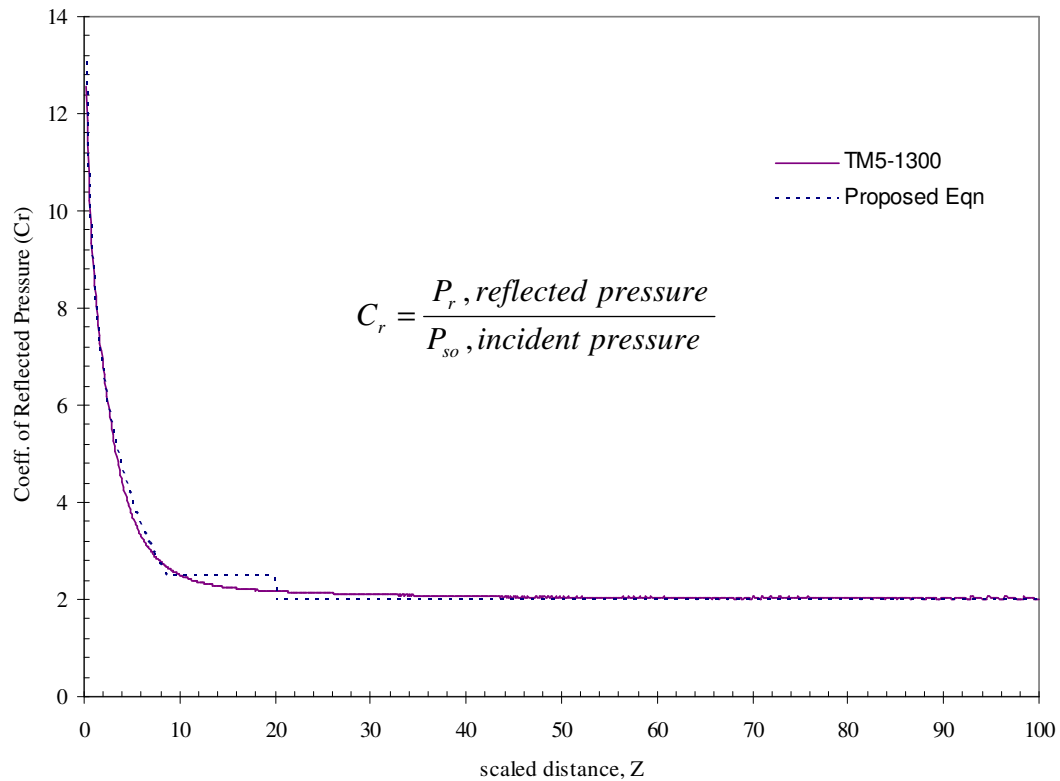


Fig. 2.18. Proposed equation for coefficient of reflected pressure

$$\text{For } Z > 20, \quad C_r = 2 \quad (2.4)$$

$$\text{For } Z < 20, \quad C_r = (-2.82 \ln Z + 8.56) \quad \text{not less than } 2.5 \quad (2.5)$$

2.3.6 Confined versus unconfined blasts

In the case of internal blast scenarios, where the blast occurs inside a confined or partially confined structure, the pressure wave encounter several re-reflections based on the geometry of the enclosing space. These re-reflections can significantly aggravate the situation. In addition, the confinement effect significantly increases the duration of the pressure creating a quasi-static effect. For bridges, this scenario is very unlikely to happen due to the open space around the bridge which allows the ventilation of the pressure. For this reason, the duration of blast loading acting on the components of a bridge is very short, and it is convenient to design these components for impulsive loading. For blast loads inside box girder bridges, where multiple reflections are expected, re-reflection of blast wave needs to be considered.

2.3.7 Vapor cloud explosions

Vapor Cloud Explosion (VCE) is an accidental type of explosions that takes place due to the release of a flammable material such as liquefied gases under high pressure. If the released flammable vapor is subjected to ignition, explosion takes place producing overpressure shock waves similar to those produced by high explosives. This scenario can take place due to the crash of gasoline tankers into bridge components. The severity of the VCE depends on the properties of the flammable material, rate of release, quantity of the material, temperature, and pressure (Sundararajan, 2007). The VCE can be transformed into an equivalent TNT weight using Eq. 2.6

$$W_{TNT} = W_C (H_C / H_{TNT}) Y \quad (2.6)$$

Where:

W_{TNT} = equivalent TNT weight

W_C = weight of chemical

H_C = heat of combustion of chemical

H_{TNT} = heat of detonation of TNT = 1155 kcal/kg

Y = fraction of the mass of chemical that contributes to the explosion (The Environmental Protection Agency [EPA] recommends Y of 0.1)

2.4 Factors affecting the Behavior of Bridges during Blast loading

The factors affecting the behavior of a structure during blast scenarios can be categorized as external factors and internal factors. The external factors are those that depend on the blast scenario. They include the explosive material, standoff distance, charge weight, and the angle of incidence, while internal factors are those factors dependant on the properties of the structural element subjected to the blast load such as stiffness, mass, ductility, redundancy and continuity of the whole structure. As for the external factors, there is limited control over the charge weight that might be used in the scenario. It depends on the type of car or truck used. A small car can carry about 500 lbs of TNT, while a mid size truck can carry up to 10,000 lbs of explosives. It is crucial to direct more security measures towards vans and trucks as the amount of charge carried by them can be devastating. The standoff distance is the most critical parameter in blast scenarios. Just by increasing the standoff distance by a few feet, the pressure drops significantly. Therefore, it is essential to provide minimum standoff distance for critical bridges that are potential targets for terrorist attacks or are exposed for accidental chemical explosions. A charge

weight of 1000 lbs TNT can produce a reflected pressure of 85,000 psi at 2 ft standoff distance; this pressure drops to 2,000 psi at 20 ft, which is almost 2% of the pressure induced at 2 ft. The variation of the reflected pressure with the standoff distance is shown in Fig. 2.19.

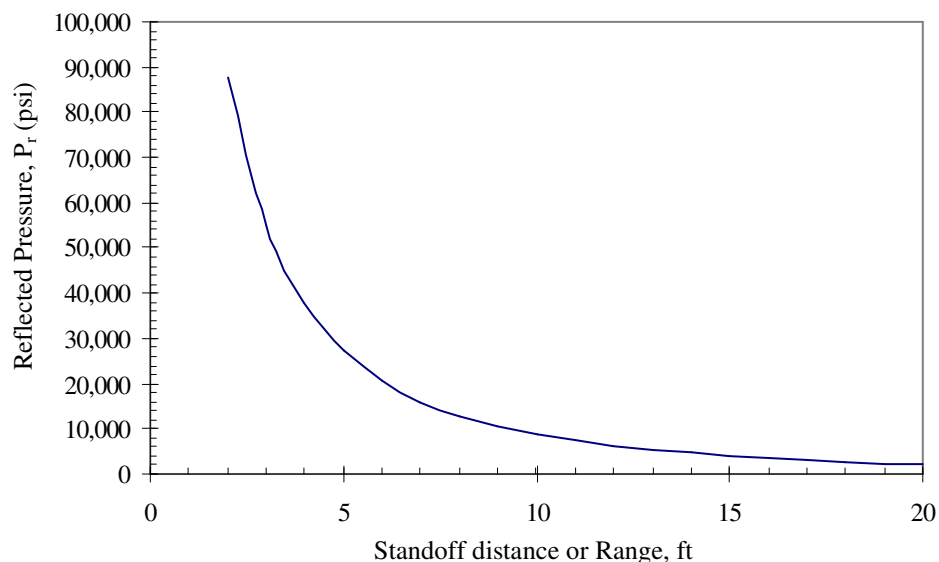


Fig. 2.19. Effect of standoff distance on pressure amplitude (A.T.-BLAST)

The behavior of structural elements depends to a great extent on their properties. The most important factors are the period of vibration and ductility of the element. Massive structures respond better than lightweight structures. Structural elements with high ductility will provide better resistance to blast loads. Also, the continuity and redundancy of the whole structure have great impact on the behavior of the structure. The structure should be designed for element removal scenarios that might occur during blast. Redundant and continuous structures exhibit localized damage rather than global collapse.

Blast loads are non-simultaneous and non-uniform. They vary along the length of the loaded member due to the variation in the range and the incident angle. For distant blast loads, the blast pressure can be approximated as uniform load. However, for small ranges, this approximation will significantly overestimate the applied blast loads.

2.5 Comparison of Blast Hazards and Earthquakes Hazards

One of the recommendations of the FHWA report “Multiyear Plan for Bridge and Tunnel Security Research, Development, and Deployment”, which was published in 2006, was to investigate the transferability of seismic design approach to blast resistant structures. Hence, it is important to understand the similarities and differences between blast loads and seismic loads. Both earthquakes and blast hazards are low risk, unpredictable, and devastating events. Earthquakes can not be predicted, prevented, or even controlled. However, blast can be controlled by adopting effective security system such as inspecting trucks and enforcing minimum standoff distances.

The major difference between earthquakes and blast loads is the loading duration. Earthquakes usually last for several seconds to a few minutes, while the duration of blast loading is significantly small. Blast loads last for only a few milliseconds depending on the charge weight and standoff distance. In addition, for blast loading, damping can be neglected due to the short loading time. The performance of a structure during an earthquake depends mainly on its global behavior, especially its overall period of the vibration. However, for blast loading, localized behavior of individual elements is expected. Regarding the method of analysis, elements subjected to blast loading can be

idealized as an equivalent single degree of freedom (SDOF) system. However, different mode shapes should be considered for seismic design. Finally, heavier structures are subjected to higher base shear during earthquakes, while massive structures have better response than lightweight structures during blast loading. This is mainly attributed to the fact that massive structures are less rigid than light weight structure. Consequently, the period of vibration of a massive structure is relatively high, and hence, it is subjected to a lower dynamic load factor as illustrated in section 2.9 and in Fig. 2.20. A comparison between seismic hazards versus blast hazards is presented in Table 2.4.

Table 2.4. Comparing seismic hazards and blast hazards

Criterion	Seismic hazards	Blast hazards
Low risk	Yes	Yes
Prediction	Unpredictable	Unpredictable
Severe damage	Yes	Yes
Can be controlled	No	Partially
Loading duration	Several seconds	Few milliseconds
Damping	Considered	Neglected
Structural behavior	Global	Localized
Mass effect	Negative	Positive

2.6 Dynamic Properties of Materials

During blast scenarios, materials are rapidly loaded by higher strain rates. Thus, plastic deformations are much less than those in the case of static loading at normal strain rates. It was found that the mechanical properties of materials during blast loading are increased. The ratio between the material property under rapid dynamic load and the

same property under static loading is defined as the dynamic increase factor (DIF). The DIF for concrete and reinforcing steel bars are presented in Table 2.5.

Table 2.5. Dynamic Increase Factor for design of reinforced Concrete (TM5-1300, 1990)

Type of stress	Far Design Range			Close-in Design Range		
	Reinforcing Bars		Concrete	Reinforcing Bars		Concrete
	f_{dy} / f_y	f_{du} / f_u	f'_{dc} / f'_c	f_{dy} / f_y	f_{du} / f_u	f'_{dc} / f'_c
Bending	1.17	1.05	1.19	1.23	1.05	1.25
Diagonal Tension	1.00	NA	1.00	1.10	1.00	1.00
Direct Shear	1.10	1.00	1.10	1.10	1.00	1.10
Bond	1.17	1.05	1.00	1.23	1.05	1.00
Compression	1.10	NA	1.12	1.13	NA	1.16

Where:

f_y = static yield strength of steel

f_{dy} = dynamic yield strength of steel

f_u = static ultimate strength of steel

f_{du} = dynamic ultimate strength of steel

f'_c = static ultimate strength of concrete

f'_{dc} = dynamic ultimate strength of concrete

2.7 Strength Increase Factor

Unlike the Dynamic Increase Factor (DIF), the Strength Increase Factor (SIF) depends mainly on the static properties of material and is independent on the rate of loading. The mechanical properties of materials specified in codes and specifications are usually the minimum values that are obtained from the standard tests. However, the average values for the material properties are higher than those values provided by the specifications. The average yield strength of steel is approximately 25% higher than the specified minimum values (ASCE, 1997). Blast hazards are considered low probability events, and hence, it is recommended to include this SIF in the design or analysis of the structural members that are subjected to this extreme load. Some of the SIF recommended by TM5-

1300 are provided in Table 2.6. The modified dynamic yield strength of steel after accounting for both the SIF and the DIF is presented in Eq. 2.7.

$$f_{dy}^* = (SIF)(DIF)f_y \quad (2.7)$$

The SIF used for concrete 1.0. This is a conservative approach due to the brittle nature of concrete. However, for the analysis of existing structures, the in-situ strength of concrete can be used in lieu of the minimum compressive strength of concrete which is measured at 28 days and does not account for the age of concrete.

Table 2.6. Strength Increase Factor (TM5-1300, 1990)

Material	SIF
Structural Steel ($f_y < 50$ ksi)	1.1
Reinforcing Steel ($f_y < 60$ ksi)	1.1
Cold-Formed Steel	1.21
Concrete	1.0

2.8 Impulsive Load Design

The design of structural elements subjected to blast loads depends mainly on the duration of blast. For confined or partially confined blast scenarios, the blast duration is long and the design is based on the quasi-static load, while for free-field unconfined blast scenarios, the blast duration is much shorter than the period of the structural element subjected to the blast load. Hence, the blast pressure will finish acting on the element before the element responds with its full deformation and most of the deformation will occur after the pressure is cleared. Consequently, the maximum response of the system occurs during its free vibration phase. In this investigation, it is assumed that the designed

bridge is located in an unconfined field, and hence the bridge design for blast will be based on the impulsive load.

2.9 Equivalent SDOF Analysis

A bridge component subjected to blast load can be idealized as an equivalent single degree of freedom system (SDOF). The equivalent mass of the SDOF system is equal to the actual mass multiplied by a load-mass coefficient (K_{LM}). This coefficient is used to equate the work done by the actual system and that of the equivalent SDOF system. Values of K_{LM} for different support conditions and loading types are tabulated in TM5-1300 (1990). The dynamic blast load acting on the structure can be idealized as an equivalent static load equal to the dynamic load amplitude multiplied by a dynamic load factor (DLF). The dynamic load factor is based on the ratio of the blast load duration (t_d) to the period of vibration of the structural element (T). Since this ratio is relatively small for the unconfined blast scenarios on bridges, DLF is a reduction factor for typical designs of bridge structures. However, for internal blasts inside buildings, the multiple reflections of the blast waves create a quasi-static loading effect. Thus, the DLF can be relatively higher than that used for bridges. The variation of DLF with t_d/T is shown in Fig. 2.20.

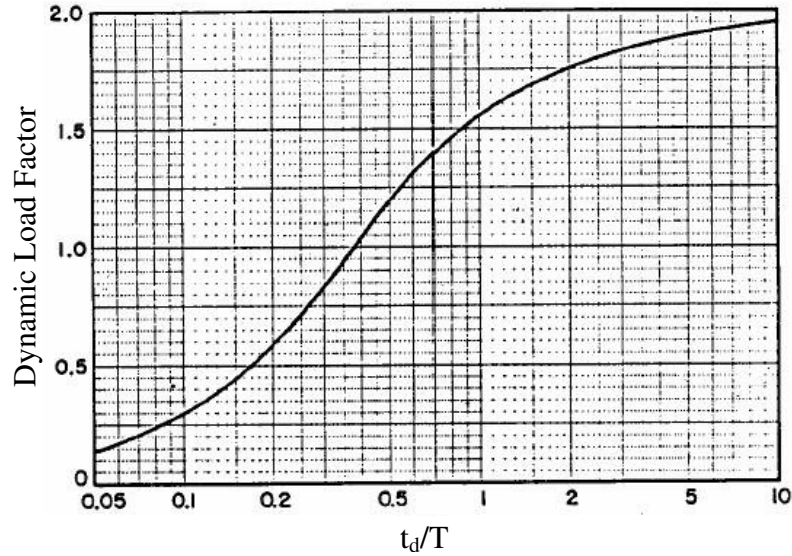


Fig. 2.20. Dynamic Load Factor for triangular load (TM5-1300, 1990)

2.10 Plastic Design of Structural Members Loaded with Impulsive Loads

Elastic design of structural elements against blast is uneconomical. Therefore, it is common to design those members do develop plastic deformations. Ductility of a structural member is defined as the ratio between the maximum deformation (X_M) to the deformation at the yield limit (X_Y). For impulsive load, if the kinetic energy is “KE”, impulse is “ i ”, mass is “ m ”, and the velocity is “ v ”, then

$$i = mv \quad (2.8)$$

$$v = \frac{i}{m} \quad (2.9)$$

$$KE = \frac{mv^2}{2} \quad (2.10)$$

$$KE = \frac{i^2}{2m} \quad (2.11)$$

The strain energy absorbed by the structure is shown in Fig. 2.21 and is expressed by:

$$W_e = R_u(X_M - 0.5X_Y) \quad (2.12)$$

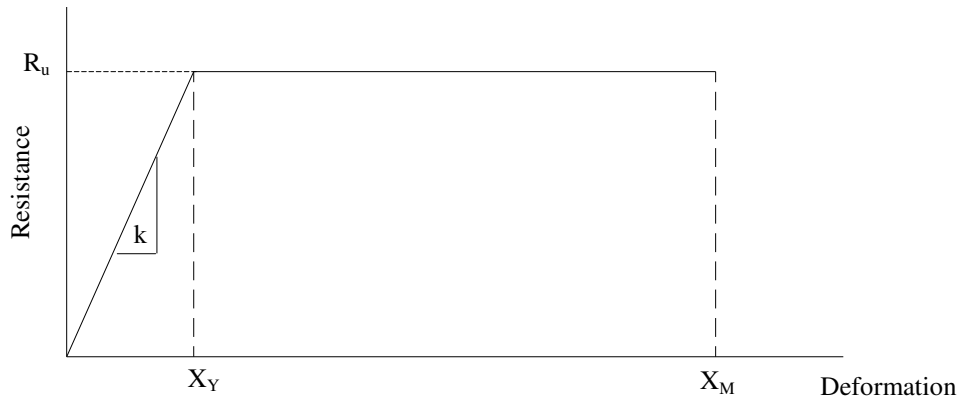


Fig. 2.21. Typical resistance curve of elastic-perfectly plastic system

$$\mu = \frac{X_M}{X_Y} \quad (2.13)$$

$$W_e = R_u X_Y (\mu - 0.5) \quad (2.14)$$

W_e = strain energy, R_u = ultimate resistance of the element, X_M = maximum deformation, X_Y = yield deformation, and μ = ductility.

The stiffness (k) and natural circular frequency of the structure (ω) are describes as:

$$k = \frac{R_u}{X_Y} \quad (2.15)$$

$$\omega = \sqrt{\frac{k}{m}} \quad (2.16)$$

Equating the kinetic energy and the strain energy, we obtain:

$$\frac{i^2}{2m} = \frac{R_u^2}{m\omega^2} \left(\mu - \frac{1}{2}\right) \quad (2.17)$$

$$i^2 = \frac{R_u^2}{\omega^2} (2\mu - 1) \quad (2.18)$$

$$R_u = \frac{i\omega}{\sqrt{2\mu - 1}} \quad (2.19)$$

The previous equations are based on the analysis provided by Mays and Smith (1995) and Kiger and Woodson (2006). To relate the structural resistance to the pressure and the dynamic load factor (DLF), the following equations are proposed.

$$i\omega = (0.5 P_r t_d) \left(\frac{2\pi}{T} \right) = (P_r) \left(\frac{\pi}{T} t_d \right) \quad (2.20)$$

Equation (19) can be expressed as follows:

$$R_u = \frac{(P_r)}{\sqrt{2\mu - 1}} \left(\frac{\pi}{T} t_d \right) \quad (2.21)$$

In the above equation, $\left(\frac{\pi}{T} t_d \right)$ is an approximation to the DLF. For values of $\left(\frac{t_d}{T} \right)$ less than 0.5, this approximation provides reasonable values close to the exact response (Chopra, 1995). However, for more accurate results, the exact DLF should be calculated from the dynamic analysis by using the dynamic load factor (Eq. 2.22):

$$R_u = \frac{(P_r)}{\sqrt{2\mu - 1}} (DLF) \quad (2.22)$$

It is clear from equation (2.22) that the required resistance of the structural element to resist impulsive load decreases with the increase in the ductility, and hence it is more economical to increase the member ductility. The recommended ductility values for

concrete structures subjected to blast loads ranges from 10 to 15, which correspond to rotation angles 2° (0.035 rad) and 4° (0.07 rad), respectively (TM5-1300, 1990).

2.11 Pressure-Impulse (P-I) Diagrams

Pressure-Impulse diagrams, also known as damage assessment diagrams, are often used to evaluate the behavior of a specific SDOF structural element when subjected to blast loads. This graphical solution was first introduced by Baker (1973). P-I diagrams can be used to predict the damage level in a specific structural member due to the pressure and impulse values produced by a certain blast scenario. In P-I diagrams, the behavior of the structural member is classified into 3 main regions, Quasi-Static (Q-S) loading, Impulse loading, and Dynamic loading, which are designated as region I, region II, and region III, respectively as shown in Fig. 2.22.

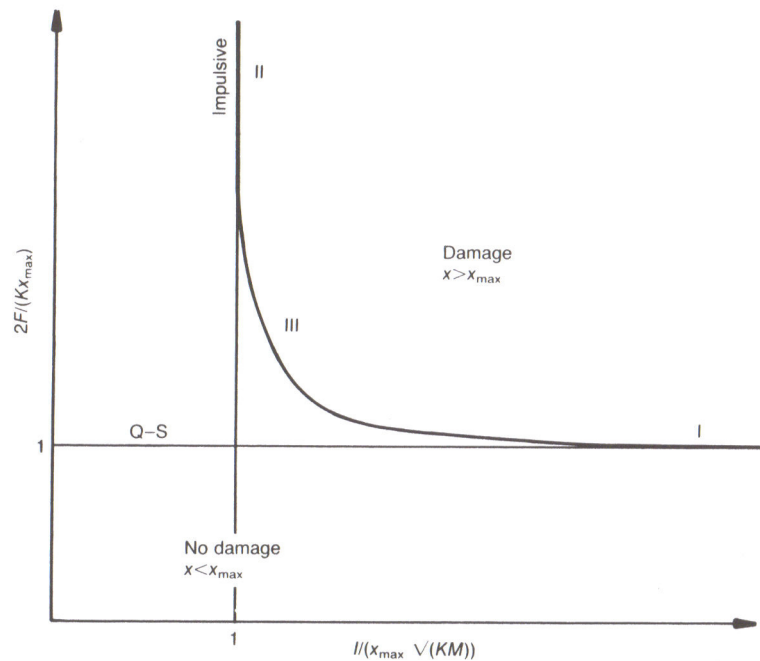


Fig. 2.22. Typical normalized P-I diagram for a SDOF system (Mays and Smith, 1995)

If the ratio between the blast duration to the period of vibration of the structure is relatively high ($t_d/T \gg 1$), the structure will reach its maximum deformation while the blast load is still in action, and the behavior of the structural element will be dominated by the pressure created by the blast and the effect of the impulse is insignificant (Mays and Smith, 1995). This phase is similar to the behavior of structures under constant load and is defined as the quasi-static loading phase. The dynamic displacement of the quasi-static phase is a function of the peak blast load and the stiffness of the structure and its maximum value is equal to twice the value of the static displacement.

On the other hand, if the ratio between the blast duration to the period of vibration of the structure is relatively small ($t_d/T \ll 1$), the structure will reach its maximum deformation in the free vibration phase after the blast load has cleared. Hence, the behavior of the structural element will be dominated by the Impulse created by the blast and the effect of the pressure is insignificant. Using the principle of conservation of energy, the maximum dynamic displacement can be approximated as $(\pi t_d)/T$. The quasi-static load and the impulsive load are illustrated in Figs 2.23 and 2.24, respectively.

The transition region between region I and region II is known as the dynamic loading (region III). In this case, the ratio between the blast duration to the period of vibration of the structure is close to one ($t_d \sim T$). The analysis of the structural response under dynamic loading is cumbersome as it requires solving the dynamic equation of motion of the structure. The boundaries of these three regions are expressed in Eqs. 2.23 through 2.25 (Mays and Smith, 1995).

$$\frac{t_d}{T} > \frac{20}{\pi} \quad \text{Quasi-static Loading (Region I)} \quad (2.23)$$

$$\frac{t_d}{T} < \frac{1}{5\pi} \quad \text{Impulsive Loading (Region II)} \quad (2.24)$$

$$\frac{1}{5\pi} > \frac{t_d}{T} > \frac{20}{\pi} \quad \text{Dynamic Loading (Region III)} \quad (2.25)$$

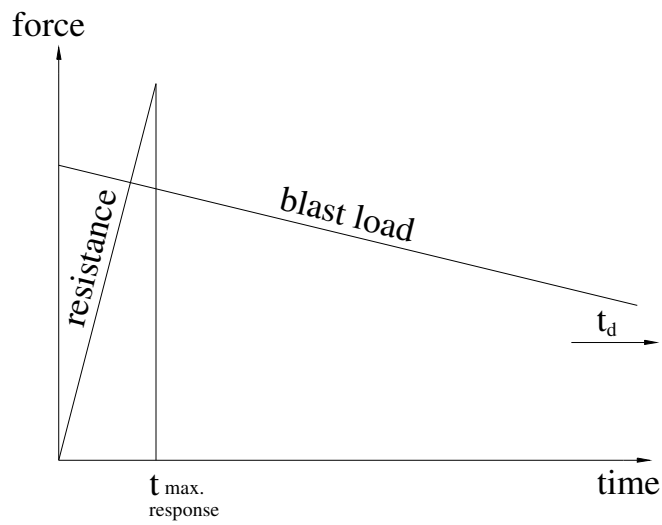


Fig. 2.23. Quasi-static loading

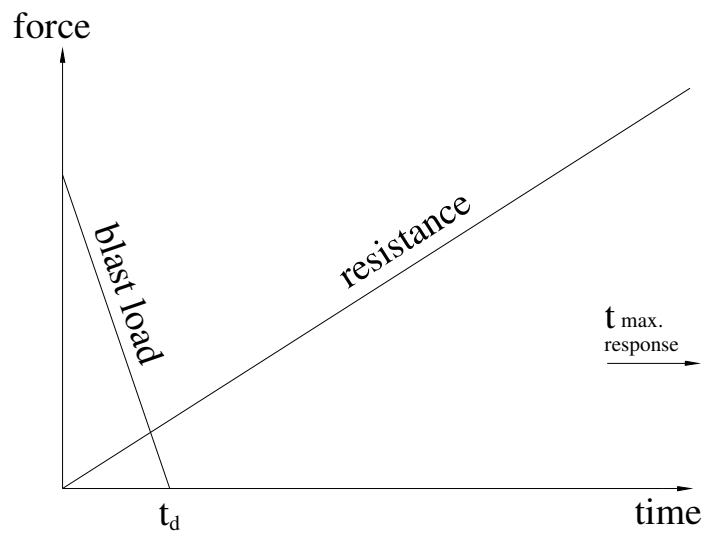


Fig. 2.24. Impulsive loading

The P-I diagram shown in Fig. 2.22 is expressed in terms of the normalized (non dimensional) pressure and impulse values. For quasi-static loading, the ratio between the maximum dynamic displacement (X_{\max}) and the static displacement (X_{st}) can be expressed as:

$$\frac{X_{\max}}{X_{st}} = \frac{X_{\max}}{F/K} = 2 \quad (2.26)$$

Hence, the normalized pressure can be expressed as:

$$\frac{2F}{K X_{\max}} = 1 \quad (2.27)$$

Where, (F) is the peak blast load, and (K) is the stiffness of the structure.

Similarly, for impulsive loading, the ratio between the maximum dynamic displacement (X_{\max}) and the static displacement (X_{st}) can be expressed as:

$$\frac{X_{\max}}{F/K} = \frac{\pi t_d}{T} = \frac{\omega t_d}{2} \quad (2.28)$$

The natural frequency of vibration (ω) can be expressed as:

$$\omega = \sqrt{\frac{K}{M}} \quad (2.29)$$

The Impulse (I) can be expressed as:

$$I = \frac{F t_d}{2} \quad (2.30)$$

Hence, the normalized Impulse can be expressed as:

$$\frac{I}{X_{\max} \sqrt{KM}} = 1 \quad (2.31)$$

P-I diagrams are generated for specific structural elements, material properties, and failure mechanism. The element type can be beams, one way slabs, two way slabs, columns, or walls. Material type can be reinforced concrete, steel, masonry, or others. For each P-I diagram, a specific failure mechanism is assumed such as flexural failure, diagonal tension, or shear. For a specific blast scenario, if the combination of pressure and impulse falls below or to the left of the curve, the structure will exhibit no damage, whereas, if it falls above or to the right of the curve, the structure will be damaged (Fig. 2.22). P-I diagrams can also be expressed in terms of the pressure and impulse values in specific dimensions as shown in Fig. 2.25

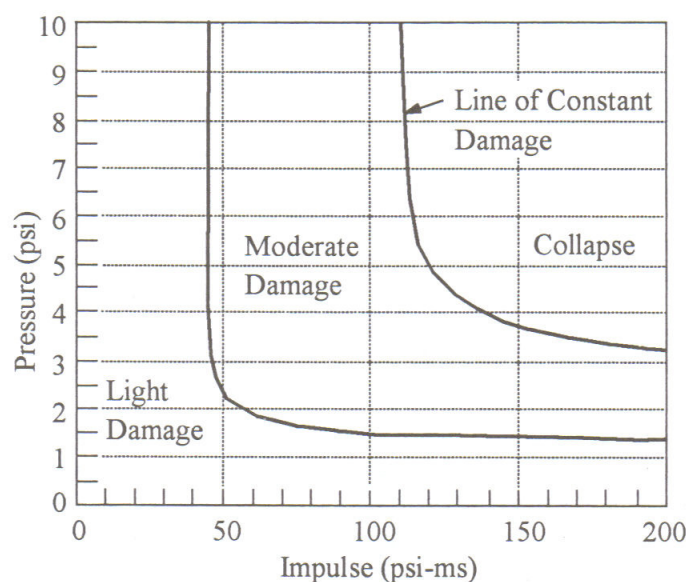


Fig. 2.25. P-I diagram expressed in specific units (ASCE, 1997)

Facility and Component Explosive Damage Assessment Program (FACEDAP) is a computer program developed by Oswald and Skerhut (1993) to perform P-I damage assessment for individual structural components as well as entire conventional buildings subjected to external blast attacks. Four damage levels 0%, 30%, 60%, and 100% are

incorporated in the diagrams. These damage levels correspond to high levels of protection, medium level of protection, low level of protection, and collapse, respectively. These damage levels were recommended by the U.S. Corps of Engineers and they correspond to specific ductility limit and support rotation induced in the structure. Some of these values are presented in Table 2.7. The percentage of damage in the entire structure can be determined based on weighted calculation of the damage level induced in each member.

Table 2.7. Performance criteria for typical structural components (TM5-1300, 1990)

Component Type	Light damage		Moderate damage		Severe damage	
	μ^*	θ^{**}	μ	θ	μ	θ
RC Beam	1	1	5	2	20	4
Steel Beam	3	2	10	6	20	12
One-Way Masonry Wall	0.25	0.5	0.5	0.75	1.0	1

* μ = ductility limit

** θ = support rotation in degrees

FACEDAP P-I diagrams are generated for a range of scaled standoff distance (Z) ranging between 3 and 100, and thus they can not be used for blast hazards at close proximity. Furthermore, they are developed for a specific failure mechanism and do not take into account the combination of various failure mechanisms. Since these P-I diagrams are generated based on various assumptions and approximations, they have limited accuracy and reliability and should not be used when high accuracy is required (Oswald and Skerhut, 1993). For more accurate results, theoretical P-I diagrams can be validated based on experimental data obtained from blast testing of structural members.

In brief, P-I diagrams can be used as a preliminary tool to determine the damage level in structural components. However, they should not be used if high accuracy level is required. Some of the shortcomings of P-I diagrams include the uncertainties in the assumed level of damage, and the effect of combined failure mechanisms. Furthermore, P-I diagrams are generated in terms of the pressure and the impulse values generated by the blast and they can not be used to determine the minimum standoff distance that should be provided to the structural components in order to resist a specific charge weight. It will be more convenient to develop blast response spectra in terms of the charge weights and the standoff distance rather than the pressure and impulse values.

2.12 Synopsis

- The pressure induced due to the detonation of an explosive device is divided into two main phases; positive phase and negative phase. During the positive phase, the structure is subjected to compressive pressure, whereas it is subjected to suction during the negative phase. The amplitude of the negative phase is insignificant when compared to that of the positive phase, and hence, only the positive phase is considered in the design.
- The free field pressure waves produced by a detonation are defined as the incident pressure waves. When these incident pressure waves encounter a solid surface, they undergo reflection and the structure is loaded by the reflected pressure. The amplitude of the reflected pressure is significantly higher than that of the incident pressure waves, and therefore it is important to account for the effect of the reflected pressure waves on the design of structural members subjected to blast hazards.

- The factors affecting the behavior of a structure during blast scenarios can be categorized as external factors and internal factors. External factors depend on the blast scenario. This includes the explosive material, standoff distance, charge weight, and the angle of incidence, while internal factors are dependant on the properties of the structural element subjected to the blast load such as its stiffness, mass, ductility, redundancy and continuity of the whole structure.
- The blast wave parameters such as the amplitude of the incident and reflected pressure, impulse, and blast duration depend mainly on the weight of the explosive charge and the standoff distance between the explosive device and the structural element. The intensity of the pressure is directly proportional to the cubic root of the charge weight, whereas it is inversely proportional to the standoff distance. However, the standoff distance is the dominant parameter in determining the intensity of the pressure. The same pressure can be produced from different blast scenarios as long as the ratio between their standoff distances is proportional to the cubic root of their charge weights.
- The effect of blast waves on bridges is classified as a free-field unconfined blast scenario. The open space around the bridge allows for the ventilation of the pressure waves and hence, the duration of the blast load acting on the bridge components is relatively short when compared with the period of the structure. Consequently, the maximum structural response occurs during the free vibration phase and the bridge components can be designed for impulsive loading.
- Blast loads are non-simultaneous and non-uniform. They vary along the length of the loaded member due to the variation in the range and the standoff distance. For distant

blast loads, the blast pressure can be approximated as uniform load. However, for small ranges, this approximation significantly overestimates the applied blast loads. The blast pressure distribution along the length of the loaded member can be approximated as a triangular pressure with its maximum value occurring at the point of the shortest perpendicular distance from the detonation source. This peak pressure decreases linearly by a slope of 1:2, and thus the pressure drops to zero with a horizontal distance that is equal to twice the value of the standoff distance.

- Pressure-Impulse (P-I) diagrams can be used as a primary tool to determine the damage level induced in a specific structural member due to the pressure and impulse values produced by the blast scenario. P-I diagrams lack accuracy due to the uncertainties in the assumed failure mechanism and level of damage. It will be more convenient to develop blast response spectra in terms of the charge weights and the standoff distance rather than the pressure and impulse values.

CHAPTER 3

RESPONSE SPECTRA FOR BLAST LOADS

The behavior of bridges subjected to blast loads depends mainly on the standoff distance and the charge weight used in the blast scenario. It is hard to predict the charge weight that might be used in an attack. The charge weight can vary from few pounds to thousands of pounds depending on the size of used vehicles. It is important to prevent blast scenarios involving large trucks. More security measures should be directed to these types of trucks. A typical small car can carry about 500 lbs. This can increase to 1000 lbs for vans. Hence, this analysis will be based on the previous two values of charge weights. There are also uncertainties associated with the explosive material used in the attack. The explosive materials used by terrorists are usually not sophisticated and are not expected to have TNT equivalence more than one. Therefore, TNT will be used as the default explosive material.

3.1 Variation of Blast Pressure along the Length of Loaded Members

The distribution of blast pressure along the length of the loaded member has significant effect on the behavior of that member. For large values of standoff distance, the pressure can be assumed to be uniform along the length of the member, while for small values of standoff distance, this approximation can significantly overestimate the pressure. When a structural member is subjected to a blast, the peak pressure occurs at the point having the shortest perpendicular distance from the blast source. This point has the minimum range. Furthermore, the value of the angle of incidence at this point is zero, and hence, the reflected pressure is maximized. However, the peak pressure decreases as we move away from this point of maximum pressure. This decrease in the pressure is due to the increase in the range (R) as well as the increase in the angle of incidence as shown (α) in Fig. 3.1. For very small values of standoff distances, this decrease is very steep. If the length of the member is relatively bigger than the standoff distance, the angle of incidence at the tips of the member becomes significantly large, and the pressure approaches the incident pressure.

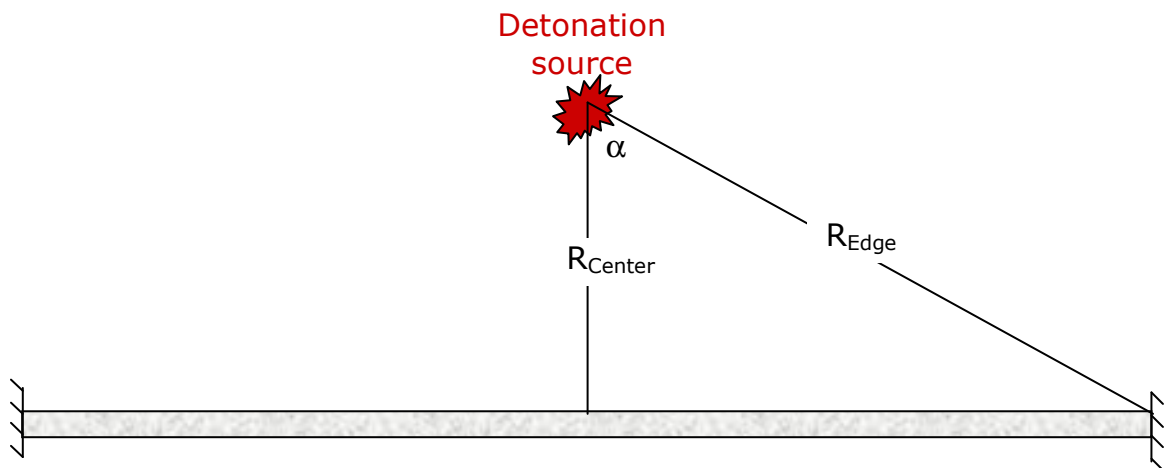


Fig. 3.1. Variation of range and angle of incidence along the length of the loaded member

It is important to develop a simplified procedure to represent the pressure distribution for different blast scenarios. The variation of blast pressure along the length of the loaded member was plotted for different values of standoff distance as shown in Fig. 3.2. This figure was developed using the AT-Blast software which is a numerical representation of the blast wave parameter charts of the United States Department of Defense (TM5-1300, 1990).

To compare, the distribution of pressure for different standoff distances, the pressure is presented in percentile values. The peak pressure in each case is considered to be the 100 percentile. It was observed that for a 50 ft standoff distance, the pressure drops to 83% of the peak value along a distance of 15 ft. The drop in pressure increases with the decrease in the standoff distance. For a 5 ft standoff distance, the pressure drops to less than 50% of the peak pressure along a distance of 5 ft, while for a standoff distance equal to 2 ft, the pressure drops to 50% with only a 2 ft distance along the length of the member. Based on the presented curve, the pressure distribution can be approximated by a triangular pressure that decreases linearly by a slope of 1:2 (see Appendix A, Fig A2). In other words, the pressure drops to zero with a horizontal distance equal to twice the value of the standoff distance. This approximation is valid for different values of standoff distance. It was clarified that the distribution of the pressure depends mainly on the standoff distance, while it is independent on the charge weight as demonstrated in Fig. 3.3.

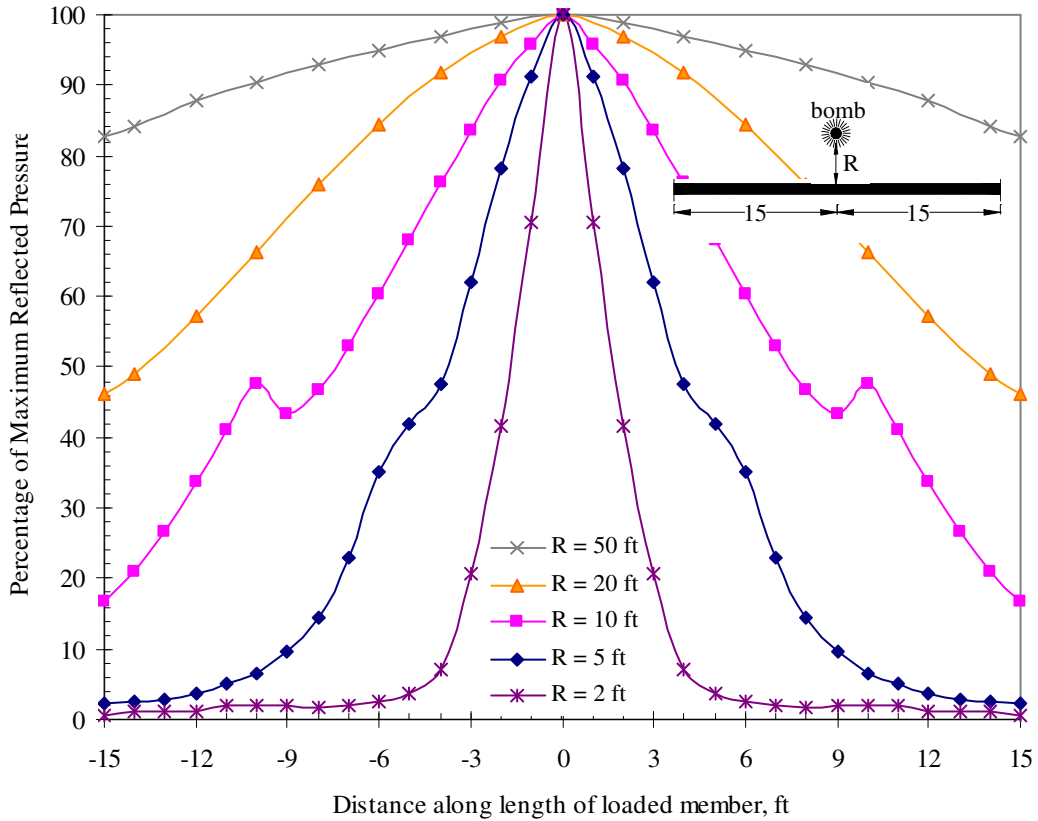


Fig. 3.2. Distribution of blast pressure along the length of the loaded member for different values of standoff distances

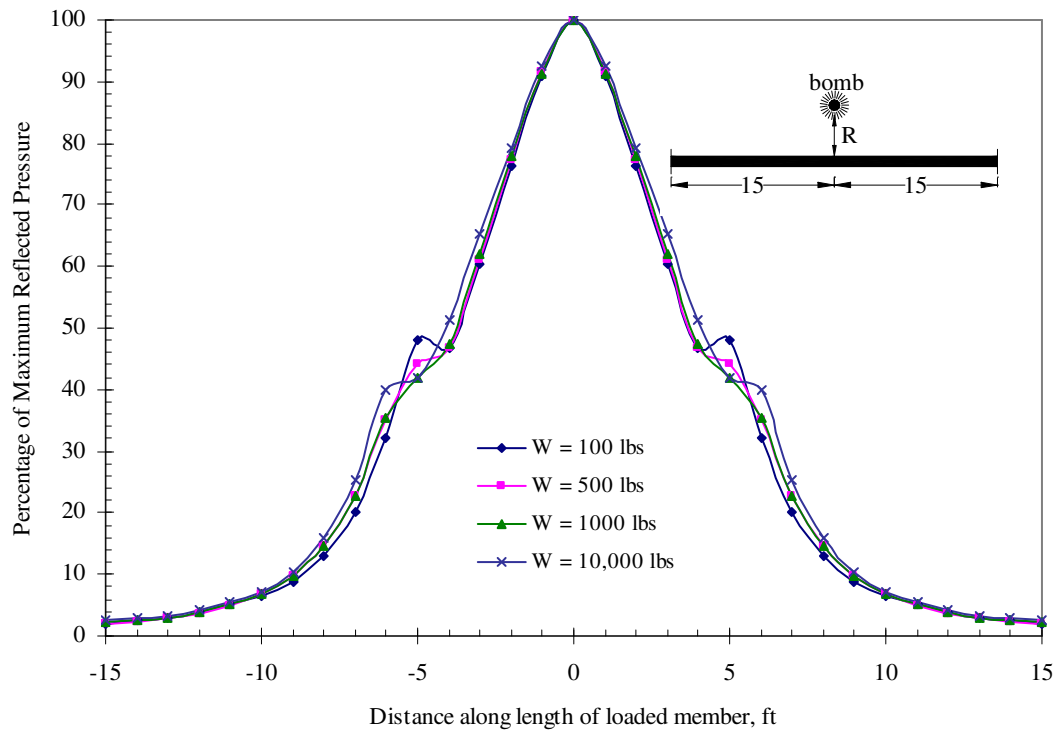


Fig. 3.3. Distribution of blast pressure along the length of the loaded member for different charge weights ($R = 5$ ft)

Unless the detonation charge is located exactly at the midspan of the member, the blast load distribution will be unsymmetrical. For most members, the blast pressure will have a trapezoidal / triangular shape. To simplify the design, the trapezoidal blast pressure can be converted to an equivalent uniform pressure. The value of this uniform pressure is equal to the peak value of the triangular pressure multiplied by a correction factor “C”, such that the area under both pressure distributions is the same (Eq. 3.1). This approximation can yield reasonable results. However, more accurate results can be obtained by analyzing the structural member under the effect of the trapezoidal blast load.

$$C = \frac{\text{area under the triangular pressure distribution}}{\text{loaded length}} \quad (3.1)$$

3.2 Elastic Blast Pressure Response Spectra

Estimating the blast loads on a member due to specific blast scenario is a cumbersome procedure. There are different combinations of charge weights and standoff distances. Each case has its particular values of pressure and duration. In addition, the equivalent static pressure that acts on the member depends on the dynamic load factor (DLF), and hence, the period of the structural element. To facilitate the design, it is essential to have response spectra similar to those used in seismic design. For the seismic response spectra, the global period of the structure is used to estimate the spectral acceleration which is then multiplied by the total mass of the structure to give the base shear. However, in blast loading, the equivalent static pressure can be computed directly based on the charge weight, the standoff distance, and the local period of the structural element. These response spectra can be generated in two different ways. Firstly, they can be generated

for constant charge weights and variable standoff distances (Figs 3.4 and 3.5). Secondly, they can be generated for variable charge weights and constant standoff distances (Figs 3.6 through 3.8). In addition, they can be generated for specific damping values. Nevertheless, the effect of damping can be neglected due to the short loading duration.

In this study, all the response spectra were generated based on numerical solutions of the triangular impulse of the blast scenario. Newmark's constant average method was used for the numerical analysis (Chopra, 1995). The analysis is based on Eq. 2.22 which was derived in the previous chapter. The response spectrum for a constant charge weight of 500 lbs and variable standoff distances is presented in Fig. 3.4. This spectrum is based on zero damping constant. A similar spectrum for a charge weight of 1000 lbs is presented in Fig. 3.5. The standoff distances used in these curves ranged from 2 ft to 50 ft. Response spectra for constant values of standoff distances and variable charge weights are presented in Figs. 3.6, 3.7, and 3.8 for standoff distances of 3 ft, 8 ft, and 20 ft, respectively.

It can be observed from these curves that pressure values decrease with the increase in the period of the structure. This is attributed to the fact that the DLF decreases with the increase in the period. Flexible members are subjected to less pressure values compared to stiff members. It is also observed that the pressure values dropped with the increase in the standoff distance. The equivalent static pressure for a standoff distance of 2 ft dropped to less than 50% with only one additional foot of standoff distance. On the other hand, the drop in pressure is much less significant for standoff distance larger than 6 ft. In

all these spectra, it is assumed that the structural member has a ductility value of one (elastic response spectra). The equivalent elastic static pressure obtained from these curves will be modified based on the ductility of the member. The plastic static pressure is obtained by dividing the elastic static pressure by a ductility factor (R_f). The equation for this factor is:

$$R_f = \sqrt{2\mu - 1} \quad (3.2)$$

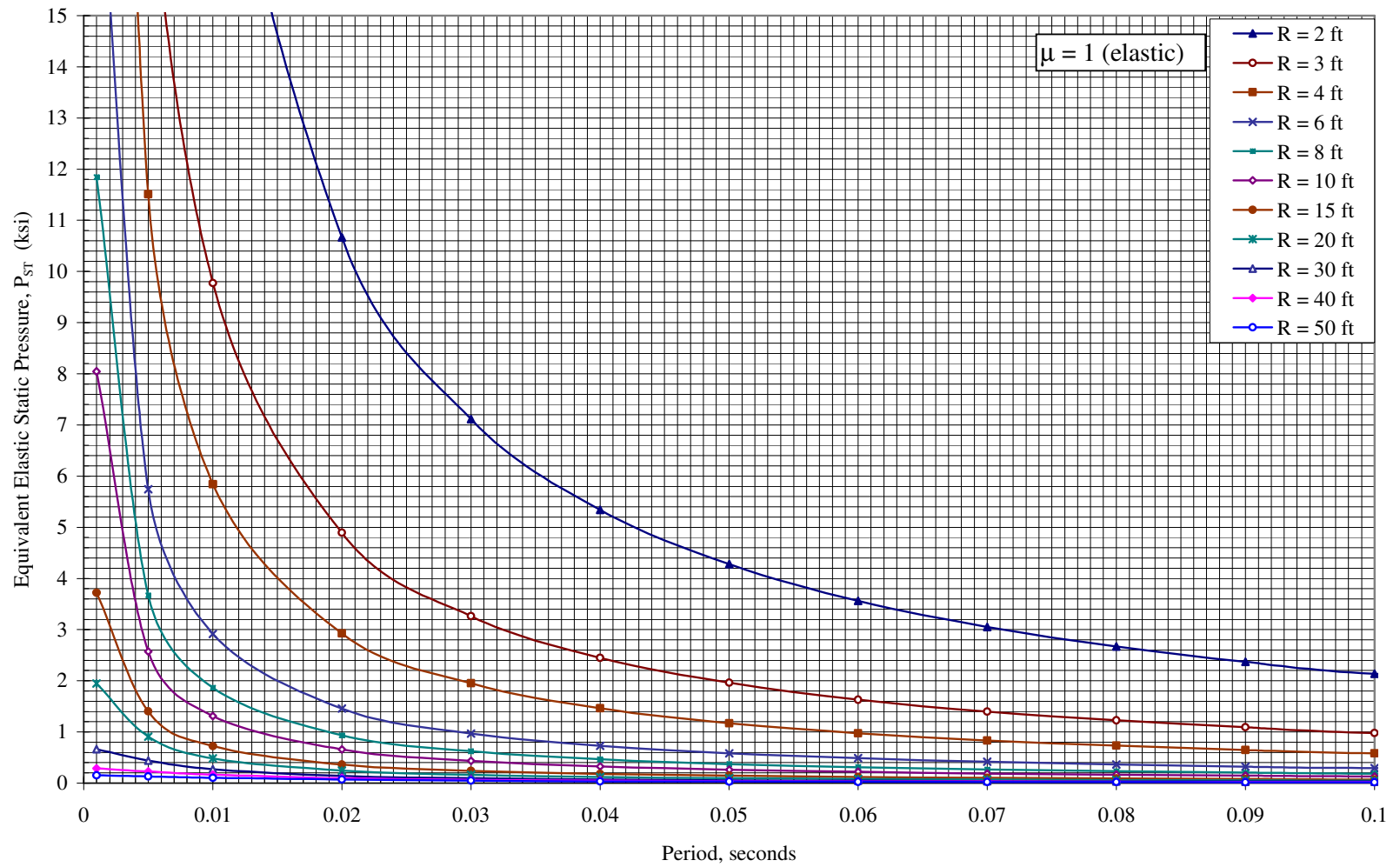


Fig. 3.4. Response Spectra for W = 500 lbs (zero damping)

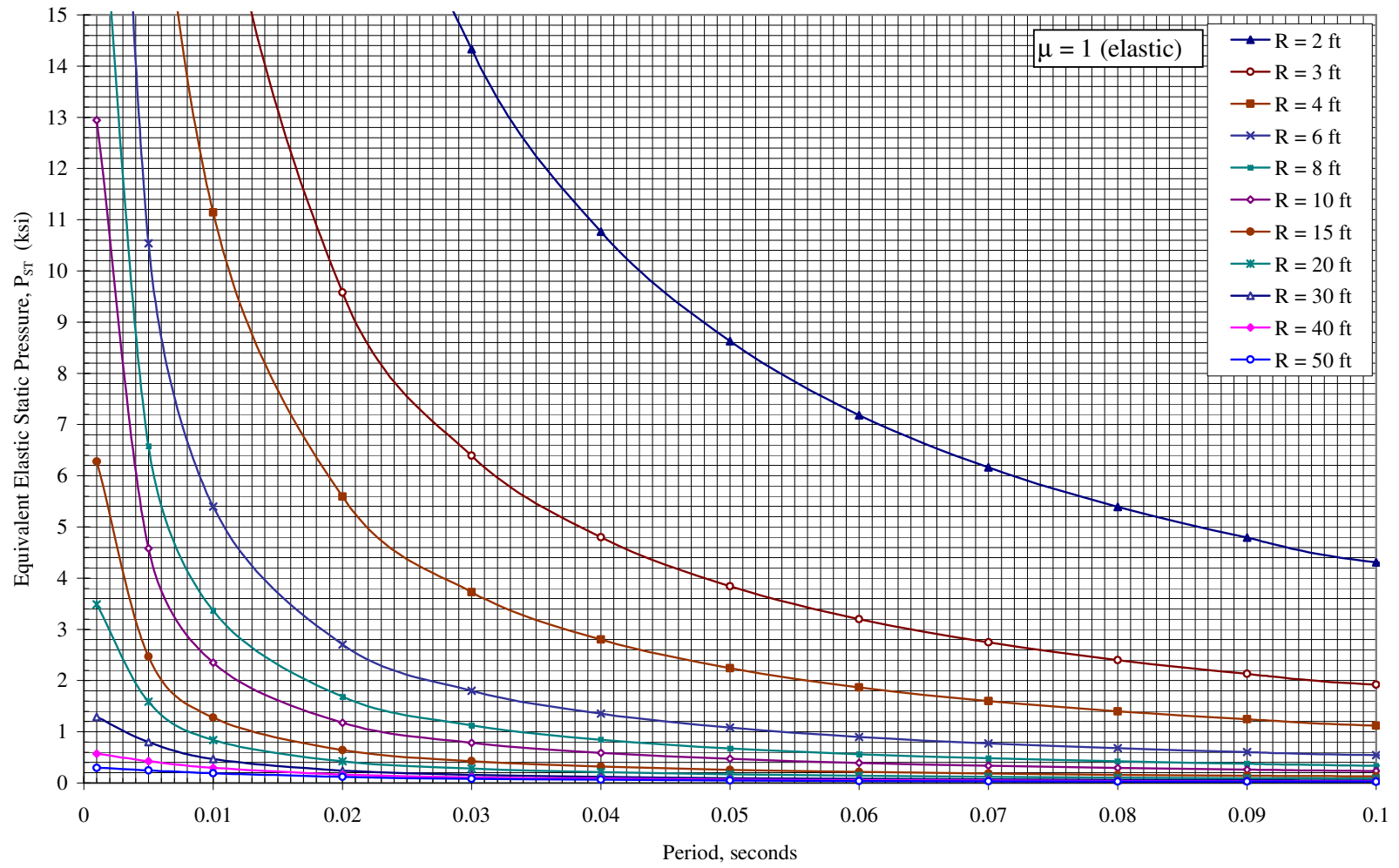


Fig. 3.5. Response Spectra for W = 1000 lbs (zero damping)

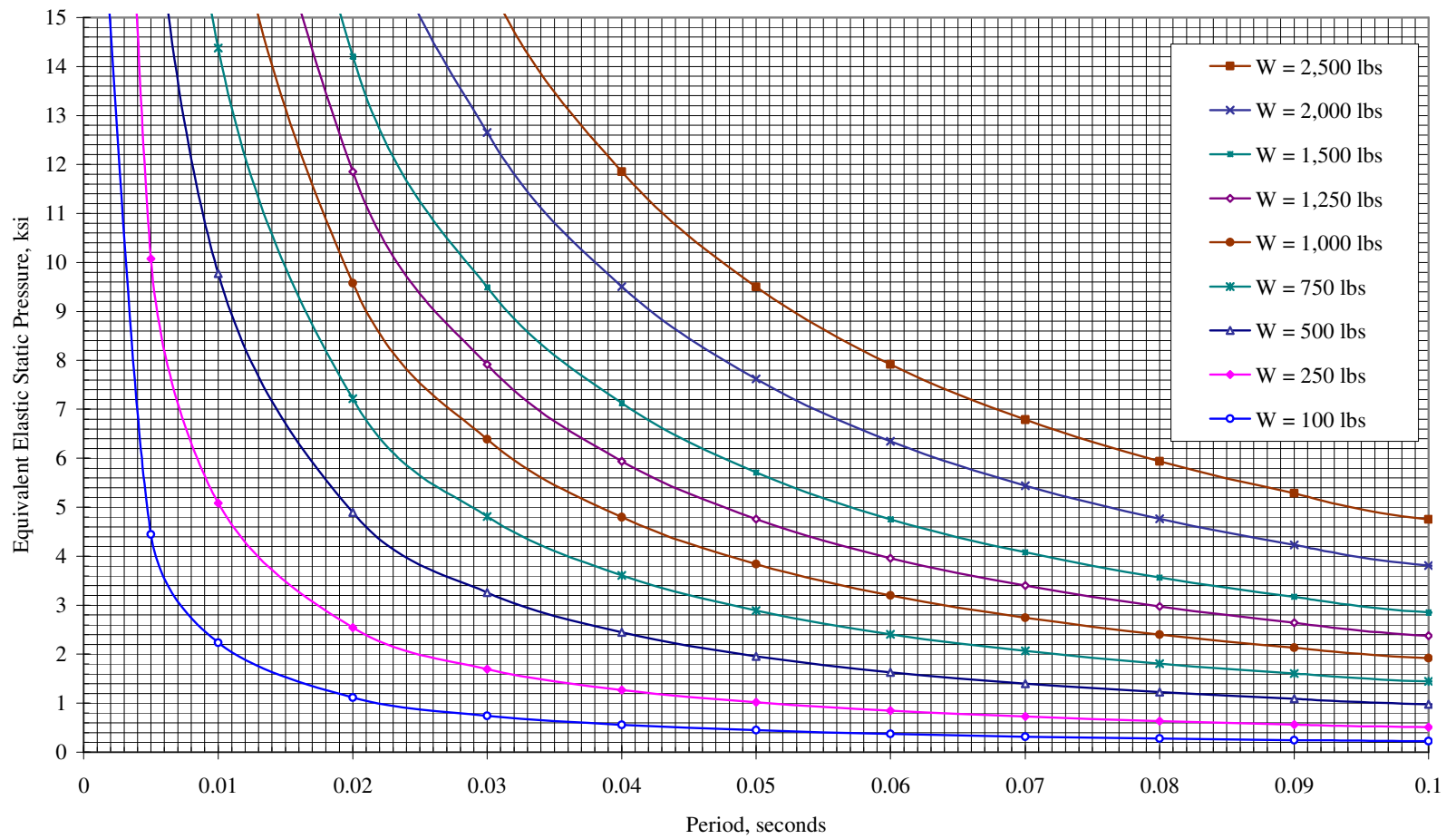


Fig. 3.6. Response Spectra for R = 3 ft (zero damping)

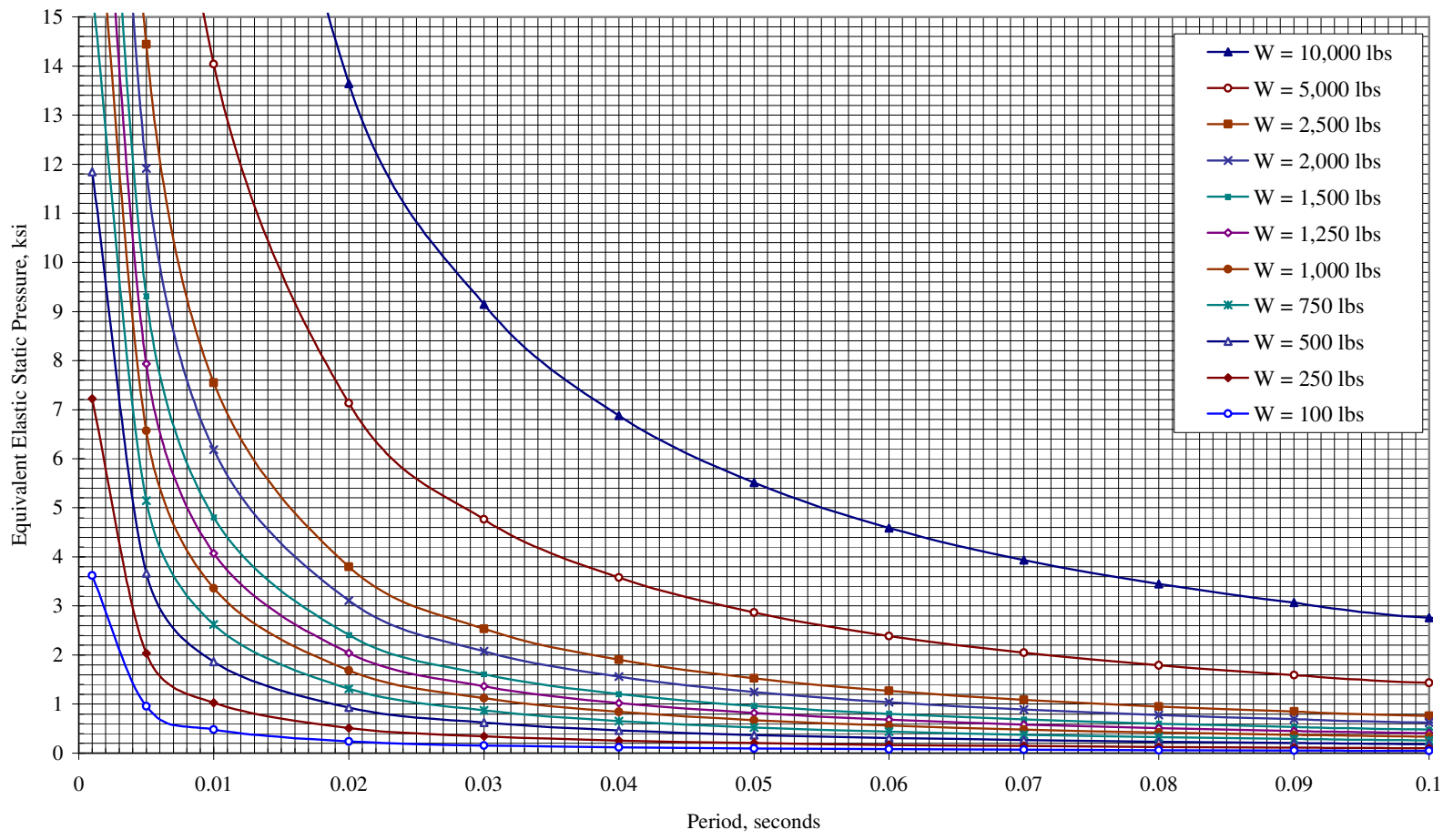


Fig. 3.7. Response Spectra for R = 8 ft (zero damping)

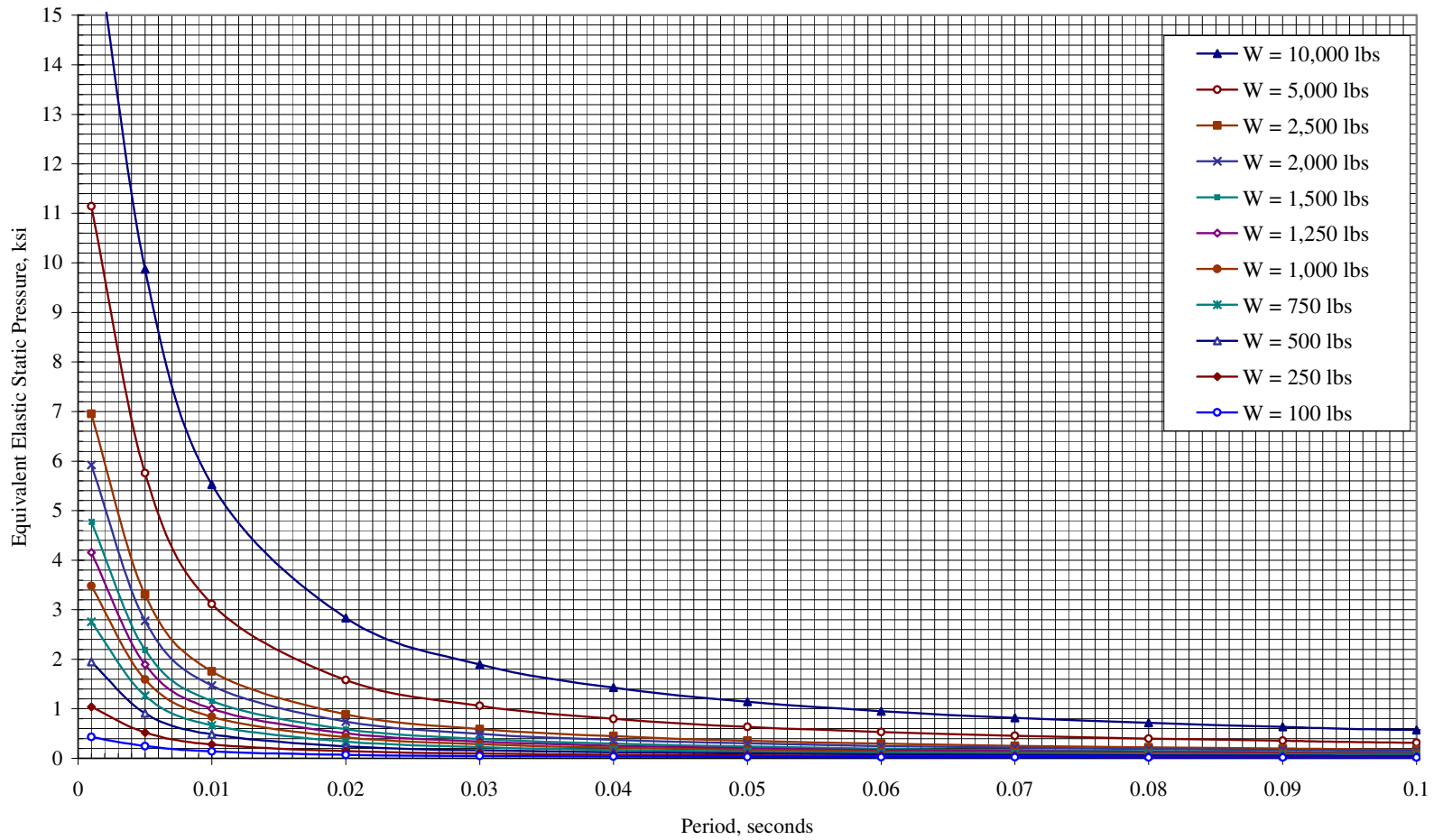


Fig. 3.8. Response Spectra for R = 20 ft (zero damping)

These response spectra can be used for the design as well as the analysis of structural members subjected to blast loads. In addition, they can be used to determine the minimum standoff distance that should be provided to a member to resist specific blast scenario. Using the response spectra for design is summarized as follows:

3.2.1 Designing a member for a specific charge weight and standoff distance

Step1: The period of the structural member is calculated based on its mass and stiffness.

These values are computed based on the design for other types of loads acting on the member.

Step2: For a specific probable blast scenario, use the response spectra for the anticipated charge weight and standoff distance.

Step3: Read the equivalent elastic static pressure from the vertical axis based on the period, charge weight, and standoff distance.

Step 4: The equivalent elastic static pressure is multiplied by the correction factor “C” derived in Eq. 3.1.

Step 5: Divide the result by the ductility factor (R_f) derived in Eq. 3.2, based on the provided ductility, to get the equivalent plastic static pressure.

Step 6: Multiple this plastic static pressure by the tributary width of the member to obtain the equivalent uniform load.

Step 7: Use this uniform load to calculate the maximum shear and bending moment acting on the member.

Step 8: Check the adequacy of the member to resist the applied staining actions. If the member is not adequate, revise the design and repeat steps 1 through 7.

3.2.2 Calculating the minimum required standoff distance for a member

Step1: The period of the structural member is calculated based on its mass and stiffness.

These values are computed based on the design for other types of loads acting on the member.

Step2: Based on the properties of the structural element calculate the maximum uniform plastic pressure that the member can withstand.

Step3: Multiply this plastic static pressure by the ductility factor (R_f) derived in Eq. 3.2 to obtain the maximum elastic static pressure.

Step4: For a specific charge weight, the minimum standoff distance can be computed based on the equivalent elastic static pressure and the period of the structure.

Step 5: Based on the computed standoff distance, the equivalent elastic static pressure is divided by the correction factor “C” derived in Eq. 3.1 to give a revised elastic static pressure.

Step 6: Enter the response spectrum using the revised elastic static pressure to compute the revised standoff distance.

Step 7: Repeat steps 5 and 6 until the standoff distance converges to a constant value.

The above design steps are illustrated in detailed examples that are provided in the Appendix (A.1 and A.2).

To study the effect of damping, the response spectra were generated based on damping values of 0%, 3%, 5%, and 10%. The results are shown in Fig. 3.9. It was observed that the pressure dropped with the increase in the damping constant. For a specific damping

value, this drop was constant for all blast scenarios. Hence, the drop in pressure due to damping is independent on the charge weight and the standoff distance. The percentile drop in pressure for damping values of 3%, 5%, and 10% was about 4.5%, 7.3%, 13.7%, respectively. It is observed that the relationship is linear. For every 1% of damping, the pressure drops 1.4% of the undamped pressure value. For most structural members, the damping values are less than 5%, and hence, the damping does not have a significant effect on the pressure values and can be ignored. Damping values can be increased through utilizing higher mechanical damping devices. However, mechanical dampers are likely to be damaged during the blast. Furthermore, due to the significantly small duration of the blast, mechanical dampers will not have enough time to be engaged to reduce the blast pressure acting on the structure.

3.3 Inelastic Blast Pressure Response Spectra

The blast pressure response spectra can be generated for specific ductility values. In this case, the equivalent plastic static pressure values are obtained directly from the response spectra without using the ductility factor (R_f). The inelastic plastic pressure response spectra for a charge weight of 500 lbs and various ductility limits is shown in Fig. 3.10. A similar spectrum for a charge weight of 1000 lbs is shown in Fig. 3.11. Figures 3.10 and 3.11 are generated for two values of standoff distances; 2 ft and 10 ft.

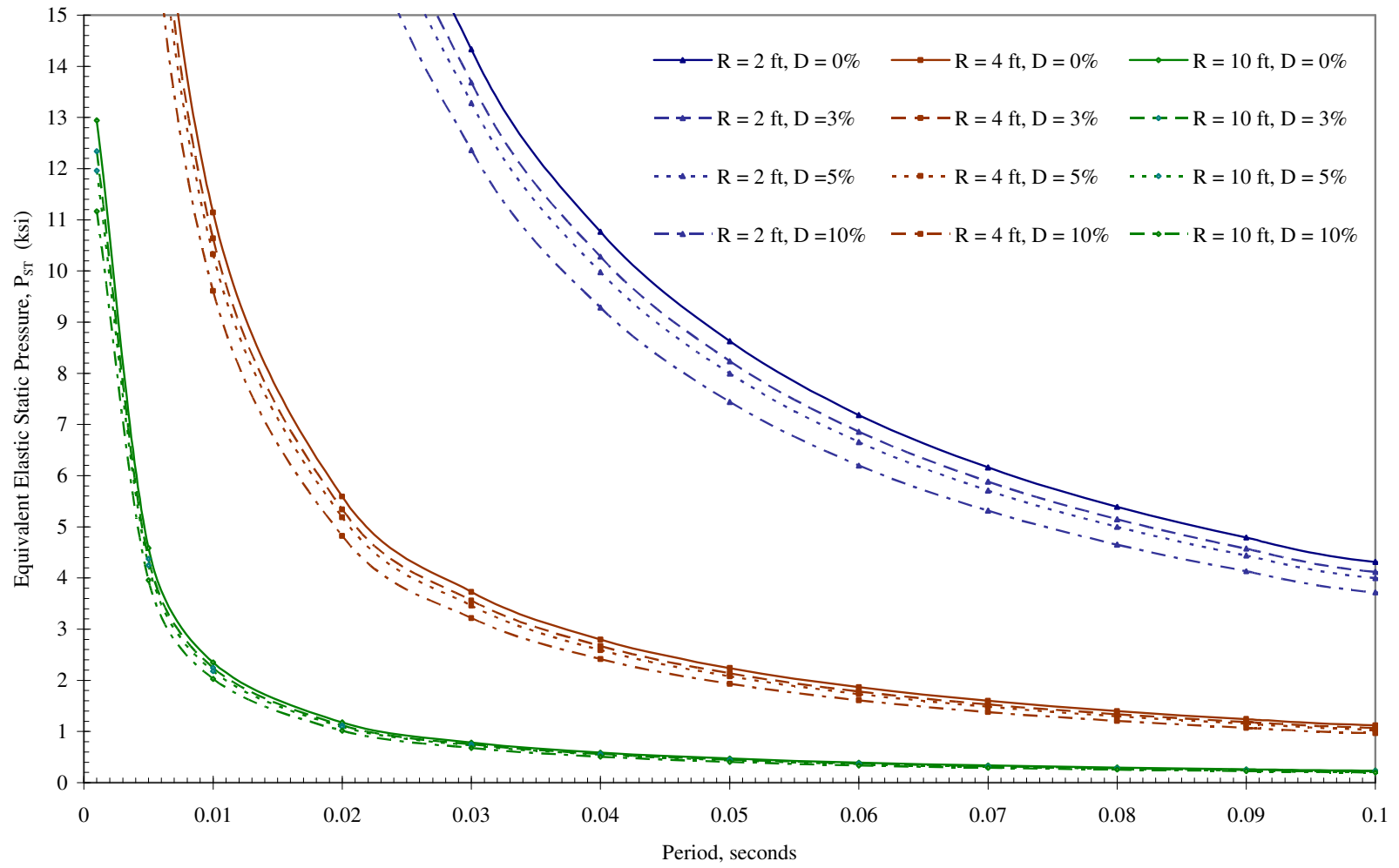


Fig. 3.9. Effect of Damping on the equivalent static pressure (W = 1000 lbs)

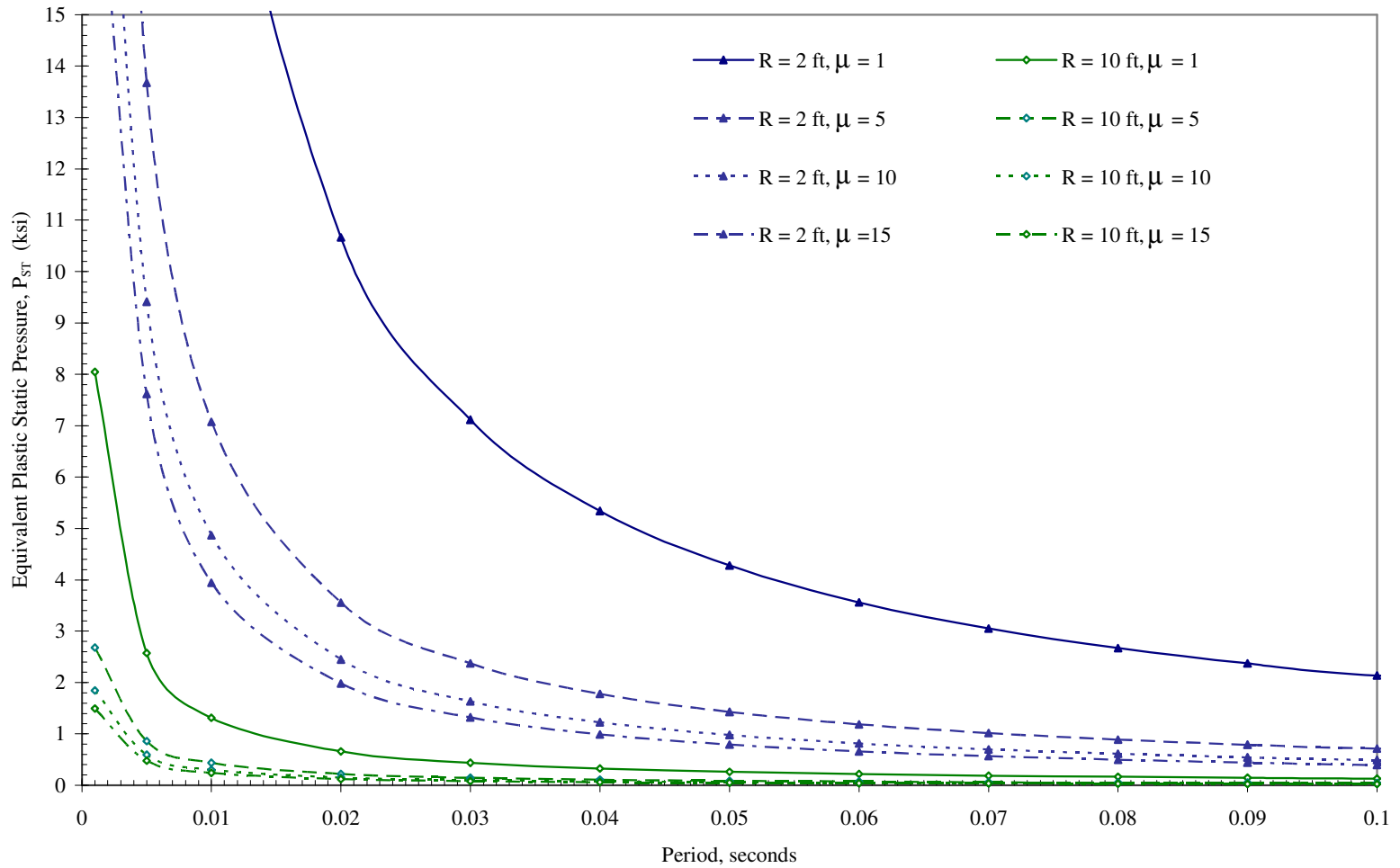


Fig. 3.10. Plastic pressure values for various ductility limits ($W = 500$ lbs)

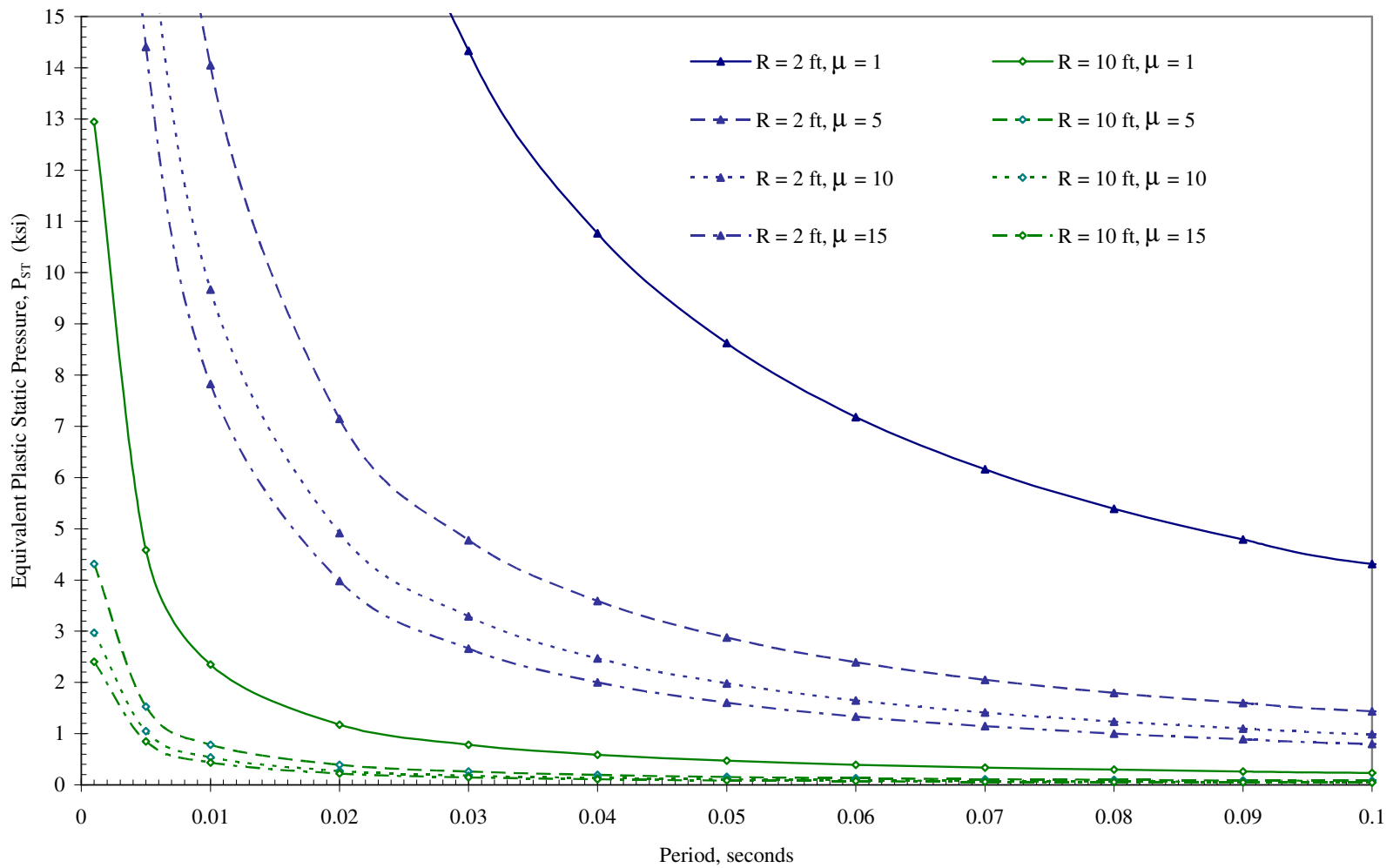


Fig. 3.11. Plastic pressure values for various ductility limits ($W = 1000$ lbs)

CHAPTER 4

ANALYTICAL INVESTIGATION

4.1 Analysis Methods

Researchers have used several analysis methods to simulate the behavior of structures subjected to blast loads. The simplest analysis is based on idealizing an individual structural element as a single degree of freedom model (SDOF). The impulsive blast load is converted to an equivalent concentrated static force acting on the SDOF element. If the material properties were considered linearly elastic, the analysis is referred to as linear elastic static analysis. More accurate results can be obtained by taking into account the nonlinear behavior of the materials, and hence the analysis becomes nonlinear static analysis. The main advantage of static analysis method is that it is simple and fast. On the other hand, it does not account for dynamic behavior of the structure. Furthermore, it does not account for the interaction between the response of structure and the blast load. In reality, the blast loads are spherical or hemispherical waves that apply pressure on the loaded elements, and hence converting the blast load to a single concentrated force is not an accurate representation of the actual blast scenario.

More accurate results can be obtained by using non-linear dynamic analysis methods. Unlike elastic static analysis, non-linear dynamic analysis accounts for the plastic behavior of structural elements by taking into consideration the nonlinear properties of materials. Non-linear dynamic analysis method is more realistic as it accounts for the ductility, yielding, cracking, and damping. In general, SDOF analysis can be used to provide preliminary analysis to individual structural elements subjected to distant blasts. However, this method lacks accuracy if applied for close range blasts. Another major disadvantage is that SDOF analysis does not simulate nor predict the failure mechanism of the structure when subjected to an extreme blast scenario (Williamson and Winget, 2005).

A more rigorous analysis can be performed by using the finite element method. The main advantage of the finite element analysis (FEA) is that it takes into account the interaction between the blast loads and the structural response. There are several commercial FEA softwares available in the market. Most of these softwares simulate blast loading as pressure-time histories. Third party softwares, such as A.T.-Blast, are used to convert the blast scenario into an equivalent pressure which is then applied to the structure. The magnitude of this pressure varies according to the charge weight and the standoff distance. Although FEA softwares are more accurate than other SDOF analyses, they are not representative to the actual scenario. Blast loads are non-simultaneous and non-uniform. They vary along the length of the loaded member due to the variation in the range and the incident angle. For distant blast scenarios, the blast pressure can be approximated as uniform pressure load. However, for small ranges, this approximation will significantly over estimate the blast loads. Furthermore, FEA is limited to the

nonlinear dynamic behavior. It does not track how the collapse of the structure is triggered and it does not account for elements separation and collision that takes place during the stages of collapse.

4.2 ELS Software

4.2.1 Applied element method

The main focus of this part of the study is to evaluate the local and global behavior of bridges subjected to blast loads, and to simulate and predict their failure mechanisms during blast scenarios. In order to obtain accurate results, it is important to represent the blast loads realistically as much as possible. This will require a software that can represent the behavior of the structure during the various stages starting from the application of loads until the complete collapse. Recently, Applied Science International (ASI) released a 3D analysis program named “Extreme Loading for Structures” (ELS). This software is based on the applied element method (AEM) which was developed by Kimiro Meguro and Hatem Tagel-din during the late 90’s (Tagel-Din, 1998). AEM is characterized by its unique ability to track the structural collapse behavior during the several stages throughout the lifetime of the structure. This includes the application of loads, elastic stage, crack initiation and propagation, reinforcement yielding, nonlinear behavior, large displacements, element separation, elements collision, and energy dissipation during collision (ELS Technical Manual, 2006).

When a structure is subjected to conventional loads, the rules of continuum mechanics apply and the behavior can be represented by the FEM. However, when the structure is

subjected to extreme loading cases such as earthquakes, blasts, and impacts, the behavior of structure is controlled by the separation and collision of its elements, and hence the rules of continuum mechanic will no longer apply. In this case, the behavior of the separated elements can be simulated by using the discrete element method (DEM). Although DEM is well representative of the separation and collision, it can not represent the continuum elements. A major advantage of AEM lies in its wide range of applications as it can represent both the continuum as well as the discrete behavior of structures. Therefore, it can realistically simulate the behavior of the structures before and during collapse. Hence, AEM is preferred over FEA and DEM. A comparison between the three methods of analysis is presented in Fig. 4.1.

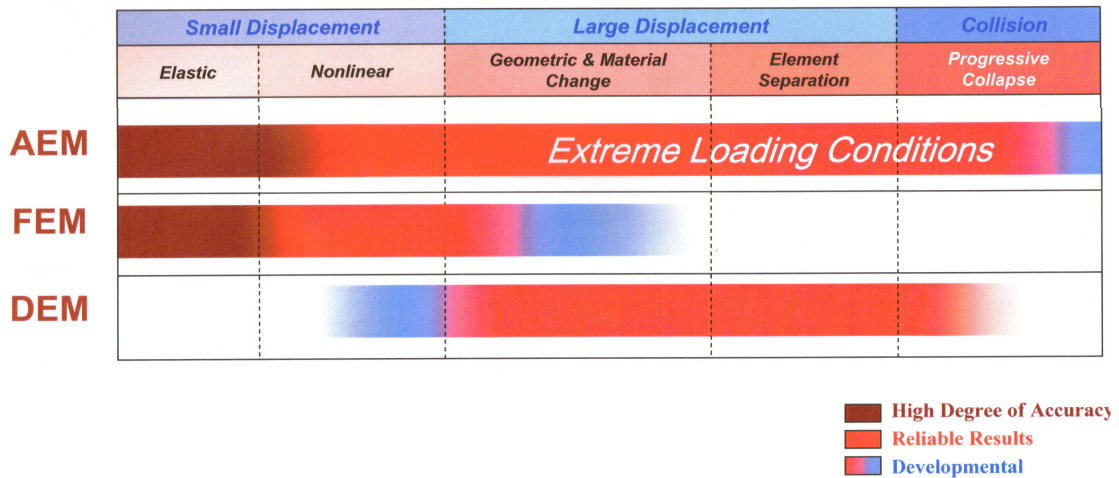


Fig. 4.1. Comparison between AEM, FEM, and DEM (ELS Technical Manual, 2006)

4.2.2 Connectivity between elements

FEA is usually based on modeling structural elements either as frame elements or shell elements. Adjacent elements are connected together through their common nodes, and

consequently partial connectivity is not allowed, and the failure and separation of elements can not be simulated. Conversely, in AEM, elements are modeled as 3D shapes which are connected together by springs along their surfaces (Fig. 4.2). Therefore, adjacent elements are not restricted to share common nodes, and therefore, this leads to simplified meshing in comparison to FEA. In AEM, partial connectivity can be achieved between adjacent elements if they share a portion of the surface (Fig. 4.3). During analysis, partial connectivity may occur if some of the springs fail, while other springs remain intact.

AEM allows for the separation between the adjacent elements if the applied forces exceed the separation strain between these elements. After separation, these 3D elements are free to collide with one another according to the loading scenario. ELS implements the auto-element contact detection system to simulate the behavior of colliding elements. This includes several types of contacts such as, corner to face, edge to edge, and corner to edge (ELS Technical Manual, 2006).

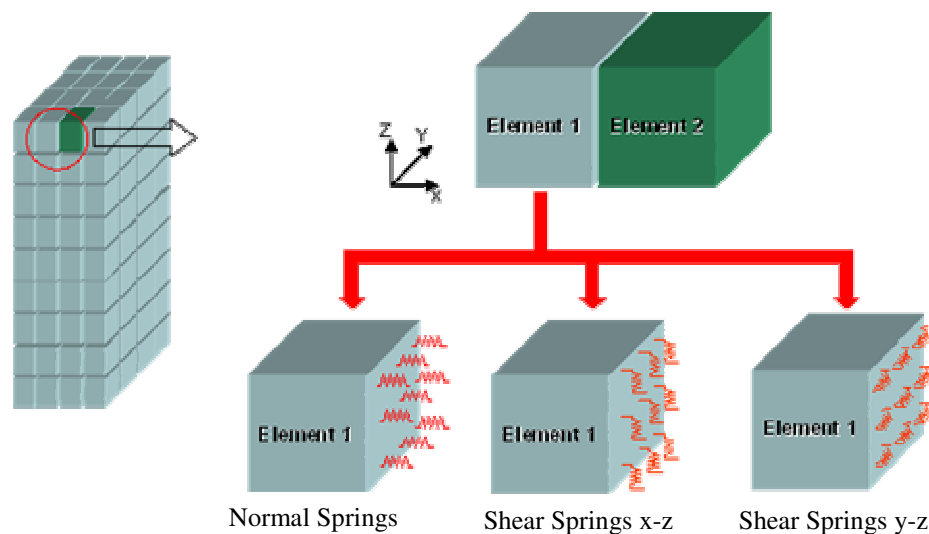


Fig. 4.2. Connectivity springs between adjacent elements (ELS Technical Manual, 2006)

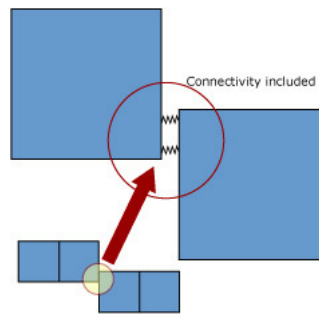


Fig. 4.3. Partial connectivity in AEM (ELS Technical Manual, 2006)

4.2.3 Collapse analysis

ELS can predict whether or not the collapse of the structure will occur under certain loading conditions. If collapse occurs, ELS can simulate how this collapse is initiated and whether it will be partial or total collapse. These simulations can be used to identify the structural vulnerabilities and to investigate how to enhance the behavior of the structures in order to prevent disproportionate collapses. ELS software was used to simulate the blast scenario that hit the Murrah Federal Building in Oklahoma City in 1995 (ASI, 2004). The simulation was very similar to the actual collapse of the building. This indicates that ELS software can be used to predict the behavior of structures subjected to blast loads and to track their failure throughout the various stages of collapse.

4.2.4 Blast wave model

The choice of ELS software was mainly based on its ability to create and simulate realistic blast conditions without using any other third party software. ELS software uses a free-field blast wave model. The magnitude of the pressure is generated based on the charge weight and the standoff distance from the detonation source. In analysis, the

detonation of the blast can be set to a specific time. After detonation, pressure waves travel from the detonation source towards the surrounding elements. When the wave front encounters a solid surface, the pressure is assumed to act perpendicular to the loaded surface. The pressure value is obtained based on Friedlander's equation (Baker, 1973) [Eq. 4.1].

$$P_{so}(t) = P_{\max} \left(1 - \frac{t}{T_s} \right) e^{-\frac{bt}{T_s}} \quad (4.1)$$

Where:

- P_{so} = incident pressure value
- t = time measured since wave arrival
- P_{\max} = peak static overpressure at the wave front
- T_s = duration of the positive phase
- b = wave decay parameter

This blast wave model does not take into consideration the effect of the incident angle on the amplification of the blast pressure, and hence, all structural elements are assumed to be loaded by the incident pressure. This assumption underestimates the magnitude of the actual pressure acting on the structure. In fact, when the incident pressure (P_{so}) waves created by the detonation encounter a solid surface, the pressure undergoes reflection. This reflection is mainly attributed to the compression of air molecules of the pressure wave when they decelerate suddenly and are brought to rest. At this incident, the structure is loaded by the reflected pressure (Mays and Smith, 1995). This reflected pressure (P_r) is of significantly higher amplitude than the incident pressure. The value of

the reflected pressure depends on the angle of incidence between the detonation source and the point under consideration. It also depends on the value of the incident pressure.

The coefficient of reflection (C_r) is defined as the ratio of the reflected pressure to the incident pressure (Eq. 4.2). For distant explosions, the value of C_r is in the order of 2, while for close blast scenarios, C_r can get as high as 13.

$$P_r = C_r P_{so} \quad (4.2)$$

For our study, the results of the blast analysis obtained using ELS software will be then multiplied by the coefficient of reflection (C_r), which was developed earlier in equations (2.4) and (2.5). This will ensure more realistic representation of the blast event. Since C_r changes with the change in the value of the incident pressure P_{so} , therefore, the relation between the reflected and the incident pressure is a non-linear relationship.

4.3 Response of Concrete Columns Subjected to Blast Loads

In this section, ELS software will be used to perform blast analysis for concrete columns subjected to blast loads. The results will be compared with the values obtained from the SDOF analysis using the blast loading response spectra that were developed earlier in this investigation.

The cross sectional properties, dimensions, and reinforcements of the column were based on that of a typical concrete bridge. The cross section was assumed to be circular with 3.5 ft diameter and the column height was assumed to be 18 ft. The column was assumed to

be fixed at both the top and bottom. This assumption is deemed reasonable since the column is monolithically connected to the footing at the bottom and to the cap beam at the top. The reinforcement consisted of 16 # 8 bars longitudinal reinforcement and # 3 stirrups @ 12 inches with 3 inches cover. The compressive strength of concrete and yield strength of steel used in the analysis were 3 ksi and 60 ksi, respectively.

The blast scenario is assumed to be the result of an explosive device located below the bridge deck. The blast load has a charge weight of 1000 lbs of TNT explosives. This weight represents that of an average size van. The main parameter considered in the analysis is the effect of the standoff distance on the behavior of the concrete columns. In this analysis, the standoff distance varied from 5 ft up to 100 ft. The charge is assumed to be located at 3 ft above the ground surface. This distance represents the center of gravity of a typical car trunk.

4.3.1 ELS analysis

The analysis was recorded over a period of 0.1 second with a time step increment of 0.0001 second. It was observed that the time step increment is a crucial parameter in the analysis of structural elements subjected to blast loads. This time step should be a very small value to monitor the rapid changes that take place in the behavior of the structure. If the time step is not small enough, the obtained results can be inaccurate and misleading. As expected, the time at which the maximum response is recorded increased in a curvilinear manner with the increase in the standoff distance (Fig. 4.4).

The results obtained from ELS included the maximum shear and its location, maximum moments and its location, shear envelope, bending moment envelope, crack pattern, and deformed shape. These results are obtained for each blast scenario and then plotted together for comparison. The results are presented in Figs. 4.6 through 4.10. A typical time-history response of a concrete column subjected to a distant blast load is shown in Fig. 4.5.

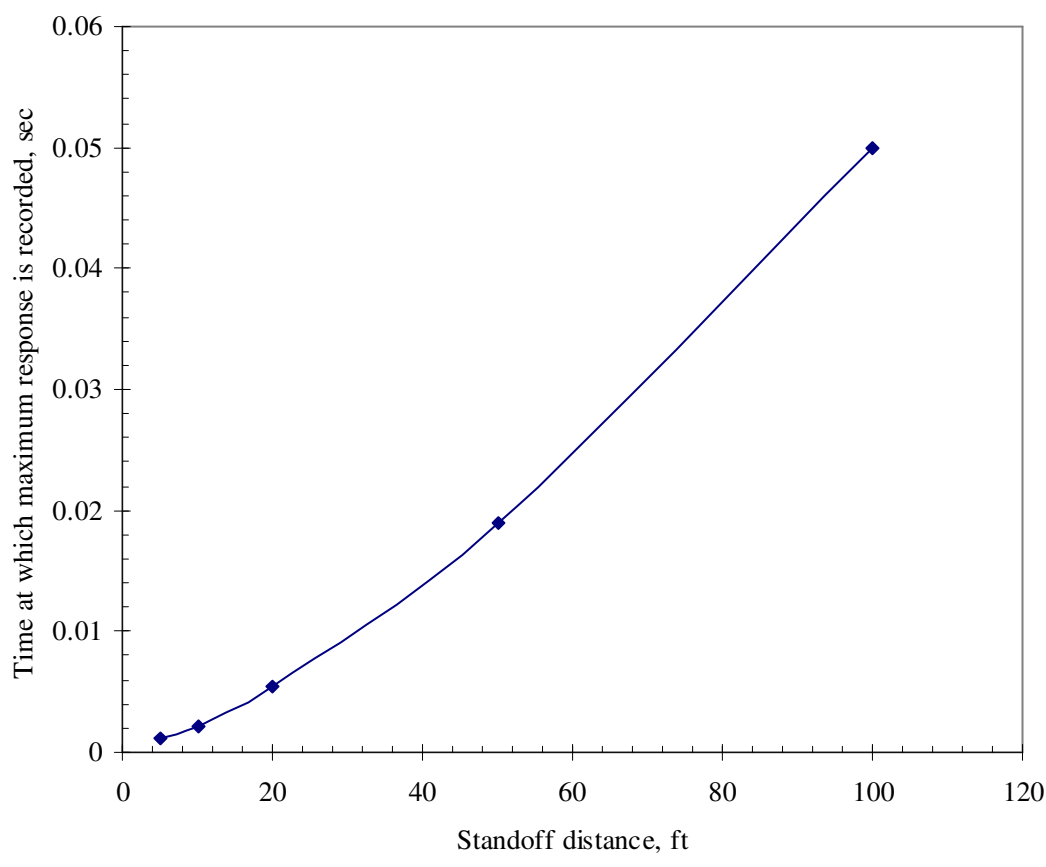


Fig. 4.4. Effect of the standoff distance on the time of maximum response

From these results, several observations were made. For distant blasts, the bending moment diagram (BMD) and the shear force diagram (SFD) were similar to that of a fixed beam subjected to uniform distributed load (Figs. 4.7 and 4.8). The maximum negative moment was generated at the location of the fixed supports, and the maximum positive moment was generated at the mid span of the column. The moment and shear envelopes indicated that the column undergoes reversible response (Figs. 4.9 and 4.10). However, the magnitude of the reversed shear and moment is usually smaller than the initial magnitude. For standoff distance exceeding 20 ft, the magnitude of the reversed response was about 50% of the initial. The cracks induced in the columns subjected to the distant blast were mainly minor flexural cracks initiated at the supports and the midspan, which are the location of the maximum negative and positive moments, respectively. A schematic of the deformed shape and cracking of the column is shown in Fig. 4.6. For clarity, the deformed shapes were multiplied by a scaling factor of 10.

However, with the decrease in the standoff distance, more localized behavior was observed. The SFD became nonlinear with its peak value at bottom support which is closer to the detonation source (Fig. 4.7). The maximum positive moment shifted from the midspan to the level of the detonation source (Fig. 4.8). Furthermore, the magnitude of the reversed response started to decrease with the decrease in the standoff distance. The effect of the standoff distance on the magnitude of the reversed response is shown in Fig. 4.11. This decrease can be attributed to the plastic behavior of the columns due to the higher degree of damage and the intensive cracking. It was also observed that more cracks were induced with the decrease in the standoff distance (Fig. 4.6). These cracks were spread all along the column height, but they were very intense at the level of the

detonation source. Additionally, these cracks propagated throughout the whole cross section of the column. This can be attributed to the formation of shear cracks in addition to the flexural cracks. For blast scenarios in close proximity, concrete breaching occurred at the level of the detonation source. The intensive cracking and the breaching of concrete led to the failure of the column and its final collapse.

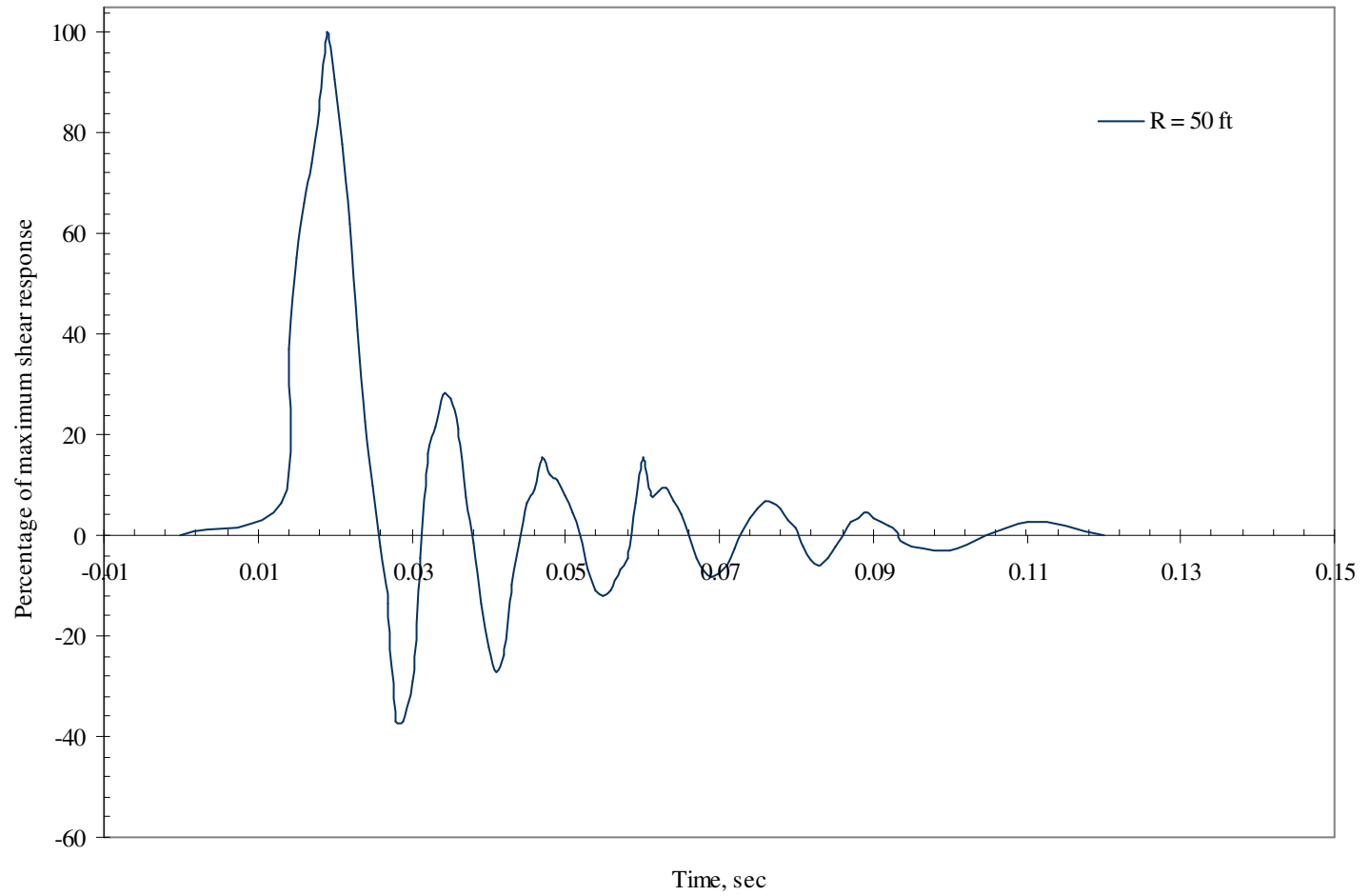


Fig. 4.5. Typical time-history response of a concrete column subjected to distant blast load

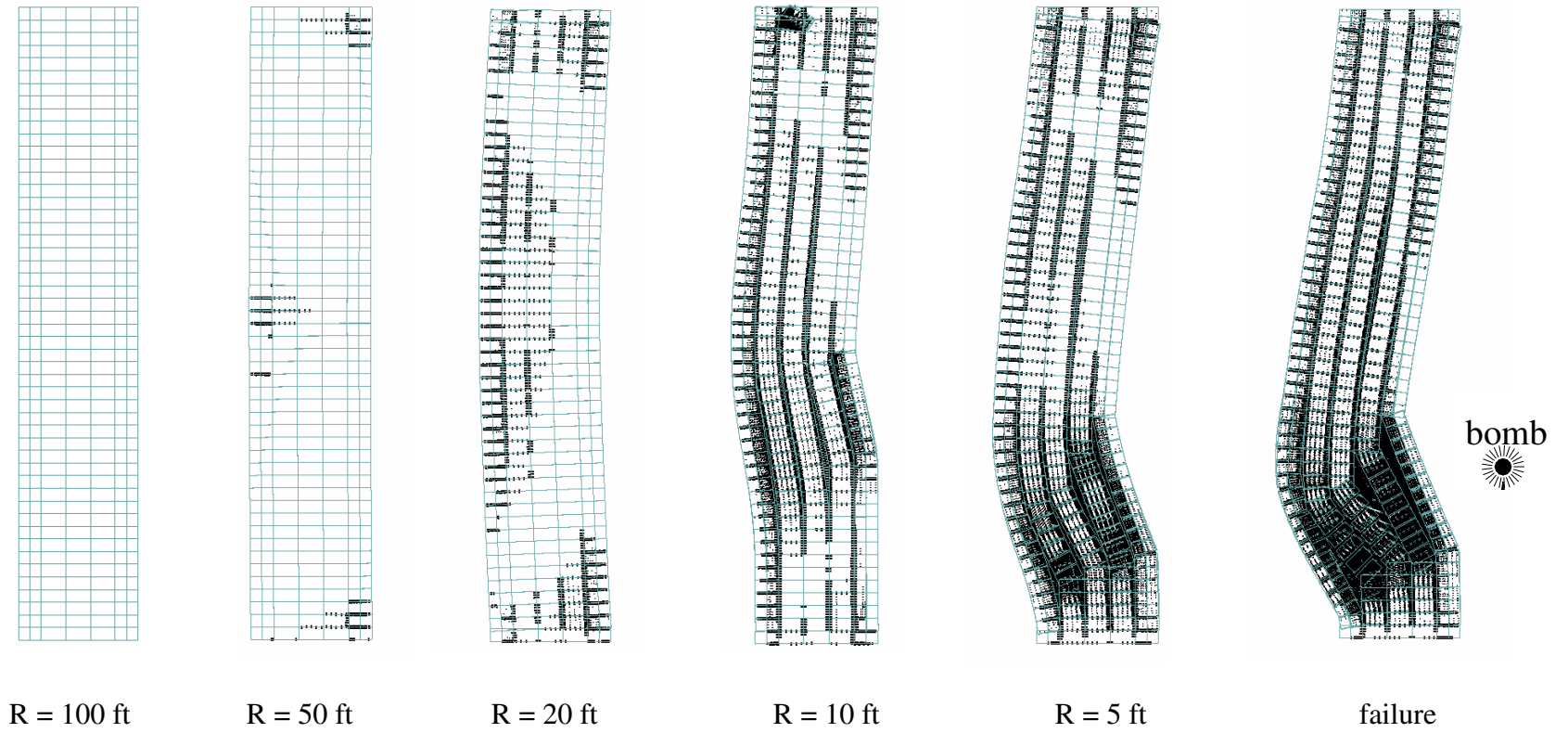


Fig. 4.6. Schematics of cracks developed in a concrete column due to variable standoff distances

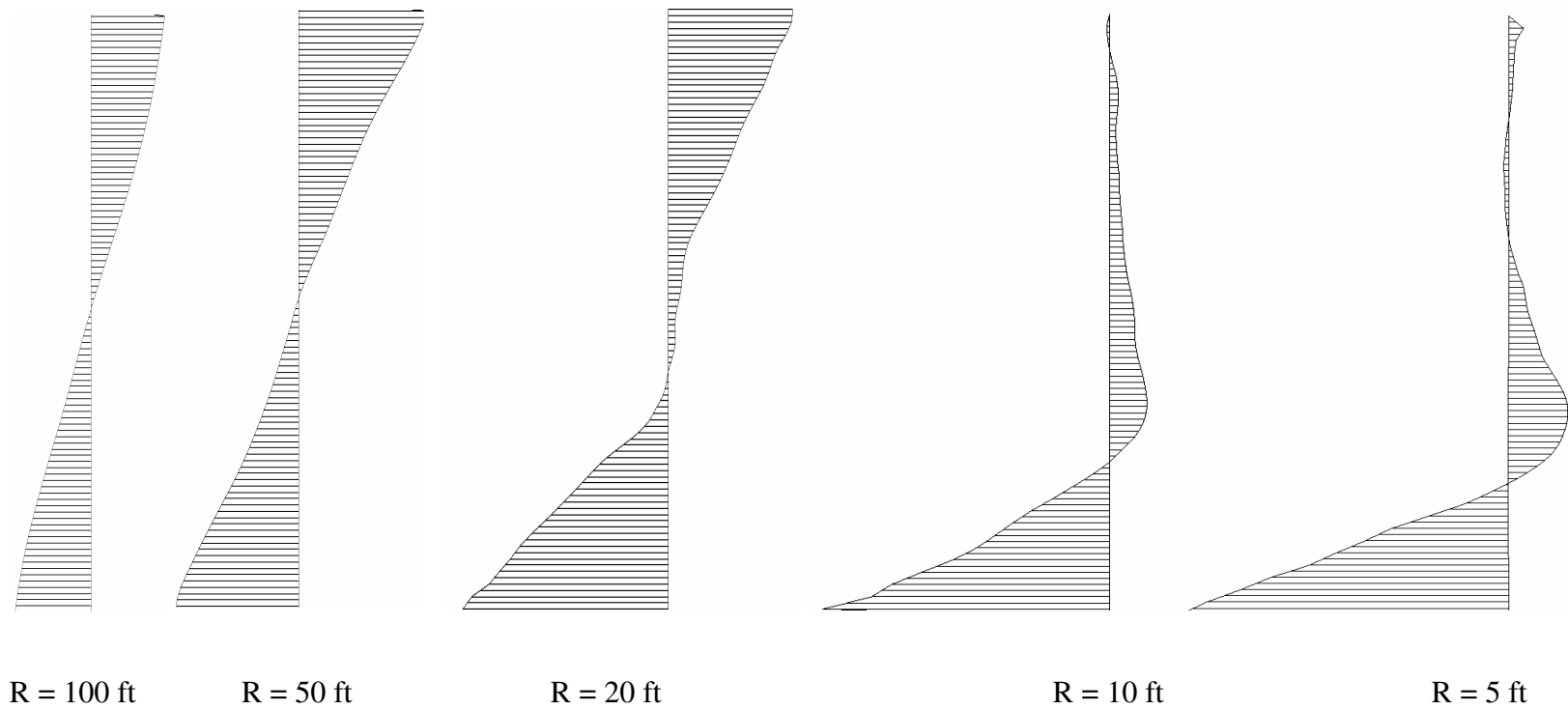


Fig. 4.7. Schematics of SFD developed in a concrete column due to variable standoff distances

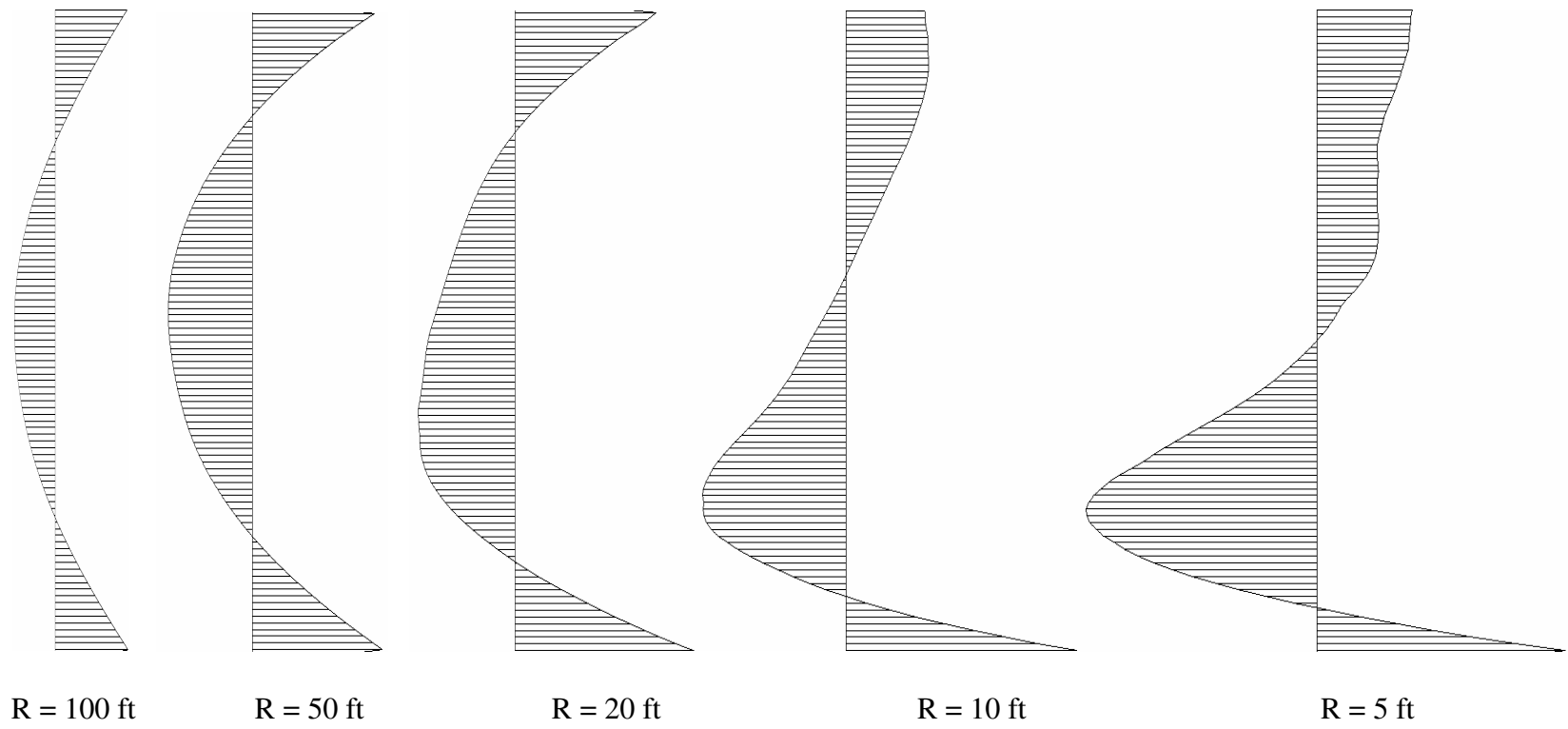


Fig. 4.8. Schematics of BMD developed in a concrete column due to variable standoff distances

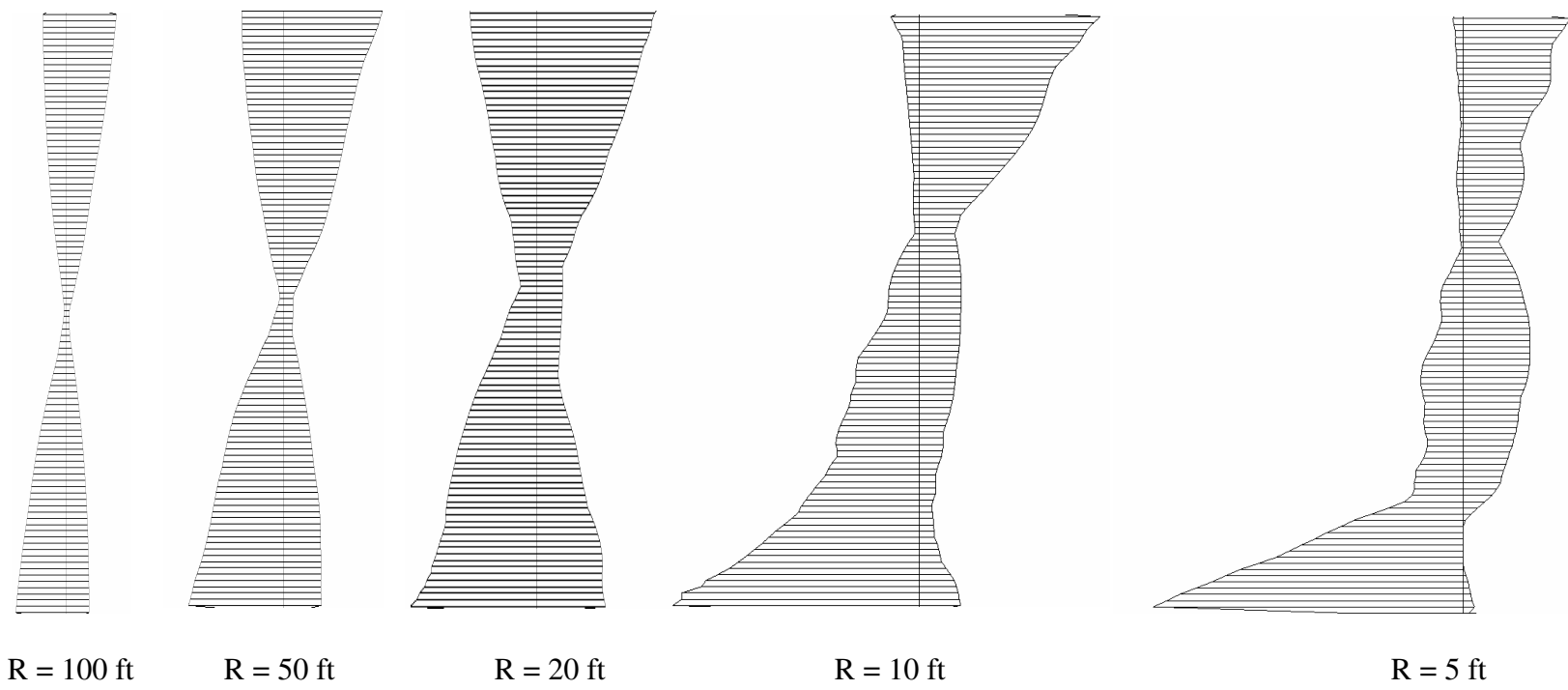


Fig. 4.9. Schematics of shear envelope developed in a concrete column due to variable standoff distances

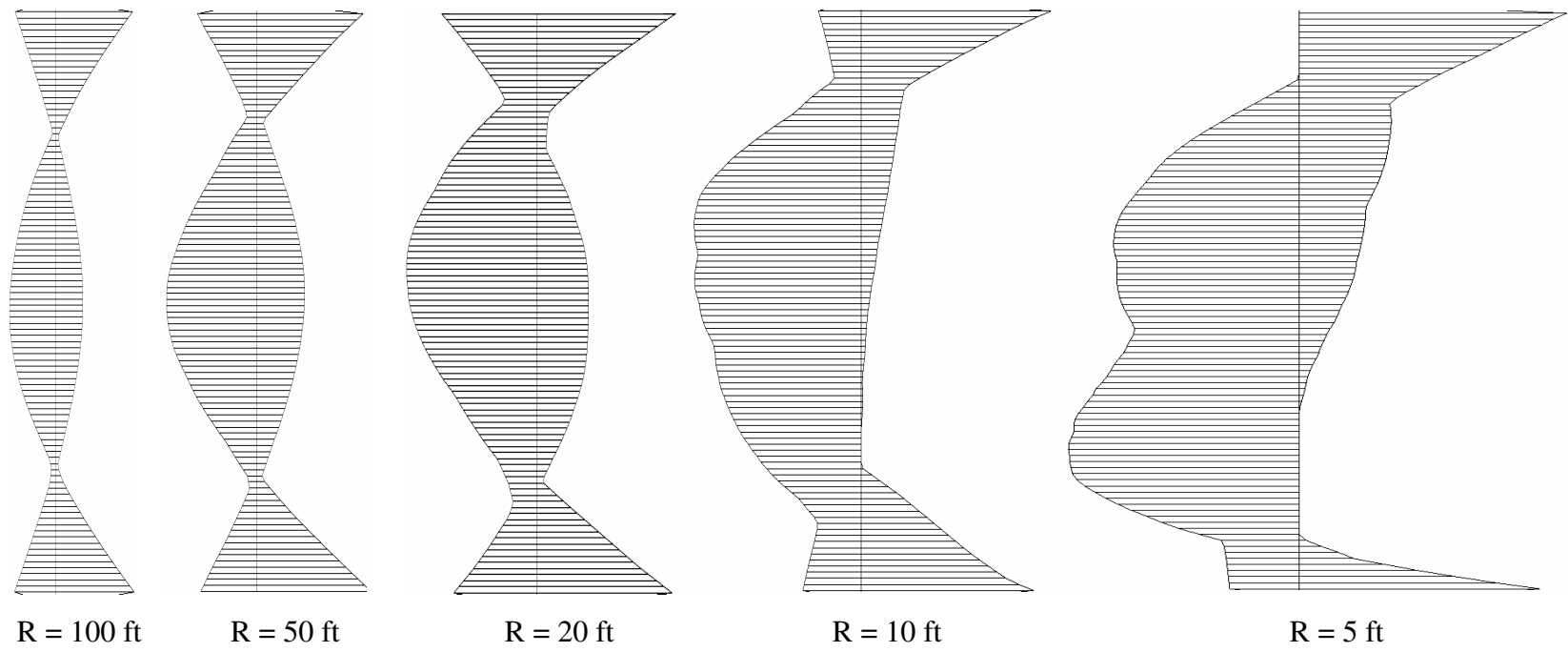


Fig. 4.10. Schematics of bending moment envelope developed in a concrete column due to variable standoff distances

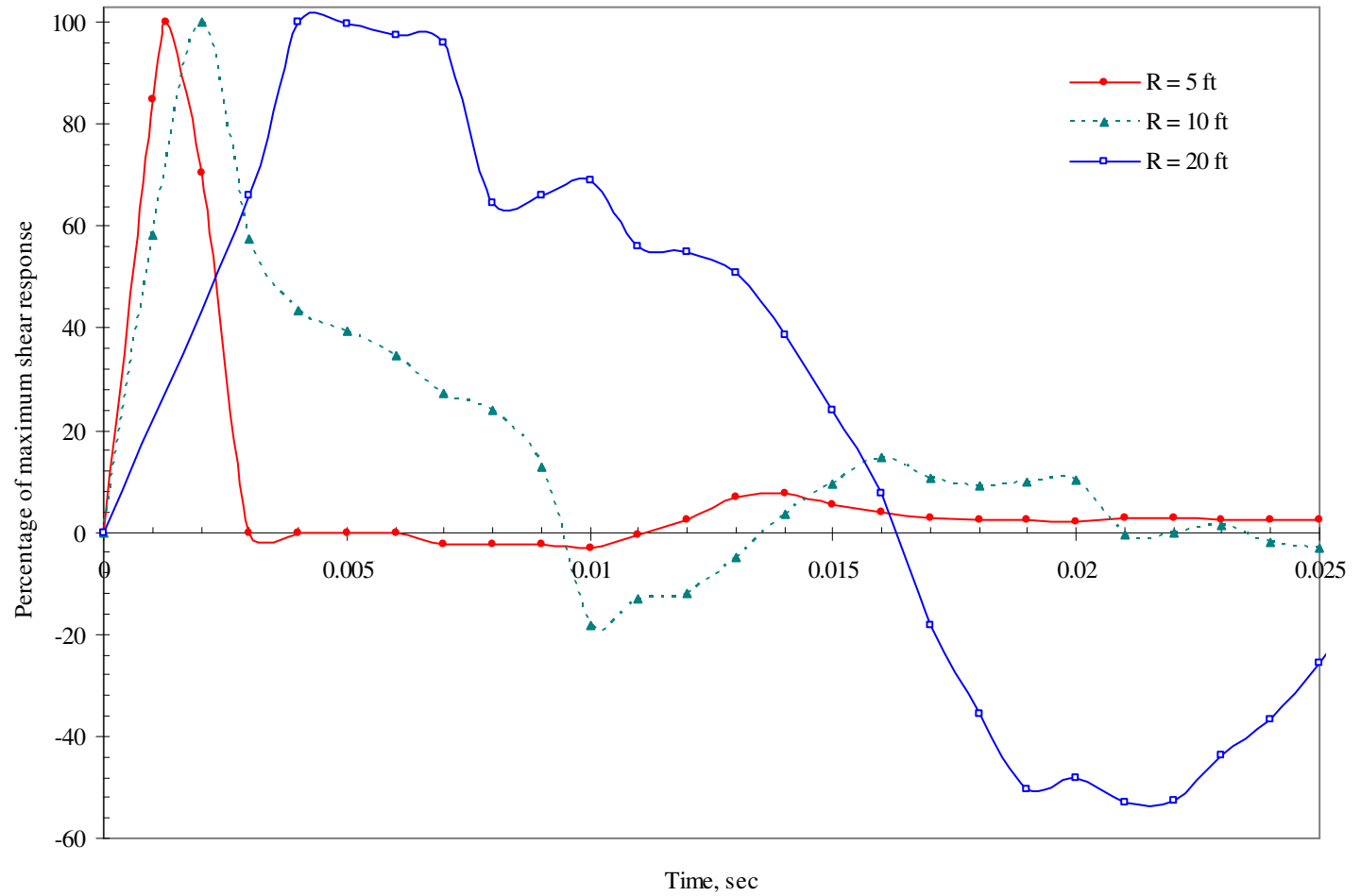


Fig. 4.11. Effect of the standoff distance on the magnitude of the reversed response

From the above results, it can be concluded that distant blasts can be approximated as a uniformly distributed load. On the other hand, as the standoff distance decreases, this approximation lacks accuracy as the structural element undergoes localized behavior at the level of the detonation source. Furthermore, the nonlinearity in the shape of the shear diagram for close proximity should be taken into consideration during the design.

In the earlier analysis, the charge weight was assumed to be a constant value. However, in reality, the charge weight can vary from a few lbs up to thousands of lbs depending on the size of the vehicle used in the blast scenario. To examine the effect of the variation in the charge weight on the behavior of columns, ELS was used to run several simulations. Two parameters were considered in the analysis; the standoff distance and the charge weight. The used standoff distance varied from 2 ft up to 100 ft. The charge weight was assumed to vary as 50, 100, 200, 500, and 1000 lbs (Fig. 4.12). The small values of the charge weight such as 50 and 100 lbs represents the typical blast scenario due to a hand charge or a small brief case. Hence, these values are usually expected to be located near the columns at small standoff distance values. On the other side, the heavier charge weights represent the vehicle bombings of an average size car or van, and hence, they are more likely to occur at larger standoff distances.

To observe the relationship between the charge weight and the column response, the maximum shear developed in the column was plot versus the charge weight for variable standoff distances (Fig. 4.13). From this figure, it can be seen that the maximum shear induced in the column increased with the increase in the charge weight. Yet, the effect of the charge weight is far less significant than the effect of the standoff distance on the

response of the column. These results are in good agreement to the conclusion drawn earlier from the blast loading response spectra. For standoff distance more than 10 ft, the relationship between the charge weight and the column response can be approximated as a linearly increasing relation. The slope of this linear relation increases with the decrease in the standoff distance, while for standoff distances less than 10 ft, the relationship tends to be a curvilinear relation as shown in Fig. 4.13.

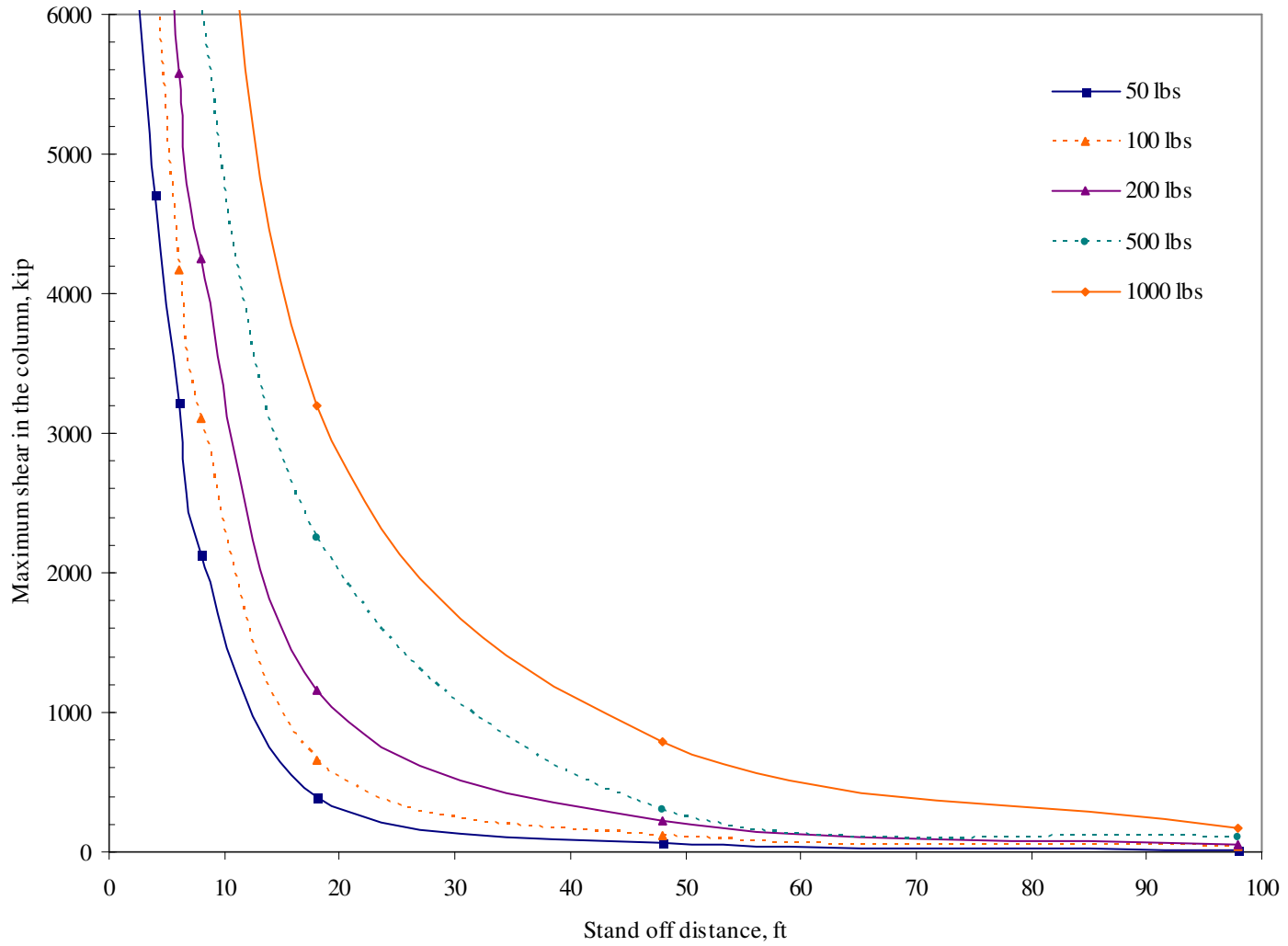


Fig. 4.12. Response of concrete column to various blast scenarios

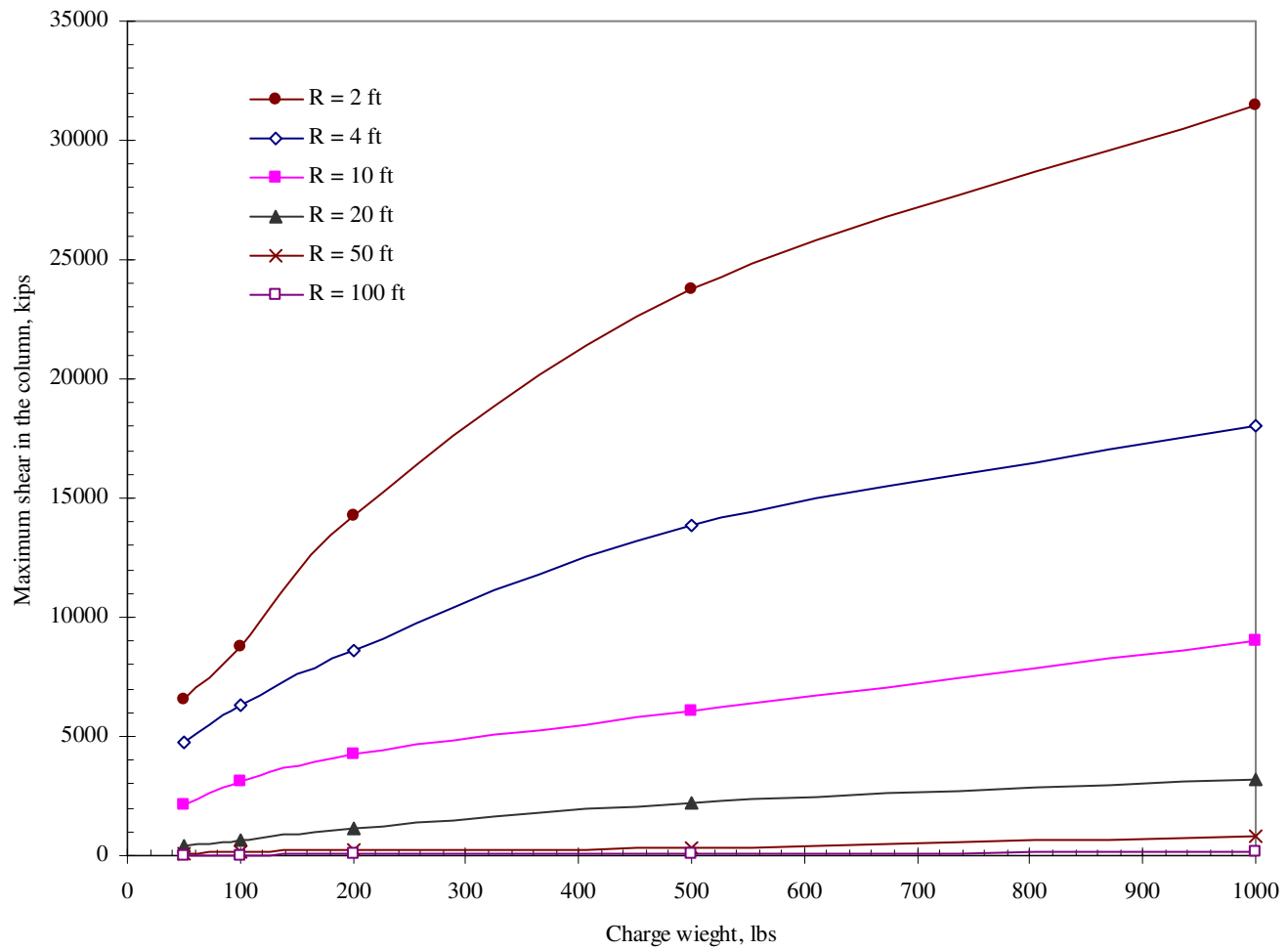


Fig. 4.13. Effect of the charge weight on the maximum shear developed in the column

4.3.2 Response spectral analysis – Approximate Analysis

The response spectral analysis is an approximate method in which each column is idealized as an equivalent single degree of freedom system (SDOF). The equivalent period of vibration of the SDOF system is calculated using Eq. 4.3. The actual mass of the column was multiplied by a load-mass coefficient (K_{LM}). This coefficient is used to equate the work done by the actual system and that of the equivalent SDOF system. Values of K_{LM} for different support conditions and loading types are tabulated in TM5-1300 (1990). For a column with fixed supports subjected to distributed load K_{LM} is equal to 0.77, 0.78, and 0.66 for the elastic, elasto-plastic, and plastic analysis, respectively.

$$T = 2\pi \sqrt{\frac{M K_{LM}}{K_E}} \quad (4.3)$$

Where:

T	= period of vibration	M	= actual mass
K_{LM}	= load-mass coefficient	K_E	= equivalent stiffness

An elastic design of structural elements against blast is uneconomical. Therefore, it is more cost-effective to design those members to develop plastic deformations. The behavior of a concrete column fixed at both its ends and subjected to uniform blast pressure is shown in Fig. 4.14. The column behaves linearly elastic until the formation of plastic hinges at the fixed supports. Plastic hinges at the support are formed due to the yielding of the negative-moment steel. At this point, the column enters the elasto-plastic phase and the stiffness value changes to match that of a simply supported column. Finally, when the deformation of the column reaches its plastic limit (X_P), this will result in the yielding of the positive moment steel and thus the plastic behavior until the final collapse.

To simplify the analysis procedure, TM5-1300 adopts a simplified bilinear curve with an equivalent stiffness value of K_E such that the area under the actual curve and the simplified bilinear curve are the same. It was reported that the difference between both approaches is negligible, and hence the equivalent stiffness can be used with good accuracy (TM5-1300, 1990). The elastic stiffness (K_e), elasto-plastic stiffness (K_{ep}), and the equivalent stiffness (K_E) of a concrete column subjected to uniform load are presented in Eqs. 4.4, 4.5, and 4.6, respectively. The values of K_E for different loading configurations and support conditions are tabulated in TM5-1300.

$$K_e = \frac{384EI}{L^3} \quad (4.4)$$

$$K_{ep} = \frac{384EI}{5L^3} \quad (4.5)$$

$$K_E = \frac{307EI}{L^3} \quad (4.6)$$

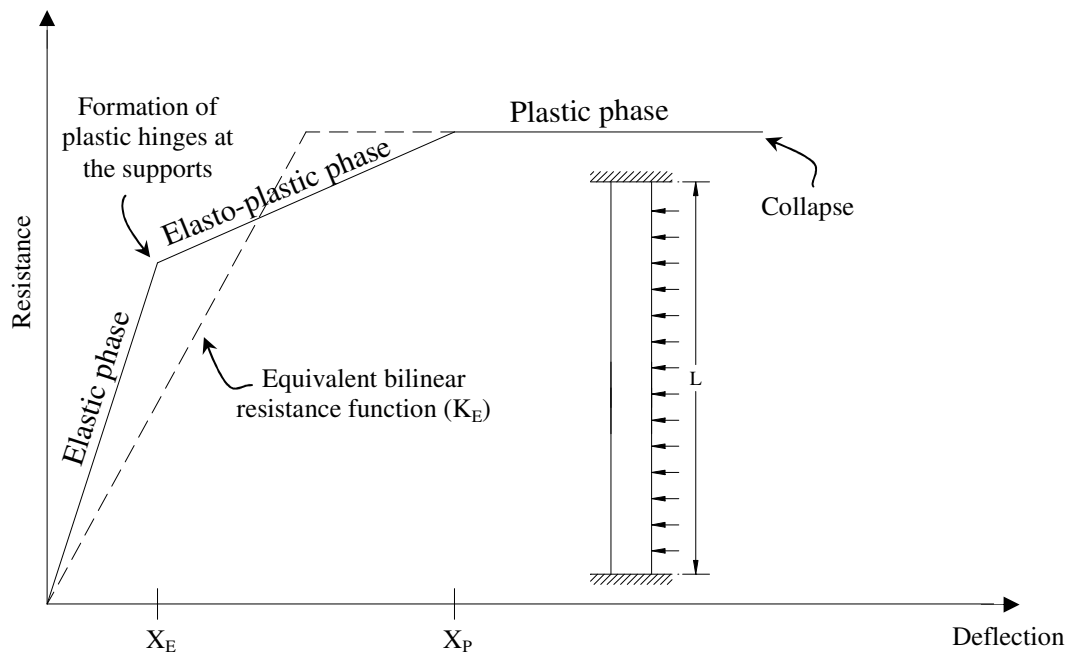


Fig. 4.14. Resistance curve for concrete columns with fixed supports

Blast loads are non-simultaneous and non-uniform. They vary along the length of the loaded member due to the variation in the range and the incident angle. Earlier in this investigation, it was proved that the blast pressure distribution can be represented by a triangular pressure that decreases linearly with a slope of 1:2. In other words, the pressure drops to zero with a horizontal distance equal to twice the value of the standoff distance (Fig. 4.15). To transform the triangular blast pressure to an equivalent uniform pressure, the load correction factor (C) which was developed in Eq. 3.1 should be applied.

The calculation of the equivalent static load on a typical column subjected to a blast scenario is presented herein. The column is assumed to be subjected to a TNT detonation of 1000 lbs placed at standoff distance that varies from 5 ft up to 100 ft from the column. The specific weight of concrete is assumed to be 150 pcf. The inertia of the cracked section is assumed to be 0.7 of the inertia of the uncracked section. Since the column has a circular cross section, only 80% of the column diameter is considered as its tributary width that is subjected to the perpendicular blast pressure. Damping was ignored in the analysis. The provided calculation is based on a standoff distance of 50 ft. Similarly, the calculation can be repeated for other values of the standoff distance.

1000 lbs at 50 ft

$$\begin{aligned} \text{Elastic modulus of concrete, } E_{con} &= 57000\sqrt{f'_c} \\ &= 57000\sqrt{3000} = 3,122,018 \text{ lb/in}^2 = 450,000 \text{ k/ft}^2 \end{aligned}$$

$$\text{Area of concrete, } A = \pi r^2 = \pi(1.75^2) = 9.62 \text{ ft}^2$$

$$\text{Gross moment of inertia, } I_g = \frac{1}{4}\pi r^4 = \frac{1}{4}\pi(1.75^4) = 7.37 \text{ ft}^4$$

Cracked moment of inertia, $I_{cr} = 0.7I_g = 5.16 \text{ ft}^4$

Density of concrete, $\gamma_{con} = 0.15 \text{ kips/ft}^3$

Self weight of column = $\gamma_{con} AH = (0.15)(9.62)(18) = 26 \text{ kips}$

$g = 32.2 \text{ ft/sec}^2$ $M = (26/32.2) = 0.807 \text{ kip-sec}^2/\text{ft}$

$K_{LM} = 0.66$ for the plastic behavior

$$K_E = \frac{307EI_{cr}}{L^3} = \frac{(307)(450,000)(5.16)}{18^3} = 122,231 \text{ kip/ft}$$

For typical bridge piers, the column height is significantly longer than the column depth. Therefore, the effect of the shear stiffness on the period of vibration of the structure is usually minimal and can be neglected.

$$T = 2\pi \sqrt{\frac{M K_{LM}}{K_E}} = 2\pi \sqrt{\frac{(0.807)(0.66)}{(122,231)}} = 0.0131 \text{ sec}$$

From the blast pressure response spectrum (Fig. 3.5), equivalent elastic static pressure = 0.164 kip/in^2

Tributary area = $(0.8 \times 3.5) (18) = 50.4 \text{ ft}^2 = 7,258 \text{ in}^2$

Calculating the load correction factor (C):

$$C = \frac{\text{area under the triangular pressure distribution}}{\text{loaded length}}$$

$$= \frac{(1+0.85)(0.5)(15) + (1+0.97)(0.5)(3)}{18} = 0.935 \text{ (Fig. 4.15)}$$

Support shear = $(0.164 \text{ kip/in}^2) (7,258 \text{ in}^2) (0.935) (0.5) = 557 \text{ kips}$

$$\text{Fixed end moment} = \frac{\omega L^2}{12} = \frac{(61.9)(18)^2}{12} = 1,671 \text{ kip-ft}$$

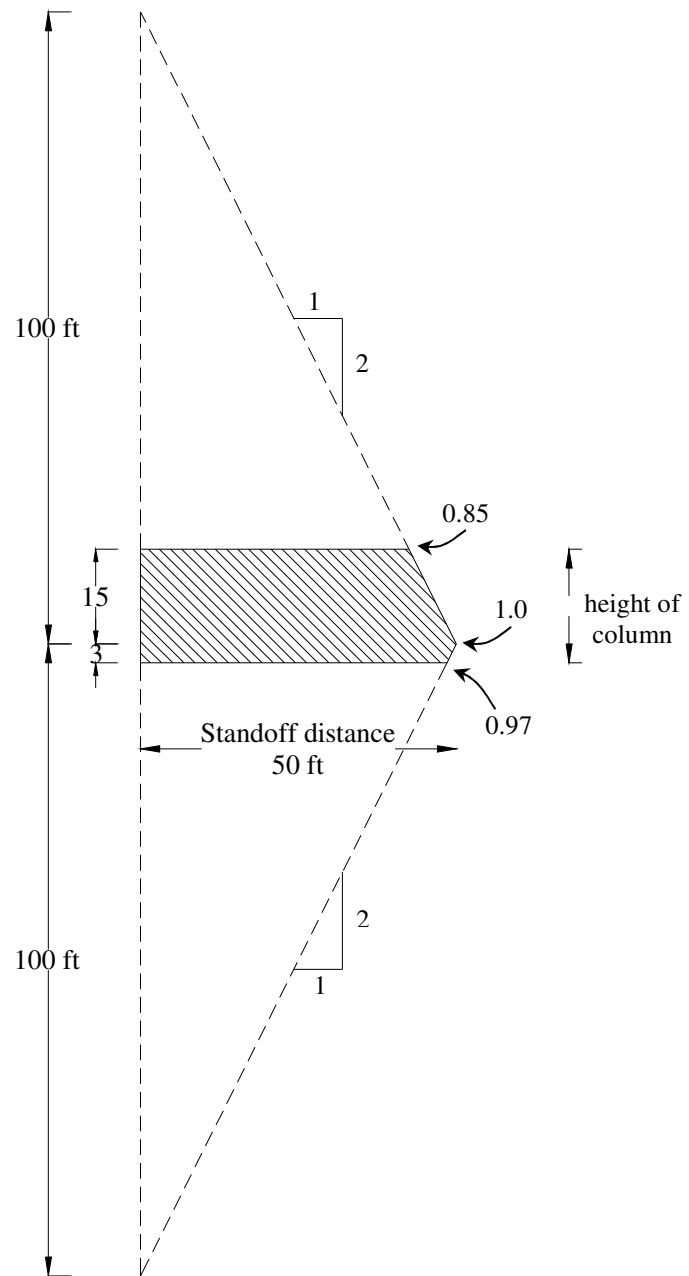


Fig. 4.15. Pressure distribution along the length of the column

4.3.3 Comparisons and discussions

The results obtained from ELS analysis were compared with those obtained from the SDOF equivalent static analysis using the blast loading response spectra. It was observed that for large values of the standoff distance, the two methods are in good agreement. However, as the value of the standoff distance decreases, the difference between the two methods starts to increase. For small values of standoff distances, the approximate SDOF analysis using the blast pressure response spectra yields more variability. Based on the results obtained from the current investigation, it is recommended to use more rigorous analysis methods for standoff distance values less than 20 ft.

The maximum shear responses calculated using ELS analysis versus the SDOF static analysis are compared in Fig. 4.16 and Table 4.1. The SDOF static analysis using an equivalent uniformly distributed load tends to underestimate the shear value for small values of the standoff distance. This can be attributed to the nonlinearity in the shape of the shear diagram which was not taken into consideration when using the SDOF analysis. For large values of the standoff distances, the shear diagram is linearly symmetrical with the top and bottom supports carrying the same share of the shearing force. However, for small values of the standoff distance, the shear diagram becomes nonlinear and the share of the bottom support – which is closer to the detonation source – tends to increase at the expense of the top support. When the standoff distance is smaller than 10 ft, the shear force at the top support was almost insignificant when compared with that of the bottom support (Fig. 4.6). For clarity, the summation of shear forces at both supports was calculated, and then compared using ELS analysis and SDOF analysis (Fig. 4.17 and

Table 4.2). It was observed that the total shear at both supports obtained using SDOF analysis and ELS were in good agreement for all the values of the standoff distance. This illustrates the effect of the nonlinearity in the shape of the shear force diagram on the behavior of structural elements subjected to close proximity of blast loads.

Therefore, for small values of the standoff distance in the SDOF analysis, it could more realistic to represent the blast pressure by equivalent concentrated load acting at the level of the detonation source. This will result in higher shear value at the support closer to the detonation source. More conservative results can be obtained if the total value of shear is assumed to act at the support which is closer to the detonation source. Furthermore, in the SDOF analysis, it was roughly assumed that 80% of the column diameter is subjected to the blast pressure. Further investigations are required to determine a practical value for the portion of the cylindrical face subjected to blast loading.

Table 4.1. Comparison between the maximum shear values of ELS versus SDOF

R	Z	C_r	ELS values	modified ELS values*	SDOF	% difference
5	0.5	10.5	2620	27510	12406	-55
10	1	8.5	1150	9775	4382	-55
20	2	6.6	580	3828	1952	-49
50	5	3.6	220	792	557	-30
100	10	2	64	128	133	4

Table 4.2. Comparison between the total shear values of ELS versus SDOF

R	Z	C_r	ELS values	modified ELS values*	SDOF	% difference
5	0.5	10.5	2620	27510	24812	-10
10	1	8.5	1150	9775	8764	-10
20	2	6.6	810	5346	3904	-27
50	5	3.6	420	1512	1114	-26
100	10	2	128	256	266	4

* *modified ELS values = (ELS values) x (C_r)*

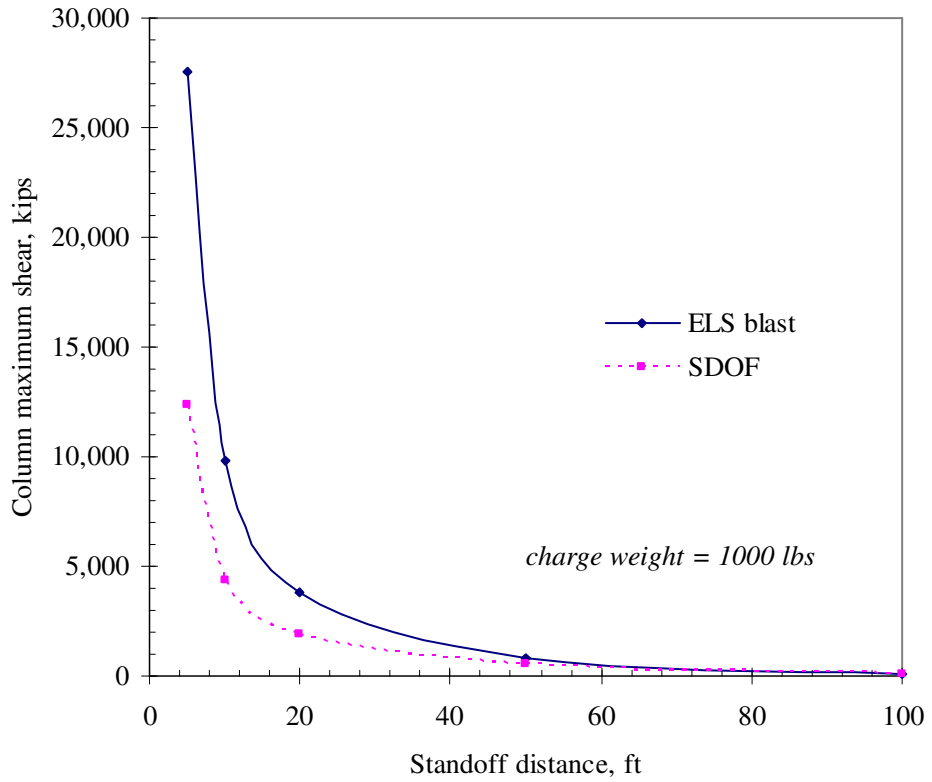


Fig. 4.16. Maximum shear calculated using ELS analysis versus SDOF analysis

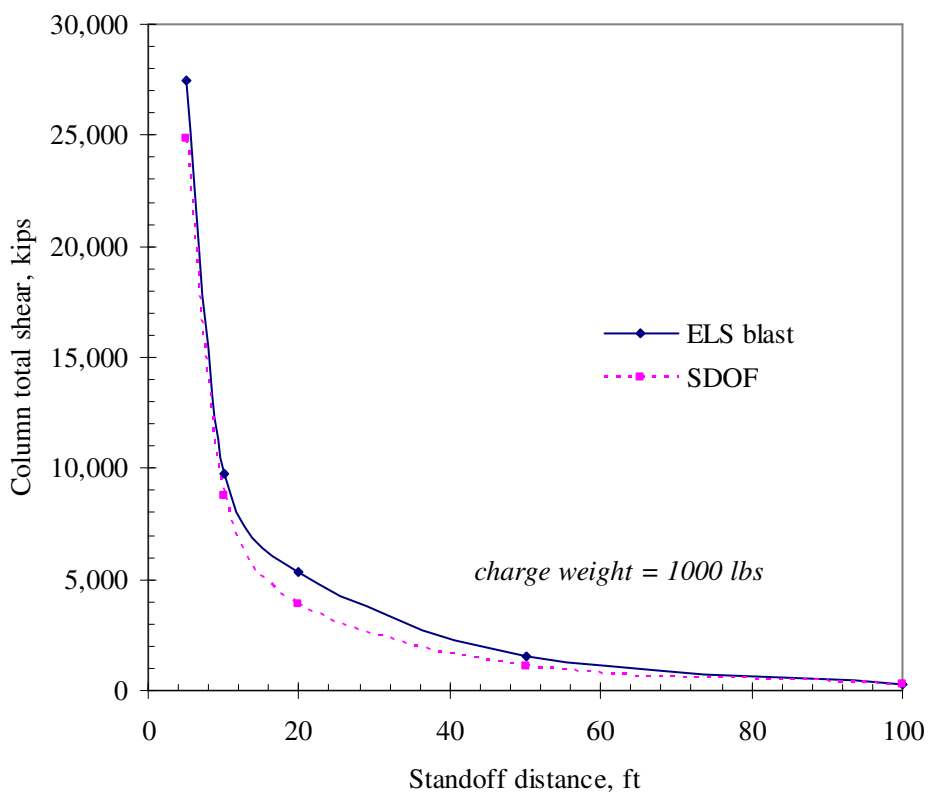


Fig. 4.17. Summation of total shear calculated using ELS analysis versus SDOF analysis

From the analytical investigation performed on the response of concrete columns subjected to blast hazards, the following observations were made:

- For distant blasts, it was observed that the blast pressure acting on the column was similar to that of a uniformly distributed load. Flexural cracks were developed at the location of maximum bending moments. However, with the decrease in the standoff distance, more localized behavior was observed. The shear force diagram became nonlinear and the maximum moment was recorded at the level of the detonation source. In addition to the flexural cracks, shear cracks were formed. These cracks were induced throughout the length of the column and propagated through its entire cross section. For close proximity blast scenarios, failure of the column took place due to the intensive cracking and the breaching of concrete.
- The results obtained from ELS analysis were compared with those obtained from the single degree of freedom (SDOF) static analysis using the blast loading response spectra. It was observed that for large values of the standoff distance, the two methods are in good agreement. However, as the value of the standoff distance decreases, the difference between the two methods starts to increase. The SDOF static analysis using an equivalent uniformly distributed load tends to underestimate the shear value for small values of the standoff distance. This can be attributed to the nonlinearity in the shape of the shear diagram which was not taken into consideration when using the SDOF analysis.

CHAPTER 5

BRIDGE GLOBAL RESPONSE TO BLAST LOADS

To understand the global behavior of bridges subjected to blast loads, a typical prestressed concrete girder superstructure bridge will be analyzed using the ELS software. The bridge geometry, materials, dimensions, and details are based on the FHWA design example (Wassef et al, 2003). In this example, the design of the bridge was based on the second edition of the AASHTO-LRFD Bridge Design Specification. To simplify the analyzed model, minor modifications were applied to the original bridge details (Figs 5.1 and 5.2). The bridge consisted of two simple spans; each 110 ft long. For live loads, continuity between the two spans was achieved using a common concrete deck supported on the prestressed girders. The thickness of the deck slab was 8". The top and bottom reinforcement for the deck slab were assumed to be the same. This reinforcement consisted of #5 @ 7" in the transverse direction perpendicular to the prestressed girders and #5 @ 12" in the longitudinal direction. The concrete compressive strength and steel yield strength used in the analysis of the deck slab were 4 ksi and 60 ksi, respectively.

The prestressed girders were AASHTO Type VI. The girders were spaced at 9'-8". For prestressing, grade 270 steel strands were used. The total prestressing force was 1600 kips with a constant eccentricity of 31". The stirrups used for the prestressed girders were extended upward in the deck slab to provide composite action. The prestressed girders were supported on 3.5" thick elastomeric bearing pads (Fig. 5.3). To support the girders laterally, 12" thick concrete diaphragms were provided between the girders at the ends and at third-points along the length of each span. A common 36" thick intermediate concrete diaphragm was provided between both spans.

The substructure consisted of multi-column intermediate bent having 4 circular columns spaced at 14'-1". The column diameter and height are 3.5' and 18', respectively. The column reinforcement consisted of 16 # 8 bars longitudinal reinforcement and # 3 stirrups @ 12 inches with 3 inches cover. The column reinforcement was extended upward in the 4' x 4' cap beam and downward in the concrete footing. Reinforcement for the cap beam consisted of 14 # 9 at the top, 9 # 8 at the bottom, and 4 # 7 on each side. The footings were 12' x 12' with a depth of 3'. The compressive strength of concrete and yield strength of steel used in the analysis of the substructure were 3 ksi and 60 ksi, respectively. A cross section of the bridge from the design example (Wassef et al, 2003), and the reinforcement details of the bridge model which is analyzed using ELS are presented in Figs. 5.1 and 5.2, respectively.

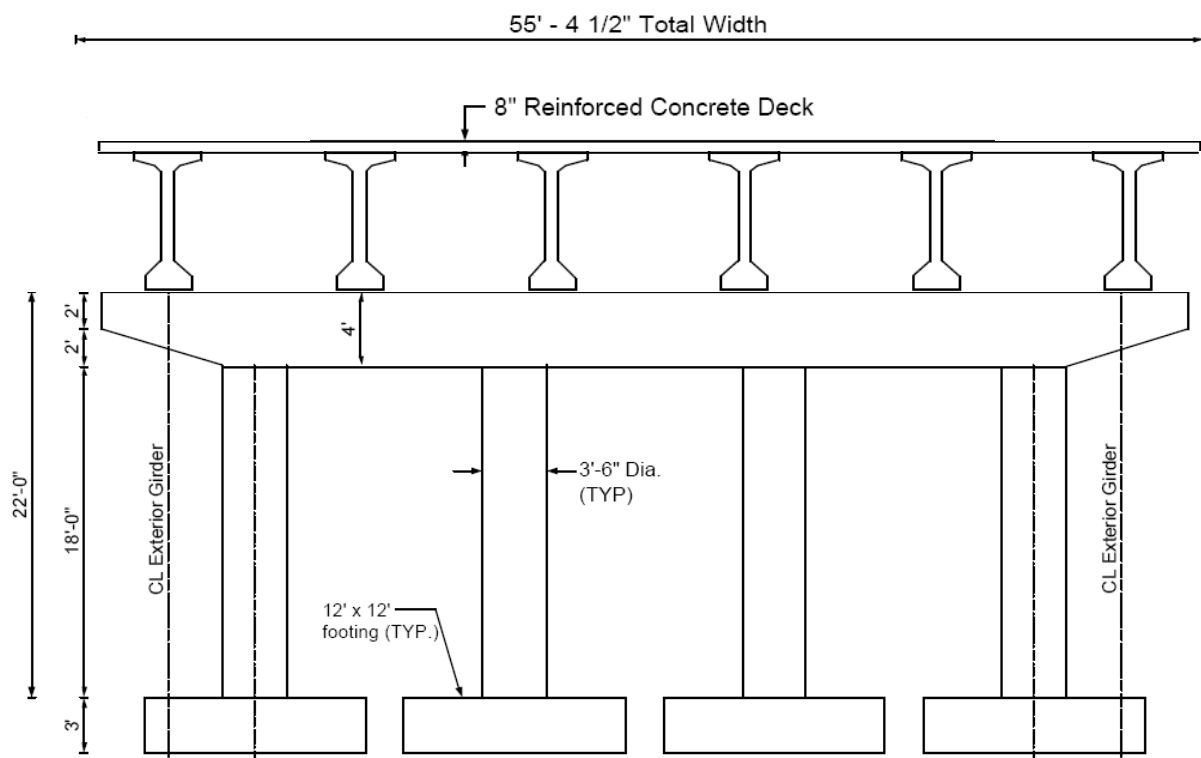


Fig. 5.1. Cross section of bridge (Wassef et al, 2003)

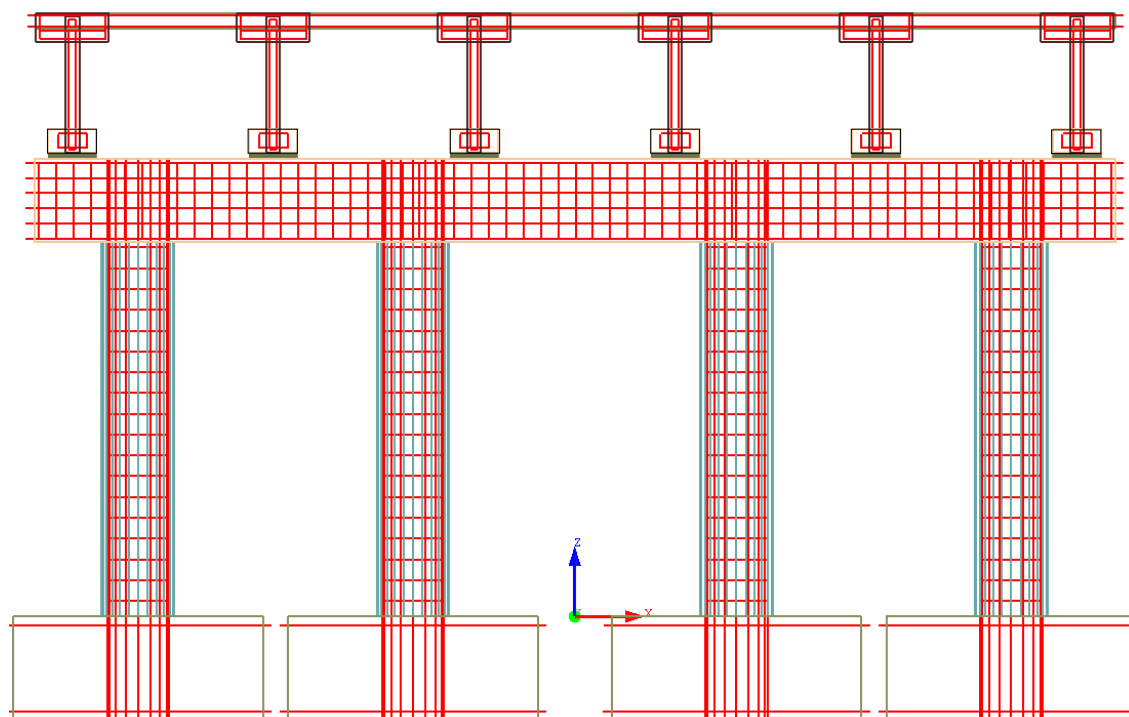


Fig. 5.2. Reinforcement details of the bridge model (ELS)

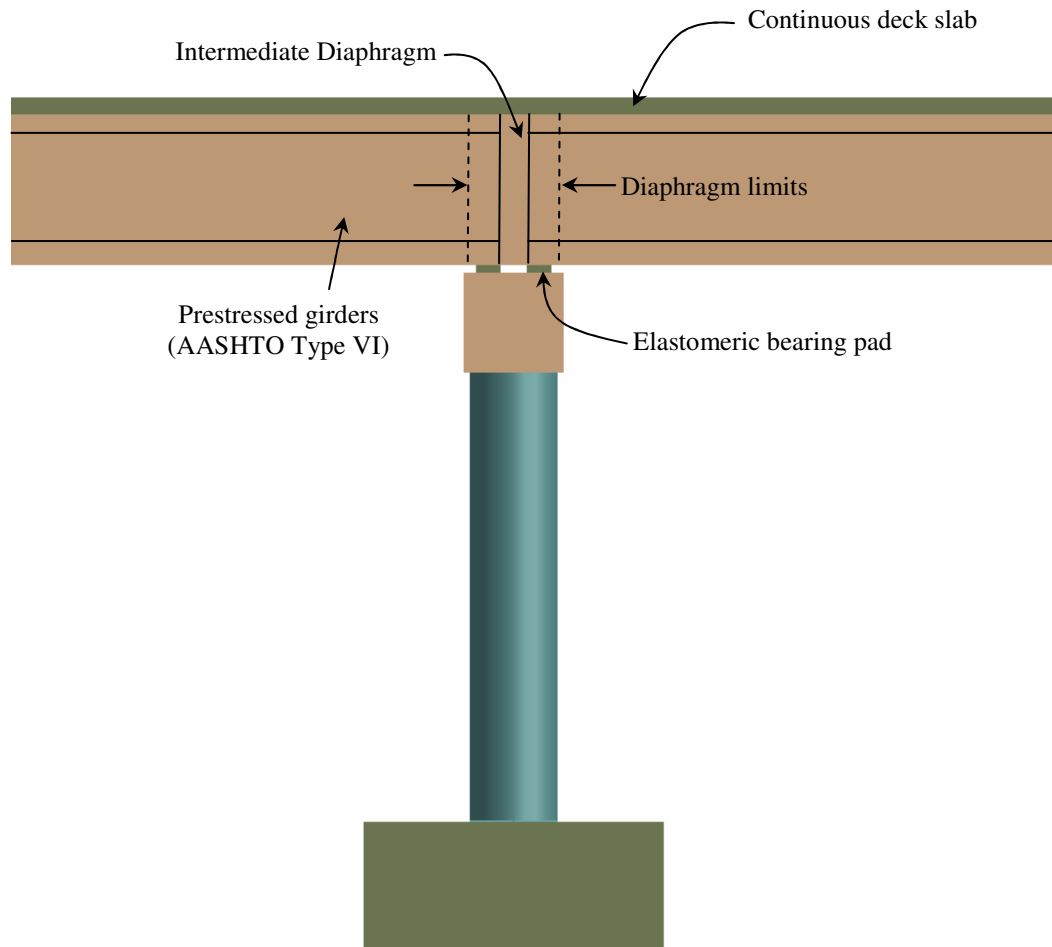


Fig. 5.3. Prestressed girders supported on elastomeric bearing pads

The bridge model will be analyzed for several blast scenarios. These scenarios can be classified into two main categories; above deck and below deck. For each one of these two categories, the detonation charge is assumed to be located either closer to the middle of one of the bridge spans or closer to the intermediate bent. In the blast analysis, the bridge is assumed to be free from any traffic. Hence, only the self weight of the bridge is taken into consideration. A perspective view of the bridge model prior to being subjected to the blast scenario is presented in Fig. 5.4.

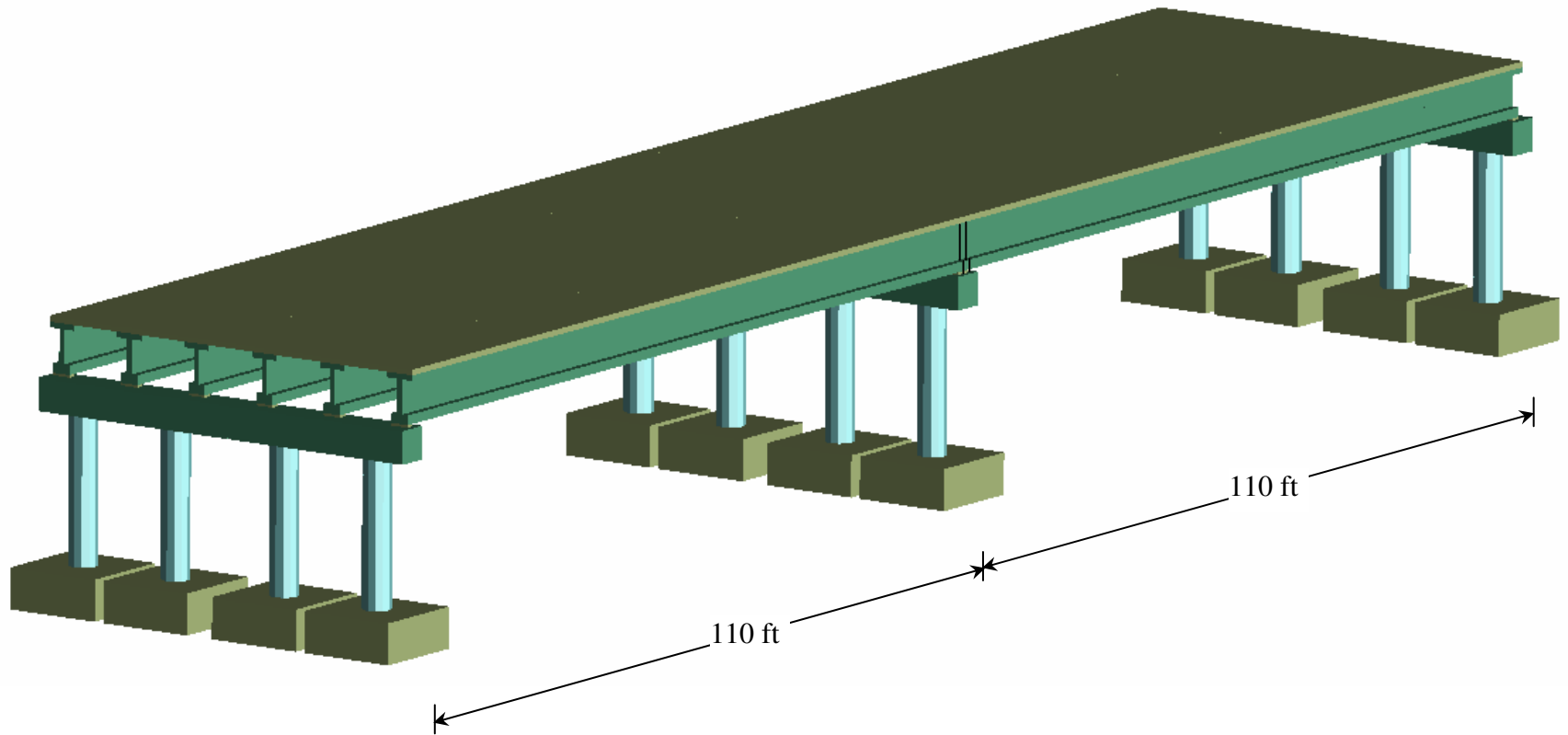


Fig. 5.4. View of the bridge model prior to being subjected to blast scenarios

(End diaphragms are not shown for clarity)

5.1 Below Deck Blast Scenario

The below deck blast scenario can be a result of a vehicle explosion, a hand charge, or a small brief case. For the vehicle explosion, the location of the vehicle can be at midspan or somewhere in-between the midspan and one of the bents. If the vehicle is located closer to midspan, the standoff distance between the columns and the detonation source is usually large, and hence, the threat to the columns is minimal. In this scenario, the deck slab and concrete girders will be subjected to uplift pressure from the blast. This uplift pressure can be devastating because the slab and girders were not designed to withstand this uplift force. Another extreme scenario can occur if the vehicle is located closer to the bent or if hand charges are attached to one or more columns. In this case, the columns are subjected to severe damage due to the insufficient standoff distance. In this case, the blast waves may result in loss of one or more columns, and may lead to the potential collapse of the bridge. The results of these extreme cases are presented herein.

5.1.1 Blast scenario close to the bridge midspan

When the bridge is subjected to a below deck detonation at midspan, the hemispherical blast waves travel towards the bridge structure. For typical bridges, the height of the bridge deck above the ground level is less than midspan length, and hence, the girders and deck are the first structural elements affected by the blast. For conventional design, the steel reinforcement of the deck slab is designed to carry the stresses produced by the dead and live loads applied to the bridge. At the middle of the deck slab between adjacent girders, the bottom fiber of the slab is subjected to tensile stresses, and hence, primary steel reinforcements are located at the bottom of the slab. This arrangement is reversed

for the slab section above the girders to resist the negative moment. However, this typical steel reinforcement is insufficient for resisting blast loads. When the deck slab is subjected to blast pressure from below, the top fiber of the deck slab will be subjected to tensile stress. If the top reinforcement is not sufficient, then the slab will crack and eventually fail (Fig. 5.5). Due to the uncertainty in blast scenarios, the top and bottom reinforcement of the deck should be the same throughout the cross section. Furthermore, if the number of shear connectors between the deck slab and the prestressed girders is insufficient, the uplift pressure created by the blast can separate the deck from the girders. Hence, shear connectors must be designed to withstand additional tensile forces created by the blast loads.

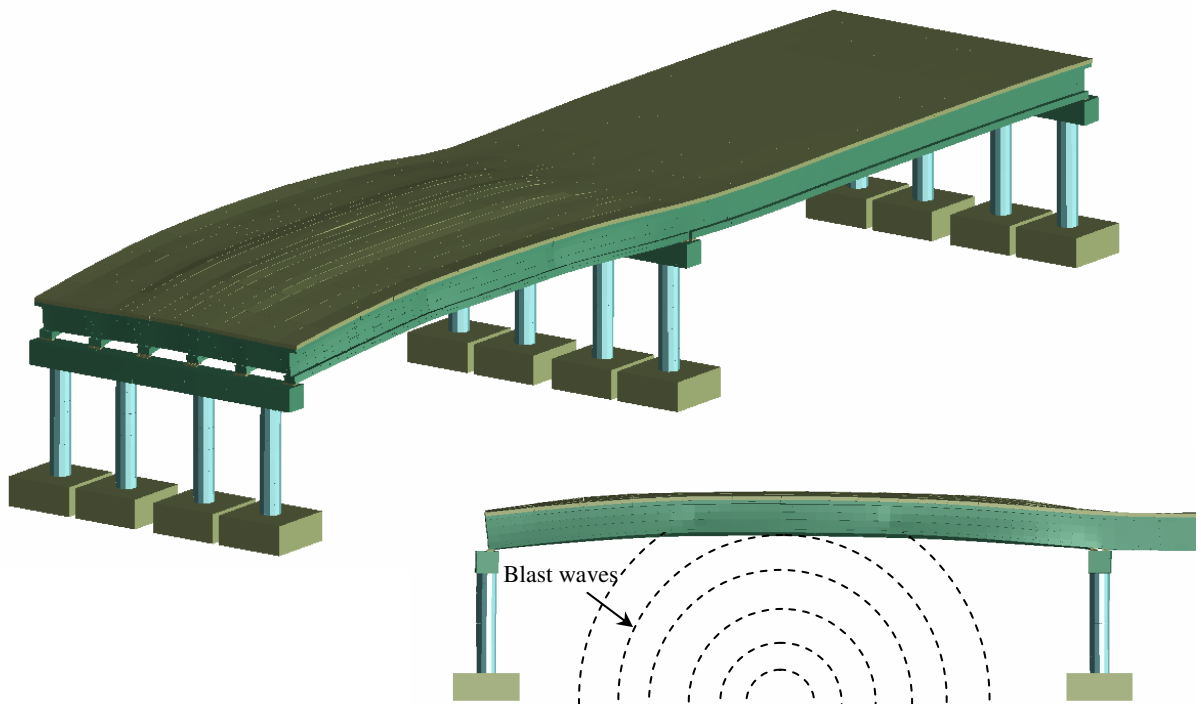


Fig. 5.5. Response of deck slab to a blast scenario from below (scale 1:15)

The behavior of the girders is governed by the superposition of: 1) its response due to the self weight of the bridge structure, 2) the uplift pressure resulting from the blast scenario. To verify the shear and moment diagrams obtained using ELS, SAP 2000 was used to replicate the response of a typical prestressed girder subjected to uplift pressure. Schematics of the shear force diagram (SFD) and bending moment diagram (BMD) of the bridge girders are presented in Figs. 5.6 and 5.7, respectively.

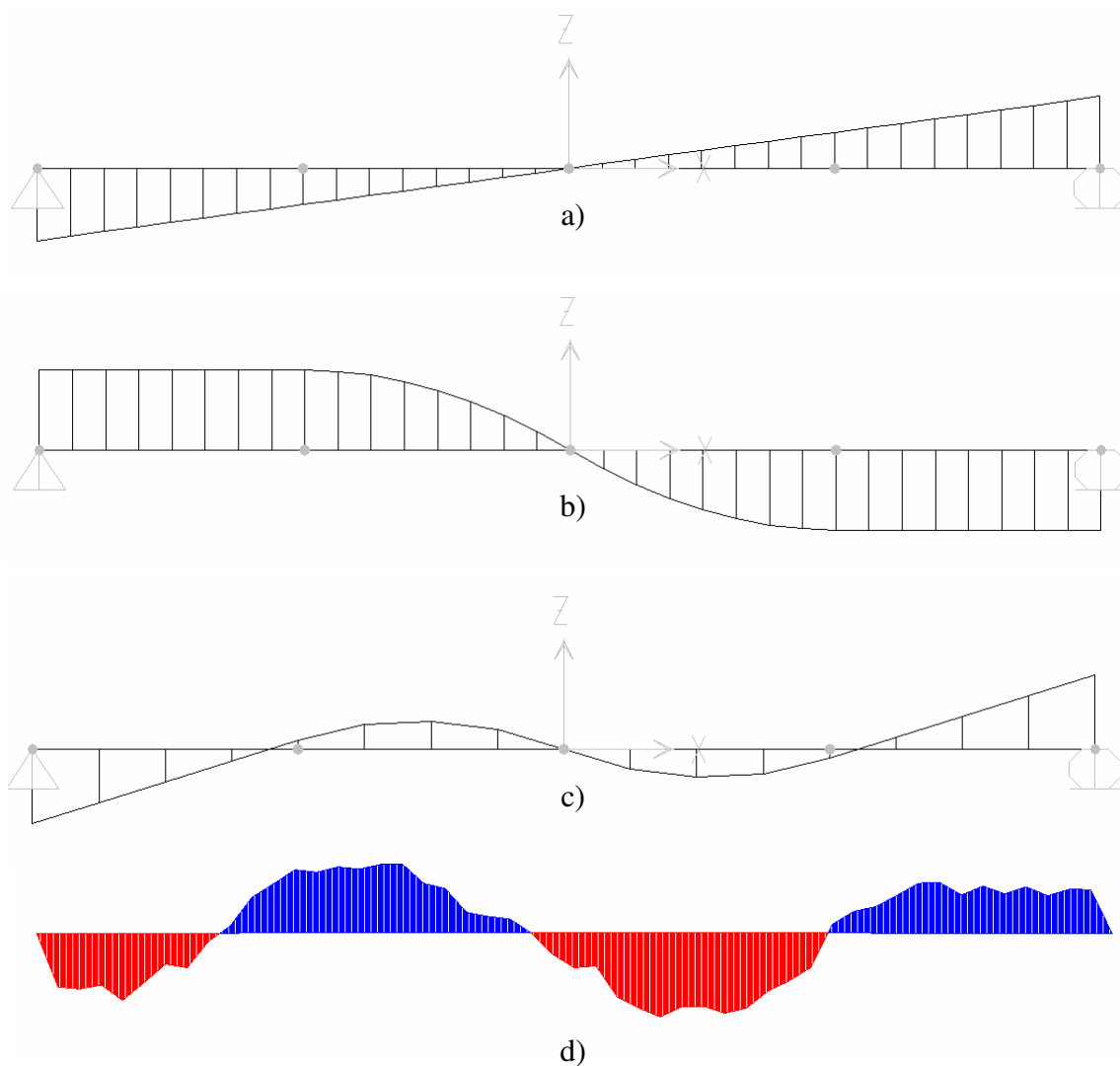


Fig. 5.6. Schematics of the SFD of a bridge girder subjected to below-deck blast scenario
a) self weight b) blast load c) resultant d) ELS resultant

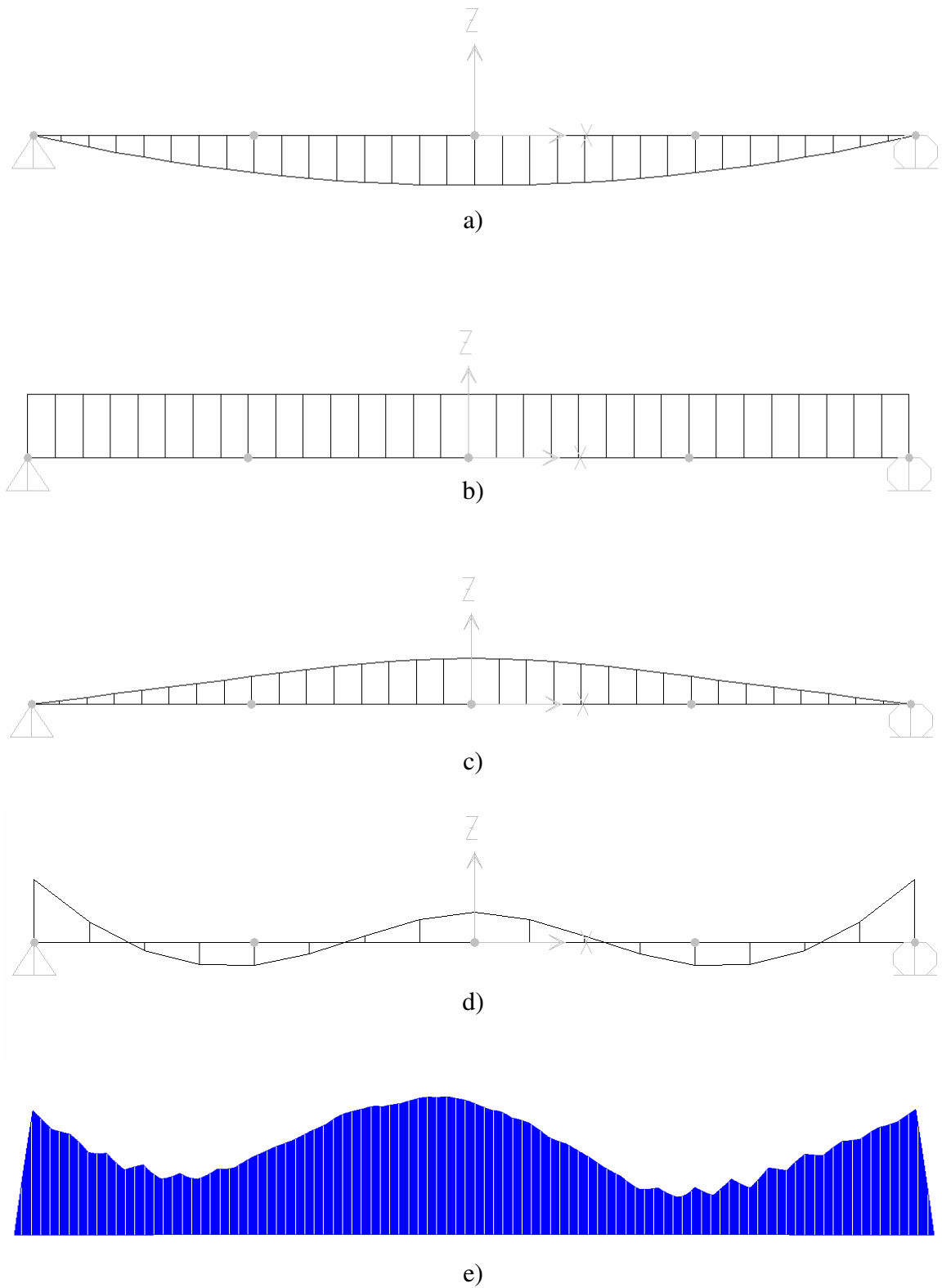


Fig. 5.7. Schematics of the BMD of a bridge girder subjected to below-deck blast
 a) self weight b) prestressing c) blast load d) resultant e) ELS resultant

From the simulation performed on the bridge model using ELS, it was observed that the behavior of the bridge model due to a blast scenario located at midspan below the deck depends on the type of bearing between the girders and the substructure. If the girders are only resting on the elastomeric bearing (free bearing), then they are not restrained against upward movement. In this case, if the uplift forces acting on the girders exceed the gravity loads, then the girders will move vertically upward departing from the substructure. If the blast scenario takes place at an exterior span of the bridge, it is more likely to have this separation between the girders and the substructure over the abutment rather than over the intermediate pier (Fig. 5.8). This is mainly because the gravity loads at the abutment are of lesser value than those at the intermediate pier. Furthermore, the deck slab provides some continuity at the intermediate pier. Hence, it is important to implement more mitigation measures at the abutments where it is more likely to encounter separation between the girders and the substructure.

A possible mitigation technique against this vertical movement is to restrain the girders against uplift. A typical fixed bearing connection consists of shear studs embedded in the bottom flange of the concrete girders and welded to a steel plate at the bottom of the girders. This plate is connected to another sole plate which is then connected to the abutment by anchor bolts (Fig. 5.9). This detail can be sufficient to prevent the upward movement for small values of uplift pressure. However, if the uplift pressure created by the blast scenario exceeds the capacity of the anchor bolts, then the girders will be released and they can move vertically similar to the case of the free bearing. If the anchor bolts are strong enough to withstand the tensile forces, another mode of failure can take

place due to the separation between the bottom flange and the web of the concrete girders (Fig. 5.10).

After the girders are uplifted, they will rebound back on the substructure. If the provided seat width is not enough, the girders will fall to the ground and this can result in the collapse of one or more spans of the bridge. Furthermore, the blast waves can result in the lateral movement of the abutment and this can aggravate the situation (Fig. 5.11). Hence, it is important to ensure that the seat width is long enough to hold the rebounding girders.

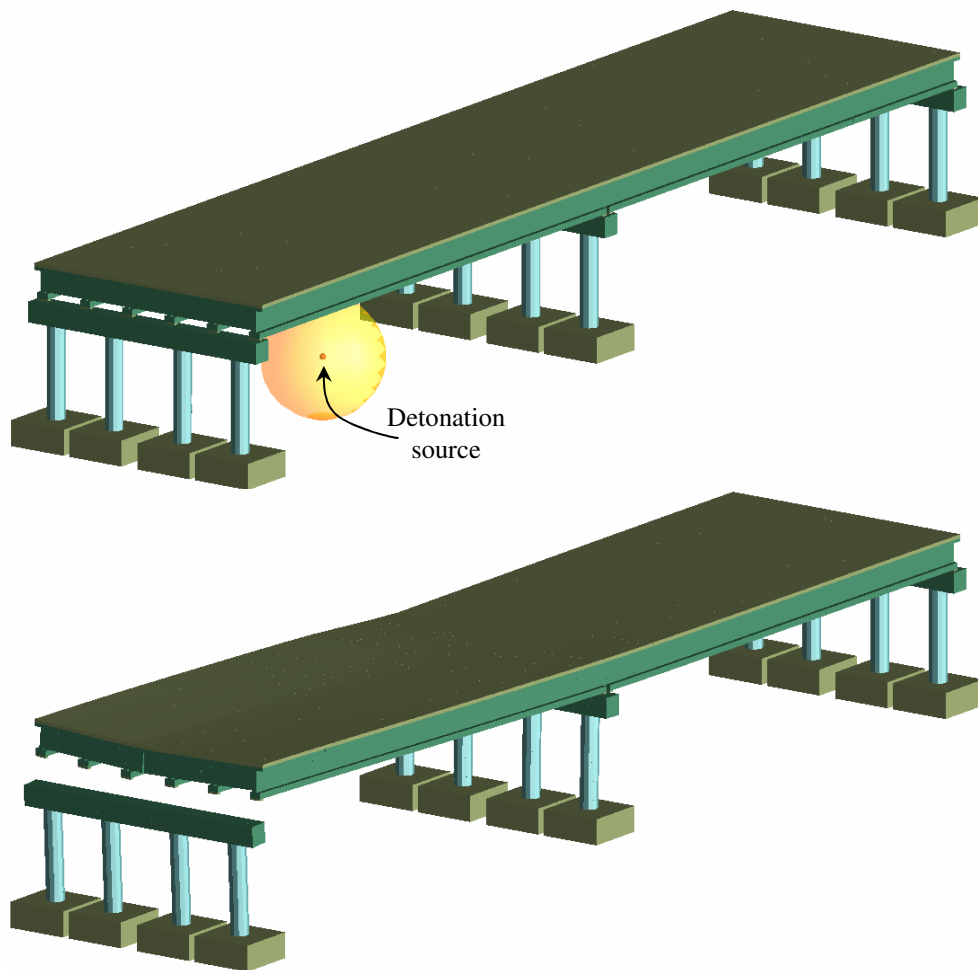


Fig. 5.8. Separation between the girders and the abutment

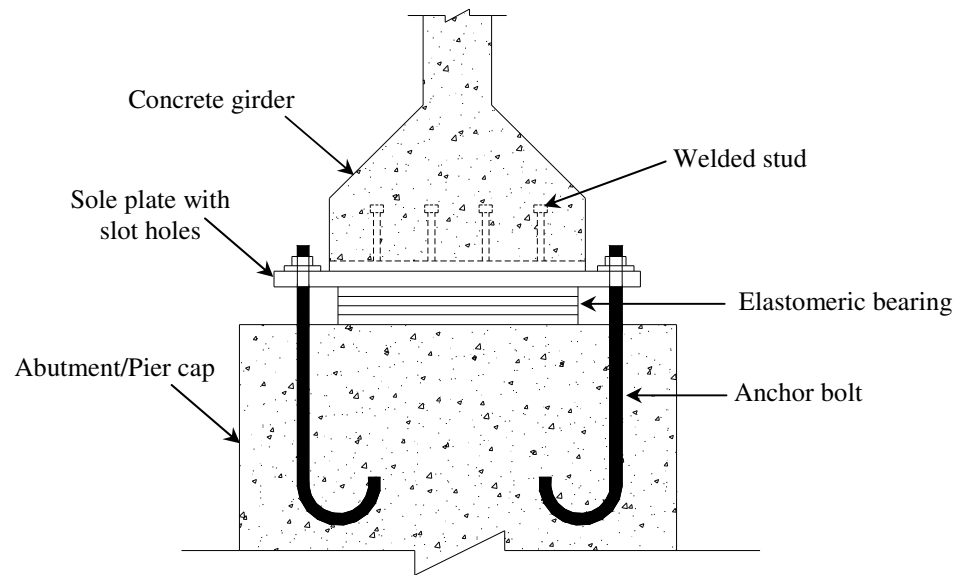


Fig. 5.9. Fixed bearing connection

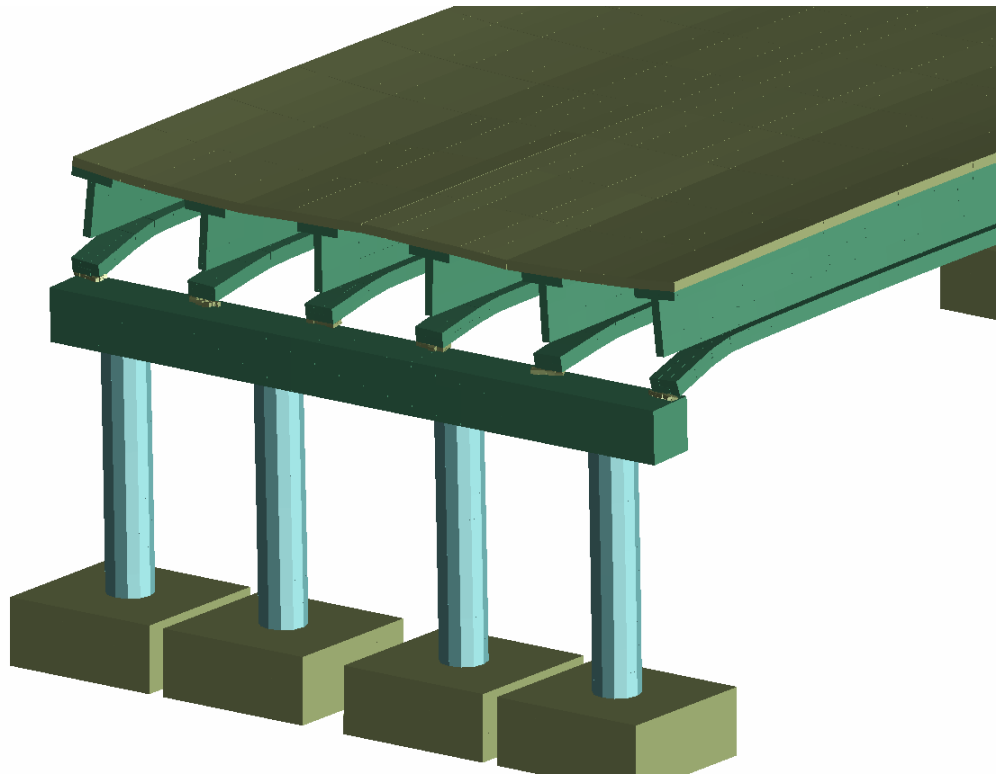


Fig. 5.10. Separation between the bottom flange and the web of the prestressed girders

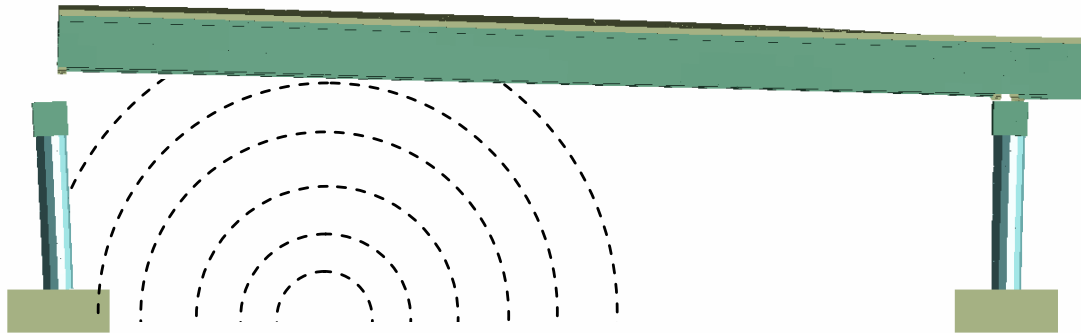


Fig. 5.11. Lateral movement of abutment due to blast waves

The behavior of concrete columns subjected to blast scenarios was discussed earlier in this study. Schematics of the SFD and BMD of a bridge column subjected to below-deck blast scenario close to the midspan are presented in Fig. 5.12. It was observed that the maximum shear was recorded at the bottom of the column at the intersection with the footings, while the shear at the top of the column was smaller in magnitude. In addition, the maximum negative moment was recorded at the bottom support, while the top support was mainly subjected to positive moment. This behavior can be attributed to the elastomeric bearing pads which allow for relative rotation between the cap beam and the prestressed girders. Therefore, the upper support of the column is less rigid than its lower support.

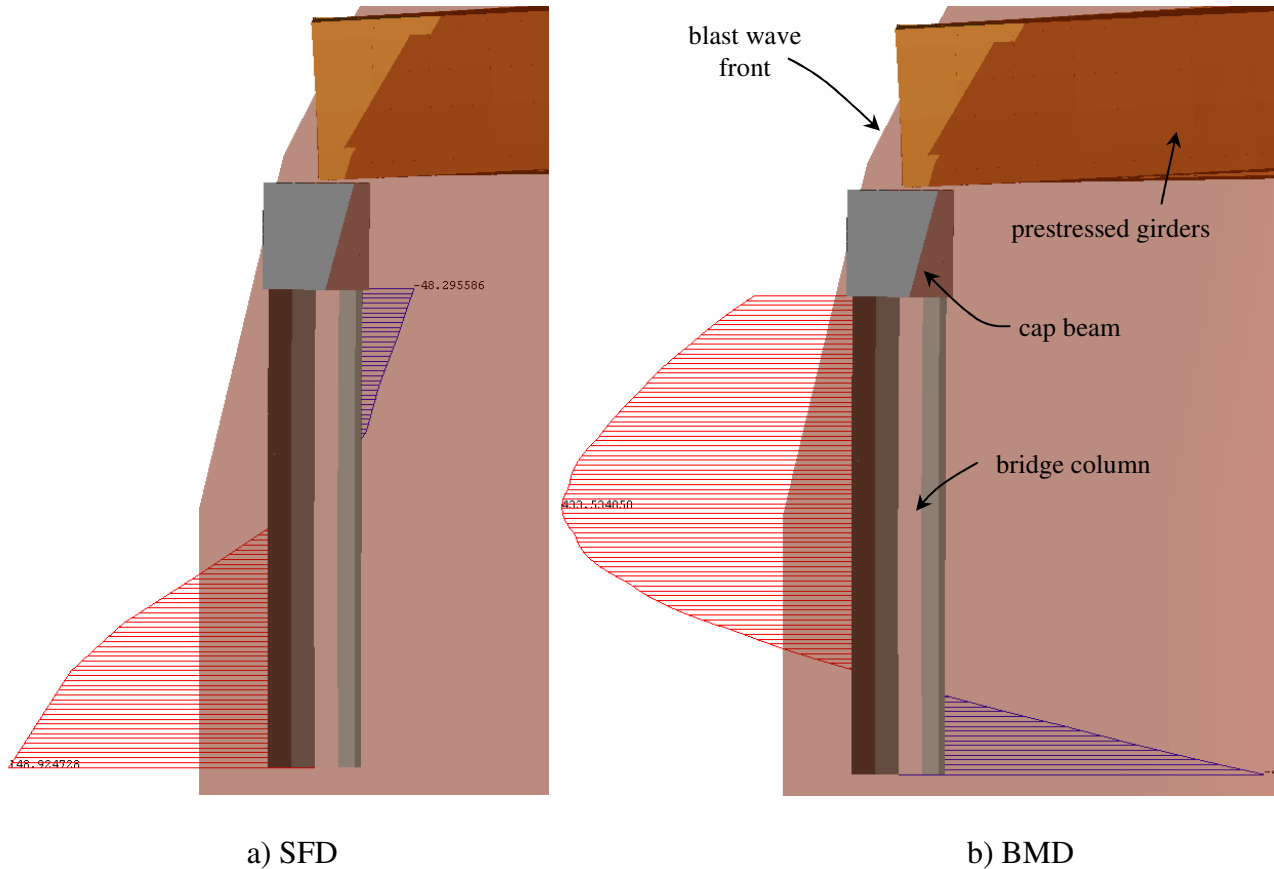


Fig. 5.12. Schematics of the SFD and BMD of a bridge column subjected to below-deck blast scenario

It was also observed that the blast waves resulted in the transverse movement of the girders (Fig. 5.13). This can apply significant torsional forces on the girders. Therefore, it is essential to provide lateral stiffness by providing sufficient number of concrete diaphragms. Concrete diaphragms are preferable over steel cross frames because they exhibit more stiffness, and enhance the continuity of the bridge in the transverse direction. As a result, all girders act together as a single unit instead of having individual behavior for each girder

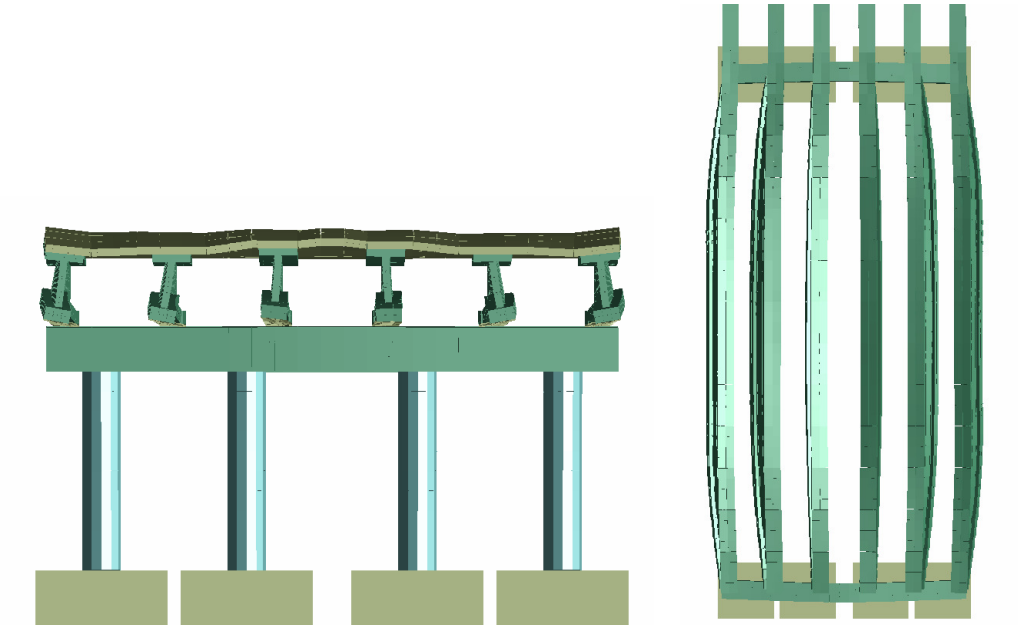


Fig. 5.13. Lateral displacement of bridge girders (scale 1:20)

5.1.2 Blast scenario between the midspan and the bridge pier

To examine the effect of blast scenarios located somewhere between the midspan and the bridge pier, the bridge was subjected to a blast detonation located 10 ft away from the intermediate pier below the deck slab. It was observed that the failure of the bridge is initiated by the cracking at the top fiber of the deck slab followed by the flexural failure of the prestressed girder (Fig 5.14). As a result of the blast wave pressure, the intermediate bent was subjected to lateral bending (Fig. 5.15). The magnitude of this bending depends to a great extent on the standoff distance between the pier and the detonation source. The best mitigation measure is to provide minimum standoff distance so as to prevent blast scenarios at close proximity to the pier. To mitigate the lateral bending of the bent, the columns should be designed to exhibit significant plastic behavior and energy absorption capacity. This can be achieved by using ductile fiber reinforced concrete (FRC) and closely spaced stirrups.

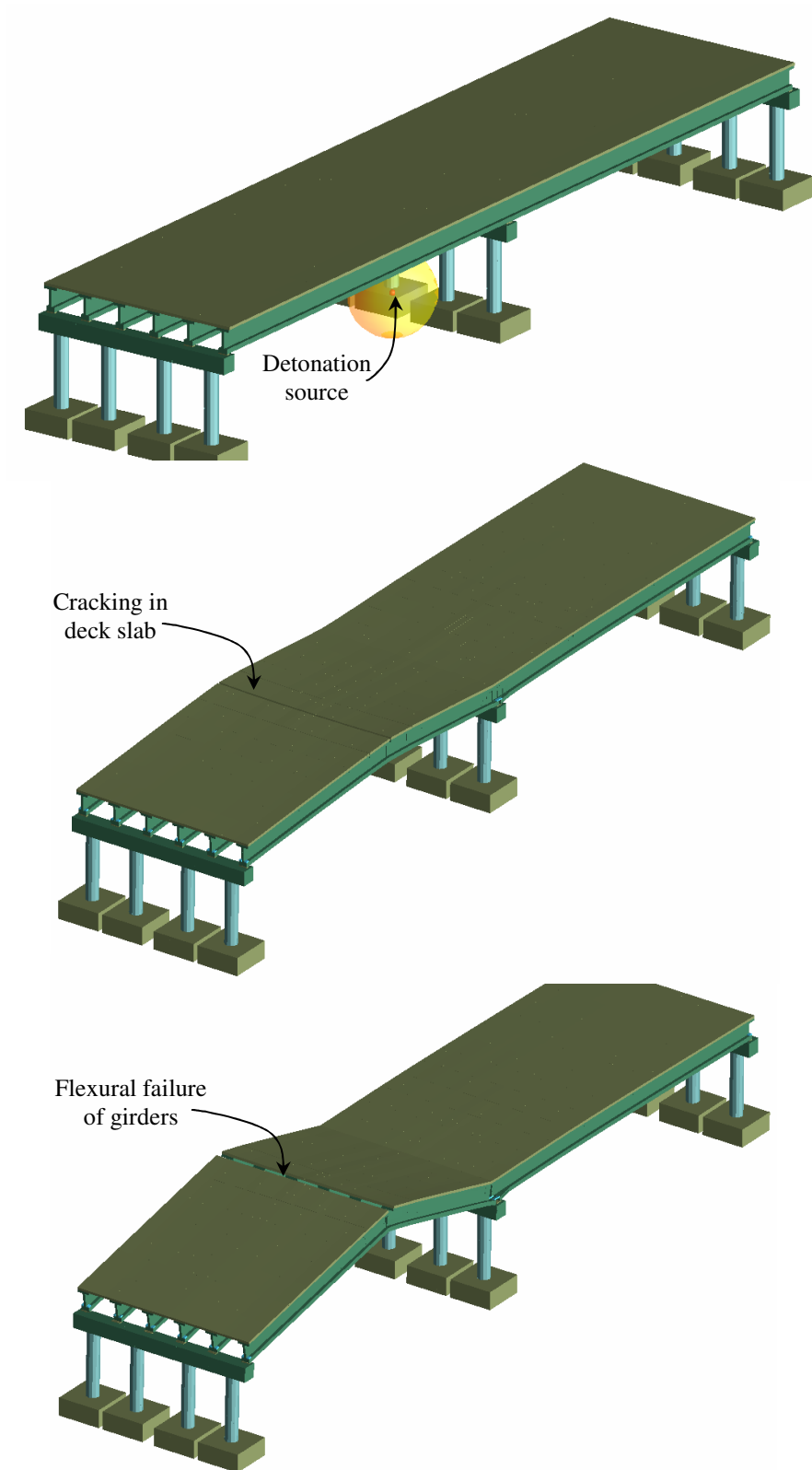


Fig. 5.14. Response of the bridge model to a below-deck detonation between the midspan and the pier

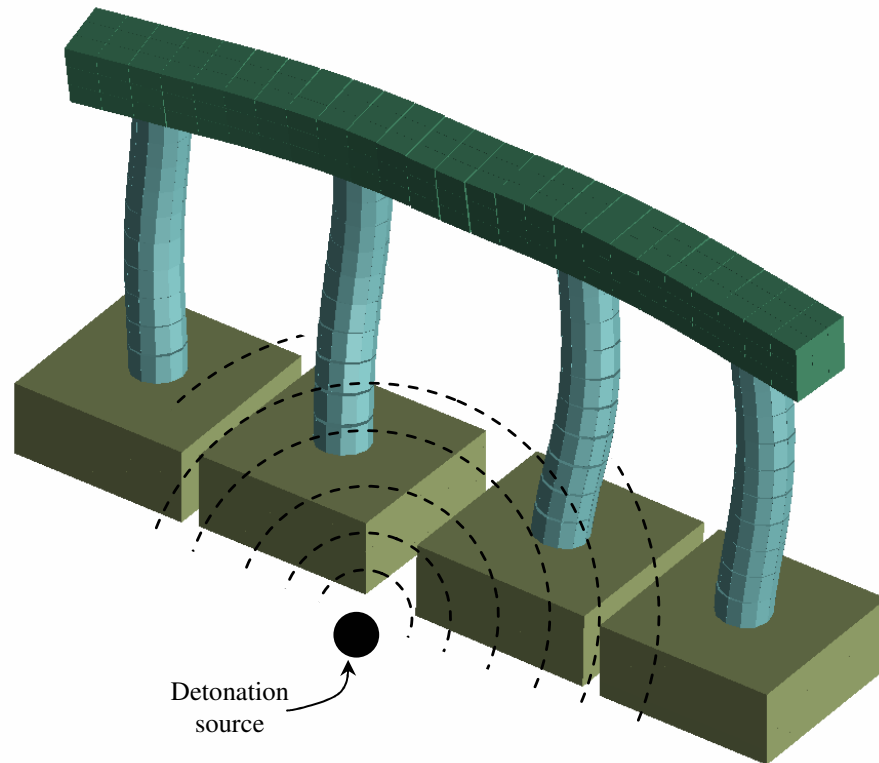


Fig. 5.15. Intermediate bent subjected to lateral bending (scale 1:50)

5.1.3 Blast scenario underneath the bridge bent

To examine the effect of blast scenarios at close proximity to the pier, the bridge model was analyzed for a detonation charge located exactly at the location of the pier at the center of the bent columns. The nature of this blast scenario depends to a great extent on the type of pier and the spacing between its columns. If the columns are closely spaced, then it is more likely for the blast to be a result of a small charge weight either hand emplaced or embedded in a brief case. However, if the spacing between the columns is large enough to allow the passage of a vehicle loaded with explosives, then this blast scenario can become devastating. As explained earlier, if the bearing does not restrain the bridge girders against uplift, then the blast waves can result in lifting the bridge over the

pier. This behavior depends on the charge weight used in the attack. Small charge weights are expected to trigger localized damaged, whereas heavier charges can result in lifting the bridge. Furthermore, the blast pressure can trigger flexural cracks at the top fiber of the deck slab as well as the bridge girders (Fig. 5.16). Hence, it is recommended to restrain the upward movement of the superstructure. The deformed shape of the pier cap is presented in Fig. 5.17.

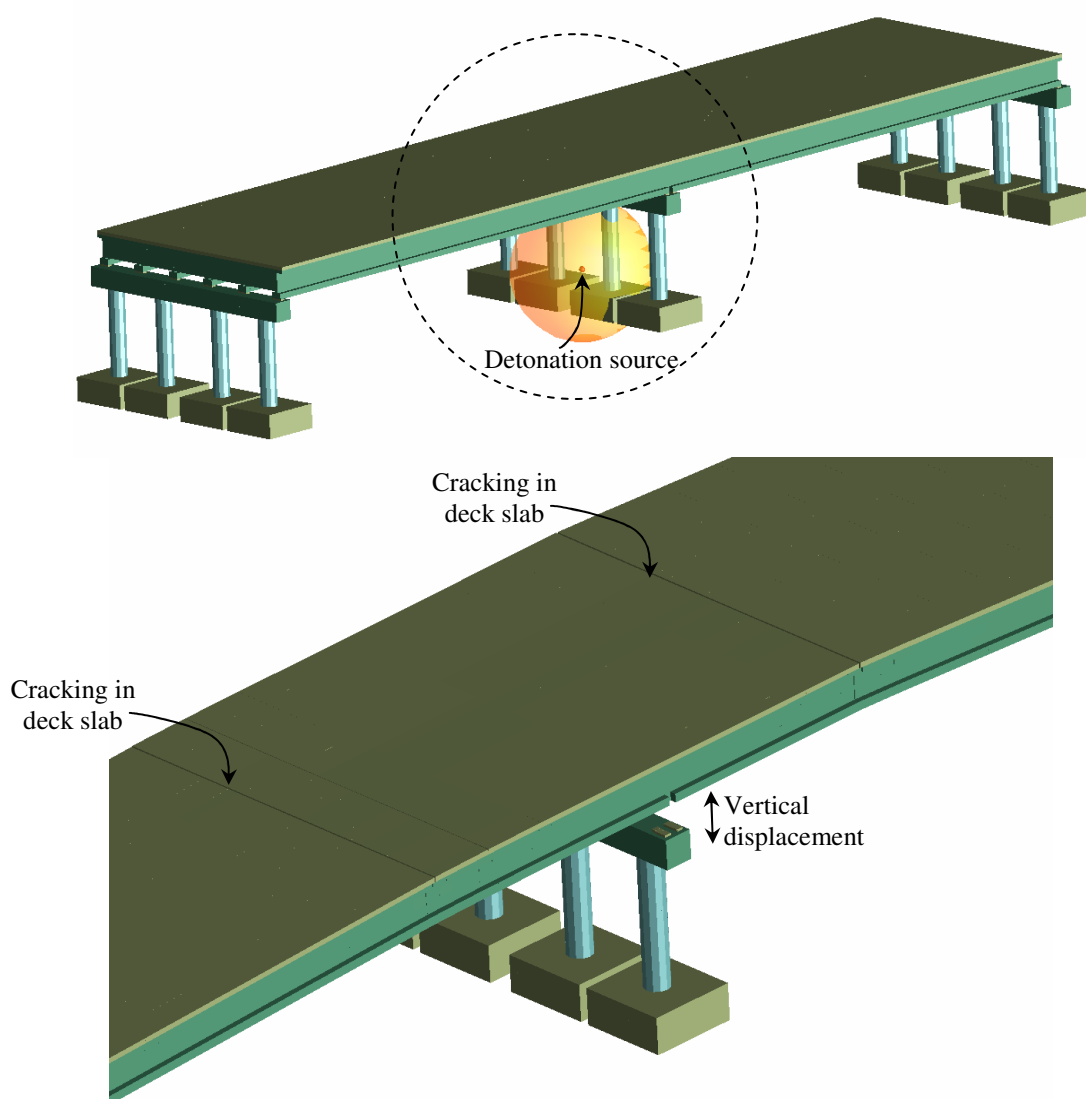


Fig. 5.16. Rising of bridge superstructure if the girders are not restrained against upward movement

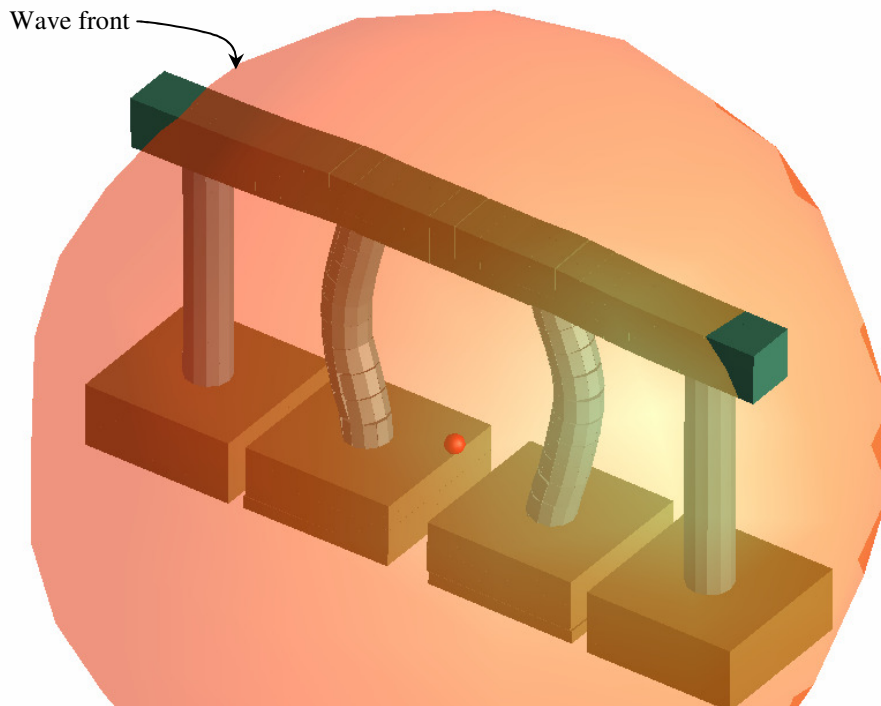


Fig. 5.17. Deformed shape of the intermediate bent (scale 1:25)

The behavior of the bridge superstructure at the intermediate pier is dependant on the bearing type. For expansion bearings, relative movement between the adjacent spans of the bridge is expected. However, for fixed bearings where the girders of adjacent spans are connected by a common concrete diaphragm, the two adjacent spans behave integrally.

The bridge model was analyzed for the case of integral piers where the girders are rigidly connected to the pier cap. It was observed that the failure is initiated at the columns either by tensile failure of columns due to uplift or by separation between the columns and the pier cap (Fig. 5.18). For the integral piers at the far ends of the span, the failure was

initiated by cracking of the cap beam followed by separation between the cap beam and the columns (Fig. 5.19). This behavior is mainly attributed to the upward movement of the superstructure as a result of the blast waves.

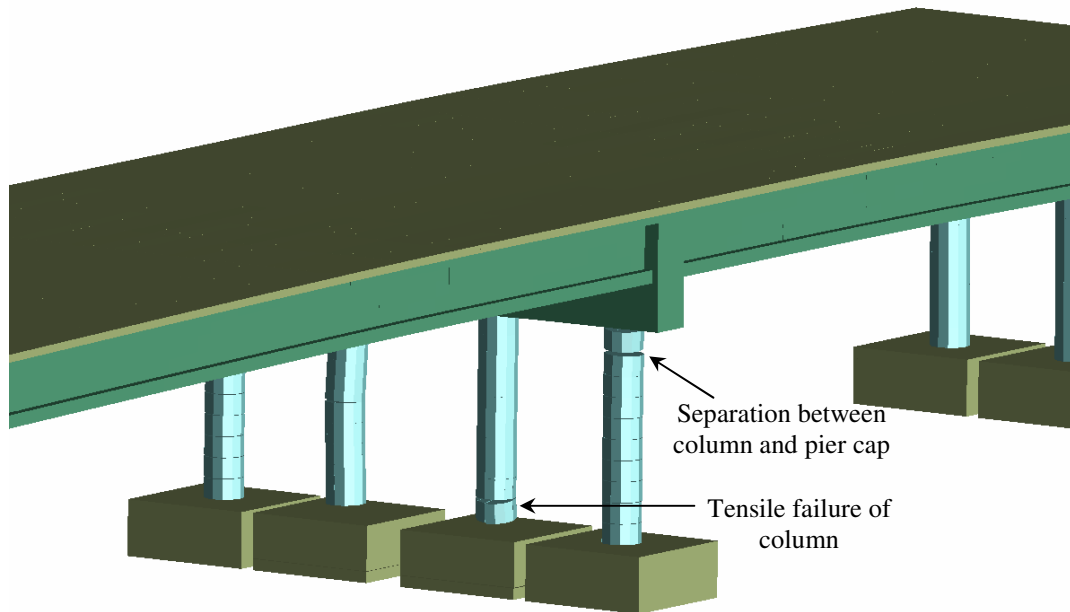


Fig. 5.18. Failure in concrete columns for integral piers

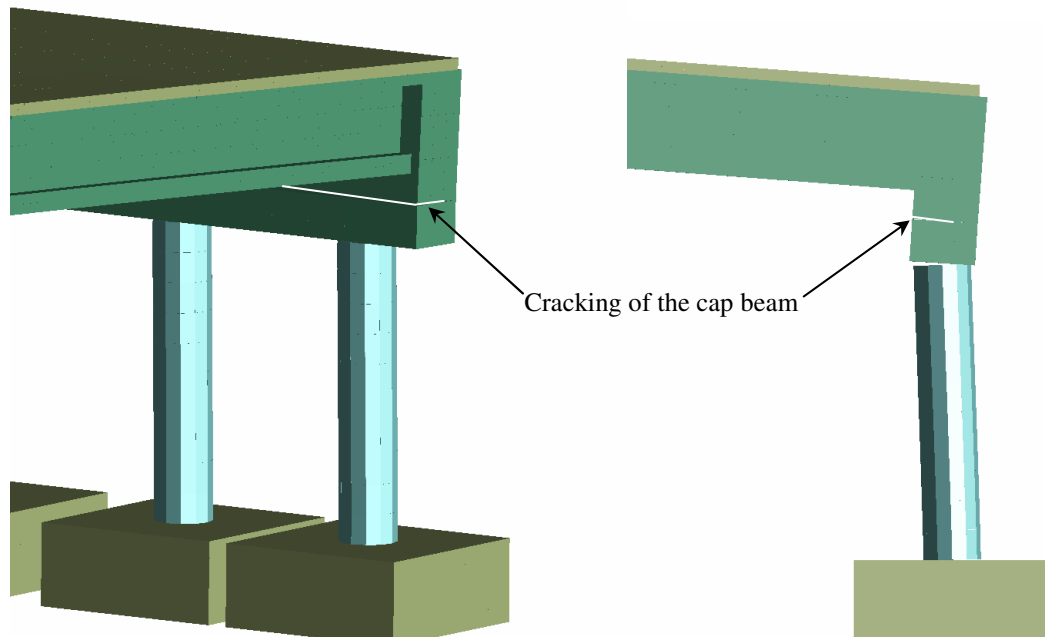


Fig. 5.19. Cracking at the pier cap and separation between the cap beam and columns

5.1.4 *Hand charge attached to one or more of the columns*

Although the weight of hand emplaced charges is usually small, it can be devastating if it results in the failure of a critical structural component such as the pier columns (Fig. 5.20). Therefore, it is recommended that the pier cap and columns be designed to exhibit sufficient redundancy to resist the removal of one or more of its columns and redistribute the load without collapse. This can be achieved by designing the pier cap for several column removal scenarios and taking the envelope of all these cases as the final design. If the blast resulted in the failure of the pier, this can trigger the collapse of the two adjacent spans sharing this pier (Fig. 5.21). Furthermore, it can result in the potential progressive collapse of the whole structure.

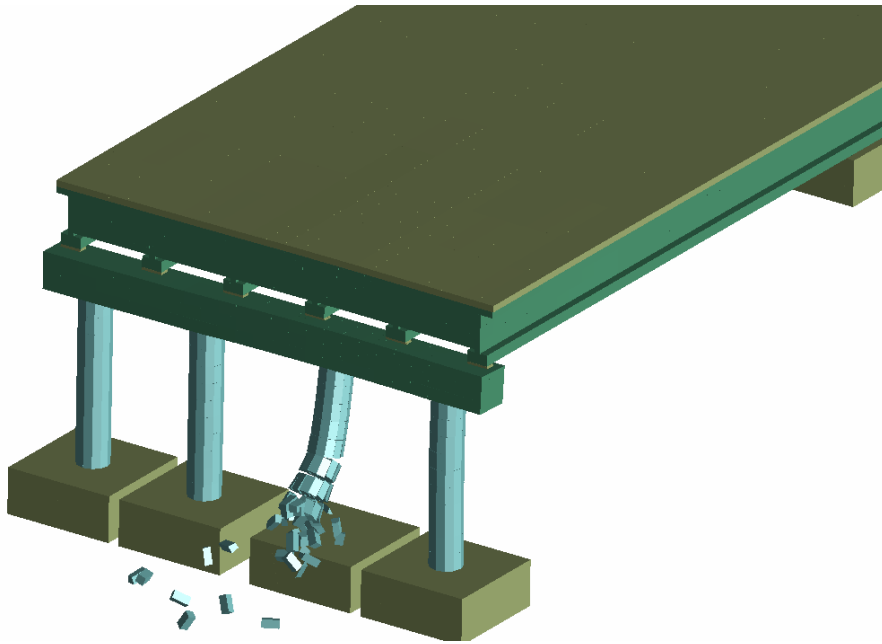


Fig. 5.20. Failure in concrete column as a result of a hand emplaced charge

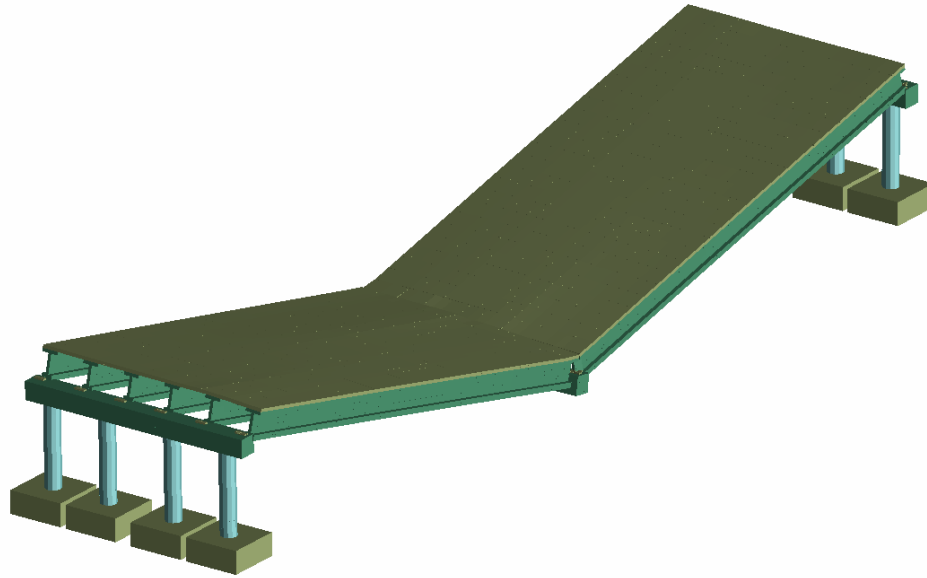


Fig. 5.21. Bridge collapse due to the failure in the intermediate pier

5.2 Above Deck Blast Scenario

The behavior of bridges due to blast scenarios above the deck depends mainly on the size of the vehicle used in the attack. Small vehicles can carry about 500 lbs, whereas big trucks can carry as much as 20,000 lbs of explosives. The standoff distance is measured from the top of the deck slab to the centroid of the detonation charge, and hence, it usually ranges from 3 to 5 ft depending on the height of the vehicle. For this analysis, the standoff distance is taken as 3 ft.

Although the average standoff distance for blast scenarios above the deck is much smaller than that below the bridge deck, it was observed that below-deck blast scenarios can be more devastating than above-deck blast scenarios. This is mainly attributed to the uplift pressure created by detonations located below the deck slab, while for above-deck

blast scenarios; the bridge is loaded in the same direction of the gravity loads. Therefore, for the same amount of explosives, it is expected to encounter more damage if the blast scenario takes place below the bridge deck. Two cases were considered in the analysis: 1) the explosive vehicle is located close to the midspan 2) the explosive vehicle is located close to bent. The results of these two extreme cases are presented herein.

5.2.1 Blast scenario close to the bridge midspan

For comparison, the weight of explosives used in this scenario was the same as that used for the below-deck blast scenario at midspan. It was observed that blast resulted in minor crushing at the top of the deck slab at mid span. However, the bridge remained intact. To examine how the failure can take place, the charge weight was increased to 3 times the original value. In this case, severe crushing was observed at the deck slab around the midspan (Fig. 5.22). This was followed by the flexural cracking of the pier cap and the buckling of the concrete columns (Figs 5.23 and 5.24). This is mainly attributed to compressive forces resulting from the blast pressure. One of the hazards associated with the blast scenarios above the bridge deck is due to the falling debris which can result in severe injuries to individuals below the bridge (Fig. 5.25).

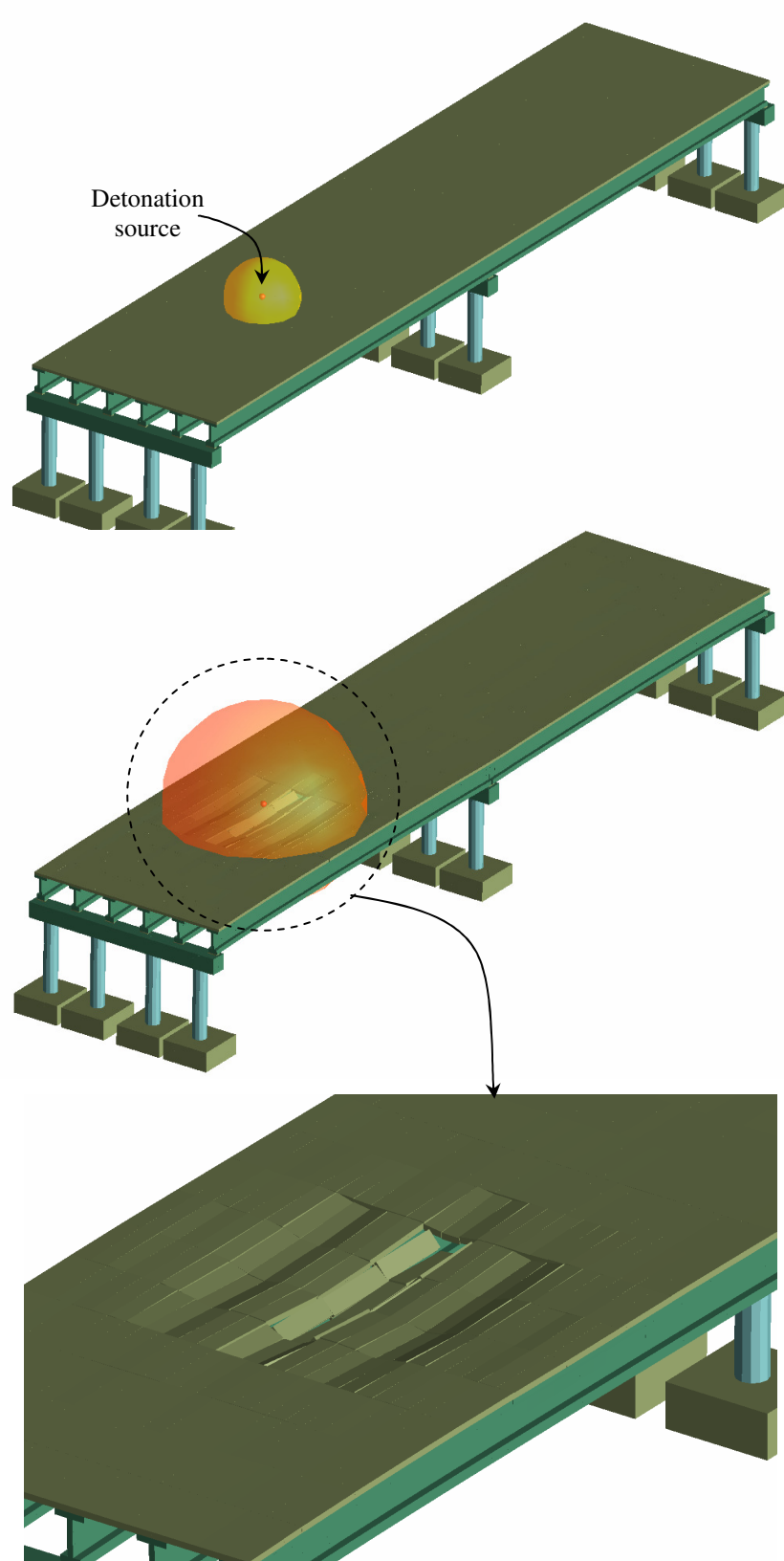


Fig. 5.22. Crushing of concrete at the top of the deck slab

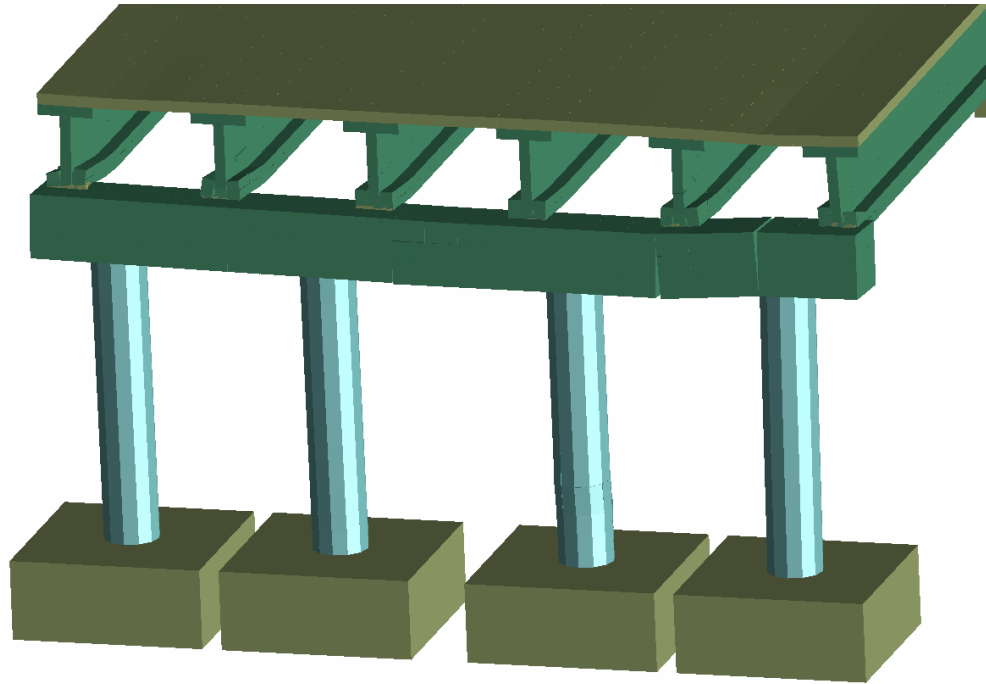


Fig. 5.23. Initiation of flexural cracks in the cap beam

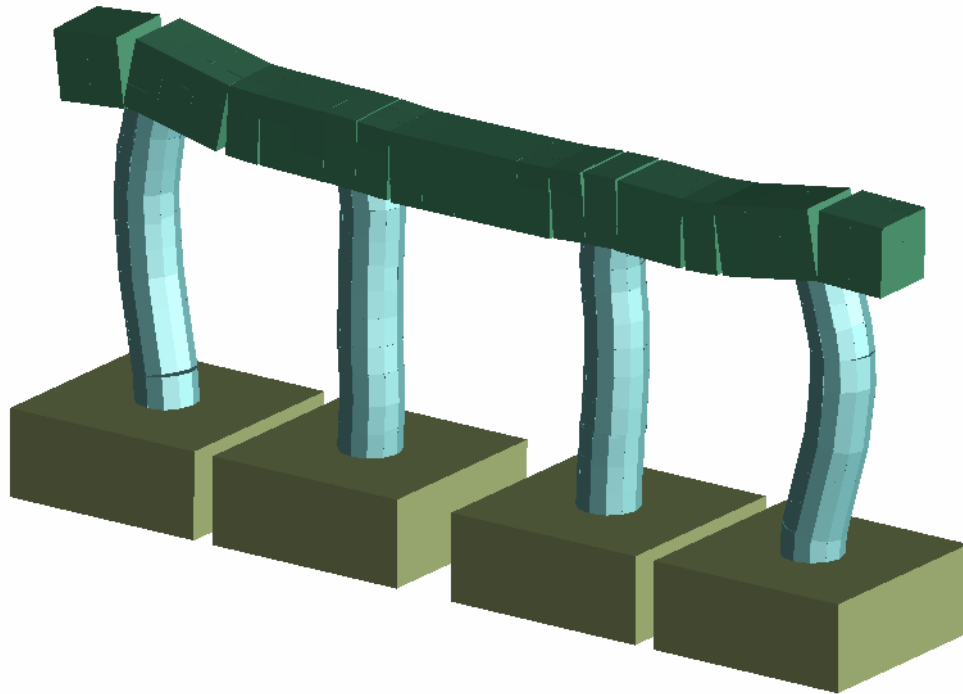


Fig. 5.24. Severe flexural cracking of pier cap and buckling of concrete columns

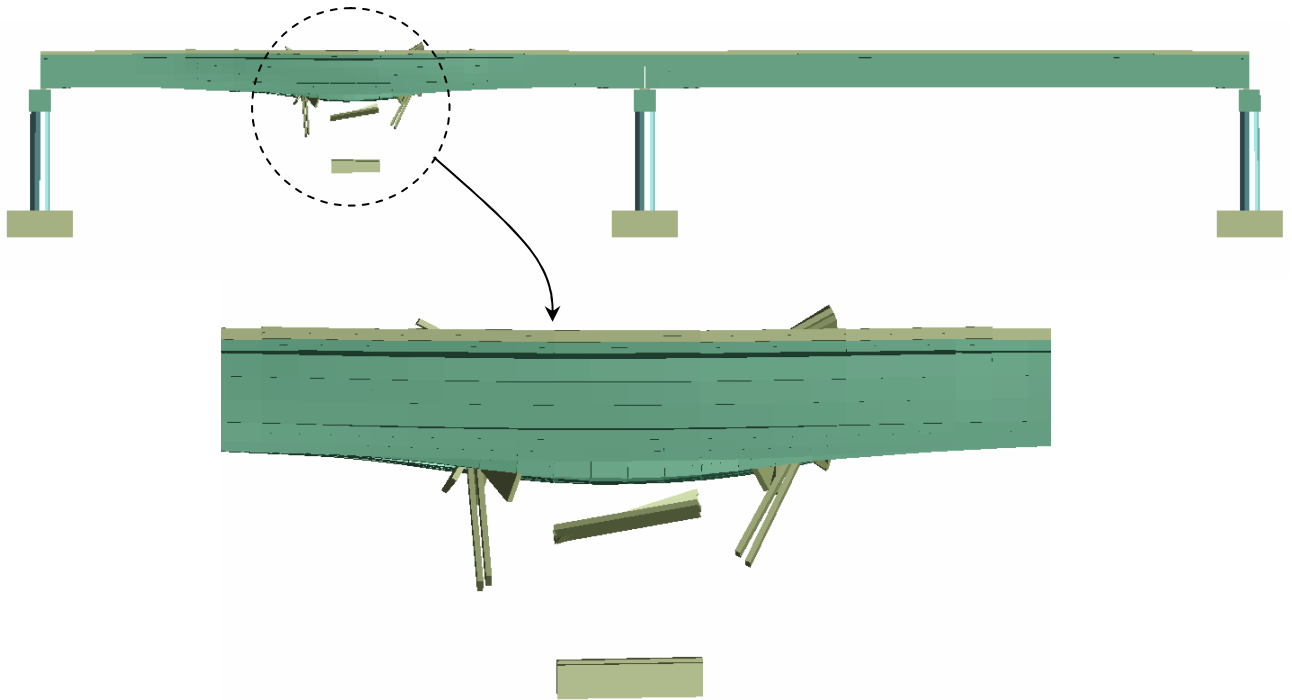


Fig. 5.25. Hazards of falling debris

5.2.2 Blast scenario close to the bridge bent

From the analysis of the blast scenario when the explosive vehicle is located close to the bridge bent, it was observed that the behavior of the bridge was very similar to the case when the vehicle is at the midspan (Fig. 5.26). The failure is initiated by the crushing of concrete at the top of the deck slab followed by the intensive flexural cracking of the pier cap and the buckling of the columns.

Based on the results obtained from these computer simulations, mitigation measures for protecting bridges against blast attacks were evaluated. The use of high-performance fiber reinforced composite columns, multiple columns; confinement, cable systems, and other details in conjunction with protective measures are presented in the next chapter.

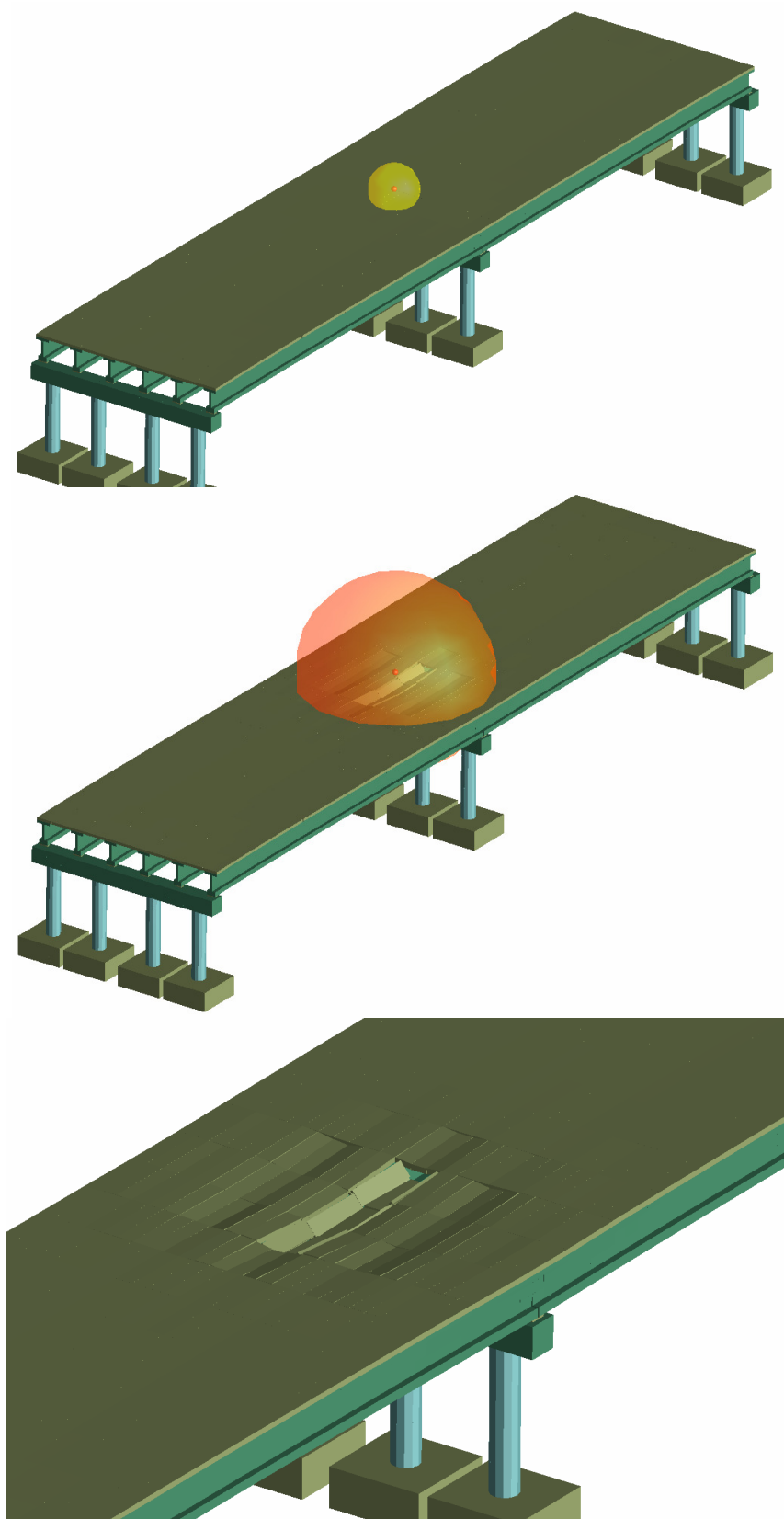


Fig. 5.26. Response of the bridge model to an above-deck detonation at the bent

5.3 Results and Discussion

The global behavior of a typical highway bridge subjected to blast hazards was evaluated using ELS software. The bridge model was subjected to several blast scenarios from above and below the bridge deck. For each scenario, the bridge model was analyzed for variable blast locations and charge weights. Based on the analyses results, the following observations were made:

- For the same charge weight, it was observed that below-deck blast scenarios are more devastating than above-deck blast scenarios. This is mainly due to the uplift forces created by the below-deck blast scenarios. When the bridge model was subjected to a below-deck detonation at midspan, the primal threat was on the bridge superstructure. For conventional design, the bridge superstructure is designed for gravity load, and hence the uplift forces created by the below-deck explosion can be devastating. If the uplift forces acting on the bridge superstructure exceeded the effect of the gravity loads, the girders will move vertically upward departing from the substructure. After the girders are uplifted, they will rebound back on the substructure provided that adequate seat width is provided.
- When the bridge model was subjected to a blast detonation located close to the intermediate pier, it was observed that the failure is initiated by the cracking at the top fiber of the deck slab followed by the flexural failure of the girders. The intermediate pier was subjected to a combined effect of lateral bending and uplift forces. These uplift forces can result in the tensile failure of the column or the separation between the column and the pier cap.

- The bridge model was analyzed under the effect of hand emplaced charges attached to one of the substructure columns. Even though the weight of the hand charge is relatively small when compared to that of a vehicle bomb, it can be devastating due to its close proximity and can result in the failure of the structural member to which it is attached to.
- When the bridge model was subjected to a blast scenario located above the deck, it was observed that the failure can take place due to the crushing of the deck slab followed by the flexural cracking of the pier cap and the buckling of the substructure columns. This is mainly attributed to the compressive forces produced by the blast.

CHAPTER 6

PROTECTION TECHNIQUES TO MITIGATE BLAST HAZARDS

This chapter deals with evaluation of protection measures that can be implemented to reduce the vulnerability of bridges to blast hazards and other extreme events. The use of these protection measures will increase the cost of the bridge and in certain cases this increase is significant and can be prohibitive. The selected protection measures and the associated additional cost should be addressed early on in the design process so that the bridge owner and the public are aware of the impact of including extreme-event-design on bridge geometry, functionality, clearance, aesthetics, and cost. An example of the cost impact of some of the protection measures is provided in appendix C.

Protection measures can be classified into two main categories: 1) protection measures related to blast scenario, and 2) protection measures related to the structural elements. The impulsive load created by the blast scenario depends on the standoff distance and the charge weight, and hence, by controlling these two parameters, the magnitude of the blast load can change significantly. Additionally, the behavior of the structure subjected to

blast load is sensitive to its geometry, continuity, properties of the materials, and the availability of alternate load paths to prevent its progressive collapse. Various protection techniques and protective measures for bridges were investigated and the results are presented herein.

6.1 Minimum Standoff Distance and Maximum Charge Weight

Through the literature review, it was clear that the standoff distance is the key factor in determining the damage produced by a blast scenario. Therefore, the most effective protection measure is to provide a minimum standoff distance to protect the critical components in the bridge. Standoff distance can be provided by using barriers or obstacles to prevent vehicles from coming too close to the protected element. Nevertheless, in many cases it is practically difficult to utilize barriers as they will interrupt traffic to a certain extent. In addition to the standoff distance, the blast pressure depends on the charge weight used in the attack. Therefore, more security measures should be directed to heavy trucks as they can carry up to 20,000 lbs of explosives. The type and material of barrier, wall or obstacle used to enforce the minimum standoff distance should be very ductile and capable of high energy absorption. The use of High Performance Fiber Reinforced Composites (HPFRC) in these elements can provide the required ductility and high energy absorption capacities needed to maintain the design standoff after a blast event.

6.2 Highly Ductile Concrete Materials

It is uneconomical and unpractical to design structures to be blast-proof. The design philosophy is mainly based on allowing the structure to be damaged but preventing the total collapse of the structure. Therefore, the structural elements should be designed to exhibit large plastic deformations. The required resistance of the structural element to resist impulsive blast loads decreases with the increase in the ductility of the element. The recommended ductility values for concrete structures ranges from 10 to 15, which corresponds to rotation angles 2° and 4° , respectively (TM5-1300, 1990).

The ductility of concrete is enhanced with proper confinement. Yet, it is impossible to achieve those high ductility levels using conventional reinforced concrete. Hence, it is essential to utilize innovative materials that are capable of exhibiting higher levels of ductility and energy dissipation such as High Performance Fiber Reinforced Concrete (HPFRC). A comparison between the moment-curvature curve of HPFRC using SIFCON matrix and conventional confined reinforced concrete (RC) is presented in Fig. 6.1. This curve was generated using USC_RC program. The confined ultimate strain of concrete for RC and HPFRC is taken as 0.02 and 0.06, respectively. From the curve, it is observed that the ductility of HPFRC is significantly higher than that of conventional reinforced concrete.

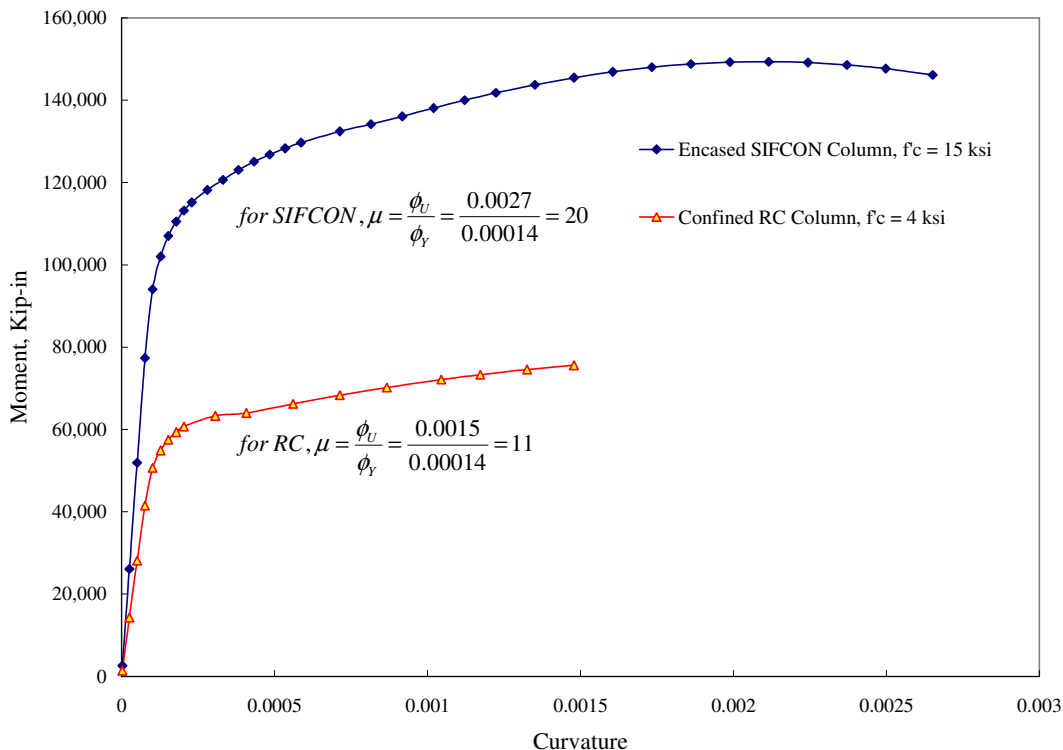


Fig. 6.1. Moment-curvature curve of HPFRC versus RC

Fiber-reinforced concrete (FRC) consists of discontinuous discrete fibers embedded in cement based matrix. Based on the desired properties, fine aggregate or a combination of fine and coarse aggregate may be added to the mix. FRC is characterized by its improved tensile and flexural strength in comparison to the regular concrete. Furthermore, based on the volume fraction of the fibers, FRC structures can exhibit high levels of ductility. The mechanical properties of FRC depend on the properties of the matrix, type of fiber, fiber length, volume fraction of the fibers, fiber orientation, and bond between the fibers and the surrounding concrete (Zia P. et al, 1991).

Several types of fibers are being used in FRC. These fibers can be classified as metallic, mineral, or polymeric fibers. Metallic fibers are usually made of steel or stainless steel, while mineral fibers are usually glass fibers. The most common types of polymeric fibers are aramid, polyester, and carbon fibers (Balaguru and Shah, 1992).

The load deflection relationship of FRC is linearly elastic until cracking. When the matrix cracks, the tensile stresses are transferred to the fibers below the neutral axis. Depending on the volume and strength of the fiber, the maximum load may drop or increase after the first cracking. With sustained loading, nonlinear plastic deflection occurs due to the separation between the fibers and the matrix. The post peak behavior indicates the high energy absorption (toughness) of FRC. Toughness is a measure of the energy absorption capacity of the material and hence its ductility. Ductility of a structural member is described as its ability to sustain inelastic deformation without significant loss in its load carrying capacity prior to failure. Therefore, toughness is of great importance for the safety of structures, especially for structures subjected to seismic or blast loading. When a ductile structural member is loaded close to its maximum carrying capacity, the inelastic deformation produced will allow significant warning time to ensure the safety of lives and allow enough time to start the rehabilitation process. Ductile structures allow effective redistribution of loads and moments and hence they exhibit large deformations while still sustaining the applied loads. The toughness index increases with the increase in the fiber volume fraction, and the increase in the fiber aspect ratio (Balaguru and Shah, 1992). Slurry Infiltrated Fiber Concrete (SIFCON), Slurry Infiltrated Mat Concrete (SIMCON), and Engineered Cementitious Composites (ECC) are the most common types

of highly ductile concrete materials. The properties of these different types were studied and the results are presented herein.

6.2.1 SIFCON

Slurry infiltrated fiber concrete (SIFCON) is a cementitious composite with high volume fraction of steel fibers. The volume fraction of fibers in ordinary FRC does not exceed 2%. For volume fractions more than 2%, it becomes very difficult to mix the composite. To overcome this obstacle, a new technique was introduced for SIFCON. This technique involves infiltrating a pre-placed stack of steel fibers with cementitious slurry (Lankard, 1984). The cement based slurry contains only fine aggregate as using large aggregates may lead to improper infiltration. External vibration may be used to facilitate the infiltration of the slurry. This process results in utilizing high volume fractions of steel fibers. The volume fraction of steel fibers can be as high as 20% (Balaguru et al., 1992).

Load deflection curve of SIFCON is characterized by the relatively long post-peak plastic plateau. This indicates the ability of the material to develop large plastic deformation without significant drop in its load carrying capacity. SIFCON is characterized by its superior ductile behavior and energy absorption capacity which makes it a practical material for structures subjected to dynamic loads such as seismic or blast loads. The toughness of SIFCON is much higher than that of the conventional FRC. Furthermore, the high volume fraction of steel fibers significantly increases the load carrying capacity of the material. The load carrying capacity of SIFCON depends to a great extent on the volumetric ratio of the used fibers (Fig. 6.2).

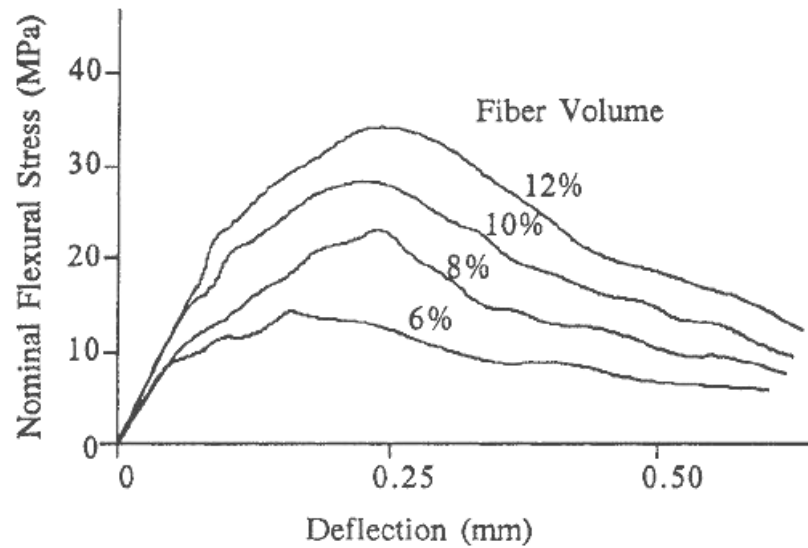


Fig. 6.2. Effect of the fiber volume fraction on the flexural behavior of SIFCON (Josifek and Lankard, 1987)

Like other types of FRC, the flexural failure is initiated by the cracking of the matrix followed by a plastic deformation plateau due to the pull-out of fibers. Normally, FRC fibers are randomly distributed, while steel fibers are pre-placed in SIFCON which ensures a more uniform distribution. This uniform distribution improves the flexural capacity as well as the toughness of the composite. The flexural load-deflection curve for SIFCON is close to the behavior of an elastic perfectly plastic material (Parameswaran et al., 1994). Recently, steel bars were used to reinforce SIFCON. This application proved to provide high strength and high ductility especially under extreme cyclic loading. A comparison between the load deflection response of reinforced concrete and reinforced

SIFCON beam is shown in Fig. 6.3. The ductility of reinforced SIFCON beam can be 3 times higher than the ductility of reinforced concrete

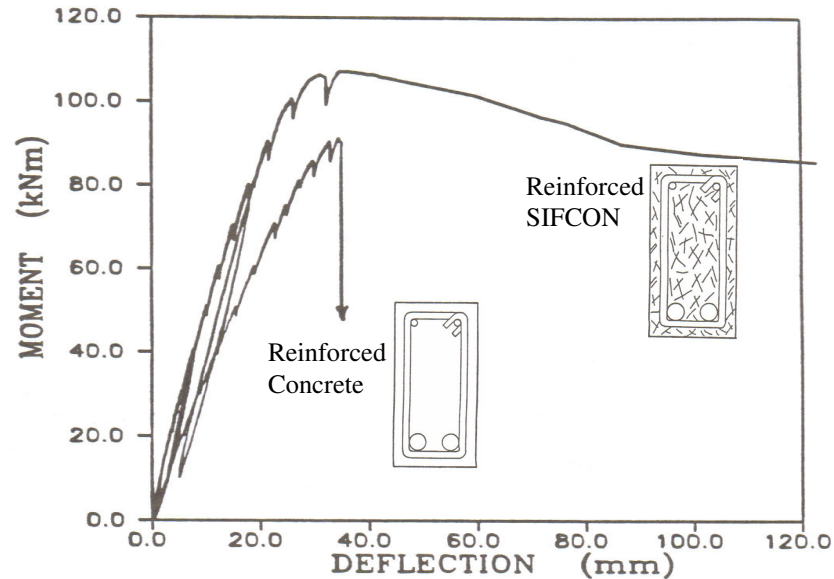


Fig. 6.3. Load-deflection curve for reinforced concrete versus reinforced SIFCON (Fritz et al, 1992)

6.2.2 SIMCON

Although SIFCON offered several advantages, the high cost associated with this type of composites remains a major concern. Due to the high volume of fibers and the cost of the skilled labor, the application of SIFCON was limited to special structures such as military shelters and some types of pavements. These obstacles were overcome by using Slurry infiltrated mat concrete (SIMCON). Instead of using discrete discontinuous fibers, steel fiber mats are used in SIMCON. The flexural capacity of SIFCON composite with a

certain volumetric ratio of fibers can be achieved by SIMCON using almost half the amount of fibers that was used in SIFCON (Hackman et al., 1992). The main advantage of SIMCON lies in the pre-formed fiber mat which can utilize fibers with aspect ratios exceeding 500. This is almost 5 times the aspect ratio of the discrete fibers used in SIFCON. Since fibers are arranged in a mat, the handling problems are minimized. These higher values of the aspect ratio permit a better bonding between the fibers and the surrounding matrix, and hence improve the flexural behavior.

Hackman et al. (1992) compared the flexural behavior of SIMCON versus SIFCON specimens. It was observed that using SIMCON with fiber volumetric ratio of about 3.5% can yield almost 75% of the flexural strength of SIFCON specimens having a fiber volumetric ratio of 14%. When the fibrous volume in SIMCON was increased to 5.7%, the flexural strength was about 85% of that of the SIFCON specimens. This proves that the flexural capacity of SIFCON composites can be achieved by SIMCON using only a small fraction of the fiber ratio. The extremely high flexural strength of SIMCON with fewer amounts of fibers gives it an advantage over SIFCON. Furthermore, the energy absorption capacity of SIMCON is much higher than that of SIFCON. Hackman et al. (1992) reported that SIMCON specimens with only 25% of the volume of fibers used in SIFCON specimens exhibited 15% higher energy absorption capacity.

6.2.3 ECC

During the last decade, Engineered Cementitious Composite (ECC) emerged as a promising material that can possess the advantages of both steel and concrete. ECC is a special type of ultra ductile FRC. The unique characteristics of ECC are based on the

microstructure tailoring of the composite to achieve enhanced mechanical properties. The main philosophy is to utilize the fibers to bridge across the matrix cracks. Hence, the fiber type, matrix properties, and the bond between the fibers and the matrix are the main factors that control the behavior of ECC (Li, 2003). The tensile strain of ECC can reach as high as 5% with fiber volume fraction less than 3%.

Conventional concrete or FRC specimens are characterized by the strain softening following the initiation of the first crack. Conversely, ECC exhibits strain hardening due to the development of multiple cracks (Fig. 6.4). The crack pattern of ECC is characterized by the small crack spacing (0.5 to 5 mm) and small individual crack widths (less than 200 micrometer). The small crack width is attributed to the bridging fibers which prevent the opening of the cracks. To obtain this multiple cracking behavior, the cracking strength of the matrix should be less than the maximum bridging stress of the fibers. Furthermore, the strain hardening behavior is very sensitive to the fiber/matrix interface. A too weak interface can result in the pull-out of fibers, while a too strong interface can prevent the stretching of the fibers across the bridged crack (Li, 2003). To achieve the desired ductile behavior, the fiber volumetric fraction and the bond between the fibers and the matrix should be micromechanically engineered. Polyvinyl alcohol (PVA) fibers are most commonly used in ECC. These polymeric fibers are tailored by controlling their surface coating to achieve the desired bond with the matrix.

ECC is characterized by its high ductile behavior. It is commonly referred to as “bendable concrete” (Fig. 6.5). Unlike conventional concrete, the shear behavior of ECC

is considerably ductile, and hence it responds very well under extreme cyclic loading. Furthermore, its energy absorption capacity is much higher than that of any other type of FRC. ECC can exhibit very large deformation while sustaining the applied loads. Steel reinforcements can be used in ECC to form an elasto-plastic material (R/ECC) that can sustain large strain values (Li, 2003).

The structural applications of ECC are numerous. ECC can be prepared using different techniques. It can be cast, extruded, or sprayed. Furthermore, ECC can be produced as self compacting material. Its high energy absorption capacity makes it suitable for extreme loading cases that require high ductility. It was observed that R/ECC performs excellently under seismic loads (Fisher and Li, 2002). Moreover, ECC can be used in the plastic hinge regions of precast concrete members. ECC can be used in the repair and retrofitting of existing structures. It has high fatigue endurance and good resistance for freeze and thaw. The initial cost of ECC is relatively high. However, this cost can be justified by observing the life cycle cost of the structure. ECC structures require minimum repair even under extreme loading cases. When ECC is subjected to an extreme loading case, its behavior is characterized by the development of multiple cracks of small width. These cracks can be sealed with the use of adhesives, and hence ECC provides potential for constructing self-healing structures (Li et al., 1998).

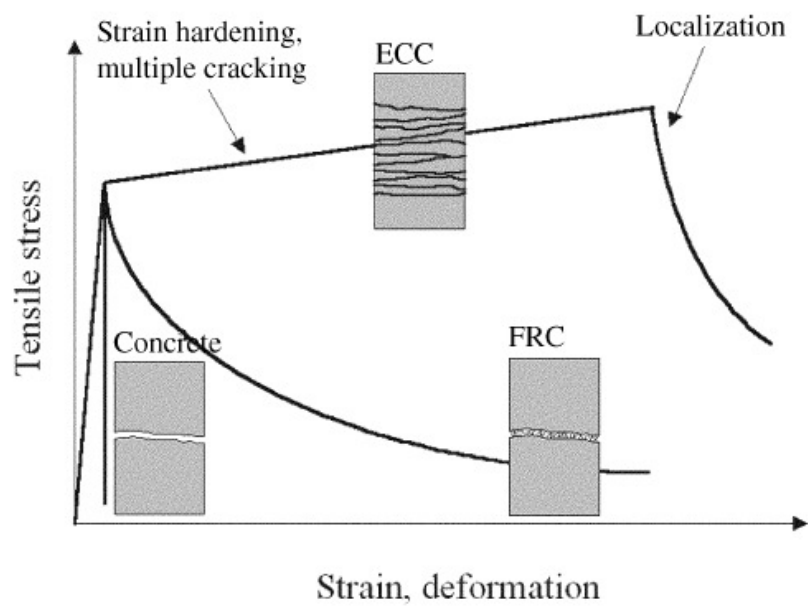


Fig. 6.4. Tensile stress strain behavior of concrete, FRC, and ECC (Li, 2003)

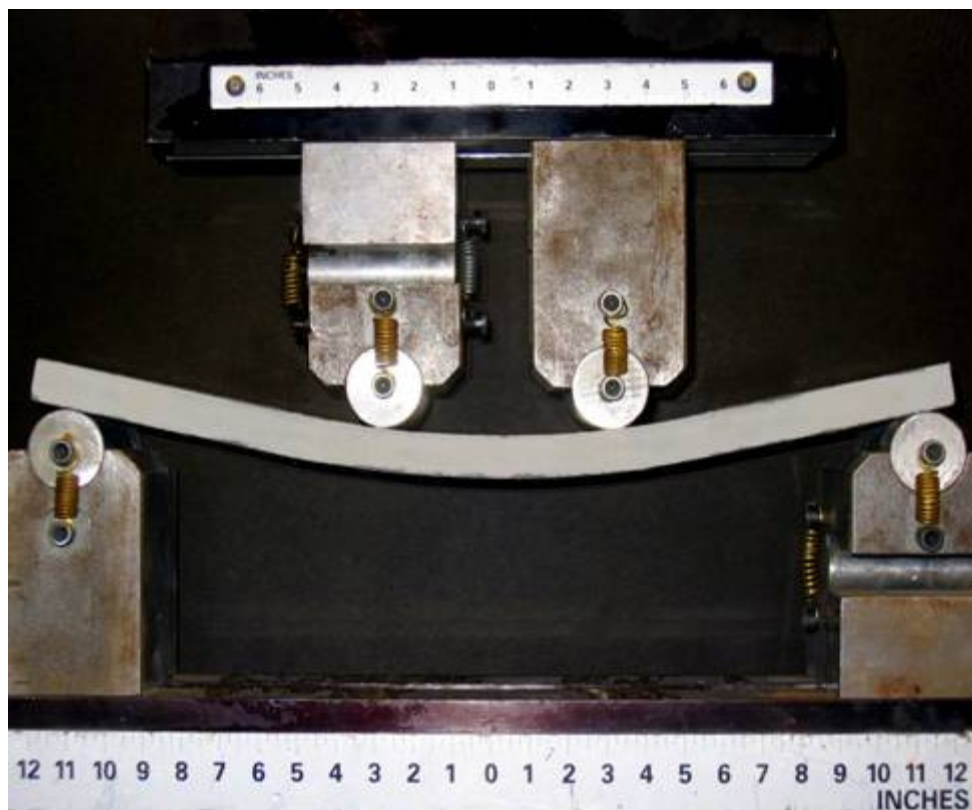


Fig. 6.5. Bendable ECC (Li, 2003)

Concisely, Engineered Cementitious Composite (ECC) gained potential as a highly ductile concrete with superior energy absorption capacity. The superior ductile behavior of ECC was demonstrated through several experimental investigations. Using micromechanical tailoring approach, small fraction of fibers is used to achieve superior mechanical properties. Its energy absorption capacity is much higher than that of any other type of FRC. Its high energy absorption capacity makes it suitable for extreme loading cases that require high ductility. Furthermore, ECC can be used for the repair and rehabilitation of existing structures to improve their performance. However, further research is required to investigate the properties of ECC and to develop its design guidelines.

6.3 Redundancy and Continuity

The integrity of the overall bridge is vital to prevent the horizontal spread of the damage to adjacent areas. Progressive collapse occurs when local failure of a primary structural element leads to a chain reaction of structural failures, and results in the collapse of all or disproportionately large part of the structure. Proper design and detailing can significantly reduce the possibility of progressive collapse. This can be achieved by providing sufficient continuity, redundancy, and energy-dissipating capacity in the structural members to transfer the loads from the locally damaged region to adjacent regions capable of sustaining these additional loads without collapse.

For multiple span bridges, intermediate piers should be designed to withstand the removal of one or more of its supporting columns. Hence, if a hand charge is attached to

one of the column, this shall not lead to the collapse of the entire structure. Some of the provisions for impact design of bridges can be implemented to improve its redundancy during blast hazards. The New Jersey Turnpike Authority recommends a minimum area of 30 ft² for single column bents. A more effective techniques is to provide multiple column bents to reduce the vulnerability of the bridge to progressive collapse (Figs. 6.6 and 6.7)



Fig. 6.6. Multiple column straddle bent (Route 130 East Brunswick, NJ)



Fig. 6.7. Close view of the multi column bent

In order to provide adequate redundancy, the cap beam should be designed for column-removal scenarios. The loss of the edge columns can be very devastating due to the cantilever behavior of the cap beam, and hence, redundancy can be provided by using double and triple edge columns as shown in Fig. 6.8. This will ensure that the bridge will remain intact even if one of the edge columns is lost due to any extreme event such as earthquake, blast, or vehicle impact. Redundancy can also be provided using wall piers constructed using HPFRC or a combination of HPFRC walls and columns as shown in Figs 6.9 and 6.10, respectively.

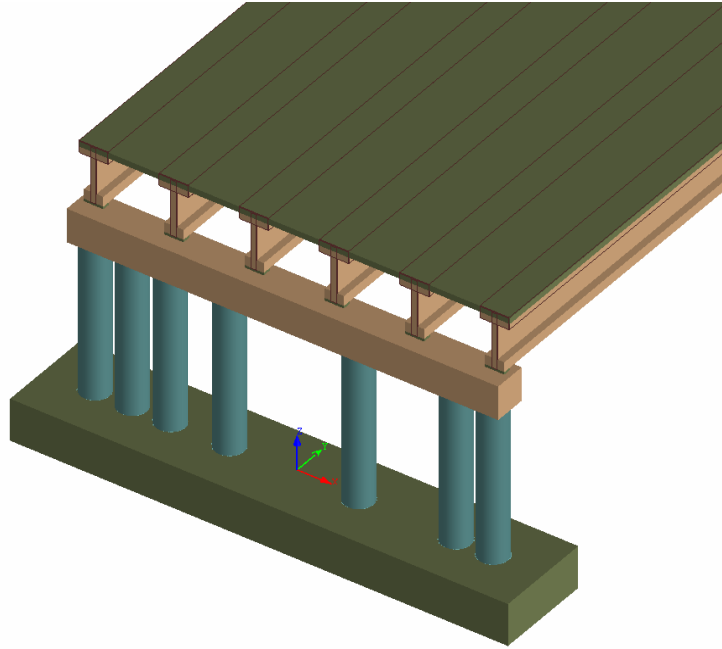


Fig. 6.8. Increased pier redundancy using double and triple edge columns

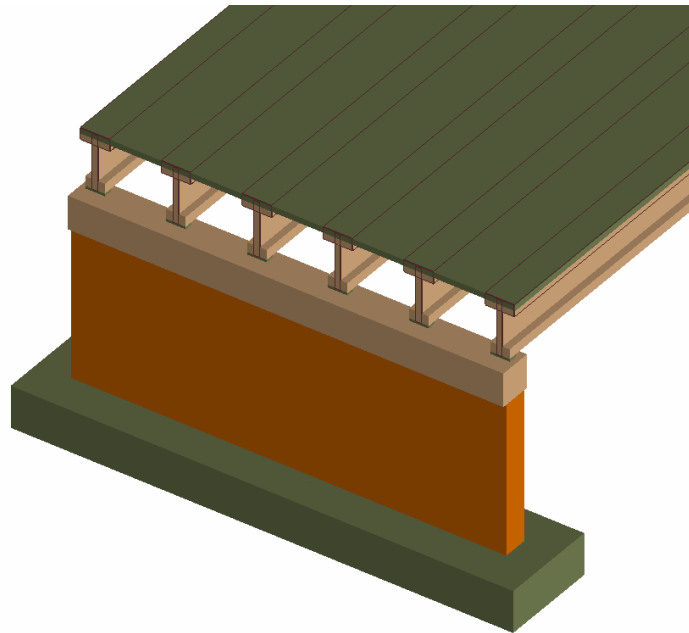


Fig. 6.9. HPFRC wall piers

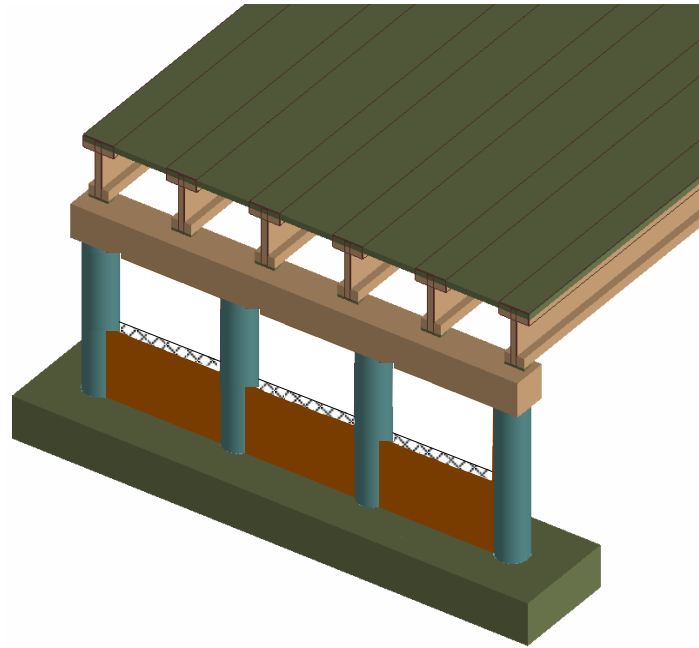


Fig. 6.10. Combinations of HPFRC walls and columns

Furthermore, using steel encased HPFRC columns can increase the energy absorption capacity and provide more redundancy. The steel casing can be tightly attached to the external skin of the concrete section as shown in Fig. 6.11 (a) or it can be offset from the concrete section by a hollow distance such as 6 to 12 inches as shown in Fig. 6.11 (b). This hollow distance enhances the standoff distance of the structural member without additional material cost.

Filler materials such as foam or sand can be used to fill the hollow space, and hence, improve the energy dissipation capacity of the member. Anchorage of these columns to the foundation is very critical and the connection of the pier to the footing should be through mechanical anchorage capable of developing the full ductility of the structural

element. This will require minimum embedment of the steel casing into the footing with mechanical anchorage which is likely to result in a massive foundation.

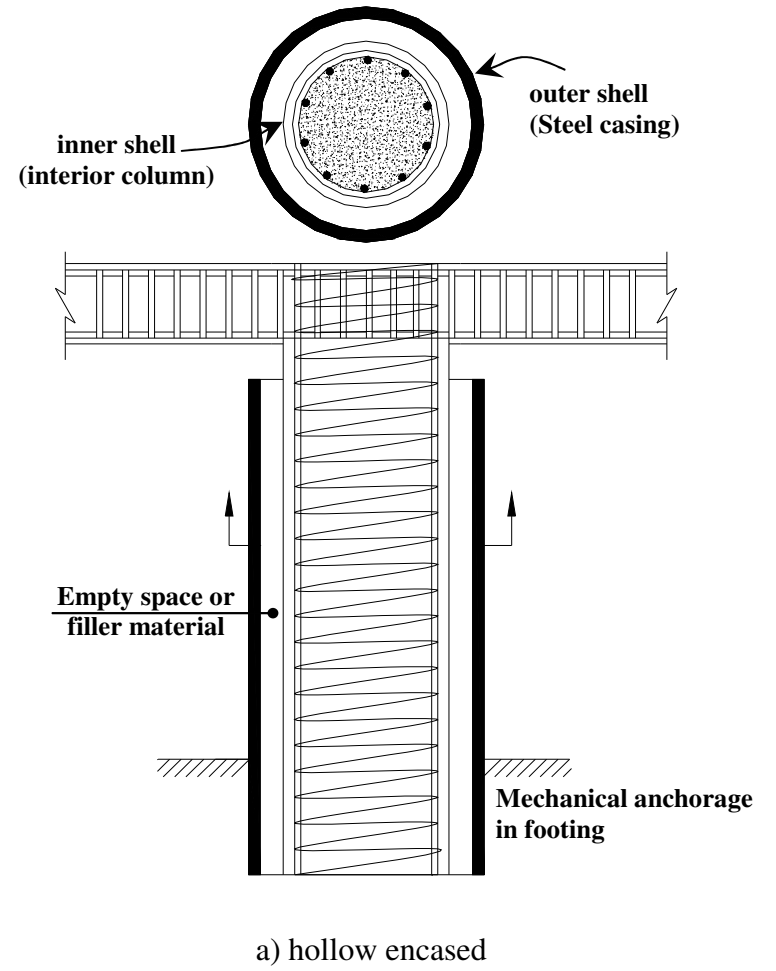
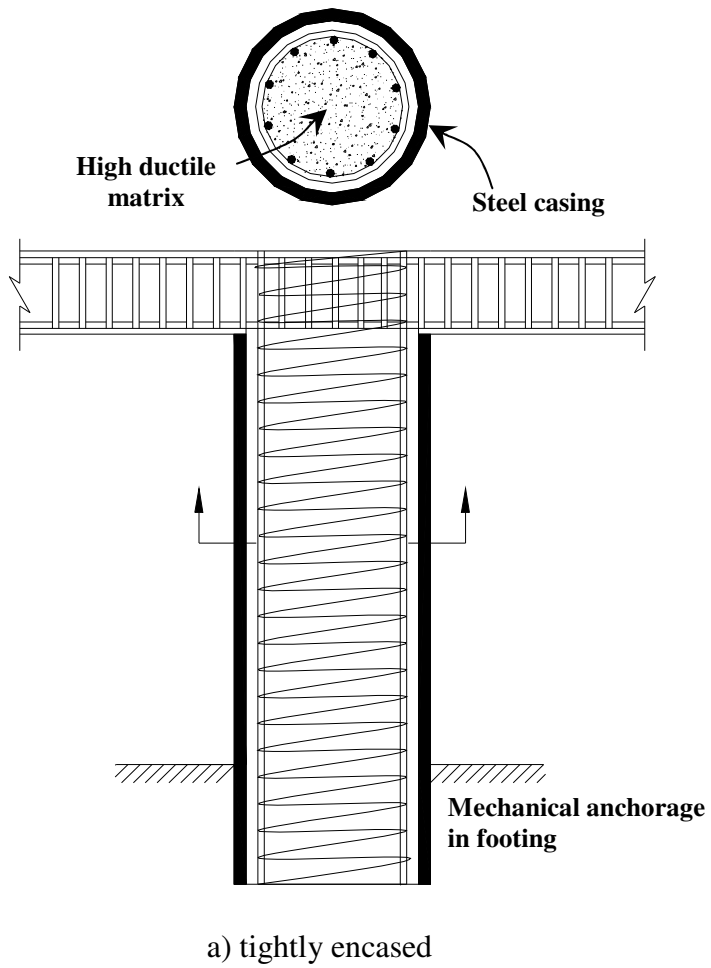


Fig. 6.11. Encased composite HPFRC columns

Steel encased HPFRC columns can deliver ductility values of 10 to 20. As shown in Fig. 6.1, a 4 ft diameter steel encased HPFRC column has almost twice the ductility of the conventional reinforced concrete column of the same diameter. Figures 6.12 and 6.13 show the ductility values obtained from encased HPFRC columns for various pipe thicknesses, and confinement ratios, respectively. These figures demonstrate that the ductility values recommended for blast design can be achieved using these types of columns. It is observed that the ductility of the encased columns increases with the increase in the pipe thickness as well as the increase in the ultimate strain of concrete.

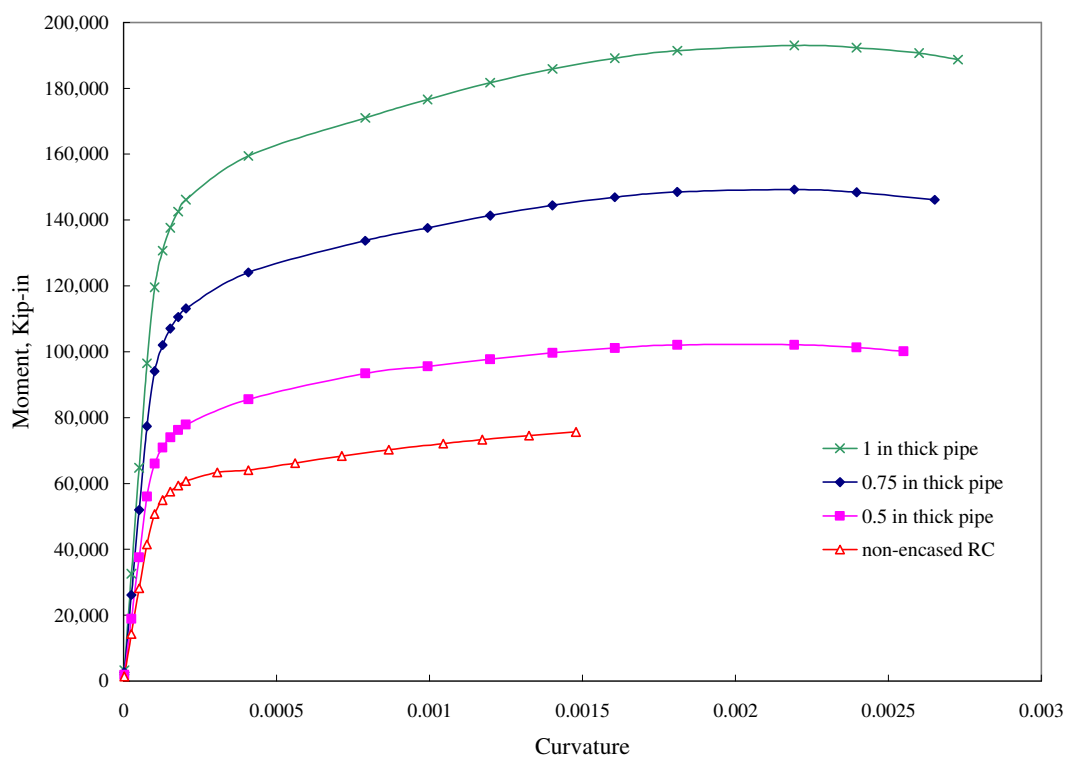


Fig. 6.12. Effect of pipe thickness on the moment curvature curve

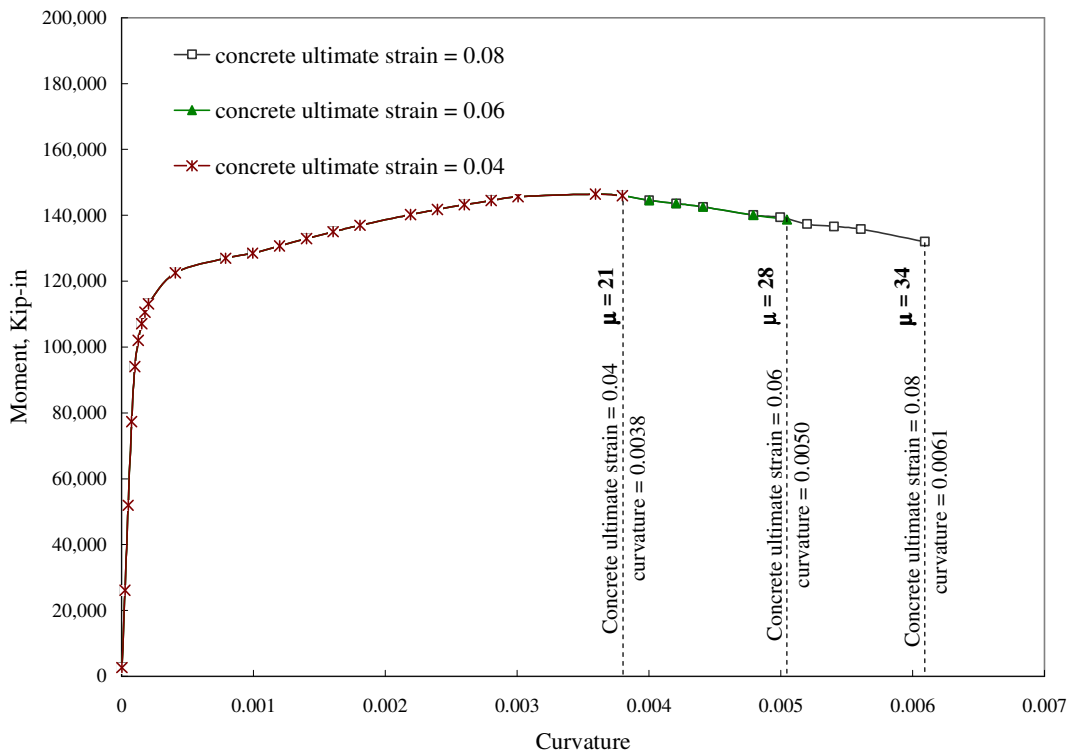


Fig. 6.13. Effect of concrete ultimate strain on the moment curvature curve

6.4 Collapse Prevention using Auxiliary Cable Systems

Recently, the catenary action of cable systems has been experimentally evaluated to prevent the progressive collapse of buildings (Astaneh et al., 2001). This innovative technique is based on providing number of cables to bridge the gap created by the collapsed member and hence, prevent the progressive collapse of the structure as shown in Figure 6.17. If this technique is utilized in bridges, it can localize the damage induced in one of the bridge spans, and prevent this damage from extending to the adjacent spans. Furthermore, the cables can support the damaged span and prevent its collapse on the roadway/waterway below. This can save the lives of those above and below the bridge. It can also insure that the roadway below the bridge remains serviceable for emergency

vehicles. The applicability of using systems of cables in bridges were studied and the various parameters associated with the design of these cables such as their length, area, material, deviation saddle location, and anchorage were evaluated.

If an intermediate pier is destroyed, the equilibrium condition of the deformed structure depends on the catenary action developed in the cables system as well as the catenary action developed in the superstructure of the bridge. The catenary action developed in the superstructure depends on the superstructure material, superstructure dimensions, and connection type between the adjacent spans. Concrete superstructures have relatively poor tensile capacity in comparison to steel superstructure. For catenary action to develop in the superstructure, it is important to have continuity between the adjacent spans. If the failed pier is located underneath an expansion joint, then there will be no catenary action in the superstructure. Quantifying the catenary action that can develop in the superstructure is complicated and further experimental research is required to examine this phenomenon. For this investigation, it is assumed that the entire load is being resisted by the cables system, i.e. the contribution of the catenary action developed in the superstructure is ignored. This assumption yields more conservative results as any contribution from the superstructure will be considered as reserved capacity.

The cable system technique consists of passing a number of cables through holes provided in the diaphragms connecting the superstructure of concrete girders or through the vertical stiffeners in steel girders (Figs. 6.14 and 6.15). Under regular loading conditions, the cable system is inactive and is not carrying any load. However, when one

of the intermediate piers is destroyed due to an extreme event such as vessel collision, accidental impact of trucks, fire, or blast attacks, the bridge superstructure starts to deflect at the location of the damaged pier inducing elongation in the cables. This deflection will stop when a state of non-linear geometrical equilibrium is reached between the vertical force resulting from the dead and live loads on the superstructure, and the tensile forces induced in the cable system. The end diaphragms/stiffeners and their corresponding anchorages should be designed to withstand the total tensile force induced in the cables at the state of equilibrium.

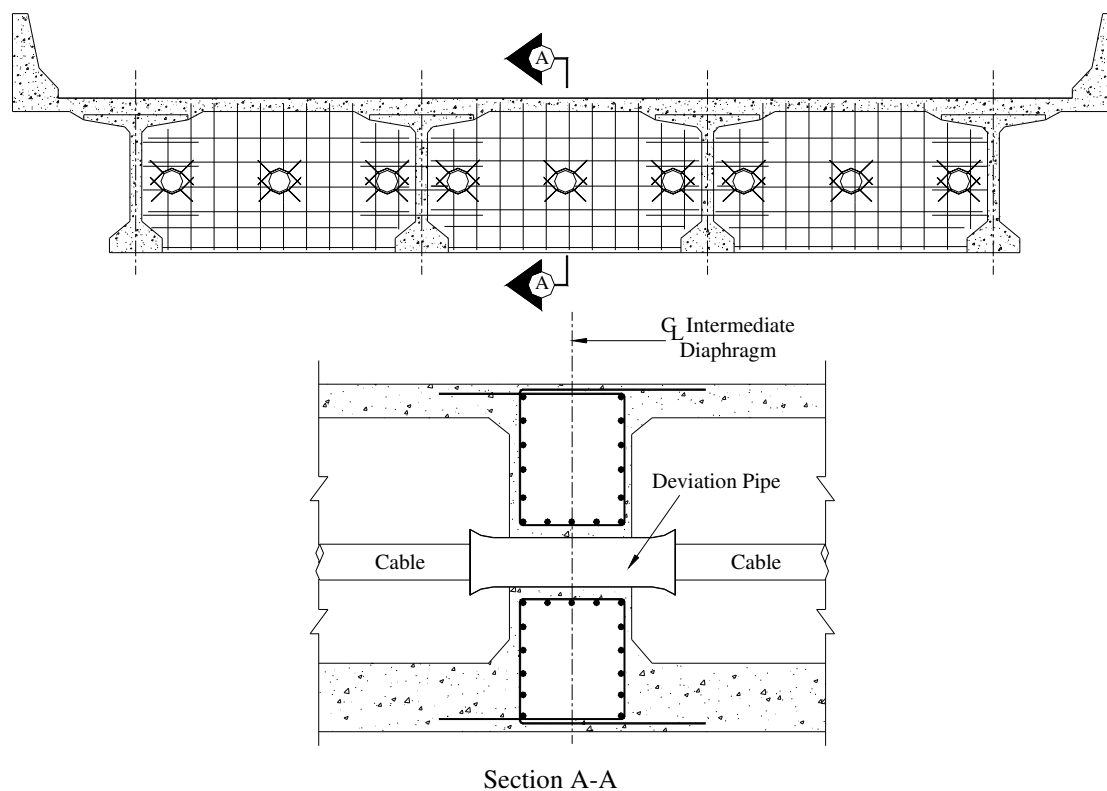


Fig. 6.14. Typical detail of cable system in concrete girders

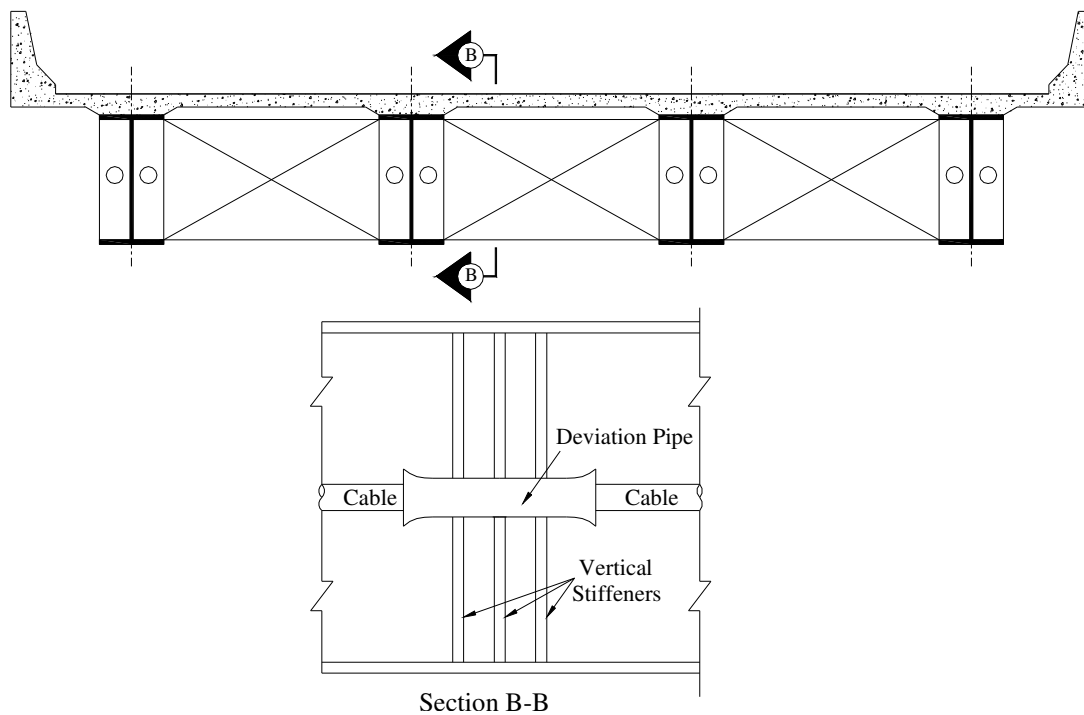


Fig. 6.15. Typical detail of cable system in steel girders

The equilibrium condition depends on the area of the cables, their material properties, and the geometry of the deformed system. It is important to eliminate any sag in the cables. The induced forces in the cables can be computed using the structural equilibrium of the deformed system (Popov, 1990) or Castigliano's first theorem (Oden, 1967).

6.4.1 Equilibrium of the deflected system (Popov, 1990)

The deflected shape for a two-span bridge is shown in Fig. 6.16.

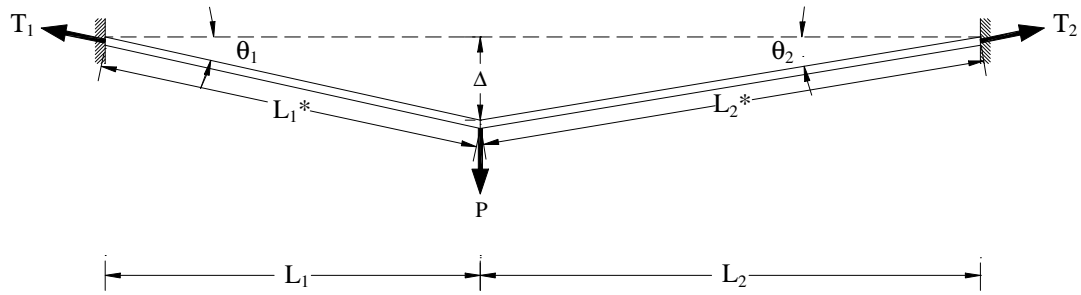


Fig. 6.16. Equilibrium of deflected system of cables for a two-span bridge

The equilibrium equations can be expressed as follows:

$$\tan \theta_i = \frac{\Delta}{L_i} \quad \text{and} \quad \Delta = (L_i)(\tan \theta_i)$$

$$\cos \theta_i = \frac{L_i}{L_i^*} \quad \text{and} \quad L_i^* = \frac{L_i}{\cos \theta_i}$$

$$\text{Elongation in each cable segment} = \frac{T_i L_i^*}{AE} = (L_i^* - L_i)$$

$$T_i = AE \left(\frac{L_i^* - L_i}{L_i^*} \right) = AE \left(1 - \frac{L_i}{L_i^*} \right)$$

$$T_i = AE(1 - \cos \theta_i) \quad (6.1)$$

$$P = T_1 \sin \theta_1 + T_2 \sin \theta_2 \quad (6.2)$$

Where:

P = applied load including the dynamic effect (dynamic factor of 2 is recommended)

T_i = Tensile force induced in i^{th} cable segment

Δ = deflection at the location of the damaged pier

L_i = initial length of i^{th} cable segment

L_i^* = deformed length of i^{th} cable segment

θ_i = rotation angle of the deformed i^{th} cable

If both spans have the same length, then Eq. 6.2 can be expressed as:

$$P = 2T \sin \theta \quad (6.3)$$

$$P = 2AE(1 - \cos \theta)(\sin \theta) \quad (6.4)$$

For design purposes, the required area of the cables can be expressed as:

$$A_{req} = \frac{P}{2E(1 - \cos \theta)(\sin \theta)} \quad (6.5)$$

For multiple span bridges, the deformed shape of the cable system is shown in Fig. 6.17.

In this case, the induced tensile force in the cables and the required cable area can be expressed by Eqs 6.6 and 6.7, respectively (Astaneh et al., 2001).

$$T = \frac{2LAE(1 - \cos \theta)}{(\sum L)(\cos \theta)} \quad (6.6)$$

$$A_{req} = \frac{P(\sum L)(\cos \theta)}{4LE(1 - \cos \theta)(\sin \theta)} \quad (6.7)$$

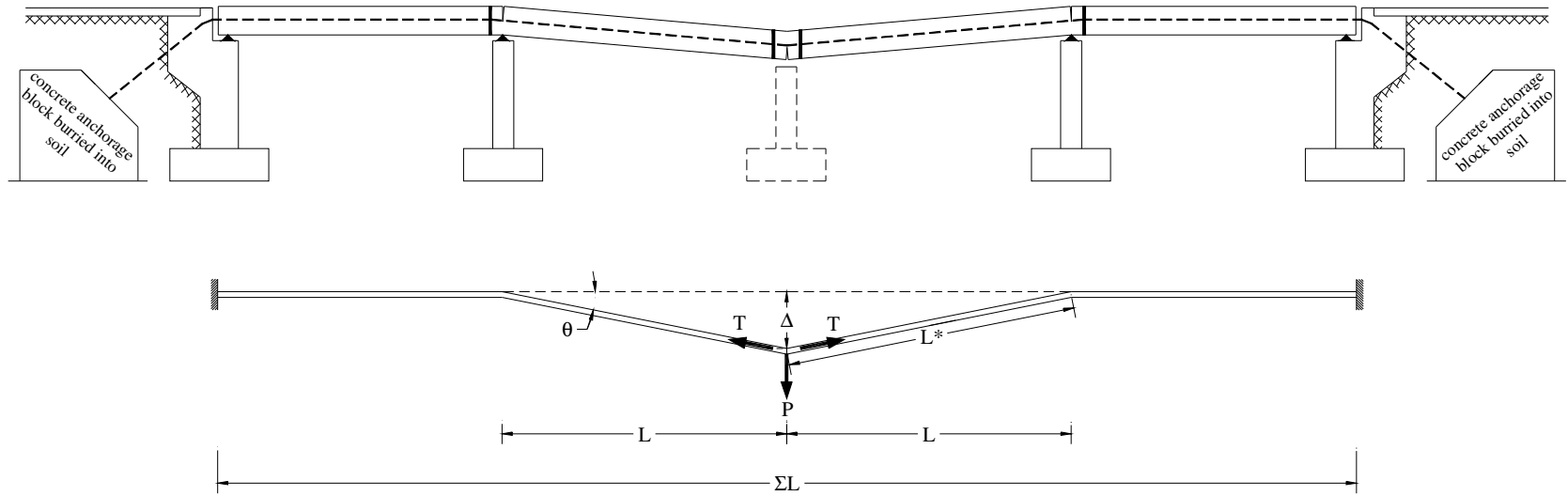


Fig. 6.17. Equilibrium of deflected system of cables for a multiple-span bridge

6.4.2 Castigliano's first theorem (Oden, 1967)

The tensile forces induced in the cables can also be expressed using Castigliano's first theorem (Oden, 1967). The required area of the cable is presented in Eq. 6.8. The results obtained using Eq (6.8) are in very good agreement with those obtained using Eq. (6.7) (Astaneh et al., 2001).

$$A_{req} = \frac{P(\sum L)(L^2)}{2E\Delta^3} \quad (6.8)$$

The analysis of the catenary action induced in the cables depends on the equilibrium of the deformed system, and hence, the required area of the cables is not solely dependant on the applied loads. However, it depends on several other factors. From Eqs 6.7 and 6.8, it can be observed that in order to minimize the area of cable required to resist the vertical loads, one or more of the following conditions should be provided:

- Reduce the applied loads (P)
- Reduce the total length of the cable ($\sum L$)
- Reduce the square of the deflected segment length (L)
- Increase in the elastic modulus of cable material (E)
- Increase the deflection at the damaged pier (Δ)

The external applied loads depend on the summation of the dead weight of the superstructure and the live load acting on the bridge at the time of failure, and hence, we have no control over these applied loads. Since the required area of cables is inversely proportional to Δ^3 , then it is most economic to increase the value of Δ in order to minimize the area of cables. For most bridges, Δ will be limited by the required clearance for emergency vehicles to operate during the high consequence event. In addition, the

required area of cables can be minimized by using innovative material that has higher values of elastic modulus such as 12K high modulus carbon fiber tows which have an elastic modulus of 92,000 ksi. However, the anchorage of carbon fiber cables should be designed carefully to eliminate the possibility of rupture. Additionally, the required area of the cables increases with the increase in the total length of the used cable. Therefore, it can be more economical to use multiple short cable systems instead of one long cable system throughout the entire length of the bridge. Each one of these multiple cable systems will extend along two adjacent spans. A schematic of this technique is shown in Fig. 6.18. Cable 1 will be anchored behind the left abutment and behind column 2; cable 2 will be anchored behind columns 1 and 3; and cable 3 will be anchored behind the right abutment and behind column 2. However, the main disadvantage associated with using multiple cable systems is that it involves using more anchorages than that used for a single cable system.

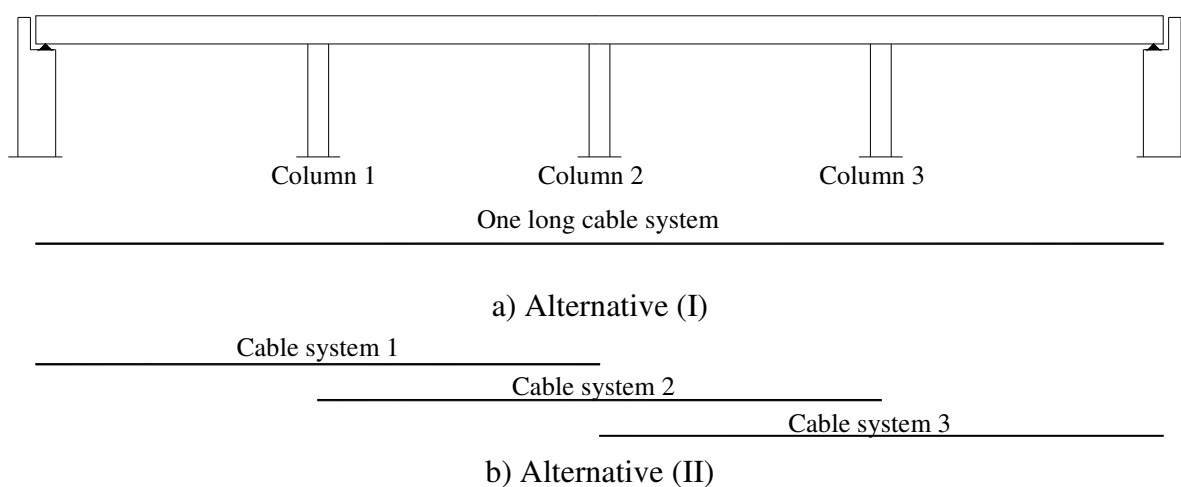


Fig. 6.18. Long single cable system versus multiple short cable systems

For small values of deflection (Δ) and angle of rotation (θ) it can be observed that the required area of the cables is not governed by the applied loads, and hence, the induced stress in the cables is very low which indicates that the cables are not used efficiently. Whereas for higher values of Δ and θ , the stress level in the cables increases and the cables are utilized more efficiently. The effect of the angle of rotation on the required area of cables and the corresponding stress induced in the cables is shown in Fig. 6.19. This curve is generated for a typical two-span bridge; each span is 110 ft long. The modulus of elasticity of the cables is taken as 29,000 ksi. All values in Fig. 6.19 are based on a unit applied force (P), and hence, the required area obtained from this curve should be multiplied by the value of the total vertical applied load.

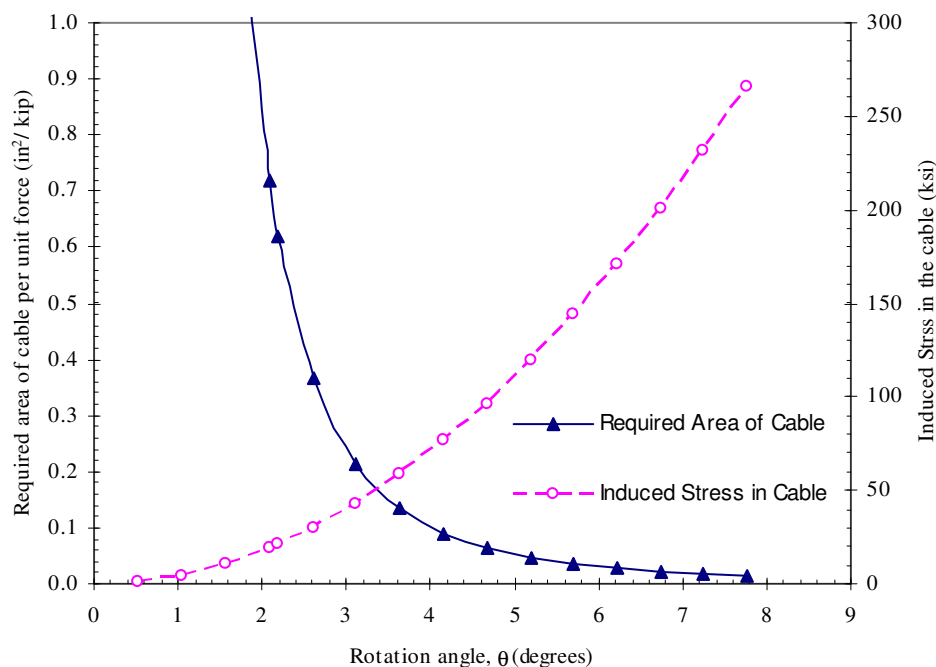


Fig. 6.19. Effect of the angle of rotation on the requires area of the cables

6.4.3 Prestressed cable system

In order to minimize the required area of cables, it can be efficient to utilize prestressed cables. In this case, equilibrium equation (6.3) for the case of two-equal spans will be as follows:

$$P = 2(T_0 + \delta T) \sin \theta \quad (6.9)$$

Where:

T_0 = initial tensile force in the cable due to prestressing

δT = additional tensile force induced in the cable due to equilibrium

The initial elongation of the cable due to the prestressing force will not have any effect on the geometrical equilibrium. Consequently, the required area of the cables will be a function of the additional tensile force induced in the cables at the extreme event. A schematic of this behavior is shown in Fig. 6.20.

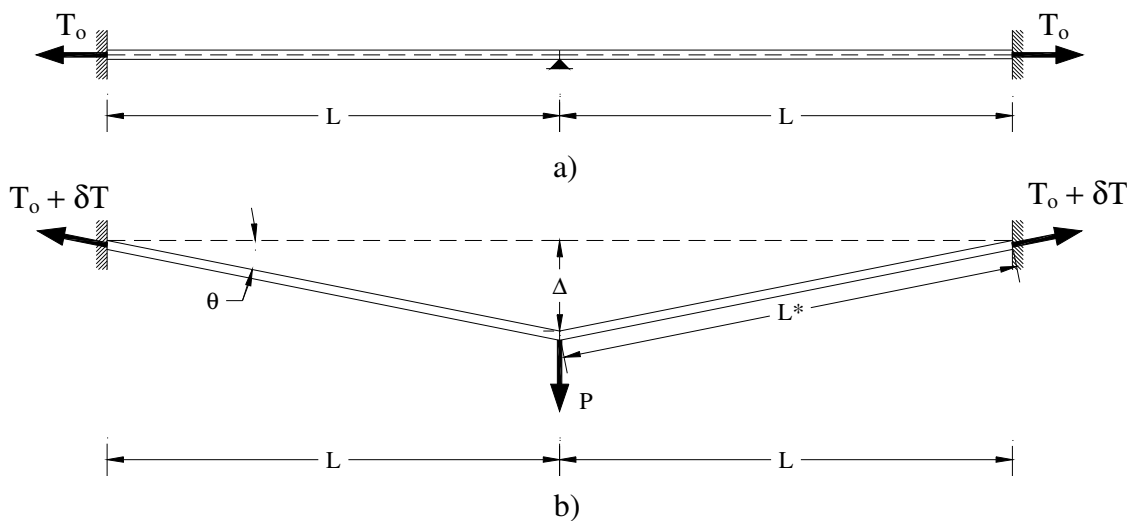


Fig. 6.20. Prestressed cable system a) initial prestressing b) final equilibrium

δT can be expressed as:
$$\delta T = AE(1 - \cos \theta) \quad (6.10)$$

The required area is:
$$A_{req} = \frac{P - 2T_o \sin \theta}{2E(1 - \cos \theta)(\sin \theta)} \quad (6.11)$$

If prestressed cables are used, then the effect of this prestressing force on the superstructure should be considered in the design. It is recommended to keep the center of gravity of the cable system close to the center of gravity of the girders. This will minimize the effect of bending moment resulting from the eccentricity of the cables. Furthermore, it is essential to design the anchorage properly to ensure that the prestressing force will not be released at the time of failure.

6.4.4 Anchorage details of cable system

The anchorage design of the cable system is provided by extending the cables over a saddle in the abutment backwall. Cables are anchored in the soil behind the abutment wall or in a concrete block buried behind the abutment wall as shown in Fig. 6.21. For multiple-span long bridges in which only specific piers are to be protected, the cables can be anchored at the ground within the span behind the columns as shown in Fig. 6.22. However, this should be discussed with the traffic engineers to ensure that the roadway underneath the bridge is wide enough for the traffic. In case of prestressed cables, it will be difficult to prestress the cables if they are anchored in concrete blocks behind the abutments or behind the columns. Providing live end anchorage near the intermediate diaphragms can simplify the constructability of the cables. In this case, the cables will

have dead anchorage in the concrete blocks behind the abutments and/or behind the columns and live anchorage within the spans near the diaphragm.

In conclusion, the catenary action developed in the cables system is a promising technique that can be utilized to localize the damaged that can occur in a certain span of the bridge, isolate the destroyed pier, prevent the progressive collapse from extending to adjacent spans of bridge, and reduce the number of casualties. Further research is required to provide a detailed method of analysis and detailing procedure for the use of cable systems. The design of catenary forces in cable systems is illustrated in a detailed example provided in appendix B.

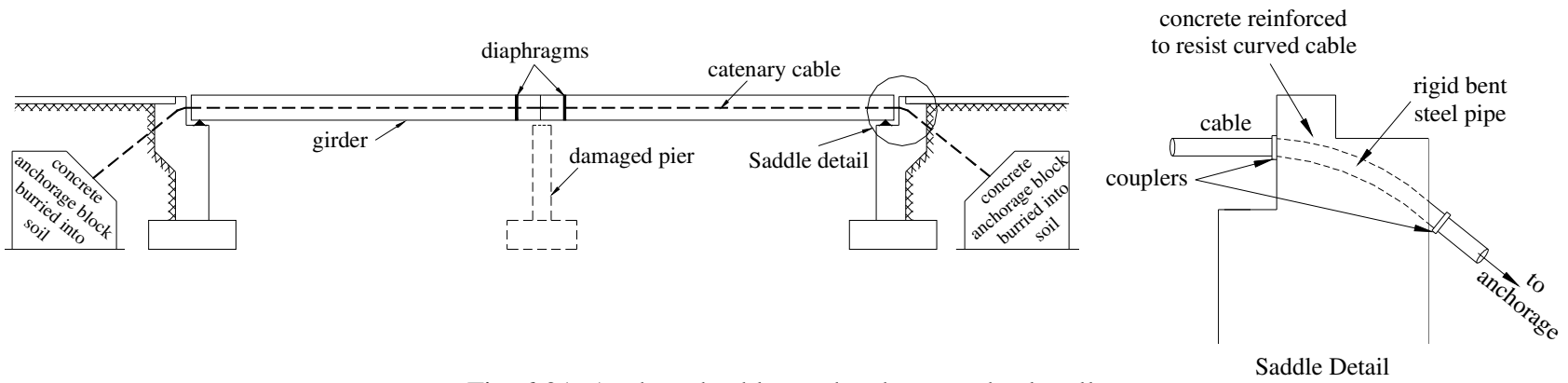


Fig. 6.21. Anchored cables at the abutment backwall

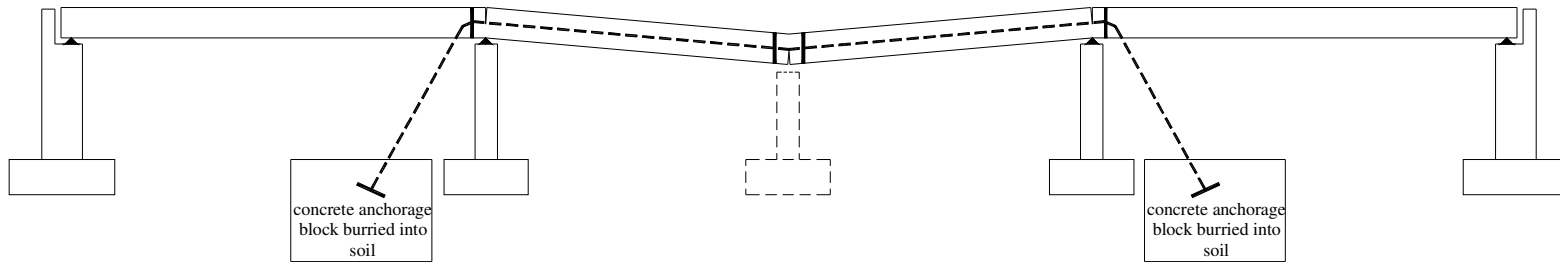


Fig. 6.22. Anchored cables behind columns

CHAPTER 7

CONCLUSIONS AND RECOMMENDATIONS

7.1 Summary

The increased threat of terrorist attacks against infrastructural and transportation targets is an alarming phenomenon and a matter of national security. Bridges are very important elements in the transportation system. The importance of bridges, their national significance, and the casualties associated with a damaged bridge make them attractive targets to terrorists. Consequently, critical bridges should be protected against blast hazards. There are no codes or design guidelines available for protecting bridges against blast, and hence, it is essential to analyze the effect of blast loads on critical bridge components and to evaluate the global response of bridges subjected to various blast scenarios. This research examined the fundamentals of blast loads including blast wave parameters, wave propagation, reflected blast pressure, impulse, and the factors affecting the behavior of structural members subjected to blast loads. Blast load response spectra were developed to transform the dynamic blast load into an equivalent static load. These spectra can be used to perform a simplified SDOF analysis of structural elements subjected to blast loads. To evaluate the global response of a typical highway bridge

model subjected to blast hazards, a computer simulation was performed using ELS software. The bridge model was subjected to various blast scenarios. For each scenario, the vulnerable elements were identified. Based on the results obtained from the computer simulations, protection measures were proposed. This includes using materials with high energy absorption capacities such as high-performance fiber reinforced composites, redundant superstructure components, superstructure continuity, and cable systems to prevent progressive collapse and minimize the damage.

7.2 Conclusions and Recommendations

- Efficient security systems are the most effective way to minimize the potential of terrorist attacks. This includes security surveillance, cameras, preventing parking under the bridge, proper lighting of the site, and truck and van inspections. It is crucial to direct more security measures to vans and trucks as the amount of charge carried by them can be devastating.
- The standoff distance is the most critical parameter in blast scenarios. It is essential to enforce minimum standoff distance for critical bridges that are potential targets for terrorist attacks or are exposed to accidental chemical explosions.
- Dynamic analysis of structures subjected to blast hazards is cumbersome and time consuming. In order to simplify the analysis, blast pressure response spectra were proposed. These spectra are based on transforming the dynamic blast load generated by the explosive device into an equivalent static load using numerical solution of the impulsive blast load. Blast pressure response spectra can be used to analyze the effect of blast loads on a structural component, design this structural member to

withstand the blast pressure, and to estimate the minimum required standoff distance that should be provided for the structural member to prevent its collapse under a specific blast hazard.

- The global response of critical bridges subjected to blast hazards should be investigated to identify the vulnerable structural elements and to predict the failure mechanism of the bridge. Analysis softwares such as Extreme Loading for Structures (ELS), Dytran, and others are effective tools for simulating the behavior of bridges under blast loads and for tracking their failure throughout the various stages of collapse.
- For critical bridges that might be subjected to below-deck blast scenarios, it is recommended to provide the same top and bottom reinforcement to the deck slab throughout the cross section. It is also important to provide sufficient number of shear connectors between the deck slab and girders for full composite action to prevent the separation of the deck from the superstructure girders. To resist the uplift forces and to prevent the separation between the girders and the substructure, it is recommended to use a fixed bearing connection to resist the tensile forces created by blast.
- In case the girders are uplifted from the substructure during the blast scenario, it is important to ensure that the seat width is long enough to hold the rebounding girders and prevent the progressive collapse of the bridge. Hold down devices may also be required in some cases to minimize impact and rebound.
- Blast waves can result in transverse movements of the girders and can apply significant torsional forces on them. Therefore, it is essential to provide lateral

stiffness by utilizing a sufficient number of diaphragms. For concrete girders, concrete diaphragms are preferable over steel cross frames because they exhibit more stiffness to enhance the continuity of the bridge in the transverse direction. As a result, all girders act together as a single unit rather than having individual behavior for each one.

- Structural elements should be designed to exhibit large plastic deformations and high ductility limits. It is essential to utilize High Performance Fiber Reinforced Concrete (HPFRC) materials such as SIFCON, SIMCON, and ECC, due to their high energy absorption capacities.
- The use of highly ductile concrete materials such as SIFCON and ECC encased in steel columns produces ductility levels ranging from 10 to 20 which are two to three times higher than the ductility of conventional concrete and are expected to meet the ductility requirements for blast design.
- Redundancy and continuity of the bridge structure are essential to prevent its progressive collapse and minimize the induced damage during blast hazards. Redundancy can be enhanced by providing double and triple edge columns for the substructure bents, using HPFRC wall piers, and combinations of HPFRC walls and columns.
- A cable system can be designed to provide an alternate load path to support the structure following an extreme event. Catenary action developed in the cable system can be utilized to localize the damage that may occur in certain spans of the bridge, isolate the destroyed pier, prevent the progressive collapse from extending to adjacent spans of bridge, and reduce the number of casualties. Cable layout, number

and locations of diaphragms, and anchorage systems are key factors in designing an efficient, functional, constructable, and cost effective cable system.

7.3 Future Research

- There is a need for experimental testing of structural members subjected to blast loads. Those members should be monitored throughout the experimental tests by special sensors. The stress, strains, and deflections should be recorded and compared with the corresponding theoretical values.
- Further research is required to provide analysis and design guidelines, detailing, and layout schemes for the use of cable systems as an alternate load path to support bridge girders following a major blast event.
- Further research is required to investigate the use of ECC in bridge piers, walls, and other structural elements, and to develop its design guidelines.
- Available software programs for simulating bridge response to blast loads are still undergoing further development and evaluation. Care should be taken when using these software programs for evaluating bridge response especially when evaluating parameters such as angles of incidence and reflected pressures.
- Analysis and design guidelines should be developed to provide a detailed analysis and design procedures for critical bridges subjected to blast hazards. These guidelines should take into account both the local and global behavior of critical bridges.

APPENDIX A

A.1 Using the Blast Response Spectra to Design a Structural Element Subjected to a Specific Blast Scenario

This example illustrates the use of the blast response spectra to design a flexural member subjected to a blast event of 1000 lbs located at a standoff distance of 20 ft. The span of the designed member is 20 ft. The compressive strength of concrete and the yield strength of steel are: $f'_c = 4000$ psi, and $f_y = 60,000$ psi

Step 1: The period of the structural member is calculated based on its mass and stiffness.

These values are computed based on the design for other types of loads acting on the member.

Assume the member has square cross section 3ft x 3ft with the same top and bottom reinforcement of 8 # 8 bars.

$$b = 36 \text{ in}$$

$$d = 36 - 2.5 \text{ in cover} - 1.0 \text{ in bar}/2 = 33 \text{ in}$$

$$\begin{aligned} \text{Elastic modulus of concrete, } E_{con} &= 57000\sqrt{f'_c} = 57000\sqrt{4000} \\ &= 3,605,000 \text{ lb/in}^2 = 519,120 \text{ kip/ft}^2 \end{aligned}$$

$$\text{Density of concrete, } \gamma_{con} = 0.15 \text{ kips/ft}^3$$

$$\text{Area of concrete, } A = 3 \times 3 = 9.0 \text{ ft}^2$$

$$\text{Area of steel, } A_s = 8 \times 0.79 = 6.32 \text{ in}^2$$

$$\text{Modular ratio, } n = \frac{E_s}{E_c} = \frac{29000}{3605} = 8.04$$

$$n A_s = (8.04)(6.32) = 50.84 \text{ in}^2$$

$$c = \frac{-nA_s + \sqrt{nA_s(nA_s + 2bd)}}{b} = \frac{-50.84 + \sqrt{50.84(50.84 + (2)(36)(33))}}{36} = 8.34 \text{ in}$$

$$\text{Gross moment of inertia, } I_g = \frac{1}{12} b h^3 = \frac{1}{12} (3^4) = 6.75 \text{ ft}^4$$

$$\text{Cracked moment of inertia, } I_{cr} = \frac{bc^3}{3} + nA_s(d-c)^2 = \frac{(36)(8.34)^3}{3} + 50.84(33-8.34)^2 = 1.83 \text{ ft}^4$$

$$\text{Use an average moment of inertia, } I_a = \frac{I_g + I_{cr}}{2} = \frac{6.75 + 1.83}{2} = 4.29 \text{ ft}^4$$

$$\text{Self weight of member} = \gamma_{con} A H = (0.15)(9.0)(20) = 27 \text{ kips}$$

Assume the member is subjected to a static weight of 73 kips

Total weight on the member = 100 kips

$$g = 32.2 \text{ ft/sec}^2$$

$$M = (100/32.2) = 3.1 \text{ kip-sec}^2/\text{ft}$$

$K_{LM} = 0.66$ for the plastic behavior

$$K_E = \frac{307EI_a}{L^3} = \frac{(307)(519,120)(4.29)}{20^3} = 85,462 \text{ kip/ft}$$

$$T = 2\pi \sqrt{\frac{M K_{LM}}{K_E}} = 2\pi \sqrt{\frac{(3.1)(0.66)}{(85,462)}} = 0.031 \text{ sec}$$

Step 2: For the design blast scenario, use the response spectra for the specific charge weight and standoff distance.

Use the response spectra for 1000 lbs. A close in view of this spectrum is presented in Fig. A.1.

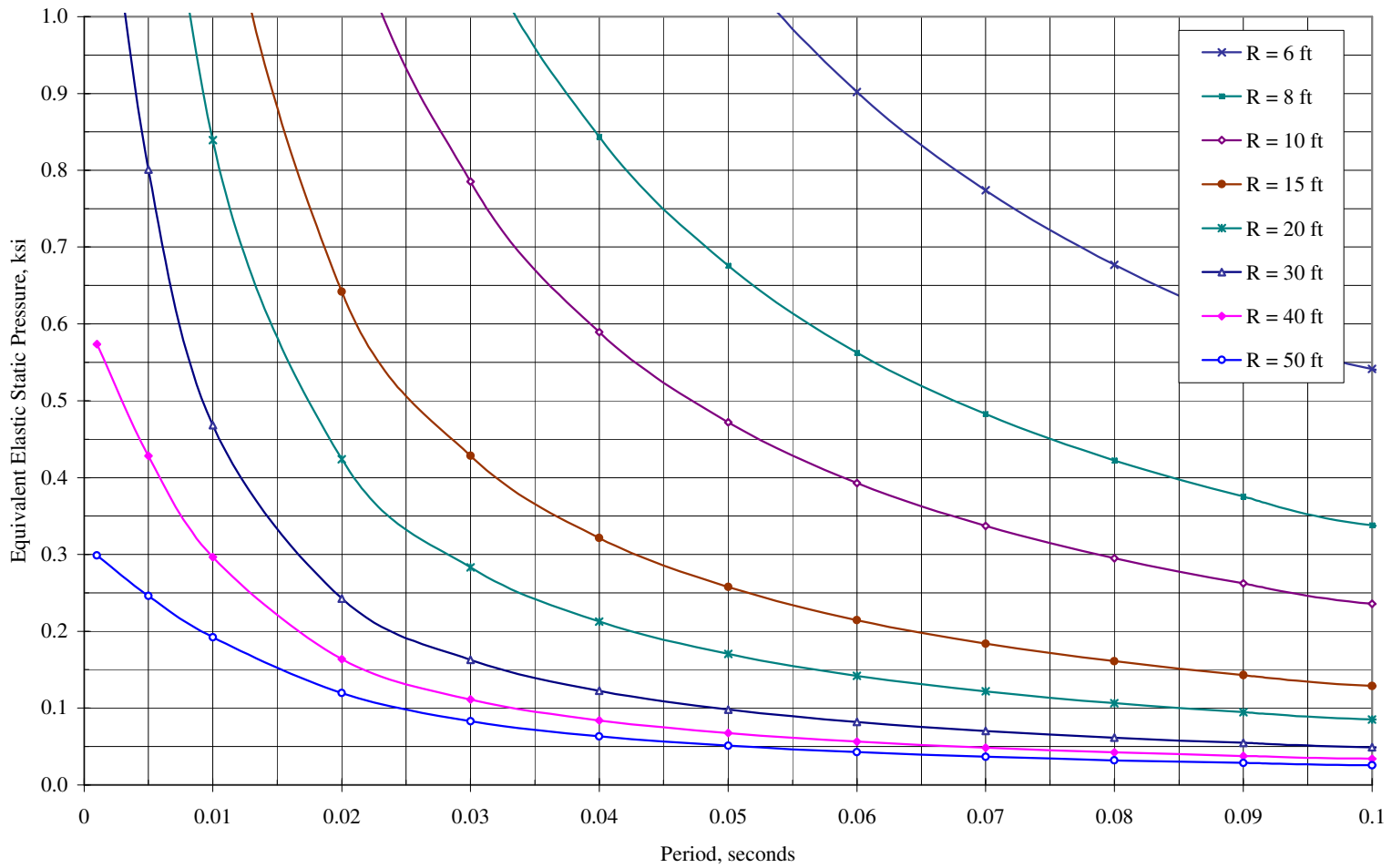


Fig. A.1. Response spectra for W = 1000 lbs (zero damping)

Step 3: Read the equivalent elastic static pressure from the vertical axis based on the period, charge weight, and standoff distance.

From the response spectrum at a standoff distance of 20 ft, the equivalent elastic static pressure = 0.277 kip/in²

Step 4: The equivalent elastic static pressure is multiplied by the correction factor “C” derived in Eq. 3.1.

Assume the detonation source is located at the midspan of the member. The pressure distribution can be approximated to a triangular pressure that decreases linearly by a slope of 1:2 as shown in Fig. A.2. In other words, the pressure drops to zero with a horizontal distance equal to twice the value of the standoff distance.

$$C = \frac{\text{area under the triangular pressure distribution}}{\text{loaded length}}$$

$$= \frac{(1+0.75)(0.5)(10) + (1+0.75)(0.5)(10)}{20} = 0.875$$

Equivalent elastic static pressure = (0.277 kip/in²) (0.875) = 0.242 kip/in²

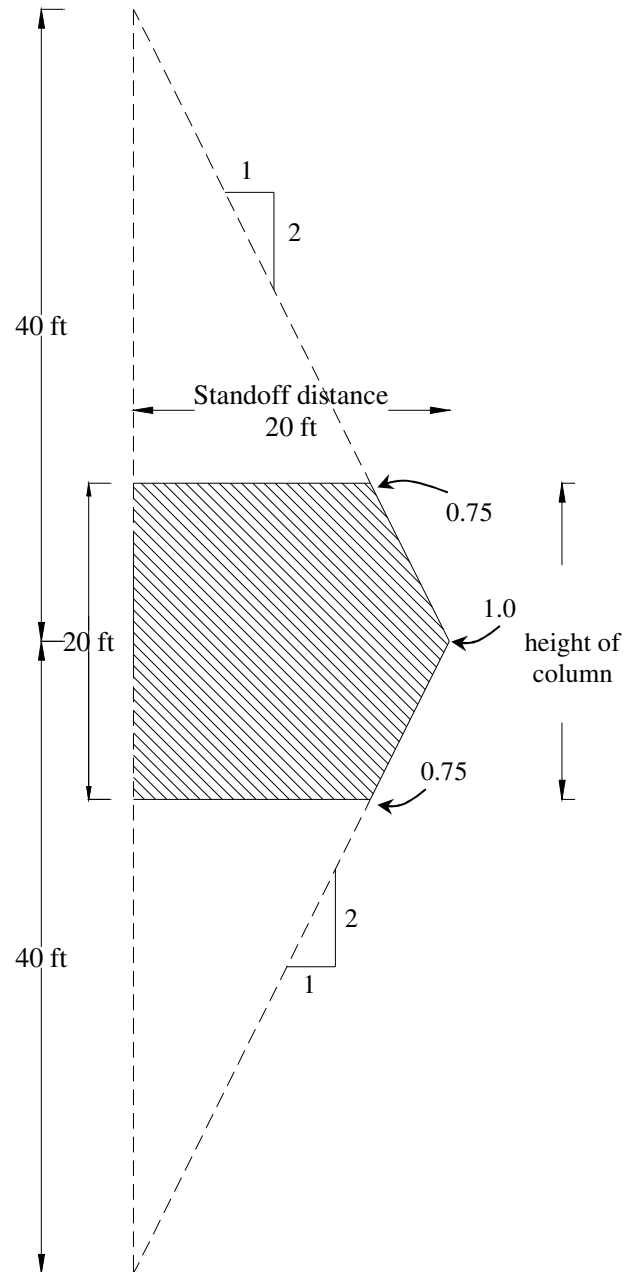


Fig. A.2. Pressure distribution along the length of the member

Step 5: Divide the result by the ductility factor (R_f), based on the provided ductility, to give the equivalent plastic static pressure.

$$\text{Assume } \mu = 5, \quad R_f = \sqrt{2\mu - 1} = 3$$

$$\text{Equivalent plastic static pressure} = (0.242 \text{ kip/in}^2) / 3 = 0.080 \text{ kip/in}^2$$

Step 6: Multiply this plastic static pressure by the tributary width of the member to obtain the equivalent uniform load.

$$\text{Tributary width} = 3.0 \text{ ft} = 36 \text{ in}$$

$$\text{Uniform load} = (0.080 \text{ kip/in}^2)(36 \text{ in}) = 2.90 \text{ kip/in} = 34.85 \text{ kip/ft}$$

Step 7: Use this uniform load to calculate the maximum shear and bending moment acting on the member.

$$\text{Support shear} = (34.85 \text{ kip/ft})(20 \text{ ft})(0.5) = 348 \text{ kips}$$

$$\text{Fixed end moment} = \frac{\omega L^2}{12} = \frac{(34.85)(20)^2}{12} = 1162 \text{ kip-ft}$$

Note: if the member is subjected to bending and shear due to conventional loads, the bending and shear values should be added to those from the blast load case.

Step 8: Check the adequacy of the member to resist the applied staining actions. If the member is not adequate, revise the design and repeat steps 1 through 7.

For dynamic bending, the design strength is calculated as the product of the material strength, the Strength Increase Factor (SIF), and the Dynamic Increase Factor (DIF).

$$f_{dy} = (\text{SIF})(\text{DIF}) f_y = (1.1)(1.17)(60) = 77.2 \text{ ksi}$$

$$f'_{dc} = (\text{SIF})(\text{DIF}) f'_c = (1.0)(1.19)(4) = 4.76 \text{ ksi}$$

Values for DIF and SIF are obtained from Table 2.5 and Table 2.6, respectively.

$$a = \frac{A_s f_{dy}}{0.85 f'_{dc} b} = \frac{(6.32)(77.2)}{(0.85)(4.76)(36)} = 3.35 \text{ in}$$

$$M_p = A_s f_{dy} \left[d - \frac{a}{2} \right] = (6.32)(77.2) \left[33 - \frac{3.35}{2} \right] = 15283 \text{ kip-in} = 1273 \text{ kip-ft} > 1162 \text{ kip-ft}$$

Hence, bending capacity is adequate

For dynamic shear,

$$f'_{dc} = (\text{SIF})(\text{DIF}) f'_c = (1.0)(1.1)(4) = 4.4 \text{ ksi}$$

The shear capacity of plain concrete is

$$V_c = 2\sqrt{f'_{dc}} bd = 2\sqrt{4400}(36)(33) = 157 \text{ kips}$$

The shear capacity of the stirrups is

$$V_s = \frac{A_v f_{dy} d}{s}$$

Assume No. 4 two-legged stirrups @ 5.0 in spacing, i.e. area per leg = 0.2 in²

$$V_s = \frac{(0.4)(77.2)(33)}{5} = 204 \text{ kips}$$

Total shear capacity = 157 + 204 = 361 kips > 348 Kips

Hence, shear capacity is adequate.

Note: if the design is inadequate, the member strength can be increase either by increasing its dimensions, increasing the reinforcement ratio, enhancing the material properties, or increasing the ductility limit.

A.2 Calculating the Minimum Required Standoff Distance for a Specific Structural Element

This example illustrates the use of the blast response spectra to determine the minimum standoff distance that should be provided to a specific member in order to resist a specific charge weight. The charge weight is assumed to be 1000 lbs. The span of the designed member is 20 ft. The compressive strength of concrete and the yield strength of steel are:

$$f'_c = 4000 \text{ psi, and } f_y = 60,000 \text{ psi}$$

Step 1: The period of the structural member is calculated based on its mass and stiffness.

These values are computed based on the design for other types of loads acting on the member.

Assume the member has square cross section 3ft x 3ft with the same top and bottom reinforcement of 8 # 8 bars.

$$b = 36 \text{ in}$$

$$d = 36 - 2.5 \text{ in cover} - 1.0 \text{ in bar}/2 = 33 \text{ in}$$

$$E_{con} = 57000\sqrt{f'_c} = 57000\sqrt{4000} = 3,605,000 \text{ lb/in}^2 = 519,120 \text{ kip/ft}^2$$

$$\gamma_{con} = 0.15 \text{ kips/ft}^3$$

$$A = 3 \times 3 = 9.0 \text{ ft}^2$$

$$A_s = 8 \times 0.79 = 6.32 \text{ in}^2$$

$$n = \frac{E_s}{E_c} = \frac{29000}{3605} = 8.04$$

$$n A_s = (8.04)(6.32) = 50.84 \text{ in}^2$$

$$c = \frac{-nA_s + \sqrt{nA_s(nA_s + 2bd)}}{b} = \frac{-50.84 + \sqrt{50.84(50.84 + (2)(36)(33))}}{36} = 8.34 \text{ in}$$

$$I_g = \frac{1}{12} b h^3 = \frac{1}{12} (3^4) = 6.75 \text{ ft}^4$$

$$I_{cr} = \frac{bc^3}{3} + nA_s(d-c)^2 = \frac{(36)(8.34)^3}{3} + 50.84(33-8.34)^2 = 1.83 \text{ ft}^4$$

Use an average moment of inertia, $I_a = \frac{I_g + I_{cr}}{2} = \frac{6.75 + 1.83}{2} = 4.29 \text{ ft}^4$

Self weight of member = $\gamma_{con} A H = (0.15)(9.0)(20) = 27 \text{ kips}$

Assume the member is subjected to a static weight of 73 kips

Total weight on the member = 100 kips

$$g = 32.2 \text{ ft/sec}^2$$

$$M = (100/32.2) = 3.1 \text{ kip-sec}^2/\text{ft}$$

$K_{LM} = 0.66$ for the plastic behavior

$$K_E = \frac{307EI_a}{L^3} = \frac{(307)(519,120)(4.29)}{20^3} = 85,462 \text{ kip/ft}$$

$$T = 2\pi \sqrt{\frac{M K_{LM}}{K_E}} = 2\pi \sqrt{\frac{(3.1)(0.66)}{(85,462)}} = 0.031 \text{ sec}$$

Step 2: Based on the properties of the structural element calculate the maximum uniform plastic pressure that the member can withstand.

For dynamic bending, the design strength is calculated as the product of the material strength, the Strength Increase Factor (SIF), and the Dynamic Increase Factor (DIF).

$$f_{dy} = (\text{SIF})(\text{DIF}) f_y = (1.1)(1.17)(60) = 77.2 \text{ ksi}$$

$$f'_{dc} = (\text{SIF})(\text{DIF}) f'_c = (1.0)(1.19)(4) = 4.76 \text{ ksi}$$

Values for DIF and SIF are obtained from Table 2.5 and Table 2.6, respectively.

$$a = \frac{A_s f_{dy}}{0.85 f'_{dc} b} = \frac{(6.32)(77.2)}{(0.85)(4.76)(36)} = 3.35 \text{ in}$$

$$M_p = A_s f_{dy} \left[d - \frac{a}{2} \right] = (6.32)(77.2) \left[33 - \frac{3.35}{2} \right] = 15283 \text{ kip-in} = 1273 \text{ kip-ft}$$

$$\text{Uniform plastic pressure from bending} = \omega_b = \frac{12M_p}{bL^2} = \frac{(12)(15282)}{(36)(240^2)} = 0.088 \text{ kip/in}^2$$

For dynamic shear,

$$f'_{dc} = (\text{SIF})(\text{DIF}) f'_c = (1.0)(1.1)(4) = 4.4 \text{ ksi}$$

The shear capacity of plain concrete is

$$V_c = 2\sqrt{f'_{dc}} bd = 2\sqrt{4400}(36)(33) = 157 \text{ kips}$$

The shear capacity of the stirrups is

$$V_s = \frac{A_v f_{dy} d}{s}$$

Assume No. 4 two-legged stirrups @ 5.0 in spacing, i.e. area per leg = 0.2 in²

$$V_s = \frac{(0.4)(77.2)(33)}{5} = 204 \text{ kips}$$

Total shear capacity = 157 + 204 = 361 kips

$$\text{Uniform plastic pressure from shear} = \omega_s = \frac{2V_n}{Lb} = \frac{(2)(361)}{(240)(36)} = 0.084 \text{ kip/in}^2$$

Maximum uniform plastic pressure is the lesser of ω_b and ω_s , hence $\omega_{\max} = 0.084 \text{ kip/in}^2$

Step 3: Multiply this plastic static pressure by the ductility factor (R_f) to obtain the maximum elastic static pressure.

$$\text{Assume } \mu = 5, \quad R_f = \sqrt{2\mu - 1} = 3$$

Maximum uniform elastic static pressure = $(0.084)(3) = 0.252 \text{ kip/in}^2$

Step 4: For a specific charge weight, the minimum standoff distance can be computed based on the equivalent elastic static pressure and the period of the structure.

Use the blast response spectrum for a charge weight of 1000 lbs. Using the period of the structure (0.031 sec) and the uniform pressure of 0.252 kip/in^2 , the standoff distance obtained from the chart is 21 ft

Step 5: Based on the computed standoff distance, the equivalent elastic static pressure is divided by the correction factor “C” derived in Eq. 3.1 to give a revised elastic static pressure.

Assume the detonation source is located at the midspan of the member. The pressure distribution can be approximated to a triangular pressure that decreases linearly by a slope of 1:2. In other words, the pressure drops to zero with a horizontal distance equal to twice the value of the standoff distance.

$$C = \frac{\text{area under the triangular pressure distribution}}{\text{loaded length}}$$

$$= \frac{(1+0.75)(0.5)(10) + (1+0.75)(0.5)(10)}{20} = 0.875$$

Revised elastic static pressure = $0.252/0.875 = 0.288 \text{ kip/in}^2$

Step 6: Enter the response spectrum using the revised elastic static pressure to compute the revised standoff distance.

Revised standoff distance = 19.5 ft

Step 7: Repeat steps 5 and 6 until the standoff distance converges to a constant value

Since the change in the standoff distances obtained in steps 4 and 6 is insignificant, there is no need to carry any further iteration.

APPENDIX B

Design of Catenary Cable System to Prevent Progressive Collapse

This example illustrates the design of a two span bridge to mitigate the removal of the intermediate pier. The design is based on utilizing steel cables to provide catenary action to resist the external applied loads, and hence prevent the collapse of the bridge. The design will be based on a two-span bridge; each span is 110 ft long. The superstructure consists of AASHTO Type VI prestressed girders spaced at 10 feet center-to-center. The deck slab thickness is 8 inches with 2 in. haunch at the location of the girders. The future wearing surface is assumed to be 2 inches. The self weight of concrete is taken as 150 lb/ft³. The weight per unit foot on each girder is calculated as follows:

$$A_{\text{girder}} = 1128 \text{ in}^2$$

$$\text{girder weight} = (1128)(0.15)/(144) = 1.18 \text{ k/ft}$$

$$\text{deck slab weight} = (8)(10/12)(0.15) = 0.98 \text{ k/ft}$$

$$\text{wearing surface} = (2)(10/12)(0.15) = 0.24 \text{ k/ft}$$

$$\text{haunch weight} = 0.09 \text{ k/ft}$$

$$\text{Parapet and guardrail} = 0.5 \text{ k/ft}$$

$$\text{Total dead load} = 1.18 + 0.98 + 0.24 + 0.09 + 0.5 = 3.0 \text{ k/ft}$$

Due to loss of pier, the total dead weight carried by the cables (P) will be:

$$P = (3.0) (110+110)/2 = 330 \text{ kips}$$

For the steel cables, assume $f_{pu} = 270 \text{ ksi}$

Due to the dynamic effect of the extreme event, this force (P) should be multiplied by a magnification factor. However, in this example this factor is assumed to be equal to 1.

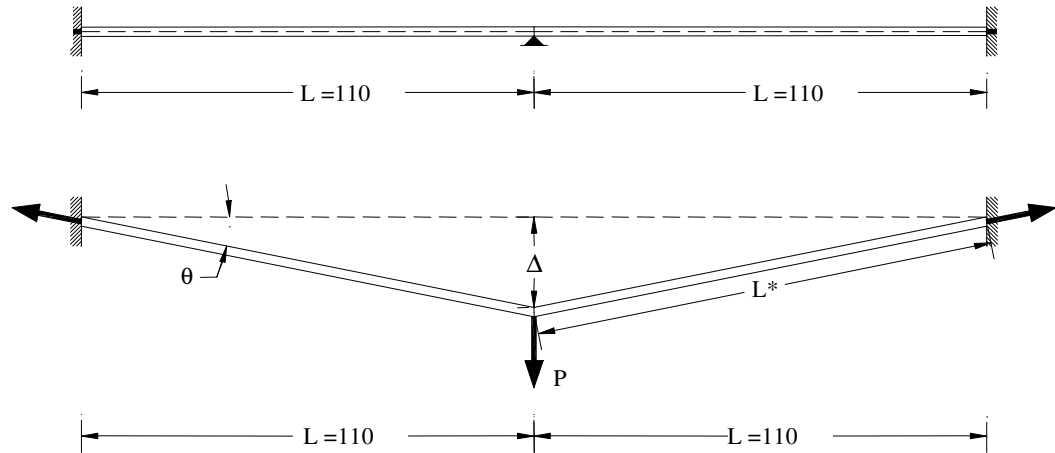


Fig. B.1. Schematic of the catenary forces in the cable system

For steel Cables, the modulus of elasticity (E) = 29000 ksi

$$P = 2T \sin \theta$$

$$P = 2AE(1 - \cos \theta)(\sin \theta)$$

Since the required area of cables is inversely proportional to Δ^3 , then it is most economic to increase the value of Δ in order to minimize the area of cables. For most bridges, Δ will be limited by the required clearance for emergency vehicles to operate during the high consequence event. For this example, it is assumed that $\Delta = 7$ ft

$$\frac{\Delta}{L} = \tan \theta = \frac{7}{110} = 0.0636$$

$$\theta = 3.65^\circ$$

$$T = \frac{P}{2 \sin \theta} = \frac{330}{2(0.0636)} = 2594 \text{ K}$$

$$A_{req} = \frac{P}{2E(1 - \cos \theta)(\sin \theta)} = \frac{330}{2(29000)(1 - \cos 3.65)(0.0636)} = 44.1 \text{ in}^2$$

$$\text{Cable stress } f = \frac{2594}{44.1} = 58.8 \text{ ksi } (0.22f_{pu})$$

Number of 0.6 in Φ diameter strands required = $44.1/0.217 = 203$ or about 7×31 - 0.6 in Φ tendons per girder. (This is a large number of tendons per girder and will not be practical to accommodate in terms of anchorages, deviation diaphragms, and space)

In order to reduce the number of cables, we can utilize the following alternatives:

1. Provide prestressing forces in the cables to reduce their number.
2. Use high modulus cables such as high-modulus carbon fiber tendons.

1. Prestressing

It is recommended to maintain the centroid of the prestressed cables at center of gravity of composite section of the superstructure to avoid introducing bending stresses in deck and girder that could further complicate the design. The amount of prestressing will be controlled by the allowable compression in the composite girder.

f_{pu} for the prestressing steel cables is assumed to be 270 ksi

$$P = 2(\Delta T_0 + T) \sin \theta \quad \text{Where } \Delta T_0 \text{ is the prestress in the two cables}$$

$$(T_0 + \Delta T) = \frac{P}{2 \sin \theta} = \frac{330}{2(0.0636)} = 2594 \text{ kip}$$

Assume

$$T_0 = 2(\Delta T) \Rightarrow 3(\Delta T) = 2594 \text{ kip}$$

$$\Delta T = 865 \text{ kip and } T_0 = 1730 \text{ kip}$$

$$A_{req} = \frac{P - 2T_0 \sin \theta}{2E(1 - \cos \theta)(\sin \theta)} = \frac{330 - (2)(1730)(0.0636)}{(2)(29000)(1 - 0.998)(0.0636)} = 14.7 \text{ in}^2$$

$$\text{initial cable stress } f = \frac{1730}{14.7} = 117.7 \text{ ksi } (0.43f_{pu})$$

$$\text{final cable stress } f = \frac{3(865)}{14.7} = 176.5 \text{ ksi } (0.65f_{pu})$$

2. High-Modulus Carbon Cables

The modulus of carbon fiber cables can range from 43,500 ksi (300 GPa) up to 92,000 ksi (640 GPa) for ultra-high modulus cables compared the 29,000ksi (200 GPa) modulus of steel. The tensile strength of these cables also ranges from 220 ksi 390 ksi. The required area of the cables is inversely proportional to their modulus of elasticity. For example, using the ultra-modulus carbon cables with $E = 87,000$ ksi (600 GPa) and $f_u = 300$ ksi, the required area in the previous example will drop from 44.1 in^2 to 14.7 in^2 without introducing any prestress in the cables. If we introduce pre-tensioning in the ultra-strength carbon cables equal to $0.3f_u = 90$ ksi, then the required area will drop from 14.7 in^2 to 9.73 in^2 .

However, for carbon cables, more attention should be paid for anchorages, deviation diaphragms and sleeves, protection against vandalism, and transverse shear behavior. Also availability, cost, and experience in using these tendons are other factors that need to be addressed when such cables are considered.

APPENDIX C

Cost Analysis of Bridge Protection Measures against Extreme Events

The security design of a specific bridge should be addressed with respect to the statewide network of bridges rather than independent project-level security design (TRB, 2007). To provide the most effective security system, all bridges within the network should be examined and their risk assessments should be identified. Consequently, for the critical bridges, extreme event protection measures are proposed. Due to the high cost of the protection measures and the limited government budget, prioritization of these protection measures is required to achieve the most cost effective design (TRB, 2007). The high cost of bridge security design can only be justified with respect to the severe consequences and casualties that are associated with a destroyed bridge. Damage to one or more critical bridges can result in hundreds of casualties. In addition, the cost of reconstructing a bridge is significantly high. This reconstruction cost can range from few millions up to several billions of dollars.

This section illustrates the impact of some protection measures on the cost of a typical highway bridge. As illustrated earlier in this investigation, it is uneconomical and unpractical to design structures to be blast-proof. The design philosophy is mainly based on allowing the structure to be damaged but preventing the total collapse of the structure. Generally, preventive security measures such as security surveillance, cameras, preventing parking over and under the bridge, and proper lighting of the site are the most cost effective and should be considered as the first step in security design. If further protection is required, protection measures are selected based on the risk assessment, bridge performance criteria, and the design level blast. The cost analysis of these

protection measures is multifaceted as it depends on the bridge type, material, geometry, location, nature of the attack, and the protection measure adopted. This protection cost can vary significantly from one bridge to another and should depend on specific case studies.

The design bridge geometry, materials, dimensions, and details are based on the FHWA design example (Wassef et al, 2003) that was used earlier in chapter 5 (Fig. C.1). The cost analysis will be divided into two main categories; 1) Protection measures for minor blast hazards 2) Protection measures for major blast hazards. In addition, these protection measures will improve the behavior of the bridge during other extreme events such as vessel impacts, truck impacts, and earthquakes. The substructure of the bridge is the most vulnerable to blast attacks and can trigger disproportionate collapse. Hence, this cost analysis will focus mainly on the protection measures of the substructure. Costs of excavation, coring, field testing, and other items are ignored in this study as they are assumed not to vary significantly between the design alternatives.

Preliminary cost of the substructure prior to any protection measures:

Columns:

Diameter of each column = 3.5 ft

Column height = 18 ft

$$\text{Area of each column} = \frac{(\pi)(3.5^2)}{4} = 9.62 \text{ ft}^2$$

$$\text{Volume of concrete per column} = (18) (9.62) = 173.2 \text{ ft}^3$$

$$\text{For the four column in the pier, volume of concrete} = (4) (173.2) = 692.6 \text{ ft}^3 = 25.6 \text{ CY}$$

Bent cap beam:

$$\text{Area of cap beam} = (4 \text{ ft}) (4 \text{ ft}) = 16 \text{ ft}^2$$

$$\text{Length of cap beam} = 55.38 \text{ ft}$$

$$\text{Volume of concrete in the cap beam} = (16) (55.38) = 886 \text{ ft}^3 = 32.8 \text{ CY}$$

For the columns and cap beam, assume steel reinforcement weight is 200 lbs/CY

Footings:

$$\text{Volume of each footing} = (12 \text{ ft}) (12 \text{ ft}) (3 \text{ ft}) = 432 \text{ ft}^3$$

$$\text{For all four footing, volume of concrete} = (4) (432) = 1728 \text{ ft}^3 = 64 \text{ CY}$$

Assume steel reinforcement weight is 125 lbs/CY

Entire substructure:

$$\text{Total volume of concrete above Footings} = 25.6 \text{ CY} + 32.8 \text{ CY} = 58.4 \text{ CY}$$

Assume the cost of concrete above footings is \$800 per cubic yard

$$\text{Cost of concrete above footings} = (\$800/\text{CY}) (58.4 \text{ CY}) = \mathbf{\$47,000}$$

Assume unit cost of steel reinforcements = \$1.4 per lb

$$\text{Cost of steel reinforcement above footings} = (200 \text{ lb}/\text{CY}) (58.4 \text{ CY}) (\$1.4/\text{lb}) = \mathbf{\$16,500}$$

$$\text{Total volume of concrete in footings} = 64 \text{ CY}$$

Assume the cost of concrete in footings is \$400 per cubic yard

$$\text{Cost of concrete in footings} = (\$400/\text{CY}) (64 \text{ CY}) = \mathbf{\$26,000}$$

Assume unit cost of steel reinforcements = \$1.4 per lb

$$\text{Cost of steel reinforcement in footings} = (125 \text{ lb}/\text{CY}) (64 \text{ CY}) (\$1.4/\text{lb}) = \mathbf{\$11,000}$$

$$\mathbf{\text{Total substructure cost} = \$100,500 \text{ per pier}}$$

Cost of the substructure including protection measures for minor blast hazards:

The protection measures utilized against minor blast hazards will consist of using high performance fiber reinforced concrete (HPFRC) in all the columns and the bent cap. The number and geometry of the columns and the bent cap will not be changed. The connection between the columns and the foundation is assumed to be through mechanical anchorage to ensure adequate ductility. The pier section designed for minor blast hazards is shown in Fig. C.2. The cost of the HPFRC varies according to the type of fibers used as well as the fiber supplier. Since HPFRC is only provided by limited suppliers, its price is job specific. In this example, it is assumed that the cost of HPFRC including testing and labor is twice that of conventional concrete that was used earlier prior to the protection measures. The unit cost of mechanical anchorage can also vary according to its type and characteristics. In this example, the cost of each mechanical anchorage is assumed to be \$7,500.

Columns:

For the four column in the pier, volume of concrete = $692.6 \text{ ft}^3 = 25.6 \text{ CY}$

Bent cap beam:

Volume of concrete in the cap beam = $886 \text{ ft}^3 = 32.8 \text{ CY}$

For the columns and cap beam, assume steel reinforcement weight is 200 lbs/CY

Footings:

For all four footing, volume of concrete = $1728 \text{ ft}^3 = 64 \text{ CY}$

Assume steel reinforcement weight is 125 lbs/CY

Entire substructure:

Total volume of concrete above Footings = 25.6 CY + 32.8 CY = 58.4 CY

Assume the unit cost of HPFRC above footings is \$1,600 per cubic yard

Cost of concrete above footings = (\$1,600/CY) (58.4 CY) = **\$93,500**

Cost of steel reinforcement above footings = (200 lb/CY) (58.4 CY) (\$1.4/lb) = **\$16,500**

Total volume of concrete in footings = 64 CY

Assume the cost of concrete in footings is \$400 per cubic yard

Cost of concrete in footings = (\$400/CY) (64 CY) = **\$26,000**

Cost of steel reinforcement in footings = (125 lb/CY) (64 CY) (\$1.4/lb) = **\$11,000**

Cost of mechanical anchorages = (4) (\$7,500) = **\$30,000**

Total substructure cost = \$177,000 per pier

Cost of the substructure including protection measures for major blast hazards:

The protection measures utilized against major blast hazards will consist of using high performance fiber reinforced concrete (HPFRC) in all the columns and the bent cap. Double edge columns will be used at each side of the pier to provide increased redundancy. For high energy absorption capacities, all columns will be encased in 3/4 inches thick steel pipe. The connection between the columns and the foundation is assumed to be through mechanical anchorage to ensure adequate ductility. The pier section designed for major blast hazards is shown in Fig. C.3.

Columns:

Total number of columns = 4 initial columns + 2 additional edge columns = 6 columns

For the six column in the pier, volume of concrete = (6) (173.2) = 1039.2 ft³ = 38.5 CY

Area of steel casing = $(\pi)(3.5 \text{ ft})(0.75/12) = 0.69 \text{ ft}^2$

Assume the steel casing extends a distance of 1 ft in both the bent cap and the footing.

Total length of steel casing = 20 ft

Volume of six casings = (6) (0.69) (20) = 82.5 ft³

Weight of steel casings = (490 lbs/ft³) (82.5 ft³) = 40,409 lbs

Bent cap beam:

Area of cap beam = (4 ft) (4 ft) = 16 ft²

Length of cap beam = 55.38 ft

Volume of concrete in the cap beam = (16) (55.38) = 886 ft³ = 32.8 CY

Footings:

Total number of footings = 6

For all six footing, volume of concrete = (6) (432) = 2592 ft³ = 96 CY

Entire substructure:

Weight of steel casings = (490 lbs/ft³) (82.5 ft³) = 40,409 lbs

Assume the unit cost of structural steel is \$1.75 per lb

Cost of structural steel = (40,409 lbs) (\$1.75 /lb) = **\$71,000**

Total volume of concrete above Footings = 38.5 CY + 32.8 CY = 71.3 CY

Assume the unit cost of HPFRC above footings is \$1,600 per cubic yard

Cost of concrete above footings = $(\$1,600/\text{CY}) (71.3 \text{ CY}) = \mathbf{\$114,000}$

Total volume of concrete in footings = 96 CY

Assume the cost of concrete in footings is \$400 per cubic yard

Cost of concrete in footings = $(\$400/\text{CY}) (96 \text{ CY}) = \mathbf{\$38,500}$

Assume steel reinforcement weight in footings is 125 lbs/CY with a unit cost of \$1.4/lb

Cost of steel reinforcement = $(125 \text{ lb}/\text{CY}) (96 \text{ CY}) (\$1.4/\text{lb}) = \mathbf{\$17,000}$

Cost of mechanical anchorages = $(4) (\$7,500) = \mathbf{\$30,000}$

Total substructure cost = \$270,500 per pier

As illustrated in this example, the cost of the substructure prior to any protection measures was \$100,500 per pier. This cost increased to \$177,000 and \$270,500 for minor protection measures and major protection measure, respectively. This represents 76% and 169% increase of the original cost of the pier, respectively. For further protection against major blast hazards, the columns diameters can be increased from 3.5 ft to 5.0 ft. In this case, the cost of each pier will be approximately \$395,000 which represents 293% increase to the original cost of the pier.

However, this percentile increase in the cost represents only the cost of the substructure and not the entire bridge. These percentages are expected to drop when compared with the cost of the entire bridge. The increase in the cost can also vary depending on the characteristics of each bridge. Protection measures for the superstructure such as

increased seat width, additional deck reinforcements, and hold down devices are less expensive in comparison with the protection measures utilized in the substructure.

Based on this limited study of the cost analysis of protection measures for piers, it is expected that the increase in the cost of a typical bridge designed for a major blast hazard is approximately 10% to 15% of the total cost of the bridge.

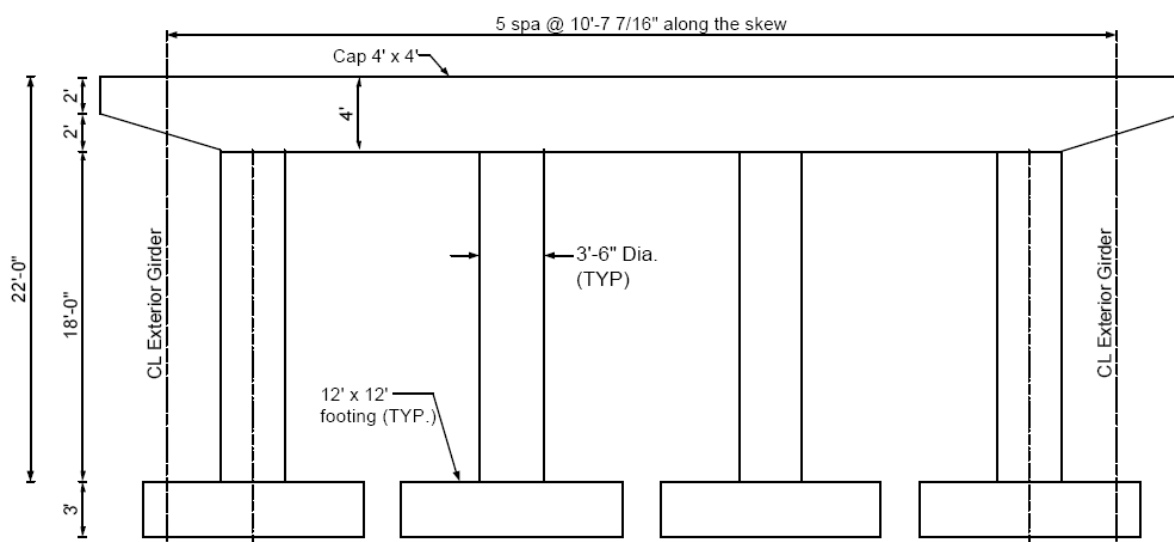


Fig. C.1. Pier section prior to any protection measures

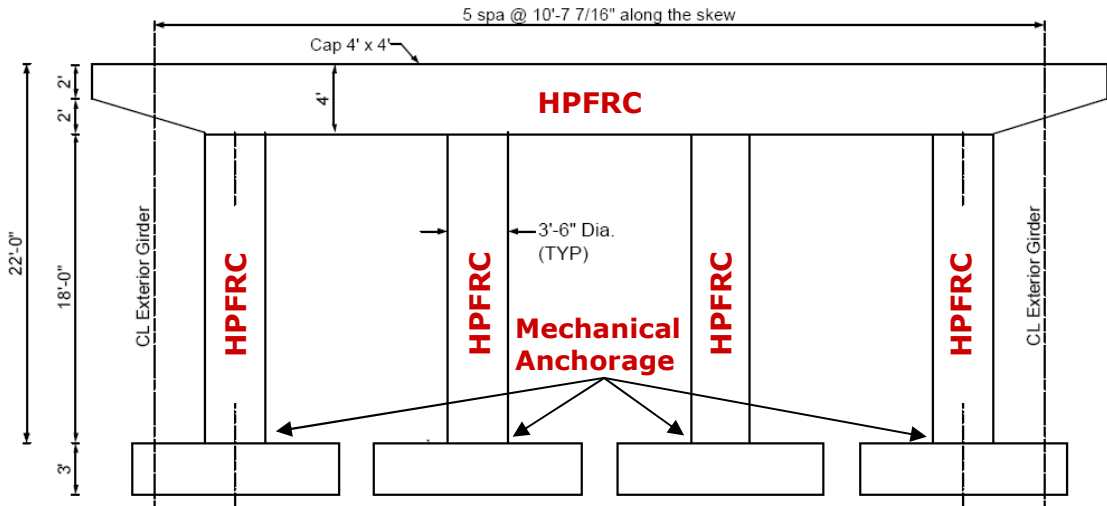


Fig. C.2. Pier section designed for minor blast hazards

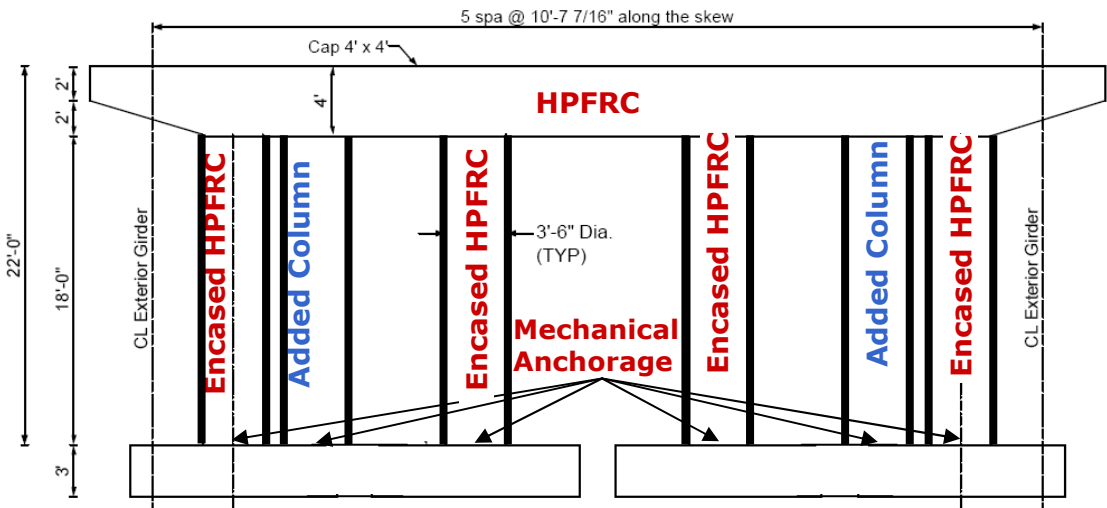


Fig. C.3. Pier section designed for major blast hazards

REFERENCES

American Association of State Highway and Officials (AASHTO), "Load and Resistant Factor Design, Bridge Design Specifications," 2003.

Applied Science International (ASI), "Computer Simulation of the Alfred P. Murrah Federal Building Bombing Event, 1995," ASI, 3221 Wellington Court, Raleigh, NC 27615, September, 2004. www.AppliedScienceInt.com.

ASCE, "Design of Blast Resistant Buildings in Petrochemical Facilities," American Society of Civil Engineers (ASCE), 1997.

Astaneh-Asl, A., Jones, B., Zhao, Y, and Hwa, R., "Progressive Collapse Resistance of Steel Building Floors", Report Number UCB/CEE-Steel-2001/03, Department of Civil and Environmental Engineering., Univ. of California, Berkeley, 2001.

AT-Blast (Anti-terrorism) Version 2.0 Software, Developed by Applied Research Associates (ARA), Inc.

Balaguru, P. N., and Shah, S. P., "Fiber Reinforced Cement Composites," McGraw-Hill, New York, 1992, xii, 530 pp.

Baker, W.E. "Explosions in air", University of Texas Press, 1973.

Cable News Network (CNN) "Davis defends public warning about California bridges" 11/02/2001. <http://archives.cnn.com/2001/US/11/02/inv.bridge.threat/index.html>

Chopra, A. K., "Dynamics of structures-theory and applications to earthquake engineering", Prentice Hall, 1995.

ELS Technical Manual (Extreme Loading for Structures), Developed by Applied Science International (ASI), LLC, 3221 Wellington Court, Raleigh, NC 27615, January 2006.

Federal Highway Administration (FHWA), "Recommendations for Bridge and Tunnel Security, Blue Ribbon Panel Report" Report No. FHWA-IF-03-036, AASHTO, Washington, D.C., September 2003, p. 55.

Federal Highway Administration (FHWA), "Multiyear Plan for Bridge and Tunnel Security Research, Development, and Deployment," Publication No. FHWA-HRT-06-072, AASHTO, Washington, D.C., March 2006, p. 59.

Federal Highway Administration (FHWA), "National Bridge Inventory (NBI) Report," The National Bridge Inventory Study Foundation, 2006.

Fischer, G. and Li, V. C. "Effect of matrix ductility on deformation behavior of steel reinforced ECC flexural members under reversed cyclic loading conditions," *ACI Structures Journal*, Vol. 99, Issue 6, 2002, pp.781-790

Fritz, C., Naaman, A., and Reinhardt, H., "SIFCON Matrix in RC Beams," *Proc., High Performance Fiber Reinforced Cement Composites*, ACI, 1992.

Hackman, L. E., Farrell, M. B., and Dunham, O. O., "Slurry Infiltrated Mat Concrete (SIMCON)," *Concrete International*, 1992, pp 53-56.

Hopkinson, B., "British Ordnance Board Minutes" 13565, 1915

Josifek, C., and Lankard, D., "SIFCON: Slurry Infiltrated Fiber Concrete," *Proc., Fiber Reinforced Concrete Int. Symposium*, 1987.

Kennedy, W.D., "Explosions and Explosives in Air" NDRC, Washington DC, 1946.

Kiger, S.A. and Stanley C. Woodson, "Explosion Effects and Structural Design for Blast, A Two-Day Training course" Center for Explosion Resistant Design, University of Missouri, October 2006.

Lankard, R. D., "Properties, applications: Slurry infiltrated Fiber Concrete (SIFCON)," *Concrete International*, 1984, pp 44-47.

Li, V. C., Lim, Y. M., and Chan, Y. W., "Feasibility Study of a Passive Smart Self-healing Cementitious Composites," *Composites Part B*, Vol. 29B, 1998, pp. 819-827.

Li, V. C., "On Engineered Cementitious Composites (ECC): A Review of the Material and Its Applications," *Journal of Advanced Concrete Technology*, Japan Concrete Institute, Vol. 1, No. 3, November 2003, pp. 215-230.

Mays G.C. and Smith P.D., "Blast Effects on Buildings," Thomas Telford Publications, Thomas Telford Services Ltd, Heron Quay, London, UK, 1995.

Newmark N. M., "An Engineering Approach to Blast Resistant Design," *ASCE Transactions*, Vol. 121, Paper 2786, American Society of Civil Engineers, New York, NY, 1956, pp. 45-64.

NSTB, "U.S. Towboat Robert Y. Love Allision With Interstate 40 Highway Bridge Near Webbers Falls, Oklahoma May 26, 2002" Highway accident report, National Transportation Safety Board, Washington D.C., 2002.

Oden, J.T., "*Mechanics of Elastic Structures*", McGraw Hill, New York, 1967.

Oswald, C. J. and Skerhut, D. "FACEDAP User's Manual," Southwest Research Institute and U.S. Army Corps of Engineers, Omaha (NE) District, April 1993.

Parameswaran, V., Balasubramanian, K., Ramakrishnan, V., and Krishnamoorthy, T., "Toughness of Slurry Infiltrated Fibrous Concrete (SIFCON)," ACI Special Publications, SP 142-3, 1994.

Popov, E. P., "*Engineering Mechanics of Solids*", Prentice Hall, New Jersey, 1990.

Sundararajan, "*Structural Design of Buildings and Industrial Facilities for Blast Loads and Accidental Explosions*", American Society of Civil Engineers, New York, NY, 2007.

Tagel-Din, H., "A new Efficient Method for Nonlinear, Large Deformation and Collapse Analysis of Structures," PhD Thesis, Civil Eng. Dept., University of Tokyo, September 1998.

TM 5-1300, "Design of Structures to Resist the Effects of Accidental Explosions," US Department of Defense, Washington DC, December 1990.

TRB, "Bridge Network Security Evaluation Method" Transportation Research Board, Committee: AHD35, Washington DC, 2007.

TRB, "Workshop # 156: Bridge and Tunnel Security" Transportation Research Board (TRB) 87th Annual Meeting, Washington DC, 2008.

USC_RC program, Asad Esmaeily, University of Southern California.

Wassef, W. G., Smith, C., Clancy, C. M., and Smith, M. J., "Comprehensive Design Example for Prestressed concrete (PSC) Girder Superstructure Bridge with Commentary" submitted to FHWA NHI - 04-043, 2003, pp. 381.

Williamson, E.B., and Winget, D.G., "Risk Management and Design of Critical Bridges for Terrorist Attacks," Journal of Bridge Engineering, Vol. 10, No. 1, January 2005, pp. 96-106.

Zia P., Leming M.L., and Ahmad S.H., "High Performance Concretes: A State-of-the-art Report (1989-1994)," FHWA-RD-97-030, 1991

CURRICULUM VITA

Yahia M. Tokal-Ahmed

EDUCATION:

2009 **Ph.D. Civil and Environmental Engineering**, Rutgers University, New Jersey

2005 **M.S. Structural Engineering**, Lawrence Technological University, Michigan

2002 **B.S. Civil and Environmental Engineering**, Cairo University, Egypt

PUBLICATIONS:

Yahia Tokal and Husam Najm, "Bridge Protection Measures for Blast Loading," *submitted to ASCE Journal of Bridge Engineering* for review, 2008

Yahia Tokal and Husam Najm, "Response of Bridge Structures Subjected to Blast Hazards," *submitted to ASCE Journal of Structural Engineering* for review, 2008

Grace, N., Enomoto, T., Tokal, Y., Abdelmohti, A., "Flexural Behavior of Precast Concrete Box Beams Post-tensioned with Unbonded Carbon Fiber Composite Cables," *PCI Journal*, July-August 2008

Y. Tokal and H. Najm, "Protecting Bridges against Blast Loads," Bridge Engineering association, *New York City Bridge Conference*, August, 2007

Grace, N., Abdelmohti, Tokal, Y., A., "Use of CFRP-DCI/CFCC/Steel in Prestressed Box Beam Bridges," *submitted to ACI Journal for review*, 2006

Yahia Tokal, "Flexural Response of Box Beam Bridges Prestressed using Carbon Fiber Composite Cables (CFCC)," *Masters Thesis*, Lawrence Technological University, Southfield, MI, December 2005

Grace, N., Singh, S., Tokal, Y., "Development of CFCC Reinforced and Prestressed Box Beam Highway Bridges," *Final Report*, Submitted to Tokyo Rope. Co. Ltd, Japan, 2005